Reconciling wind energy development with bird conservation: A comparative study of flight behaviour in raptors to understand and mitigate wind turbine collision risk

Tonio Schaub

NNT : 2024AIXM0092

THÈSE DE DOCTORAT

Soutenue à Aix-Marseille Université
le 10 avril 2024 par

Tonio SCHAUB

Reconciling wind energy development with bird conservation: A comparative study of flight behaviour in raptors to understand and mitigate wind turbine collision risk

Discipline
Sciences de l'environnement

Spécialité
Écologie

École doctorale
ED 251 – Sciences de l'environnement

Laboratoire/Partenaires de recherche
Institut Méditerranéen de Biodiversité et d'Écologie marine et continentale
ENGIE Lab CRIGEN
University of Groningen
Dutch Montagu's Harrier Foundation

Composition du jury

Beth SCOTT	Rapportrice
Professeure, University of Aberdeen, UK	
Olivier DURIEZ	Rapporteur
Maître de conférences HDR, Université de Montpellier	
Virginie BALDY	Présidente du jury
Professeure des universités, Aix-Marseille Université	
Ana RODRIGUES	Examinatrice
Directrice de recherche, CNRS Montpellier	
Christian KERBIRIOU	Examinateur
Maître de conférences, Sorbonne Université	
Alexandre MILLON	Directeur de thèse
Maître de conférences HDR, Aix-Marseille Université	
Raymond KLAASSEN	Co-encadrant
Maître de conférences, University of Groningen, NL	
Caroline DE ZUTTER	Co-encadrante
Ingénieure de recherche, ENGIE Lab CRIGEN	

Affidavit

I, the undersigned, Tonio SCHAUB, hereby declare that the work presented in this manuscript is my own work, carried out under the scientific supervision of Alexandre MILLON, in accordance with the principles of honesty, integrity and responsibility inherent to the research mission. The research work and the writing of this manuscript have been carried out in compliance with both the French national charter for Research Integrity and the Aix-Marseille University charter on the fight against plagiarism.

This work has not been submitted previously either in this country or in another country in the same or in a similar version to any other examination body.

Groningen, 13 February 2024

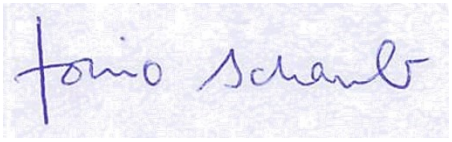

List of publications and conference contributions

1) Publications produced in the context of this thesis:

   1. Albert, P., Bourrioux, J.-L., Falkdalen, U., Lee, S., Millon, A., Persson, T. & **Schaub, T.**: Breeding dispersal of an adult female Hen Harrier from France to Sweden. Fåglar i Jämtland-Härjedalen 2022(2): 17-19.
   2. **Schaub, T.,** Millon, A., De Zutter, C., Buij, R., Chadœuf, J., Lee, S., Mionnet, A. & Klaassen, R.H.G. 2023: How to improve the accuracy of height data from bird tracking devices? An assessment of high-frequency GPS tracking and barometric altimetry in field conditions. Animal Biotelemetry 11:31. [Chapter 3]
   3. **Schaub, T.,** Klaassen, R.H.G., De Zutter, C., Albert, P., Bedotti, O., Bourrioux, J.-L., Buij, R., Chadœuf, J., Grande, C., Illner, H., Isambert, J., Janssens, K., Julius, E., Lee, S., Mionnet, A., Müskens, G., Raab, R., van Rijn, S., Shamoun-Baranes, J., Spanoghe, G., Van Hecke, B., Waldenström, J. & Millon, A.: Informed selection of wind turbine dimensions mitigates the collision risk of birds of prey. *Submitted.* [Chapter 4]
   4. **Schaub, T.,** Klaassen, R.H.G., De Zutter, C., Albert, P., Bourrioux, J.-L., Buij, R., Chadœuf, J., Grande, C., Illner, H., Janssens, K., Keller, A., Lee, S., Mionnet, A., Müskens, G., van Rijn, S., Shamoun-Baranes, J., Spanoghe, G., Van Hecke, B., Waldenström, J. & Millon, A.: Sensitivity to wind turbine collisions: Large differences in time spent flying, proportion of flights at risk height and distance from nest among raptor species. *In preparation.* [Chapter 5]

2) Conferences contributions during the period of this thesis:

   1. **Schaub, T.,** Klassen, R.H.G., De Zutter, C. & Millon, A. 2021: Analyse des comportements de vol par pistage GPS haute-résolution afin de réduire l'impact des parcs éoliens sur les populations de rapaces. Séminaire Éolien et Biodiversité, Paris, FR. [Oral presentation]
   2. **Schaub, T.,** Klassen, R.H.G., De Zutter, C. & Millon, A. 2022: Flight height distributions of five European raptor species and their implications for collision risk in relation to wind turbine design. Conference on Wind Energy and Wildlife Impacts, Egmond-aan-Zee, NL. [Oral presentation]
   3. **Schaub, T.,** Millon, A., De Zutter, C., Buij, R., Chadœuf, J., Lee, S., Mionnet, A. & Klaassen, R.H.G. 2023: High-resolution sampling and barometric altimetry substantially improve the accuracy of height data from bird-borne GPS tags. EURING Analytical Meeting & Workshop, Montpellier, FR. [Poster]

Résumé

Le développement de l'énergie éolienne est un élément majeur des stratégies visant à décarboner la production d'énergie et à atténuer le changement climatique anthropique. Cependant, il entraîne une mortalité d'oiseaux due aux collisions avec les éoliennes, en particulier chez les rapaces. Pour évaluer la sensibilité des différentes espèces aux collisions avec les éoliennes et identifier des mesures d'atténuation efficaces, des informations détaillées sur le comportement de vol sont essentielles. Dans cette étude comparative, des balises GPS miniaturisées ont été déployées pour étudier les aspects du comportement de vol liés au risque de collision chez six espèces de rapaces : le Busard cendré, le Busard Saint-Martin, le Busard des roseaux, la Buse variable, le Circaète Jean-le-Blanc et le Milan royal, ce dernier étant actuellement considéré comme l'une des espèces les plus menacées par le développement éolien en Europe. Au total, 377 individus ont été suivis dans 15 zones d'étude au sein de six pays européens.

Tout d'abord, la hauteur de vol des oiseaux étant un facteur déterminant du risque de collision, les méthodes susceptibles d'améliorer la précision des données de hauteur fournies par les balises GPS ont été évaluées. La précision la plus élevée est obtenue avec des données GPS collectées à haute fréquence (intervalle de 2-3 s entre les positions).

Ensuite, ces données à haute fréquence ont été utilisées pour déterminer les distributions de fréquence de la hauteur de vol et évaluer l'effet des dimensions des éoliennes sur le risque de collision dans les zones de reproduction des espèces. Pour cinq des six rapaces étudiés, la distribution de la hauteur de vol montre un mode prononcé et inférieur à 25 m au-dessus du sol. Par conséquent, le risque théorique de collision diminue considérablement avec l'augmentation de la garde au sol des éoliennes. De plus, le risque de collision par unité de puissance (MW) diminue avec l'augmentation du diamètre du rotor (pour une garde au sol fixe). En revanche, chez le Circaète Jean-le-Blanc, la distribution de la hauteur de vol est plus uniforme et l'effet des dimensions des éoliennes sur le risque de collision est à l'opposé des autres espèces.

Finalement, la sensibilité des espèces différentes aux collisions avec les éoliennes dans les zones de reproduction a été évaluée sur la base du temps passé en vol, de la proportion de vols à hauteur de risque de collision (32-200 m) et de la distance par rapport au nid. De grandes différences interspécifiques ont été constatées : par exemple, chez les mâles, le temps moyen passé en vol par jour varie d'un facteur 7,4 entre les espèces (le plus élevé pour le Busard cendré), et le temps total passé à hauteur de risque par an d'un facteur 6,0 (le plus élevé pour le Milan royal). Avec l'augmentation de la distance par rapport au nid, le temps passé à hauteur de risque par km^2 diminue pour toutes les espèces, avec toutefois une pente spécifique à chaque espèce.

Ces résultats indiquent que les caractéristiques élémentaires du comportement de vol peuvent générer des différences interspécifiques substantielles dans la sensibilité des rapaces aux collisions avec les éoliennes, à exposition au risque égale. Les dimensions des

éoliennes et leur emplacement par rapport aux sites de nidification s'avèrent être des aspects clés affectant le risque de collision, et offrent ainsi un grand potentiel d'atténuation dans un contexte de développement des parcs éoliens terrestres. Cependant, les effets sont spécifiques aux espèces, ce qui suggère de mener des études similaires sur d'autres espèces concernées.

Mots clés : transition énergétique, énergie renouvelable, biodiversité, suivi GPS, altitude de vol

Figure 0.1: A GPS-tagged Montagu's Harrier whose biography nicely symbolises the French-Dutch collaboration in this PhD project: when this male was GPS-tagged in the Netherlands in 2022 (study area Groningen), it turned out that he was born in northern France in 2020 (ringed as nestling). He raised young in the Netherlands in 2022 and 2023 (nest at 640 m of a wind turbine in 2022). Photo: G. Sterk.

Abstract

Wind energy development is a major component of the strategies to decarbonise energy production and mitigate anthropogenic climate change. However, it leads to bird mortality due to collisions with wind turbines, especially in raptors. To assess the sensitivity of different species to wind turbine collisions and identify effective mitigation measures, detailed information on the species-specific flight behaviour is required. In this comparative study, bird-borne GPS tags were used to investigate collision-related aspects of flight behaviour in six raptor species: Montagu's Harrier, Hen Harrier, Marsh Harrier, Common Buzzard, Short-toed Eagle and Red Kite, the latter being perceived as one the most collision-prone species in Europe at present. In total, 377 individuals were tracked in 15 study areas in six European countries.

First, as the flight height of birds is a crucial determinant of collision risk, we assessed methods which could improve the accuracy of height data from GPS tags. The highest accuracy was obtained in high-frequency GPS data (GPS fix interval of 2-3 s).

Subsequently, such high-frequency data were used to determine the frequency distributions of flight height in the breeding areas, and assess the effect of wind turbine dimensions on collision risk. In five out of six species, the flight height distributions had a pronounced mode below 25 m above ground. Consequently, the theoretical collision risk decreased substantially with increasing ground clearance of wind turbines. Moreover, with increasing rotor diameter (at fixed ground clearance), the collision risk per MW decreased. By contrast, in Short-toed Eagle, a more uniform flight height distribution and opposite effects of wind turbine dimensions on collision risk were found.

Finally, the species-specific sensitivity to wind turbine collisions in the breeding areas was assessed based on the time spent in flight, the proportion of flights at collision risk height and the distance travelled from the nest location. Large interspecific differences were found: for example, in males, the average time spent in flight per day varied with a factor of 7.4 between species (highest in Montagu's Harrier), and the total time at risk height per year with a factor of 6.0 (highest in Red Kite). With increasing distance from nest, the time spent at risk height per km^2 decreased in all species, albeit with a species-specific slope.

These results indicated that basic characteristics of flight behaviour could explain substantial differences in the sensitivity to wind turbine collisions among raptor species. The dimensions of wind turbines and their location in relation to nest sites were found to be key aspects affecting collision risk, offering a large potential for mitigation measures. However, the effects were species-specific, which calls for conducting similar studies on other concerned species.

Keywords: energy transition, renewable energy, biodiversity, GPS tracking, flight altitude, bird of prey

Résumé détaillé

La transition vers les sources d'énergie renouvelables est une composante majeure des stratégies visant à décarboner la production d'énergie et à atténuer le changement climatique anthropique (IEA, 2021). Cependant, les installations d'énergie renouvelable telles que les parcs éoliens, les parcs solaires et les centrales hydroélectriques constituent des menaces potentielles pour la biodiversité et pourraient donc renforcer la crise mondiale de la biodiversité (Pörtner et al., 2021). Pour concilier la transition énergétique et la conservation de la biodiversité, le développement des installations d'énergie renouvelable doit s'accompagner de mesures d'atténuation appropriées. Le développement de l'énergie éolienne en particulier implique la mortalité directe d'animaux volants (oiseaux, chauves-souris et insectes) par collision avec les éoliennes (Perrow, 2017). Un ensemble de mesures d'atténuation de ce risque a été proposé (Marques et al., 2014), mais leur efficacité à réduire le risque de collision pour les différentes espèces concernées reste à prouver.

Dans cette thèse de doctorat – une collaboration franco-néerlandaise entre l'Institut Méditerranéen de Biodiversité et d'Ecologie marine et continentale, ENGIE Lab CRIGEN, l'Université de Groningen et la Dutch Montagu's Harrier Foundation – j'ai étudié le risque de collision avec les éoliennes chez les rapaces (ordre des Accipitriformes). Ceux-ci sont généralement perçus comme particulièrement vulnérables aux collisions avec les éoliennes : premièrement, les rapaces présentent généralement des taux de collision élevés (Thaxter et al., 2017) et deuxièmement, ils ont une longue durée de vie avec un faible taux de reproduction, ce qui implique qu'une augmentation de la mortalité a potentiellement des impacts importants sur la croissance de la population (Carrete et al., 2009).

J'ai adopté une approche mécaniste basée sur le comportement de vol en combinaison avec des modèles de risque de collision. Conceptuellement, le comportement de vol a été divisé en différents aspects affectant le risque de collision avec les éoliennes : le temps passé à l'intérieur de la zone du parc éolien, le temps passé en vol, le temps passé à la hauteur du risque de collision (c'est-à-dire la gamme de hauteur du rotor) et le taux d'évitement peuvent être interprétés comme des variables binaires, distinguant les situations où les oiseaux sont exposés à un risque de collision, et les situations où ils ne le sont pas (Figure 0.2). Dans le cadre du modèle de risque de collision de Band (Band et al., 2007), les proportions de temps à risque pour chaque variable sont multipliées l'une par l'autre pour obtenir le nombre attendu de traversées du rotor, qui est une composante importante du risque de collision. Dans le cadre de cette thèse, les trois premiers aspects mentionnés du comportement de vol ont été étudiés, en mettant un accent particulier sur la hauteur de vol (Figure 0.2).

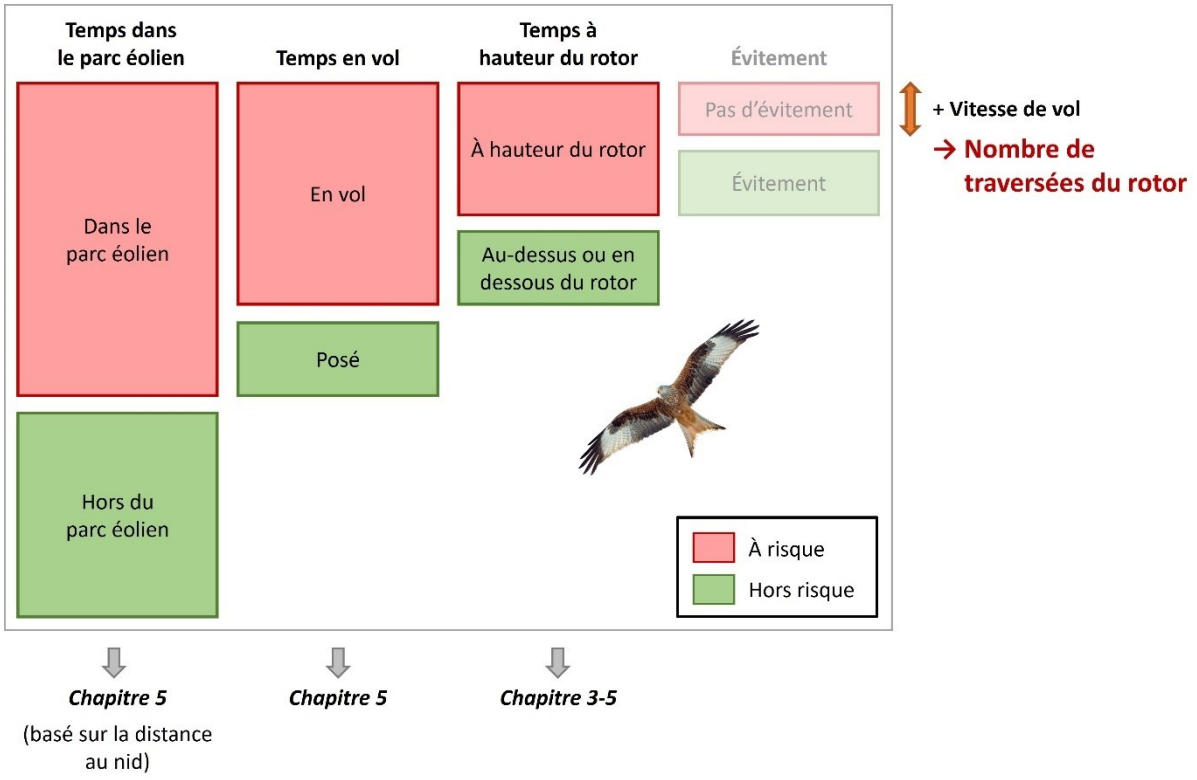

Figure 0.2 : Représentation schématique des aspects du comportement de vol affectant le risque de collision des oiseaux avec les éoliennes. Les chapitres de cette thèse dans lesquels les différents aspects ont été traités sont indiqués en bas. Le taux d'évitement n'a pas été étudié dans cette thèse. La taille des compartiments dans ce schéma n'est pas basée sur des données réelles.

Par rapport aux suivis de mortalité (recherche de cadavres autour des éoliennes), l'approche basée sur le comportement de vol et les modèles de risque de collision a l'avantage de permettre de distinguer les deux composantes du risque de collision, à savoir la sensibilité (facteurs intrinsèques) et l'exposition (facteurs extrinsèques ; Pretorius et al., 2023). En outre, il ne dépend pas de la correction complexe pour la persistance des carcasses, la détectabilité des carcasses et la variation des protocoles de recherche (Huso et al., 2017), des facteurs qui peuvent fortement biaiser les données de suivis de mortalité. De plus, comme les modèles de risque de collision incluent différents aspects du comportement de vol en plus des traits morphologiques et des caractéristiques des éoliennes, ils fournissent des aperçus mécanistes sur la façon dont le risque de collision survient. Ils offrent également de la flexibilité pour mener des études de scénarios pour des parcs éoliens planifiés, par exemple en ce qui concerne l'emplacement et la configuration spatiale des parcs éoliens et les modèles d'éoliennes utilisés (T. Schaub et al., 2020).

À l'aide de balises GPS miniaturisées, les différents aspects du comportement de vol liés au risque de collision ont été étudiés chez six espèces de rapaces, à savoir le Busard cendré *Circus pygargus*, le Busard Saint-Martin *C. cyaneus*, le Busard des roseaux *C. aeruginosus*, la Buse variable *Buteo buteo*, le Circaète Jean-le-Blanc *Circaetus gallicus* et le Milan royal *Milvus milvus* – ce dernier étant actuellement considéré comme l'une des espèces les plus menacées par le développement éolien en Europe. Dans un effort impliquant un grand nombre de partenaires de collaboration, 377 individus ont été suivis dans 15 zones

d'étude en France, Belgique, Luxembourg, Pays-Bas, Allemagne et Suède (voir chapitre 2 pour les détails sur les zones d'étude et les méthodes générales). Tout au long de la thèse, les différences de comportement de vol entre les zones d'étude ont été examinées afin d'obtenir une indication de la variation régionale, dont l'étendue détermine si les résultats peuvent être transférés d'une région à l'autre.

Les principaux objectifs de la thèse étaient les suivants :

1) Améliorer la compréhension du risque de collision avec les éoliennes chez les rapaces (sensibilité relative des six espèces aux collisions avec les éoliennes, interaction des différents aspects du comportement de vol) et
2) Évaluer l'efficacité des mesures d'atténuation sélectionnées (choix des dimensions des éoliennes, choix du site en tenant compte de la distance par rapport aux lieux de nidification).

Précision des données de hauteur fournies par les balises GPS

Les informations sur la hauteur de vol des oiseaux sont essentielles pour évaluer le risque de collision avec les éoliennes. Cependant, la collecte de données précises sur la hauteur de vol s'est avérée difficile. C'est pourquoi, dans le chapitre 3, nous avons évalué deux méthodes susceptibles d'améliorer la précision des données de hauteur obtenues à partir des balises GPS :

a) le suivi GPS à haute fréquence avec des intervalles de 2-3 s entre les positions, où le GPS reste allumé entre les positions ("mode continu" ; par opposition au suivi GPS standard à basse fréquence avec des intervalles ≥ 5 min), et
b) l'altimétrie barométrique à l'aide de capteurs de pression atmosphérique intégrés aux balises GPS.

Cette évaluation a été réalisée dans des conditions de terrain (194 balises de 10 modèles différents posées sur des oiseaux vivant en liberté), et basée sur des périodes où les oiseaux étaient immobiles au sol, ce qui implique que la hauteur réelle au-dessus du sol était connue (approximativement zéro).

Dans les données GPS à haute fréquence, l'erreur aléatoire (bruit) dans les données de hauteur a été considérablement réduite par rapport aux données GPS à basse fréquence, ce qui a permis d'améliorer la précision verticale globale (erreur absolue moyenne de 2 à 7 m selon le modèle de balise GPS, contre 7 à 30 m pour les données à basse fréquence). Les données de hauteur barométriques étaient caractérisées par un bruit relativement faible, mais par une erreur systématique (biais) plus importante, ce qui s'est traduit par une précision globale intermédiaire entre les données GPS à basse et à haute fréquence (erreur absolue moyenne de 7 à 15 m).

Des simulations ont confirmé que le bruit important présent dans les données GPS à basse fréquence pouvait avoir des effets prononcés sur la forme de la distribution des hauteurs de vol (aplatissement des distributions pointues) et sur la proportion de positions situées dans la gamme de hauteurs présentant un risque de collision, alors que l'erreur verticale restant dans les données GPS de haute fréquence et les données

barométriques n'entraînait que de faibles biais. Nous avons discuté du fait que le suivi GPS à haute fréquence, en plus de fournir la précision verticale la plus élevée, présente les avantages supplémentaires d'une précision horizontale accrue et d'une haute résolution temporelle, permettant des analyses détaillées des trajectoires de vol en 3D, par exemple en ce qui concerne l'évitement des éoliennes. Malgré le risque d'un biais systématique, l'altimétrie barométrique pourrait être une approche alternative pour obtenir des données relativement précises sur la hauteur des vols, en particulier lorsque le chargement de la batterie des balises est limitée. La précision des données altimétriques barométriques pourrait encore être améliorée par des méthodes de calibration plus avancées.

Distribution des hauteurs de vol et effet des dimensions des éoliennes sur le risque de collision

Dans le chapitre 4, nous avons déterminé les distributions de la hauteur de vol des six espèces de rapaces pendant leur séjour dans les zones de reproduction. Comme il a été démontré au chapitre 3 que la plus grande précision dans les données de hauteur était nécessaire pour déterminer correctement la forme des distribution de la hauteur de vol, cette analyse a été exclusivement basée sur des données GPS à haute fréquence (de 275 individus ; 6126 h de mouvements de vol enregistrés). Dans un deuxième temps, les distributions de la hauteur de vol ont été utilisées pour évaluer l'effet des dimensions des éoliennes (garde au sol et diamètre du rotor) sur le risque de collision à l'aide d'une adaptation stochastique du modèle de risque de collision de Band. Cette analyse a pris en compte les changements dans les caractéristiques techniques des éoliennes quand le diamètre du rotor varie (vitesse de rotation, largeur des pales, puissance nominale).

Nous avons constaté que cinq espèces sur six avaient des distributions de la hauteur de vol unimodales avec un mode prononcé inférieur à 25 m au-dessus du sol. Par conséquent, pour ces espèces, le risque théorique de collision diminuait considérablement avec l'augmentation de la garde au sol des éoliennes (par exemple de -56% à -66% lorsque la garde au sol passe de 20 à 100 m pour une éolienne dont le diamètre du rotor est de 120 m ; Figure 0.3). En outre, le risque de collision par MW diminuait avec l'augmentation du diamètre du rotor à une garde au sol fixe (par exemple de -50% à -57% lorsque le diamètre passe de 50 à 160 m pour une garde au sol de 60 m). En revanche, une distribution plus uniforme des hauteurs de vol avec un mode faible entre 120 et 260 m a été observée chez le Circaète Jean-le-Blanc. Il en résulte des résultats opposés en ce qui concerne l'effet des dimensions des éoliennes sur le risque de collision par rapport aux cinq autres espèces (risque accru avec l'augmentation de la garde au sol, risque par MW stable avec l'augmentation du diamètre du rotor pour une garde au sol fixe ; Figure 0.3).

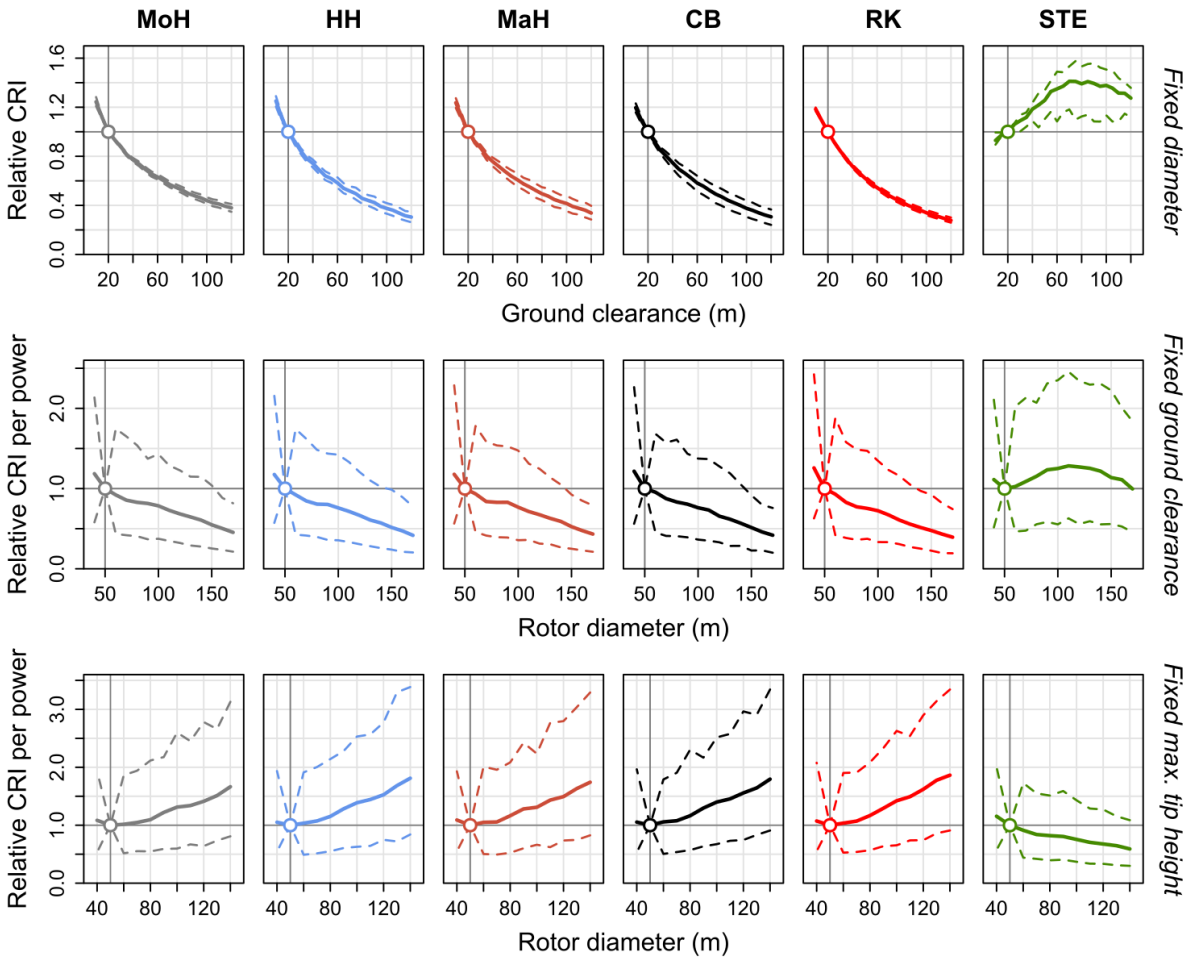

Figure 0.3 : Effet de la garde au sol (« ground clearance ») et du diamètre du rotor (« rotor diameter ») des éoliennes sur le risque de collision (« CRI ») par rapport à un niveau de référence (lignes verticales grises épaisses). Les panneaux indiquent l'indice de risque de collision par éolienne (première ligne) ou par puissance nominale (deuxième et troisième lignes), et se réfèrent à des éoliennes de 120 m de diamètre (première ligne), de 60 m de garde au sol (deuxième ligne) ou d'une hauteur maximale en bout de pale de 150 m (troisième ligne). Les lignes colorées épaisses indiquent les moyennes et les lignes en pointillé les intervalles de confiance à 95 %. MoH = Busard cendré, HH = Busard Saint-Martin, MaH = Busard des roseaux, CB = Buse variable, RK = Milan royal, STE = Circaète Jean-le-Blanc.

Ces résultats indiquent que le choix des dimensions des éoliennes a un effet important sur le risque de collision des rapaces. L'effet variant d'une espèce à l'autre, le développement de parcs éolien devrait tenir compte des espèces d'oiseaux présentes localement afin d'optimiser les dimensions des éoliennes. Pour les espèces ayant un mode de la hauteur de vol bas (c'est-à-dire probablement la majorité des espèces d'oiseaux), l'augmentation de la garde au sol atténue le risque de collision, et l'installation d'éoliennes ayant une garde au sol particulièrement faible est déconseillée. En outre, pour ces espèces, le risque de collision pour une puissance totale donnée peut être réduit en utilisant moins d'éoliennes de plus grand diamètre au lieu de plus d'éoliennes de plus petit diamètre (pour une garde au sol constante).

Sensibilité spécifique des espèces aux collisions avec les éoliennes

Le chapitre 5 a été consacré à la sensibilité des six espèces étudiées aux collisions avec les éoliennes en fonction de trois aspects du comportement de vol, à savoir le temps passé en vol, la proportion de vols à hauteur de risque et la distance parcourue depuis l'emplacement du nid. Pour ces trois aspects, nous avons constaté des variations considérables entre les espèces et les sexes en nous basant sur les données de suivi GPS de 280 individus comprenant 74 501 jours de suivi individuels (en ne considérant que les oiseaux adultes reproducteurs). Le temps moyen passé en vol par jour pendant le séjour dans les zones de reproduction variait de 0,5 (Buse variable) à 3,4 h (Busard cendré) chez les femelles et de 1,0 (Buse variable) à 7,4 h (Busard cendré) chez les mâles (Figure 0.4). La proportion de vols à hauteur de risque de collision variait entre 12,4% (Busard cendré) et 56,4% (Milan royal ; Figure 0.4). Dans les deux cas, la variation entre les zones d'étude était relativement faible, ce qui implique que les résultats peuvent être transférés dans des zones où aucune donnée de suivi n'a été collectée. La plus grande quantité totale de temps à hauteur de risque par an a été trouvée chez le Milan royal (1,7-7,4 fois plus que chez les cinq autres espèces ; Figure 0.4). Ces résultats indiquent que les caractéristiques élémentaires du comportement de vol peuvent expliquer des différences substantielles dans la sensibilité aux collisions avec les éoliennes parmi les espèces de rapaces, et confirment une sensibilité particulièrement élevée chez le Milan royal.

Le quantile de 90 % moyen de la distance du nid allait de 0,7 km (Buse variable) à 9,8 km (Circaète Jean-le-Blanc) chez les femelles, et de 1,0 km (Buse variable) à 5,6 km (Busard cendré) chez les mâles (notez qu'aucune donnée n'était disponible pour les mâles de Circaète Jean-le-Blanc), mais la variation entre les individus (et possiblement entre les zones d'étude) était considérable. Avec l'augmentation de la distance au nid, le temps passé à hauteur de risque par km^2 a diminué chez toutes les espèces. Toutefois, la pente de cette relation était spécifique à chaque espèce, impliquant que le classement relatif des espèces changeait avec la distance (par exemple, à 0-500 m du nid, la Buse variable était presque aussi sensible que le Milan royal chez les mâles). Ces résultats permettent de conclure que le risque de collision des rapaces reproducteurs peut être réduit en augmentant la distance des éoliennes au nids, et surtout en évitant la proximité directe des nids. Si des distances seuils sont appliquées, elles doivent être spécifiques à chaque espèce.

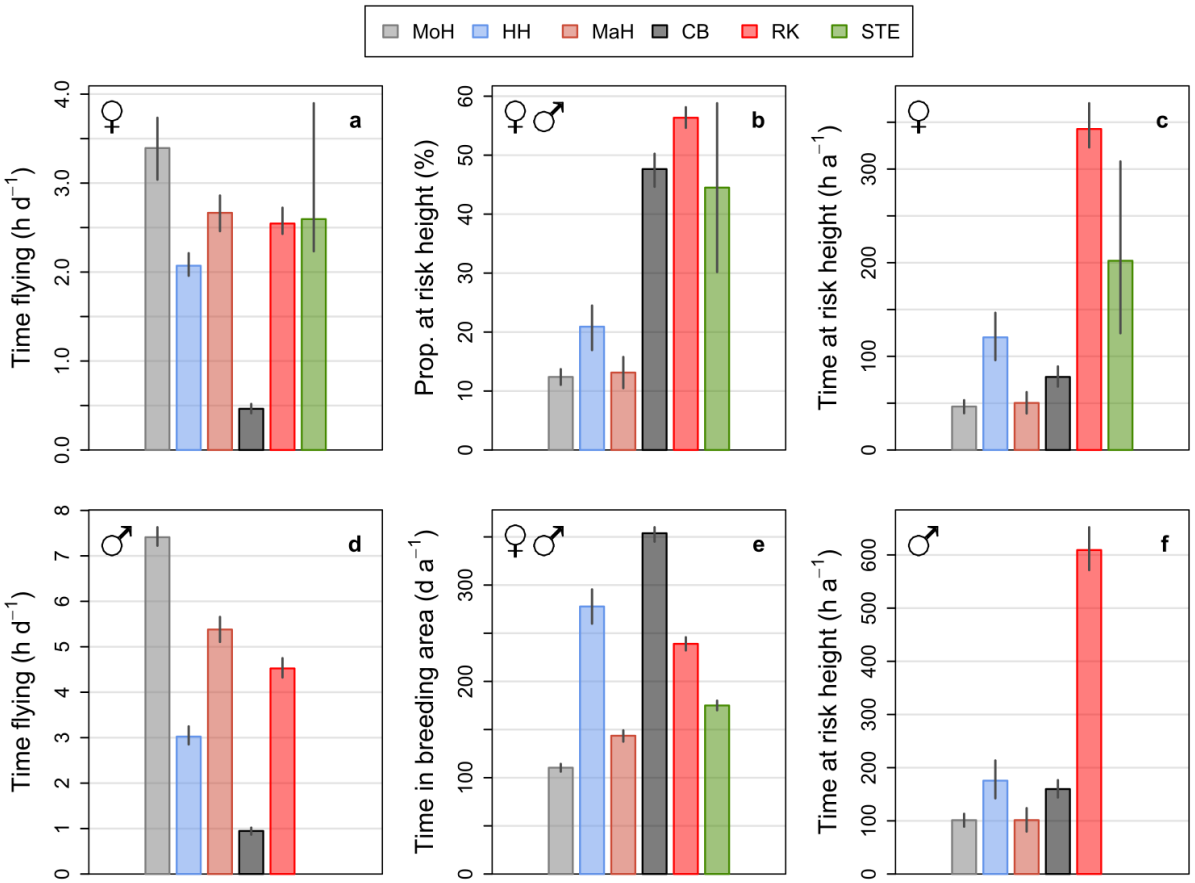

Figure 0.4 : Sensibilité des six espèces de rapaces aux collisions avec les éoliennes pendant leur séjour dans la zone de reproduction exprimée par le temps passé à hauteur de risque de collision (32-200 m) par an (**c**, **f**). Cet indice a été calculé basé sur 1) le temps passé en vol par jour (**a**, **d**), 2) la proportion de vols à hauteur de risque (**b**), et 3) le temps passé dans la zone de reproduction par an (**e**). Les barres colorées indiquent les moyennes, avec des intervalles de confiance à 95 %. Notez que les échelles de l'axe des y sont différentes pour les femelles et les mâles. Les sexes ont été regroupés en **b** et **e**. MoH = Busard cendré, HH = Busard Saint-Martin, MaH = Busard des roseaux, CB = Buse variable, RK = Milan royal, STE = Circaète Jean-le-Blanc.

Conclusions et perspectives

Les résultats de cette thèse indiquent que les caractéristiques élémentaires du comportement de vol pourraient générer des différences substantielles dans la sensibilité aux collisions avec les éoliennes parmi les espèces de rapaces. Les dimensions des éoliennes et leur emplacement par rapport aux sites de nidification se sont avérés être des aspects clés affectant le risque de collision, et offrent ainsi un grand potentiel d'atténuation dans un contexte de développement des parcs éoliens terrestres. Cependant, les effets étaient spécifiques à chaque espèce, ce qui nécessite de mener des études similaires sur d'autres espèces concernées. Comme l'augmentation de la garde au sol, qui pourrait réduire le risque de collision pour beaucoup d'espèces d'oiseaux, est actuellement souvent entravée par des réglementations légales sur la hauteur maximale en bout de pale, il est conseillé de réviser ces réglementations lorsque cela est possible. Dans l'ensemble, cette thèse illustre la valeur de l'approche visant à évaluer le risque de collision des oiseaux avec les

éoliennes sur la base de leur comportement de vol, en particulier lorsqu'elle est appliquée de manière comparative.

Pour affiner les résultats de cette thèse, de futures études pourraient étendre l'évaluation de l'effet des dimensions des éoliennes sur le risque de collision en incluant également l'évitement des éoliennes par les oiseaux à différentes échelles spatiales (par exemple, le taux d'évitement pourrait augmenter avec l'augmentation du diamètre du rotor). En ce qui concerne la sensibilité spécifique des espèces aux collisions avec les éoliennes, notre approche pourrait être étendue en incluant l'évitement et la dynamique de population des espèces considérées. L'évaluation de la variation du temps passé en vol et de la proportion de vols à hauteur de risque de collision en fonction des conditions météorologiques, de la saison ou de l'heure de la journée pourrait fournir des indications précieuses pour informer les mesures de bridage « statique » (c'est-à-dire l'arrêt des éoliennes dans des conditions prédéfinies avec un risque de collision élevé). De plus, comme cette thèse ne s'est concentrée que sur les zones de reproduction, il serait intéressant d'appliquer une perspective circannuelle sur le risque de collision, en évaluant le temps passé en vol, la distribution de la hauteur de vol et l'exposition aux éoliennes également pour les périodes de migration et d'hivernage.

Acknowledgements

I am very grateful for the opportunity to work on this PhD project over the past 3.5 years. I have very much enjoyed to collaborate with so many interesting and nice people, get to know the different species and study areas, and to work on this relevant to pic, making a (small) contribution to a sustainable future. On the one hand, this project was an exciting collaboration between a private company, two universities and a non-governmental organisation. On the other hand, it was a truly European project, with a French-Dutch collaboration at its core and additional partners in Belgium, Luxemburg, Germany and Sweden.

First of all, I would like to thank my supervisors Alexandre Millon, Caroline De Zutter and Raymond Klaassen for their support, patience and dedication to the project: Alexandre for help with making decisions, memorable catching trips, many insights into ornithology in France and nice music recommendations; Caroline for bringing in the company perspective, support with administrative issues and her positive attitude; Raymond for support and supervision since my M.Sc. thesis, lessons on catching and tagging, and many fieldwork memories.

I am grateful to ANRT and ENGIE for the funding of my PhD position (Cifre grant 2020/0448).

Thank you to the teams at IMBE (VEC group and Arbois staff), ENGIE Lab CRIGEN (Lab Environment and Society), University of Groningen (ConsEco group) and Dutch Montagu's Harrier Foundation for welcoming me as a "part-time" member.

At ENGIE Lab CRIGEN, I would like to thank in particular Anne Prieur-Vernat, Alain Quinqueneau and Nathalie Maerten for administrative support, and the Biodiversity team (Coline Bouzique, Hortense Philipot, Charlotte Gironde & Co.) for valuable exchanges.

Moreover, thank you to the ENGIE and CNR colleagues who accompanied the PhD project and provided valuable insights into the technical and business perspective on wind energy development and mitigation measures: Olivier Bedotti, Ariane Frère, Rob Versteirt, Thibaud Uhl, Pauline Millot, Olivier Moreau, Matthieu Lam, Isabella Rubini, Cédric Barbary, Mélanie Le Bris, Florian Doreau, Camille Rolin, Céline Brun, Maylis Peter, Maya Forni, Sandrine Laurent.

Thank you to the members of the PhD committee for three intense meetings and much valuable feedback: Simon Chamaillé-Jammes (CEFE), Agathe Leriche (IMBE), Bart Nolet (NIOO-KNAW) and Chris Thaxter (BTO).

Thank you to the reviewers and jury members for accepting to participate in the PhD defence: Beth Scott, Olivier Duriez, Virginie Baldy, Ana Rodrigues and Christian Kerbiriou.

Thank you to the École Doctorale 251: Jean-Christophe Poggiale and especially Isabelle Hammad for her responsiveness and patience with all my questions.

A great many people and organisations were involved in the collection of the GPS tracking data, by organising the local GPS-tracking projects, deploying GPS tags, assisting with bird captures, monitoring and protecting the nests of GPS-tagged birds, providing funding and/or allowing data use (see also p. 207). Without their contribution, this thesis would have been strictly impossible:

Alsace and adjacent Lorraine (FR): Jérôme Isambert, Arthur Keller, Sébastien Didier (LPO Alsace); Christelle Scheid (Ecofaune); Alexandre Gill (La Volerie des Aigles); Wouter Pieters and colleagues (Parc Animalier de Sainte-Croix); Alexandre Eich (Office National des Forêts)

Aumelas (FR): Alexandre Millon (IMBE); Camille Montégu, Aurélie Béa (LPO Occitanie); Simon Lee (Natural England); Colin Moffa; Carole Millon; Pierre Maigre

Aurich (DE): Celia Grande (Carl von Ossietzky University Oldenburg); Marieke Boekhoff; Felix Jachmann

Champagne (FR): Alexandre Millon (IMBE); Simon Lee (Natural England); Pascal Albert, Jean-Luc Bourrioux, José Dorey, Roland Faynot, Bernard Vacheret, Laurent Cocquyt, Gérard Crouzier, Claude Bouillon (Groupe d'Études et de Protection des Busards) ; Sylvie Dewasmes, Ninon Chinal, Chantal Pinteaux

Diepholz (DE): Luise Boldt, Thorsten Obracay and colleagues (BUND Diepholzer Moorniederung); Almut Schlaich (Dutch Montagu's Harrier Foundation)

East NL & Limburg (NL – Red Kites): Stef van Rijn, Arend van Dijk, Mark Zekhuis, René Janssen, Rick de Ruiter, Willem van Manen, Warner Jan de Wilde, Gijs Bouwmeester

Flanders (BE): Geert Spanoghe, Kjell Janssens, Tanja Milotic, Peter Desmet (INBO), Natuurwerkgroep De Kerkuil

Noordoostpolder (NL): Ralph Buij (Wageningen Environmental Research); Kjell Janssens (DMHF); Harold Boer, Jan Nagel, Jacques van der Ploeg and colleagues (Werkgroep Roofvogels Noordoostpolder); Nicolai Bolt (Province of Flevoland); Reinhard Vohwinkel

Groningen (NL): Raymond Klaassen, Almut Schlaich, Sylvia de Vries, Madeleine Postma, Jitty Hakkert, Toni Hoenders, Jan Ploeger, Popko Wiersma (Dutch Montagu's Harrier Foundation); Ben Koks; Danny Gerrets, Pien Tibbe, Gerard Sterk, Theo van Kooten and all DMHF volunteers; René Janssen (Bionet Natuuronderzoek); Henk van der Noord, Bert Toxopeus and the Marsh Harrier catching team (Collectief Groningen West); Willem Bouten and the UvA-BiTS team (University of Amsterdam); Leon Luiten (Staatsbosbeheer); all families who allowed the placement of the base station computers at their houses

Haute-Marne and adjacent Lorraine (FR): Aymeric Mionnet, Julien Rougé, Patrick Demorgny (LPO Champagne-Ardenne); Alexandre Millon (IMBE); Eric Graja (La Volerie des Templiers); Marine Felten (LOANA); Romain Vila; Lionel Dubief; Jean-Luc Bourrioux; the climbers Paul Supper and Benjamin Colonges; ENGIE Green; CNR; Boralex; EDP Renewables. Special thanks to Lucas Graja (Fauconnerie 2000) for his great fieldwork efforts and to Jérôme Chamoin for the field accomodation!

Hellwegbörde (DE): Hubertus Illner, Margret Bunzel-Drüke, Olaf Zimball, Patrick Hundorf, Christian Härting (Arbeitsgemeinschaft Biologischer Umweltschutz); Raymond Klaassen, Almut Schlaich (DMHF); Ben Koks; Thomas Laumeier (NABU-Station Münsterland)

Limburg (NL – Common Buzzards): Gerard Müskens (Müskens Fauna)

Luxembourg: Katharina Klein (natur&ëmwelt); Simone Schneider (SICONA); Stef van Rijn; Arnaud Beckers (CSD Ingénieurs); Rainer Raab (TB Raab/LIFE Eurokite); Soler

Öland (SE): Jonas Waldenström (Linnaeus University); Susanne Forslund, Helena Lager, Aron Edman (Kalmar County Administrative Board); Raymond Klaassen, Almut Schlaich (DMHF)

Provence (FR): Alexandre Millon (IMBE); Benoît Van Hecke; Olivier Hameau, Alexandre Van der Yeught, Thomas Girard (LPO PACA); Alexandre Lautier (GS Sainte-Victoire); Elvin Miller

Moreover, I would like to thank all funders of the individual GPS tracking projects for their indirect contribution to this thesis (see Table A4.3.1 for a full account); all landowners who allowed us to access their land for fieldwork, and in particular all the farmers supporting the protection of harrier nests on their fields; everyone involved in the recovery of dead GPS-tagged birds, often on a voluntary basis, in Mauritania, Morocco, Tunisia, Spain, Portugal, France, Belgium, Luxembourg, Netherlands, Germany and Sweden; Sławek Rubacha for his efforts to download the tracking data of a Montagu's Harrier "lost" in Poland; and the researchers who considered contributing data to this thesis, but where data use eventually didn't work out: Jakob Katzenberger (DDA); Martin Kolbe (Rotmilanzentrum); Theresa Spatz, Sascha Rösner (University of Marburg); Beatriz Arroyo; Paweł Mirski; Alexandre Villers.

Special thanks go out to:

- Almut Schlaich (DMHF) for diverse support across the years, including advice on stress management and enjoyable donkey walks;
- Hubertus Illner (ABU) for arousing my enthusiasm for Montagu's Harrier conservation with a lecture back in 2014, the many exchanges we had since then and numerous literature recommendations;
- Stef van Rijn for his relentless efforts to monitor Red Kites in the Benelux and the close contact we had to collect high-frequency tracking data;
- Aymeric Mionnet (LPO Champagne-Ardenne) for his indispensable role in setting up the Red Kite tracking project in the French Grand Est and great fieldwork experiences; and
- the Millon family (Alexandre, Carole, Camille, Françoise, Jean) and the Mionnet family (Aymeric, Anne-Sophie and the kids) for their great hospitality.

In addition, I am grateful to all the co-authors for their contributions to the manuscripts; Simon Lee (Natural England) for language checks; Judy Shamoun-Baranes (UvA) for constructive feedback; Joël Chadœuf for various advice on statistics; Yvonne Roelofs and Karen Blaakmeer (DMHF) for taking care of tag settings when I was unavailable; Nel Sangers and Harm Jan Kiewiet for administrative support at the DMHF; David Vallecillo and Lucile Morcelet (IMBE) and the team at CEFE Montpellier (Aurélien Besnard, Olivier Duriez, Thierry Chambert, Yohan Sassi, Arzhela Hemery, Lise Vio llat, Constance Blary) for valuable exchanges; Christophe Baehr (Météo-France/CNRS) and Bart van Stratum (UG) for help with weather data and barometric calculations; Ramunas Zydelis (Ornitela), Paweł Otulak (Milsar) and Willem Bouten (UvA-BiTS) for support with the GPS tags; Christiaan Both, Joost Tinbergen, Richard Ubels and the Flycatcher group (UG) for feedback; Ben Koks for all his work on harriers in the Netherlands and the very rewarding advice to contact Alexandre as a potential collaborator for mounting this PhD project; Gerard Sterk for the great photographs; Lisa Sánchez Aguilar for greatly improving the poster layout; Fabian Zimmer for help with the cover layout; my fellow PhD students at UG (Emma, Drew, Taylor, Koosje, Wender, Sylvia, Marie, Pieter, Renée, Iris, Alexander, Esther, Lisa S., Michella, Delip, Kasper, Izzy, Luis, Guido, Lisa B., Katrin, Maite & Co.), IMBE (Ludo, Aurélie, Emma, Karolina, Charlotte, Pauline & Co.) and CRIGEN (Farah, Gonzalo, Johanna, Hortense, Marianne, Axel & Co.) for enjoyable lunch and coffee breaks; and Marc Kuiper and Roelof Boekema for valuable physiotherapy sessions.

I would also like to thank all my friends (old and new – near and far); my dear neighbours in the ORKZ and the C2 hallway; Els, Robert, Janneke, Matan, Lev, Anne, Maurits and Elin for their warm welcome and support; Oma Gerda for keeping it up; and my parents Tilla and Georg and my sister Anna-Chiara for their support and interest and for providing a safe haven.

And finally, Pien: Thank you for the joy of being together, your support and patience, your enthusiasm for doing fieldwork, and everything else.

Thank you – Merci – Bedankt – Vielen Dank !

Title picture (next page): A pair of Montagu's Harriers performing a prey pass in the vicinity of wind turbines (study area Groningen/NL). Photo: G. Sterk.

Reconciling wind energy development with bird conservation

A comparative study of flight behaviour in raptors to understand and mitigate wind turbine collision risk

Tonio Schaub

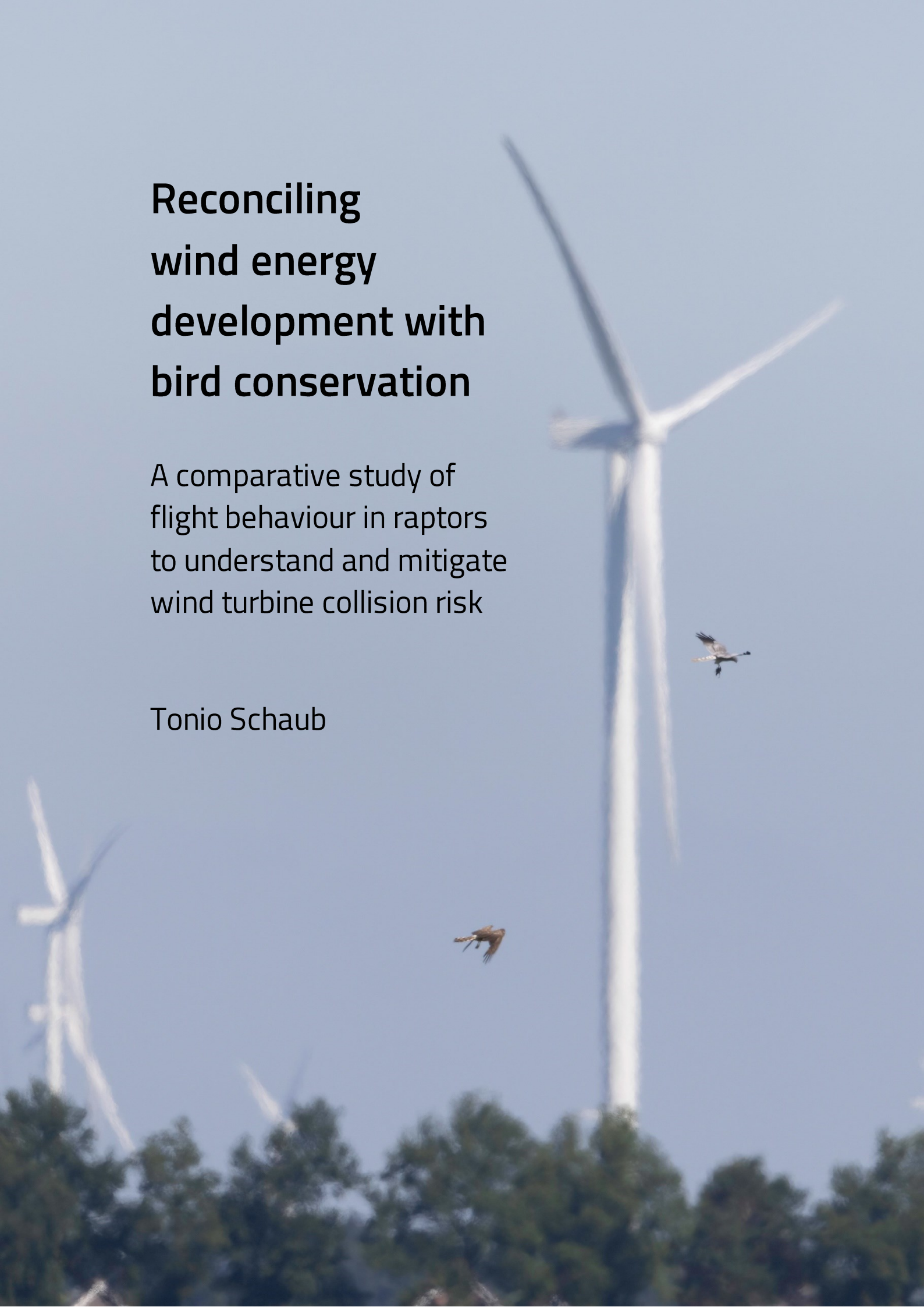

Table of contents

Affidavit 2
List of publications and conferences contributions 3
Résumé 4
Abstract 6
Résumé détaillé 7
Acknowledgements 15
List of abbreviations 21

1. Introduction 22
2. General methods 35
3. How to improve the accuracy of height data from bird tracking devices? An assessment of high-frequency GPS tracking and barometric altimetry in field conditions 45
4. Informed selection of wind turbine dimensions mitigates the collision risk of birds of prey 70
5. Sensitivity to wind turbine collisions: Large differences in time spent flying, proportion of flights at risk height and distance from nest among raptor species 89
6. Synthesis and general discussion 107

Appendix 3.1: Supplementary details on methods (chapter 3) 121
Appendix 3.2: Supplementary results – Tables (chapter 3) 128
Appendix 3.3: Supplementary results – Figures (chapter 3) 133
Appendix 3.4: Additional treatment of high-frequency GPS data (chapter 3) 141
Appendix 4.1: Additional materials and methods (chapter 4) 143
Appendix 4.2: Additional results (chapter 4) 154
Appendix 4.3: Information on local GPS-tracking projects (chapter 4) 166
Appendix 5.1: Additional materials and methods (chapter 5) 168
Appendix 5.2: Additional results (chapter 5) 177
Appendix 5.3: Information on local GPS-tracking projects (chapter 5) 189

References 191
Co-author affiliations 205

List of abbreviations

a.g.l.	Above ground level
AE	Absolute error
CB	Common Buzzard
CRHR	Collision risk height range
CRI	Collision risk index
CRM	Collision risk model
GAM	Generalized Additive Model
MAE	Mean absolute error
MaH	Marsh Harrier
MoH	Montagu's Harrier
HH	Hen Harrier
RK	Red Kite
STE	Short-toed Eagle
TDP	Ten-day period

1. Introduction

1.1. Climate change, biodiversity and wind energy development

Climate change and the loss of biodiversity are two of the most significant challenges for human societies in the 21st century. The two problems are closely interconnected: on the one hand, the loss of biodiversity and the deterioration of natural ecosystems may accelerate climate change (Pörtner et al., 2021). On the other hand, climate change is an important threat to biodiversity, which may act synergistically with other anthropogenic pressures such as habitat degradation and overexploitation (Brook et al., 2008; Nunez et al., 2019; Pörtner et al., 2021).

A key component of the strategies to reduce greenhouse gas emissions is the transition to renewable energy sources. Alongside solar energy, wind energy is an essential pillar of the energy transition (IEA, 2021). In the past decades, wind energy has strongly expanded worldwide: the total global capacity was expected to surpass 1.000 GW in 2023 (> 400.000 wind turbines; Figure 1.1), a more than 40-fold increase since 2000 (GWEC, 2023). However, to achieve the objective of net-zero emissions in 2050, the International Energy Agency expects another ca. 8-fold increase of the global wind energy capacity to be required (IEA, 2021). The expansion of wind energy has been accompanied by major technological advancements, with wind turbines increasing markedly in size and power (Serrano-González & Lacal-Arántegui, 2016; Bilgili & Alphan, 2022).

As climate change poses a threat to biodiversity and wind energy development mitigates climate change, it can generally be assumed that wind energy contributes to biodiversity conservation on a global scale. However, concerns on negative biodiversity effects of wind energy installations on a local scale have been raised. This may concern a range of organisms, such as birds, mammals, invertebrates and plants, both in terrestrial and marine habitats, through habitat alteration, habitat fragmentation, displacement and disturbance by construction and maintenance activities (Schuster et al., 2015). Moreover, as wind turbines extend far into the open airspace, they pose a collision risk to flying animals, i.e. birds, bats and insects (Perrow, 2017). Consequently, mitigation measures are required to ensure the compatibility of climate change mitigation and biodiversity conservation in the context of wind energy development.

Figure 1.1: Wind farm in an agricultural landscape (study area Alsace/FR). Photo: T. Schaub.

As governments establish plans for the expansion of wind energy (e.g. Ministère de la Transition Ecologique et Solidaire, 2020; European Commission, 2023), energy companies are encouraged to accelerate the development of wind farms. When developing and operating wind farms, these companies need to reconcile mitigation measures concerning biodiversity and the economic viability of the projects, alongside a multitude of other restrictions, for example regulations related to aviation, buffer distances to inhabited buildings and industrial safety, the availability of turbine models, the cooperation of landowners, and stakeholder expectations. In light of this complexity, the private sector is more and more appealing to the scientific community to jointly develop efficient solutions.

1.2. Effects of wind energy development on birds

Regarding negative effects of wind turbines on birds, two main processes can be distinguished: displacement and collision. Displacement indicates that the presence of wind turbines reduces bird density, or in other words, that birds visit the area around wind turbines less often than similar areas without turbines. It therefore implies the loss of suitable habitat. Displacement from wind turbines is also termed wind turbine avoidance, especially in the collision risk context (but note that displacement usually refers to the larger spatial scale only, hence corresponding to macro- and meso-scale avoidance; see section 1.5.4). Collision refers to bird mortality due to collisions with wind turbines. Conceptually, the two processes are mutually exclusive (Figure 1.2): if displacement is

complete up to a sufficient distance (no birds closely approaching turbines), the collision risk is zero. In turn, if there is no displacement, there is no habitat loss, but collision mortality is at its maximum. In practice, displacement is often incomplete (bird density reduced, but not zero; e.g. Pearce-Higgins et al., 2009), implying a combination of some degree of displacement and some degree of collision risk. For a given level of displacement, the collision risk may still vary substantially (Figure 1.2; Hötker 2017) in relation to species, wind turbine characteristics or site characteristics (e.g. zero collision risk for all levels of displacement in flightless animals).

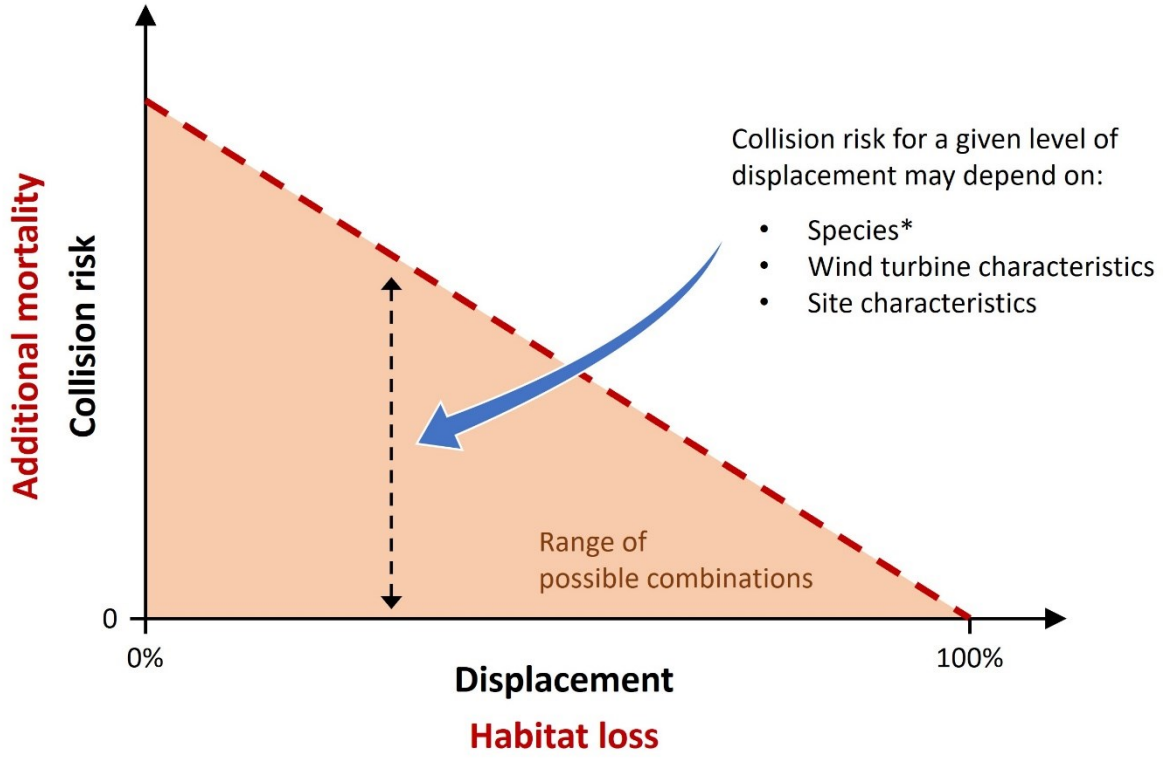

Figure 1.2: The conceptual relationship between displacement (leading to habitat loss) and collision risk (leading to additional mortality). * Including the species-specific flight behaviour (see section 1.5).

The relative importance of displacement and collision risk differs between species groups (Hötker, 2017). A recent review of available studies (predominantly from Europe and North America) identified the orders Gaviiformes, Anseriformes, Suliformes, Accipitriformes and Falconiformes to be most affected by displacement (Marques et al., 2021). However, note that studies with appropriate study design for reliably assessing displacement, i.e. before-after-control-impact (BACI; Sansom et al., 2016), are still very limited. When characterising displacement, it is important to consider both the displacement distance and the strength of the effect. A striking example is the case of Red-Throated Divers *Gavia stellata*, where the density of wintering birds was found to be reduced by > 90% within the 5 km surrounding offshore wind farms, with significant displacement effects

detectable until 10-15 km (Heinänen et al., 2020). Regarding birds of prey (synonym: raptors) of the order Accipitriformes, the focus of this thesis, about half of the available studies indicated displacement, but only up to some hundred metres (Marques et al., 2021). As a side note, also the GPS-tracking data of five species of birds of prey used in this thesis suggest only weak (large-scale) displacement, with birds regularly visiting wind farms and even breeding within the wind farm footprint (see section 2.5). However, it is crucial to differentiate between spatial scales. A lack of displacement effects on the large scale (scale of a whole wind farm, i.e. some hundred meters to some kilometres; "macro-scale") can go along with substantial wind turbine avoidance on a smaller scale (scale of individual wind turbines within a wind farm, i.e. up to some hundred metres; "meso-scale"), which have indeed been found in different raptor species (T. Schaub et al., 2020; Santos et al., 2021; Fielding et al., 2022).

Wind turbine collisions represent a source of direct anthropogenic bird mortality, besides collisions with other man-made structures like power lines, buildings or vehicles, electrocution, predation by free-ranging pets, poisoning, hunting, other forms of intentional killing, etc. (Loss et al., 2015; De Pascalis et al., 2020; Šálek et al., 2023). Usually, birds collide with the rotor blades of wind turbines (which may move with a speed of > 200 km h^{-1} at the blade tips), but also collisions with turbine towers occur in some species groups like Passeriformes and Galliformes (Dürr, 2011; Coppes et al., 2020; Smallwood & Bell, 2020). Estimating the rate of bird collisions at wind turbines is far from easy, as carcass searches are subject to a large degree of uncertainty and biases related to carcass detectability and carcass persistence, amongst others (Huso, Dalthorp, and Korner-Nievergelt 2017; see section 1.4). A meta-analysis of collision rates estimated based on carcass searches in Europe in North America suggested an overall average of 4.4 bird collisions (all species confounded) per turbine and year (De Lucas & Perrow, 2017). What is certain is that variation between sites and individual wind turbines is enormous (up to 156 collisions per year estimated for individual turbines; Brenninkmeijer & Klop, 2017). In Europe and North America, the highest collision rates are commonly found in raptors, storks, gulls, terns, doves and some species of songbirds, again with large variation between sites (De Lucas & Perrow, 2017).

To assess the effect of wind turbine collisions on bird populations, the estimated collision rate (number of collisions per year) needs to be related first to the population size to obtain a mortality rate, and then to the species-specific population dynamics (Diffendorfer et al., 2021; Duriez et al., 2022). The population effect of a given level of additional mortality depends on the species-specific pace of reproduction, with a higher impact in K-selected species (long-lived, low productivity) compared to r-selected species (short-lived, high productivity). In K-selected species, even a small amount of additional mortality can lead to population declines and increased risk of (regional) extinction (Carrete et al., 2009). Accordingly, birds of prey appear to be particularly vulnerable, exhibiting relatively high collision rates on the one hand (Barrios & Rodríguez, 2004; De Lucas & Perrow, 2017; Thaxter et al., 2017), and small population sizes and a slow pace of reproduction on the other hand. For example, Bellebaum et al. (2013) estimated that mortality through wind turbine collisions in Red Kites *Milvus milvus* in Brandenburg (Germany) were close

to the level leading to a population decline, which could be exceeded if additional wind turbines were installed.

1.3. Mitigation measures

For the mitigation of adverse effects on biodiversity, the internationally acknowledged best-practice approach is to follow the mitigation hierarchy (avoid-minimise-restore-offset; UN Global Compact & IUCN, 2012). Applying this sequence to the wind energy context implies that as a first priority, impacts on biodiversity should be *avoided* as much as possible during the planning process of a wind farm project. Secondly, the remaining impacts should be *minimised* during operation. Thirdly, impacts that could not be avoided or minimised should be *offset* (i.e., compensated) and fourthly, *restoration* should take place at the decommissioning stage (May, 2017; Bennun et al., 2021).

To mitigate wind turbine collision risk in birds, a variety of mitigation measures have been conceived (Marques et al., 2014; May, 2017). At the avoidance (pre-construction) level, informed site selection is deemed to be a key measure, implying that areas with high density of collision-prone species, including migration corridors, or more specifically areas with a high risk of birds flying at collision risk height are avoided (M. Schaub, 2012; Bright & Muldoon, 2017; May, 2017; Péron et al., 2017). At a finer scale, micro-siting allows to exclude sites with high expected collision risk based on topography, habitat, distance to nest sites or the location of particular flight corridors (Barrios & Rodríguez, 2004; Everaert & Stienen, 2007; May, 2017). Additionally, an informed selection of the wind turbine dimensions, which determine the height range swept by the rotor blades ("site selection in 3D"), may mitigate collision risk (A. Johnston et al., 2014). Using few large wind turbines (large rotor diameter, high power capacity) is often considered preferable compared to many small turbines (small rotor diameter, low power capacity; May, 2017; Thaxter et al., 2017). Therefore, the "repowering" of wind farms, i.e. the replacement of old turbines by more powerful models (Figure 1.3; Kitzing et al. 2020), which allows to increase the power capacity while decreasing the number of turbines, has been perceived as a potential mitigation measure for birds (Marques et al., 2014; Arnett & May, 2016).

Figure 1.3: "Repowering" of a wind farm: nine old small wind turbines (left; 0.5 MW, rotor diameter 40 m, ground clearance 45 m) are replaced by six new large turbines (right; 3.4 MW, rotor diameter 114 m, ground clearance 36 m; Dutch-German border, study area Groningen). Photo: T. Schaub.

Mitigation measures at the minimisation (post-construction) level include the temporary shutdown of wind turbines (also termed curtailment). The first possibility is to impose shutdown in pre-defined conditions with high collision risk, e.g. based on season, weather, time of day and/or the presence of an active nest nearby. However, such pre-defined or "static" shutdown might come at the expense of a large reduction in energy production (see below). A prominent example of efficient pre-defined shutdown schemes is curtailment at low wind speeds for bats (Adams et al., 2021). For birds, such measures may generally be less efficient (Arnett & May, 2016), possibly with the exception of shutdown during peak migration days in the case of highly concentrated migration fluxes (Krijgsveld et al., 2016).

The second possibility is to shut down wind turbines specifically when birds approach them. This "dynamic" shutdown (also termed shutdown-on-demand) requires a bird detection system, which has so far been implemented using human observers (de Lucas et al., 2012), observers in combination with radar (Tomé et al., 2017) or automatic bird detection devices based on cameras (McClure et al., 2018).

Moreover, measures increasing the visibility of wind turbines by painting the turbine towers or rotor blades have proven effective for some bird species (May et al., 2020; Stokke et al., 2020). Another proposition is to deter birds so that they do not approach the wind turbines using sound or visual cues, either permanently or only when birds are approaching a turbine, i.e. in combination with a detection system (May et al., 2015). In

addition, habitat management could be used to make the vicinity of wind turbines less attractive to birds for breeding or foraging, and in turn increase habitat quality outside the wind farm (May, 2017).

Overall, it needs to be stressed that the body of scientific studies assessing the effectiveness of the mentioned proposed mitigation measures is still very restricted, amongst others due to the difficulties of reliably quantifying and comparing collision risk (see section 1.4*)*. When evidence is available, it is commonly limited to a small number of species (e.g. McClure et al., 2018; May et al., 2020). However, the effectiveness of mitigation measures is certainly species-specific, depending on the species' flight behaviour, visual capability, behavioural responses to disturbances, habitat preferences, etc. Therefore, there is a high urgency to assess the effectiveness of mitigation measures for all species potentially affected.

Besides the *effectiveness* of the proposed mitigation measures to reduce collision risk, it is important to also consider their *efficiency*, i.e. the ratio of benefits and costs. The objective should be to identify measures reducing collision risk at low costs and involving a minimum loss of power production (Marques et al., 2014; May, 2019). This is not only relevant from the perspective of the wind energy industry, but also for biodiversity conservation: a reduced power output, for example due to restrictive curtailment regulations (e.g. shutdown during the whole breeding season), also means that more wind turbines are necessary to achieve the set targets of total wind energy production (see section 1.1). In turn, this may compromise the reduction of total collision risk brought by the initial mitigation measure, as the locally reduced collision risk would partly be offset by additional turbines elsewhere. Moreover, if mandatory mitigation measures for wind energy projects are too costly, the economic incentives might be reduced, which could slow down the energy transition and inhibit climate change mitigation, with possible negative biodiversity effects in the long term. From the industry perspective, there may also be technical or operational constraints for mitigation measures, e.g. frequent turbine shutdown may be detrimental for the material longevity of turbines.

1.4. Approaches for assessing collision risk

Conceptually, the risk an anthropogenic threat poses to a species can be divided into two components: risk = sensitivity (intrinsic factors) x exposure (extrinsic factors; Dickinson et al., 2014; May et al., 2015; Pretorius et al., 2023). Sensitivity (or hazard) refers to the "intrinsic aspects of a species' biology that determine its capability to withstand a given threat"; and exposure to the "intensity of threat acting against the species" (Dickinson et al., 2014: p. 1). In the context of collisions with wind turbines and other anthropogenic structures, sensitivity could depend on morphological aspects such as visual faculty, wing loading and manoeuvrability, behavioural aspects such as flight height and the frequency of nocturnal flights (Janss, 2000; Martin, 2011; Herrera-Alsina et al., 2013; Pretorius et al., 2023), and demographic aspects (see section 1.2). Exposure to a threat is, in general, mainly determined by geographic location (Dickinson et al., 2014).

Concerning wind turbine collision risk, this refers to the location of wind turbines in relation to the distribution range of the species (on different spatial scales; "horizontal overlap"). However, exposure also has a vertical component here, as it depends on the height range of wind turbines in relation to the species-specific flight height distribution ("vertical overlap").

Two main methodological approaches have been used to assess the collision risk of birds with wind turbines in terrestrial ecosystems. The first is to record collision fatalities based on carcass searches around wind turbines (Brenninkmeijer & Klop, 2017; Thaxter et al., 2017) in combination with procedures correcting for carcass persistence, carcass detectability and unsearched areas (Huso et al., 2017). The second approach is to study the birds' flight movements and behaviour (Ross-Smith et al., 2016; Pfeiffer & Meyburg, 2022), and subsequently derive estimates of collision risk (or the number of expected collisions) using collision risk models (Masden & Cook, 2016; Vasilakis et al., 2016; T. Schaub et al., 2020). Note that in the offshore environment, carcasses cannot be searched. Hence, the flight behaviour approach is normally the only possibility (e.g. Desholm & Kahlert, 2005; Thaxter et al., 2015; but see Skov et al., 2018 for a recent study using automatic turbine-mounted cameras for recording collisions with offshore wind turbines). Both approaches have advantages and drawbacks: the carcass search approach estimates the result (number of collisions) directly, while the flight behaviour approach is more indirect. However, the latter provides mechanistic insights on how collision risk arises, as collision risk models include different aspects of flight behaviour, morphological traits and wind turbine characteristics (Band et al., 2007; Masden & Cook, 2016). Notably, it allows to separate sensitivity and exposure, while this isn't possible using the carcass search approach alone (combination with measures of bird abundance or flux required; Krijgsveld et al., 2009). The flight behaviour approach provides more flexibility to conduct scenario studies for planned wind farms, for example regarding the location and spatial configuration of wind farms and the turbine models used (Vasilakis et al., 2016; T. Schaub et al., 2020). It also allows to make predictions for species which are not yet exposed to wind farms in their distribution range, which the carcass search approach does not. Another important disadvantage of the carcass search approach is that commonly only a small proportion of collision victims are actually found, implying that it is indispensable to correct the raw data for carcass persistence, carcass detectability and unsearched areas (Huso et al., 2017). If these corrections are not appropriately done, there may be substantial biases when comparing collision rates between species or sites (e.g. carcass detectability increasing with the size of the bird). Additionally, the uncertainty around the corrected collision rates are commonly large (e.g. Brenninkmeijer & Klop, 2017).

Concerning the flight behaviour approach, a main disadvantage is that the validation of the absolute results of collision risk models (expected number of collisions) is difficult. First, this requires reliable information on the actual number of collisions. Secondly, there is a notorious lack of reliable data on the avoidance rate, one of the species-specific input parameters (see section 1.5) with a large effect on the model outcome (Chamberlain et al., 2006). Nevertheless, collision risk models are considered suitable for relative conside-

rations, i.e. the comparison of different scenarios assuming everything else (including the avoidance rate) being equal (Chamberlain et al., 2006).

1.5. Aspects of flight behaviour

Different aspects of the flight behaviour of birds may affect the expected number of wind turbine collisions in the area of an installed or planned wind farm: the extent to which birds are present in the area (expressed as bird density or time spent within the area), the proportion of time spent in flight, the proportion of flights at the height range where collisions can take place (i.e., the rotor height range), avoidance rate and flight speed (Band et al., 2007; T. Schaub et al., 2020; Masden et al., 2021). Time spent inside the wind farm area, time spent flying, time spent at rotor height and avoidance rate can be interpreted as binary variables, distinguishing situations when birds are at risk of collision (e.g. when they are flying), and situations when they are not (e.g. when they are stationary; Figure 1.4). In the framework of the Band Collision Risk Model, the collision risk model most commonly applied in Europe (Masden & Cook, 2016), the proportions of time at risk for each variable are multiplied with each other to determine, in combination with flight speed, the expected number of rotor crossings. The number of rotor crossings is then multiplied with the collision probability per rotor crossing to obtain the expected number of collisions (Band et al., 2007). All the mentioned aspects of flight behaviour may differ importantly between species, which leads to differences in collision risk. However, note that in this conceptual framework, some aspects of flight behaviour have components of both sensitivity and exposure: for example, the proportion of time spent at rotor height depends on the birds' flight height distribution (sensitivity) and the rotor height range of the wind turbines (exposure).

1.5.1. Time spent inside wind farm

The time spent inside the wind farm area refers to the horizontal space use of birds, and may depend on a range of environmental variables such as habitat suitability (Tikkanen, Balotari-Chiebao, et al., 2018) or prey availability, territoriality, intra- and interspecific competition and the degree to which birds are displaced from the wind farm area by the presence of wind turbines (macro-scale avoidance; Marques et al., 2021). Additionally, during the breeding season, the space use of breeding birds is to a large extent determined by the nest location, in the sense that the proportion of time spent in a given area commonly decreases with increasing distance from nest (central-place foraging; Bell, 1990). The effect of all these variables is species-specific: for example, the slope of the relationship between the time spent in a given area and the distance from nest is expected to vary in line with interspecific variation in home-range size (Peery, 2000), with a steeper slope in smaller home ranges.

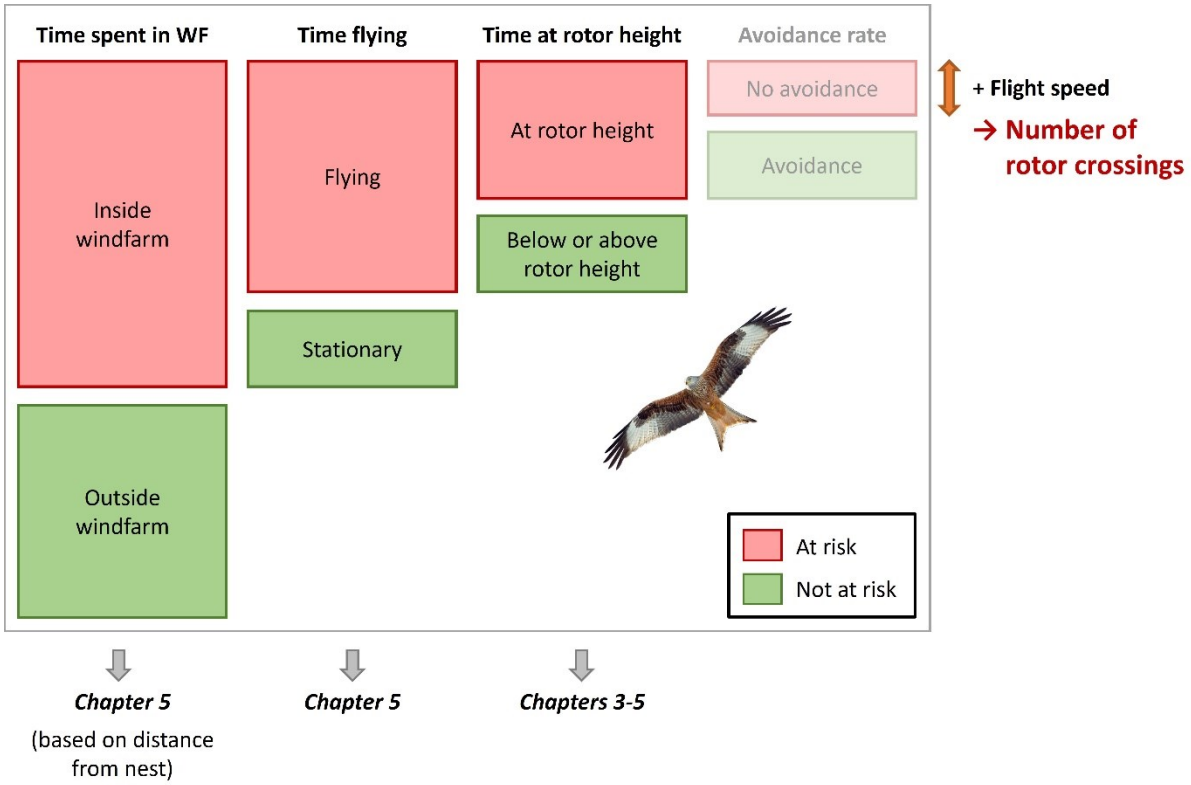

Figure 1.4: Schematic representation of the aspects of flight behaviour affecting the collision risk of birds with wind turbines. Avoidance rate refers to within-wind-farm avoidance here (meso- and micro-scale); macro-scale avoidance is included in the time spent inside the wind farm. The chapters of this PhD thesis in which the different aspects were treated are indicated at the bottom. Note that avoidance rate was not studied within this thesis. The number of rotor crossings constitutes an intermediate outcome in the Band Collision Risk Model, which is multiplied with the probability of colliding per rotor crossing to obtain the expected number of collisions (Band, Madders and Whitfield, 2007). The size of the compartments in this scheme was not based on actual data. WF = wind farm.

1.5.2. Time spent in flight

The proportion of time spent flying differs largely between bird species: globally, the extremes range from flightless species (Maderspacher, 2022) to species that fly non-stop during large parts of the year such as swifts (Liechti et al., 2013). Among birds of prey in the broad sense (i.e. Accipitriformes, Falconiformes and Strigiformes), reported values for the average time spent in flight per day vary by more than a factor of 30, with 15 min in Eagle Owls *Bubo bubo* (Grünkorn & Welcker, 2019) and 8.2 h in Montagu's Harriers *Circus pygargus* (T. Schaub et al., 2020). It can be expected that a major factor explaining these differences is foraging ecology, notably if birds forage in flight or not.

1.5.3. Time spent at rotor height

The flight height of birds is subject to large variation: it may range from just above the ground to several thousand meters above ground level (Lindström et al., 2021), amongst

others depending on the species, the purpose of the flight (e.g. foraging, displaying, commuting, migrating), the internal structure of flight paths (e.g. alternation of upwards and downwards movements in soaring-gliding flight), weather and time of day (Shamoun-Baranes et al., 2006; Bruderer et al., 2018; Pfeiffer & Meyburg, 2022). Within the possible range, birds commonly use certain heights more often than others, and the shape of the flight height distribution may vary importantly between species (Avery et al., 2011; A. Johnston et al., 2014). This results in interspecific differences in the proportion of time spent within the rotor height range of wind turbines (i.e. the height range where wind turbine collisions can occur). For example, McClure et al. (2021) reported that the proportion of flights within 50-150 m above ground level varied between 2 and 49% among species of birds of prey (in the broad sense) in southern Africa. Note that these results may be biased as the cited study relied on visual observations only (see section 1.6), but it nevertheless illustrates the possible order of magnitude of interspecific differences.

1.5.4. Wind turbine avoidance

Regarding the avoidance of wind turbines by birds, three different spatial scales are commonly distinguished: macro-scale avoidance refers to the avoidance of the wind farm area as a whole, meso-scale avoidance to the avoidance of the individual turbines inside the wind farm, and micro-scale avoidance to the avoidance of the sweeping blades (also termed "last-second evasion"; Cook et al., 2014; May, 2015). The determination of avoidance rates, especially on the meso- and micro-scale (also summarised as "within-windfarm avoidance"; Cook et al., 2014), has been notoriously difficult. Initially, avoidance rates were determined indirectly by comparing results from collision risk models assuming no avoidance with results from carcass searches from the same area (Smales et al., 2013; Vasilakis et al., 2016). However, in this way, the avoidance rate in fact acted as a model correction term, not only incorporating avoidance behaviour, but also a correction for inappropriate assumptions of the collision risk model or inaccurate input data (Cook et al., 2014). Recently, technological advancements such as high-frequency GPS-tracking and automatic camera systems have allowed to conduct behavioural studies of wind turbine avoidance on some bird species (T. Schaub et al., 2020; Santos et al., 2021; D. T. Johnston et al., 2022; Fielding et al., 2022; Mercker et al., 2023; Reichenbach et al., 2023).

1.5.5. Regional variation

In conclusion, the use of collision risk models requires knowledge on different aspects of flight behaviour, which are currently still lacking for many species. However, if data is available for a given species, information is also needed concerning the generality of results. In particular, the extent of spatial variation of flight behaviour (between sites or regions) needs to be known to assess whether results can be transferred from one region to another, where no data was collected. Many factors may lead to regional variation in flight behaviour: for example, population density could affect home range size (Efford et

al., 2016) and consequently the distance travelled from nests; prey availability could affect the time spent in flight; or regional differences in topography or weather could affect the flight height distribution in soaring birds by altering the energy landscape (Péron et al., 2017).

1.6. Methods to study flight behaviour

The flight behaviour of birds in the context of wind turbine collision risk has been studied using different techniques. Radar (Krijgsveld et al., 2009), visual observations (Hull & Muir, 2013; A. Johnston et al., 2014) and automatic cameras (Reichenbach et al., 2023) have in common that they record flight movements within a restricted spatial area regardless of the individual, although with a variable detection probability. By contrast, bird-borne tracking devices such as GPS tags register movement data of (some) individual birds regardless of the geographic location (Thaxter et al., 2015; Vasilakis et al., 2016; T. Schaub et al., 2020). GPS tags in particular allow to study bird movements and flight behaviour over extended time periods (potentially several years).

An important issue is the positional accuracy of the movement data: especially the study of flight height and meso- and micro-scale avoidance requires high accuracy both in the horizontal and vertical dimensions (few metres). In general, knowledge of the accuracy of the applied methods to assess flight behaviour is essential for a correct interpretation of results. Of the above-mentioned methods, radar has a high accuracy, but it does not directly allow for species identification, and often only flights above a certain minimum height can be tracked (Spaar & Bruderer, 1997; Krijgsveld et al., 2009; Bruderer et al., 2018). GPS positions are commonly associated with large positional error: for example, Bouten et al. (2013) reported a mean horizontal error of up to 67 m and mean vertical error of up to 26 m. However, it has been shown that reduced fix intervals increase accuracy (Bouten et al., 2013; Acácio et al., 2022). In particular, "high-frequency GPS tracking" with fix intervals of only a few seconds is a promising technique, as the GPS module remains turned on between fixes ("continuous mode"), which may substantially improve the positional accuracy (Bouten et al., 2013; Thaxter et al., 2018; T. Schaub et al., 2020). Having said that, a comprehensive analysis of the positional accuracy obtained using continuous-mode GPS tracking in different tag models is unavailable to date.

Another way to obtain more accurate height data from bird-borne tags is the use of air pressure loggers ("barometric altimetry"), which may be integrated in GPS tags. This potentially provides very accurate height data (Lato et al., 2022), but the accuracy largely depends on the possibilities to calibrate the barometric height data with reference pressure and weather data (Péron et al., 2020; D. T. Johnston et al., 2023).

1.7. Thesis outline

This PhD thesis is a comparative study of the flight behaviour of birds of prey in the context of wind turbine collision risk. Using GPS tracking, the flight behaviour in the breeding area was studied in six raptor species, i.e. Montagu's Harrier, Hen Harrier *Circus cyaneus*, Marsh Harrier *C. aeruginosus*, Common Buzzard *Buteo buteo*, Red Kite and Short-toed Eagle *Circaetus gallicus*. In a collaborative effort, 377 individual birds were tracked in 15 study areas in six European countries. A particular focus was laid on flight height, to which chapters 3 and 4 were dedicated and which also was a component of chapter 5 (Figure 1.4). Throughout the thesis, differences between study areas were examined to obtain an indication of regional variation, whose extent determines if the results can be transferred between areas.

General information on the study species, study sites and data collection was compiled in **chapter 2**. In **chapter 3**, the accuracy of height data from GPS tags ("vertical accuracy") was studied. More specifically, we assessed two methods which potentially increase vertical accuracy, i.e. high-frequency GPS tracking with fix intervals of 2-3 s (GPS remaining turned on between fixes), or barometric altimetry using air pressure loggers integrated in GPS tags. This methodological chapter served as a foundation for the following chapters.

Building on the results of chapter 3, the flight height distributions of the six study species were studied using high-frequency GPS tracking, providing highest vertical accuracy, in **chapter 4**. These flight height distributions served as a basis to assess the species-specific effect of wind turbine dimensions on collision risk, using the framework of the Band Collision Risk Model. As parameters of wind turbine size, we considered ground clearance and rotor diameter which together determine the height range swept by the wind turbine rotor. Additionally, we accounted for the increase of power capacity with increasing rotor diameter, which allowed to determine if collision risk for a given target of total power capacity could be minimised using few turbines with large rotor diameter, or many turbines with small diameter.

In **chapter 5**, we took a broader perspective on three of the aspects of flight behaviour affecting collision risk, i.e. 1) the time spent in flight, 2) the proportion of flights at collision risk height and 3) the distance travelled from the nest location, and the interplay between them. The distance from nest was considered as it represents one of the factors influencing the time spent within a wind farm for breeding birds (see section 1.5). The objectives of this chapter were to assess the species-specific sensitivity to wind turbines collisions based on flight behaviour and to improve the understanding of how inter-specific differences in sensitivity arise. The results on distance from nest could serve to guide the placement of wind turbines relative to known nest sites for minimising collision risk.

2. General methods

2.1. Collaborations

This PhD thesis was based on GPS-tracking data collected in 15 study areas in France, Luxembourg, Belgium, the Netherlands, Germany and Sweden (Figure 2.1). The compilation of the dataset was possible thanks to a large number of collaboration partners which organised the local GPS-tracking projects, did fieldwork and/or accepted to contribute the data to this study (Table 2.1). Some of the tracking projects were set up specifically for this thesis (Montagu's Harrier Aumelas, Common Buzzard Groningen, Red Kite Haute-Marne and Alsace), while others had other primary research questions related to habitat use, migratory behaviour, dispersal or mortality (Klaassen, Schlaich, et al., 2014; Schlaich et al., 2015, 2017; van Rijn & van Manen, 2019; Vansteelant et al., 2020). The period of data collection varied between the tracking projects: most started after 2016, while in Groningen (NL), Montagu's Harrier had been tracked already since 2009 (Hen Harrier and Marsh Harrier since 2012; Table A4.1.2, Table A5.1.1).

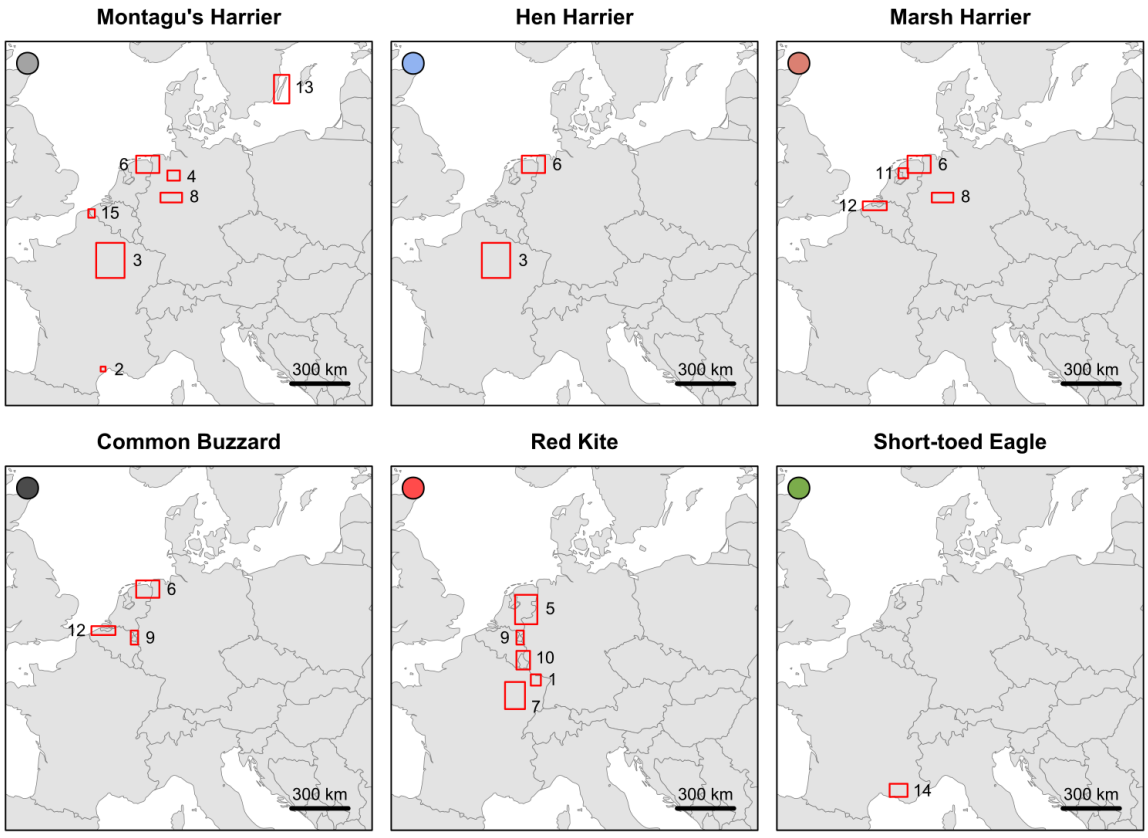

Figure 2.1: Location of the study areas within Europe per species. See Table 2.1 for study area names. Map created using the *R* package *maps* (Brownrigg et al., 2018).

Table 2.1: Overview of the main collaboration partners for the individual GPS-tracking projects from which data were included in this PhD thesis, and my personal implication in data collection. See the acknowledgements sections in chapters 3-5 for details on involved persons and organisations, including funding. Numbers in square brackets correspond to study area IDs in Figure 2.1. MoH = Montagu's Harrier, HH = Hen Harrier, MaH = Marsh Harrier, CB = Common Buzzard, RK = Red Kite, STE = Short-toed Eagle. DMHF = Dutch Montagu's Harrier Foundation. TD = tag deployment, TS = tag settings, DD = data download, NM = nest monitoring.

Study area	Species	Main collaboration partners	Implication T. Schaub
[1] Alsace (FR)	RK	LPO Alsace, Christelle Scheid, ENGIE Green, CNR	TD, TS
[2] Aumelas (FR)	MoH	LPO Occitanie, Natural England	TD, TS
[3] Champagne (FR)	MoH, HH	Groupe d'Études et de Protection des Busards, Natural England	TD, TS
[4] Diepholz (DE)	MoH	BUND Diepholzer Moorniederung, DMHF	TD, TS
[5] East NL & [9] Limburg (NL)	RK	"Working group Red Kites NL", Stef van Rijn, DMHF	TS
[6] Groningen (NL/DE)	MoH, HH, MaH, CB	DMHF, Carl von Ossietzky University of Oldenburg, University of Amsterdam, Collectief Groningen West	TD, TS, DD, NM
[7] Haute-Marne (FR)	RK	LPO Champagne-Ardenne, LOANA, ENGIE Green, CNR	TD, TS
[8] Hellwegbörde (DE)	MoH, MaH	Arbeitsgemeinschaft Biologischer Umweltschutz, DMHF	TD, TS
[9] Limburg (NL)	CB	Müskens Fauna	TS
[10] Luxembourg (LU)	RK	natur&ëmwelt, SICONA, TB Raab / LIFE Eurokite, CSD Ingénieurs, Stef van Rijn	TS
[11] Noordoostpolder (NL)	MaH	Wageningen Environmental Research, Werkgroep Roofvogels Noordoostpolder, DMHF	TS
[12] NW Flanders & [15] SW Flanders (BE)	MaH, CB, MoH	Research Institute for Nature and Forest (INBO)	TS
[13] Öland (SE)	MoH	Kalmar County Administrative Board, Linnaeus University, DMHF	TD, TS
[14] Provence (FR)	STE	LPO Provence-Alpes-Côte d'Azur, Réseau Circaète Bouches-du-Rhône	TS

2.2. Data collection

In total, the analyses comprised tracking data from 361 individual GPS tags and 377 individual birds (some tags successively deployed on several individuals): 103 Montagu's Harriers, 100 Hen Harriers, 35 Marsh Harriers, 33 Common Buzzards, 104 Red Kites and 2 Short-toed Eagles. Different data subsets, involving different numbers of individuals, were used for the three research chapters (Table 2.2).

Table 2.2: Data subsets used for the analyses of chapters 3-5. MoH = Montagu's Harrier, HH = Hen Harrier, MaH = Marsh Harrier, CB = Common Buzzard, RK = Red Kite, STE = Short-toed Eagle.

Chapter	Species	N areas	N ind.	Data selection
3 (Accuracy of height data)	MoH, HH, MaH, RK	4	204	
4 (Flight height and wind turbine dimensions)	MoH, HH, MaH, CB, RK, STE	15	275	High-frequency tracking data only
5 (Sensitivity to wind turbine collisions)	MoH, HH, MaH, CB, RK, STE	15	280	Adult breeding birds only

The majority of individuals were captured as adults (n = 273) near their nest, mostly using a mist net with a stuffed or live predator, or a stuffed conspecific, as decoy (Figure 2.2a). For harriers, also nest-traps, catching poles or a whoosh-net with carrion as bait were used. For the captures, care was taken to minimise disturbance and prevent negative effects on the breeding process. However, two adult Hen Harriers (one male, one female) deserted their nest after capture (but note that the chicks did nevertheless fledge in both cases with the support of the remaining adult). One adult STE was tagged before being released from a bird rescue centre after an injury. The remaining 104 individuals (54 Hen Harriers, 4 Marsh Harriers and 46 Red Kites) were tagged as nestlings shortly before fledging.

Twelve different models of solar-powered GPS tags from the manufacturers *Milsar*, *Ornitela* and *UvA-BiTS* (Bouten et al., 2013) were used (see Table A5.1.1 for a list of tag models). The tags were mounted as backpacks (Figure 0.1; Figure 2.2b; Figure 2.6) using a thoracic cross-strap harness (Anderson et al., 2020) made from Teflon ribbon. Tags weighed 9.7-26.3 g (1.4-6.5% of individual body weight; median: 3.1%), and 12.2-30.4 g including harness (1.6-7.7% of body weight; median: 3.8%). There were no indications of pronounced adverse tag effects: the tagged birds fulfilled their annual cycle (including migrations) and reproduced as expected. Information on possible more subtle tag effects on survival or flight performance (Longarini et al., 2023) are unavailable for the study species so far (but note that Sergio et al., 2015 showed a lack of tag effects on survival in Black Kites *Milvus migrans*).

Figure 2.2: a) A captured Montagu's Harrier is taken out of a mistnet (with a stuffed Goshawk as decoy) in a cereal field (Groningen/NL). **b**) A GPS tag is deployed on an adult Red Kite (Haute-Marne/FR). **c**) The wing length of a nestling Montagu's Harrier is measured (Groningen/NL). Photos: G. Sterk, C. De Zutter, G. Joling.

The tags transferred the recorded data remotely, either using the GSM network (*Milsar*, *Ornitela*) or local antennas (*Milsar*, *UvA-BiTS*). In the same remote way, the tags were monitored closely (mostly on a daily basis; somewhat less frequently in winter) to detect mortality events and to adjust the tag settings (e.g. GPS fix interval, GSM connection interval) according to the battery voltage. This manual adjustment of tag settings was essential to maximise the amount of high-frequency data collected (i.e. data collected with a GPS fix interval of 2-3 seconds; see chapters 3 and 4 for details), while unlinking the collection of this particular type of data from the immediate battery charging conditions (as opposed to automatic approaches based on voltage thresholds). See the methods sections of chapter 3-5 for details on tag settings.

To be able to link the flight and ranging behaviour of the tagged birds to their breeding status, information on breeding attempts (nest location, timing and breeding success) were collected in the field in most cases. This included field observations (e.g. prey passes between male and female, nest visits, fledged young in the vicinity of the nest) and/or data collected during the ringing of nestlings. On the basis of the nestlings' wing length (Figure 2.2), their age could be determined and consequently the dates of hatching and egg-laying.

Additionally, in females, the tri-axial accelerometer data collected by the GPS tags (Bouten et al., 2013) allowed to determine the dates of the onset of egg-laying and nest failure with relatively high accuracy (± 1-2 days), also in the absence of field observations. Moreover, for some male Montagu's, Hen and Marsh Harriers for which field observations were lacking or incomplete, the GPS tracks were used to infer breeding status and breeding success, as the location of an active nest is normally easily identifiable in the position data in these species.

2.3. Study species

The six study species (Figure 2.3) are medium-sized diurnal birds of prey (family Accipitridae), with wing span between 1.0 (Montagu's and Hen Harrier) and 1.9 m (Short-toed Eagle; Ferguson-Lees & Christie, 2001) and body weight between 230 g (Montagu's Harrier male) and 2.0 kg (Short-toed Eagle female; own unpublished data). Common Buzzard, Red Kite and Short-toed Eagle are known to predominantly use soaring-gliding flight, while the three species of harriers are considered facultative soaring birds, using both active flight (e.g. for foraging) and soaring-gliding flight.

All six species breed within the study areas. The tagged Common Buzzards were year-round residents, while all Montagu's Harriers, Marsh Harriers and Short-toed Eagles left the study areas outside the breeding season to winter in Africa. Also most tagged Hen Harriers and Red Kites (partial migrants) wintered outside the study areas in France or Spain. Dispersal of juvenile and adult birds out of the study areas occurred in Montagu's Harriers and Hen Harriers (e.g. Albert et al., 2022), but these data were excluded from the analyses by restricting the dataset to the defined study areas (Figure 2.1).

The six species have in common that they are associated with open habitats for foraging. Montagu's, Hen and Marsh Harriers nest on the ground in agricultural fields, reedbeds, shrubland or woodland clearings, while Common Buzzards, Red Kites and Short-toed Eagles nest in trees, generally close to the woodland edge (del Hoyo et al., 1994).

Wind turbine collisions have been documented in all six species (Dürr, 2023). Red Kite has received particular attention in the wind energy context in Europe as it is at the same time endemic to the continent and perceived to be one of the most collision-prone bird species (M. Schaub, 2012; Bellebaum et al., 2013; Dürr, 2023).

Figure 2.3: Examples of GPS tagged individuals while captured for tag deployment. From left to right and top to bottom: Montagu's Harrier (male; photo), Hen Harrier (male), Marsh Harrier (male), Common Buzzard (female), Red Kite (male), Short-toed Eagle (female). Photos: S. de Vries, M. Millet-Trebout, M. Bunzel-Drüke, S. de Vries, T. Schaub, A. Millon.

2.4. Study areas

Overall, the study areas were dominated by agricultural habitat with a varying proportion of woodland. In the two Mediterranean study areas Aumelas and Provence (FR) and on Öland (SE), (semi-)natural vegetation had a high share (low garrigue shrubs and alvar grassland). The topography varied from flat polder landscapes to hilly terrain and low mountains (Figure 2.4, Table 2.3).

Figure 2.4: Impressions from the study areas. From left to right and top to bottom: flat polder landscape with large-scale arable land in Groningen (NL); rolling hills with large-scale arable land in Champagne (FR); plateau with semi-natural garrigue vegetation in Aumelas (FR); hilly landscape with small-scale pastures in Alsace (FR). Photos: T. Schaub.

Table 2.3: Overview of landscape characteristics per study area. IDs of study areas correspond to numbers in Figure 2.1. Elevation characteristics were based on the GPS positions of the tagged birds (data from chapter 5). Species abbreviations: MoH = Montagu's Harrier, HH = Hen Harrier, MaH = Marsh Harrier, CB = Common Buzzard, RK = Red Kite, STE = Short-toed Eagle.

				Elevation a.m.s.l. (m)			
ID	**Study area**	**Species**	**Topography, vegetation and land use**	**Median**	**Min.**	**Max.**	**SD**
1	Alsace (FR/DE)	RK	Hilly; arable land and pastures with forest patches	263	193	397	41.3
2	Aumelas (FR)	MoH	Plateaus with low semi-natural garrigue vegetation, small-scale agriculture in lower parts	235	17	341	56.2
3	Champagne (FR)	MoH, HH	Hilly; large-scale arable land with forest patches	134	53	366	44.7
4	Diepholz (DE)	MoH	Predominantly flat; large-scale arable land with forest patches	45	26	84	6.3
5	East NL (NL/DE)	RK	Predominantly flat; agriculture with forest patches	9	-3	81	17.4
6	Groningen (NL/DE)	MoH, HH, MaH, CB	Flat polder landscape; large-scale arable land	-3	-11	14	1.9
7	Haute-Marne (FR)	RK	Plateaus with large-scale arable land, pastures in lower parts; forest patches	381	222	516	39.4
8	Hellwegbörde (DE)	MoH, MaH	Hilly; large-scale arable land with forest patches	103	60	260	29.6
9	Limburg (NL/BE/DE)	CB, RK	Hilly; agriculture with forest patches	143	24	326	46.4
10	Luxembourg (LU/BE/DE)	RK	Low mountains; agriculture and forests	338	136	543	88.4
11	Noordoostpolder (NL)	MaH	Flat polder landscape; large-scale arable land	-5	-10	14	1.5
12	NW Flanders (BE/NL)	MaH, CB	Flat polder landscape; large-scale arable land and industrial harbour areas	0	-23	47	2.9
13	Öland (SE)	MoH	Predominantly flat; agriculture, natural alvar grassland, forest patches	8	-2	38	5.6
14	Provence (FR)	STE	Low mountains with garrigue vegetation and forest, flat river valley with agriculture	131	42	868	80.0
15	SW Flanders (BE/FR)	MoH	Predominantly flat; large-scale agriculture	-2	-7	46	8.2

2.5. Exposure to wind turbines

The degree to which the tagged birds were exposed to wind turbines within their home ranges varied importantly between study areas and between individuals (Figure 2.5).

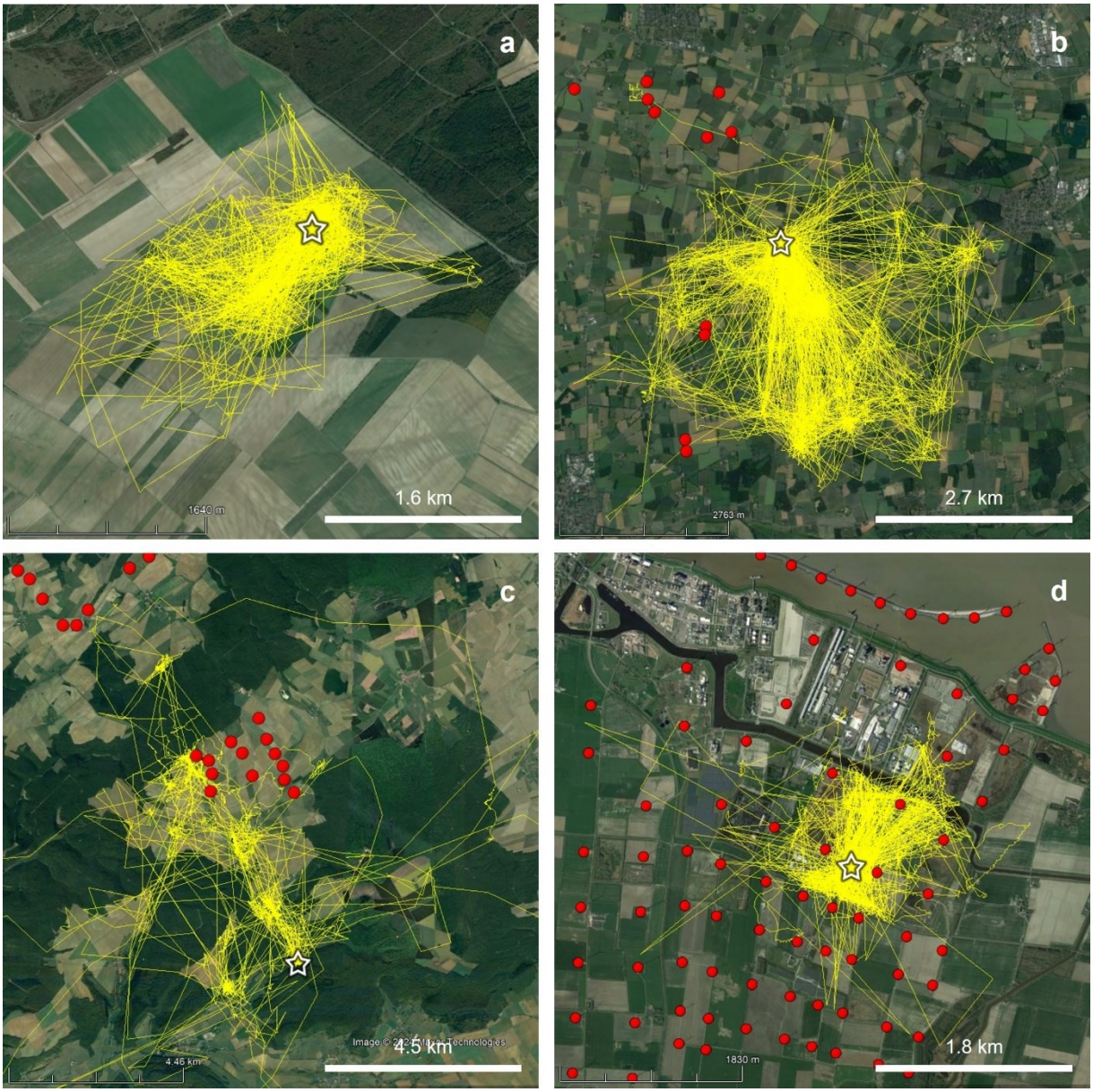

Figure 2.5: Examples of home ranges of GPS-tagged birds from this thesis showing different degrees of exposure to wind turbines (red points; stars: nest locations; yellow lines connect subsequent GPS positions;). **a**) Female Hen Harrier (Champagne/FR; nest at 6.0 km of nearest wind turbine). **b**) Male Marsh Harrier (Hellwegbörde/DE; nest at 1.9 km of wind turbine). **c**) Female Red Kite (Haute-Marne/FR; nest at 4.4 km of wind turbine). **d**) Male Common Buzzard (Groningen/NL; nest at 270 m of wind turbine). In all panels, tracking data from one month (July) are shown (incidental trips outside the map boundaries omitted in **c**). Note difference in scale. Map: *Google Earth*.

In some study areas, the tagged birds did not encounter wind turbines at all (e.g. Common Buzzards Limburg). As the other extreme, the dataset comprised some individual Montagu's Harriers, Hen Harriers, Marsh Harriers, Common Buzzards and Red Kites breeding at close vicinity of wind turbines, with distances between the nest and the nearest wind turbine below 300 m. In exceptional cases, the home ranges completely overlapped with wind farms (Common Buzzards Groningen; Figure 2.5d). Note that in this thesis, the birds' flight and ranging behaviour was studied irrespective of the distance to wind turbines, representing a first step in the assessment of wind turbine collision risk (see section 1.5). The direct interactions of the tagged birds from this dataset with wind turbines (avoidance behaviour at different spatial scales) could be studied in the future.

Figure 2.6: A GPS-tagged Red Kite (study area Luxembourg). Photo: S. van Rijn.

3. How to improve the accuracy of height data from bird tracking devices? An assessment of high-frequency GPS tracking and barometric altimetry in field conditions

Tonio Schaub, Alexandre Millon, Caroline de Zutter, Ralph Buij, Joël Chadœuf, Simon Lee, Aymeric Mionnet & Raymond H. G. Klaassen

Published in Animal Biotelemetry 11: 31 (2023)

3.1. Abstract

Background In the context of rapid development of wind energy infrastructure, information on the flight height of birds is vital to assess their collision risk with wind turbines. GPS tags potentially represent a powerful tool to collect flight height data, yet GPS positions are associated with substantial vertical error. Here, we assessed to what extent high-frequency GPS tracking with fix intervals of 2-3 s (GPS remaining turned on between fixes), or barometric altimetry using air pressure loggers integrated in GPS tags, improved the accuracy of height data compared to standard low-frequency GPS tracking (fix interval ≥ 5 min; GPS turned off between fixes).

Results Using data from 10 GPS tag models from three manufacturers in a field setting (194 tags deployed on free-living raptors), we estimated vertical accuracy based on periods when the birds were stationary on the ground (true height above ground was approximately zero), and the difference between GPS and barometric height in flight. In GPS height data, vertical accuracy was mainly driven by noise (little bias), while in barometric data, it was mostly affected by bias (little noise). In high-frequency GPS data, vertical accuracy was improved compared to low-frequency data in each tag model (mean absolute error (AE) reduced by 72% on average; range of mean AE 2-7 vs. 7-30 m). In barometric data, vertical accuracy did not differ between high- and low-frequency modes, with a bias of -15 to -5 m and mean AE of 7-15 m in stationary positions. However, the median difference between GPS and barometric data was smaller in flight positions than in stationary positions, suggesting that the bias in barometric height data was smaller in flight. Finally, simulations showed that the remaining vertical error in barometric and high-frequency GPS data had little effect on flight height distributions and the proportion of positions within the collision risk height range, as opposed to the extensive noise found in low-frequency GPS data in some tag models.

Conclusions Barometric altimetry may provide more accurate height data than standard low-frequency GPS tracking, but it involves the risk of a systematic error. Currently, high-frequency GPS tracking provides highest vertical accuracy and may thus substantially advance the study of wind turbine collision risk in birds.

3.2. Background

Flying animals have been shown to suffer mortality from collision with vertical human infrastructures (De Lucas & Perrow, 2017; Thaxter et al., 2017). In particular, collisions of birds with wind turbines can have substantial negative population impacts (Carrete et al., 2009; Bellebaum et al., 2013). This problem is expected to increase in the near future as the number of wind turbines is going to grow worldwide to fulfil the targets for renewable energy production. Therefore, there is an urgent need to quantify collision risk and identify effective mitigation measures reducing the number of casualties. However, this is currently hampered by a lack of accurate data on flight height. These are a prerequisite to reliably quantify the probability of flying within the collision risk height range and the avoidance of wind turbines in birds, two crucial components of collision risk models (Chamberlain et al., 2006; Masden et al., 2021).

Earlier methods to study flight height of birds have been relatively inaccurate (visual observations; Hull & Muir, 2013; A. Johnston et al., 2014) or provided only short sequences of accurate data without bird determination at the species level (radar; Fijn et al., 2015; Aschwanden et al., 2018). Individual-based tracking by animal-borne GPS tracking devices represents a promising source of flight height data over extended periods (Ross-Smith et al., 2016; Pfeiffer & Meyburg, 2022). However, GPS positions are associated with inherent horizontal and vertical error. The vertical error can be substantial (mean absolute error up to 30 m; Bouten et al., 2013) and potentially bias the outcomes of collision risk analyses (Péron et al., 2020). Methods have been proposed to account for the error a posteriori within a modelling framework (Ross-Smith et al., 2016; Péron et al., 2020). However, these state-space models require high levels of statistical expertise and computational capacities, and have therefore been little applied until now. Moreover, large errors increase the uncertainty around model outcomes, and particular behavioural aspects like the avoidance of wind turbines by birds require a high level of accuracy for individual data points. For these reasons, it remains critical to increase the vertical accuracy in the raw tracking data.

One possible approach to improve the three-dimensional accuracy of GPS positions is to increase the GPS fix frequency (Bouten et al., 2013; Acácio et al., 2022). The highest accuracy is expected for positions obtained when the GPS module does not turn off between successive fixes ("continuous GPS mode"). This occurs when fixes are collected at a high frequency, typically when the time interval between successive GPS fixes is below 5-20 s, depending on the GPS tag model. In this scenario, on average more satellites are used per fix compared to standard low-frequency GPS data collection, where the GPS module is turned off after every fix ("discrete GPS mode"). However, the extent of the accuracy improvement in the high-frequency mode and its consistency across different tag models remains to be demonstrated. Moreover, a downside of high-frequency GPS tracking is that it is energy demanding, usually depleting the batteries of GPS tags within hours to days (depending on battery size and solar charging conditions).

A second possibility to increase the accuracy of flight height data is the use of barometers (air pressure sensors), which are increasingly integrated into GPS tags. These sensors

operate independently from the GPS regarding the height measurement (but still depend on the GPS to determine the horizontal position, necessary to determine the height above ground). The measured air pressure is combined with local weather data in the barometric height formula to determine height (Heuck, Sommerhage, et al., 2019; Péron et al., 2020). Advantages of barometric altimetry are that it is energy-efficient, barely increasing battery demand compared to GPS fixes without pressure measurement, and that a priori accuracy is not related to sampling frequency. However, barometers need to be calibrated and the barometric height calculation requires accurate local weather data. Moreover, the assumptions of the formula regarding the stratification of the atmosphere are not always met in practice (Péron et al., 2020). Therefore, it is unclear how barometric altimetry performs under field conditions.

Here, we performed an extensive field test of these two methods to increase the accuracy in flight height data in comparison to standard low-frequency GPS height data. Our study built on a GPS tracking data set of ca. 11 million positions obtained from 194 tags of 10 models from three different manufacturers deployed on four raptor species in France and the Netherlands. Our main approach of quantifying vertical accuracy was based on stationary periods when the birds were positioned on the ground, providing a known true height above ground (i.e. approximately zero). First, we analysed the deviation of GPS and barometric height from true height for these stationary periods and assessed the consistency of the results among GPS tag models. Secondly, to extend the assessment from stationary periods to flight periods, we quantified the deviation between GPS and barometric height for both stationary and flight periods, providing an indirect measure of accuracy. Thirdly, we assessed the credibility of height profiles from high-frequency sampling and identify recurrent error patterns. Fourthly, we quantified the consequences of different levels of error for practical conservation-related questions, using the proportion of positions within the height range of wind turbine rotors as an example. Finally, we provided guidance on how to improve the vertical accuracy of tracking data from GPS tags against the background of the limitations of the different methods.

3.3. Methods

3.3.1. Data collection

We used data from 194 solar-powered GPS tags which were deployed between 2009 and 2022 on 204 individuals of four raptor species: Montagu's Harrier *Circus pygargus*, Hen Harrier *C. cyaneus*, Marsh Harrier *C. aeruginosus* and Red Kite *Milvus milvus* (Appendix 3.1: Table A3.1.1). Birds were captured during the breeding season as adults (n = 140) or as nestlings (n = 64) close to or on the nest in four study areas in France and the Netherlands (Champagne, Grand Est, Flevoland and Groningen; Figure A3.1.1).

In the Champagne, Flevoland and Groningen areas, the landscape is open and dominated by intensive arable farming, while in the Grand Est area, it is composed of a mixture

of forests, pastures and arable fields. The Flevoland and Groningen areas are flat (standard deviation [SD] of elevation above sea level [a.s.l.]: 1.7 and 1.3 m; mean: -3.1 m and -4.5 m, respectively), whereas the terrain in Champagne and especially in Grand Est is hillier (SD: 33.3 and 63.5 m; mean: 144.0 m and 311.2 m a.s.l.).

Ten different tag models from three manufacturers (*Milsar*, *Ornitela*, *UvA-BiTS*) were applied (Table A3.1.1), three of which included a barometric sensor. The *Milsar* and *Ornitela* tags transferred the recorded data remotely via the GSM network, whereas the data from *UvA-BiTS* tags were downloaded using a local antenna system (Bouten et al., 2013). GPS tags were mounted as backpacks using thoracic x-strap harnesses (Anderson et al., 2020) made from Teflon ribbon. Tags weighed 9.7-24.3 g according to the species, representing on average 3.2% of individual body weight (median 2.9%; SD 1.1%; range 1.7-6.5%; n = 207 deployments). There were no indications of adverse tag effects; the tagged birds fulfilled their annual cycle and reproduced as expected.

In spring and summer, 5 min were used as GPS fix intervals as a basic setting during daytime, except for Hen Harriers in Champagne (15 min). During night, the interval was set to 1-4 h. For autumn and winter, periods of bad weather, and incubation periods in females, the interval was increased to 1-12 h to preserve battery voltage. In addition, high-frequency data were collected using an interval of 3 s in *Ornitela* and *UvA-BiTS* tags and 1 s in *Milsar* tags. With the set interval of 1 s, *Milsar* tags collected GPS fixes at intervals of 2-3 s in practice. These GPS fix intervals were below the manufacturer-specific time thresholds for the continuous GPS mode (< 7 s for *Ornitela*, < 8 s for Milsar, < 16 s for *UvA-BiTS*). High-frequency data were collected mostly during hourly blocks (1-2 hours per day), and to a lesser extent using geofences defined around areas of interest (e.g. wind farms, fields with agri-environmental schemes). High- and low-frequency data were similarly distributed across years within tag models (Appendix 3.1: Figure A3.1.2). In tags with barometric sensor, air pressure measurements were taken alongside every GPS fix. We distinguished four methods of height data collection, i.e. low-frequency GPS (discrete mode), high-frequency GPS (continuous mode), low-frequency barometric and high-frequency barometric.

After removing positions outside of the defined study areas, the dataset comprised 10,777,644 positions with GPS height (2,881,769 from low-frequency and 7,895,875 from high-frequency sampling) and 3,610,374 with barometric height (740,306 from low-frequency and 2,870,068 from high-frequency sampling; Table A3.1.1). The number of height data varied greatly between tags (range for GPS: 111 to 614,099 positions per tag; median: 21,574; mean: 55,555; range for barometric: 3,762 to 388,140; median: 55,086; mean: 97,578), mainly as a consequence of variation in the length of the data collection period (range of the number of days with data per tag: 6-971; median: 125 d; mean: 196.6 d). For Montagu's and Marsh Harriers (trans-Saharan migrants), all individuals left the study areas in the non-breeding season, thus the dataset included only data from spring and summer. Also for Hen Harriers and Red Kites (partial migrants), the majority of individuals left the study areas in winter and for the remaining individuals fewer data could be collected in autumn and winter due to low battery voltage.

3.3.2. Data processing

All data processing and analyses were performed in *R* 4.0.3 (R Core Team, 2020). We differentiated between stationary and flight positions based on the instantaneous GPS ground speed which is recorded alongside every GPS position. The distribution of speed values typically shows two modes (one representing stationary and one representing flight positions), and we used the antimode between the two modes as threshold (Kölzsch, 2022; Appendix 3.1). The speed threshold was determined for each combination of species and tag manufacturer, separately for low- and high-frequency data (1.81-3.83 m s^{-1} and 0.85-1.86 m s^{-1} for low- and high-frequency data, respectively).

The GPS height data obtained from the tags was height above mean sea level (termed height a.s.l. hereafter), i.e. height above geoid. However, when comparing height data from different sources, it is important to verify that the same geoid model is used and if not, apply corrections (Péron et al., 2020). For *Milsar* and *UvA-BiTS* tags, the manufacturers indicated that EGM96 was used. For the *Ornitela* tags, it was possible to also obtain the height above ellipsoid, i.e. the raw height data above the WGS84 ellipsoid initially determined by the GPS module before application of a geoid model. This lead us to notice that the geoid model applied in these tags was biased compared to EGM96 in some study areas. Therefore, to obtain corrected height a.s.l. data, we used the height above ellipsoid data and applied the EGM96 geoid model with resolution of 0.25° (Agisoft, n.d.). By this correction, the height a.s.l. was offset by a mean of +3.5 m for Flevoland, +4.4 m for Groningen, 0.0 m for Champagne and -1.2 m for Grand Est. For *Milsar* and *UvA-BiTS*, it was not possible to obtain the height above ellipsoid data to apply the same test.

Furthermore, in *Milsar* tags, the GPS height data were internally and irreversibly truncated at sea level. Therefore, the lowest recorded height above ground level (termed height a.g.l. hereafter; see below) in *Milsar* tags was -197.5 m, whereas much lower values were obtained from the other tag models (Appendix 3.2: Table A3.2.1), likely leading to an underestimation of the vertical error in *Milsar* data.

The calculation of barometric height based on the pressure measurements of the tags was performed using the barometric formula describing the relationship of air pressure with height above a reference level under different meteorological conditions (ISO, 1975): $z = -\frac{T_0}{L} * (1 - \left(\frac{P}{P_0}\right)^{-\frac{LR_0}{g}})$, where z is the height above the reference level, T_0 is the temperature at reference height, L is the temperature lapse rate, P is the pressure at height z (measured by the tag), P_0 is the pressure at reference height, R_0 is the specific gas constant (287.05 J K^{-1} kg^{-1}) and g is the standard acceleration of free fall (9.81 m s^{-1}). We obtained data on T_0, L and P_0 from the global weather model ECMWF ERA5 with a temporal resolution of 1 h and a spatial resolution of 0.25° (Hersbach et al., 2018a, 2018b). The tracking data were annotated with ERA5 data using the Environmental-Data Automated Track Annotation System (Env-Data) provided by Movebank (Dodge et al., 2013), which included an interpolation of the ERA5 data to the timestamp and horizontal position of each GPS fix. The resulting height above the ERA5 model surface was transformed into height a.s.l. (see Appendix 3.1 for details).

Both for GPS and barometric height, we transformed height a.s.l. into height a.g.l. by applying the European Digital Elevation Model (EU-DEM, v1.1) with a resolution of 25 m (EEA, 2017). EU-DEM is based on the EEG2008 geoid, but the difference between EEG2008 and EGM96 (used in the GPS data and the weather model) was negligible for our study areas (mean absolute difference 0.12 m, maximum difference 0.65 m).

3.3.3. Identification of stationary positions on the ground

Our assessment of vertical accuracy was based on positions when the birds were stationary on the ground, as for these positions the true height a.g.l. was known. Note that in fact, the true height a.g.l. was not zero, but the height of the back of the bird where the tag was attached. However, as in our study species this difference was small (15-40 cm), we applied zero as true height. To identify these "ground positions", two different approaches were adopted. For the three species of harriers which are known to sit on the ground most of the time when being stationary, and for which the landscape in the study areas was relatively homogeneous with low occurrence of vertical structures (large-scale open agricultural areas), we used the digital national topographic maps *BD TOPO* for France (IGN, n.d.) and *TOP10NL* for the Netherlands (PDOK, n.d.). Positions at > 50 m from vertical structures (trees, hedgerows, buildings, electric pylons) were classified as ground positions (see Appendix 3.1 for details). The proportion of ground positions amongst stationary positions varied between 82.9 and 99.8% for the combinations of species and study area.

Contrary to the harriers, Red Kites are known to perch on trees or other vertical structures most of the time when stationary. Moreover, the landscape in the Red Kite study area was more heterogeneous with more vertical structures (more interspersed trees, hedgerows and forests; more field margins with fence poles), which were only partially included in the digital national geographic maps. Therefore, we applied a more restrictive approach by classifying the perching habitat manually by visual inspection of satellite images. We identified continuous stationary periods during daytime consisting of ≥ 2 subsequent positions in low-frequency and 20 positions in high-frequency data, with < 50 m between subsequent positions. Periods were defined as ground periods if all positions were on agricultural fields and if the mean coordinates were > 20 m away from any vertical structures or field margins visible in the satellite image. (Note that the more restrictive classification approach allowed to reduce the threshold distance compared to the harrier case.) Out of the 2,400 inspected periods (random sample), 15.7% were classified as ground periods, comprising 31,948 individual positions (8.8% of the classified positions).

3.3.4. Estimation of vertical accuracy and comparison between methods and tag models

Conceptually, we considered the error in the height data from stationary position on the ground on three levels, i.e. trueness, precision and accuracy (OIML, 2012). Trueness

refers to the deviation of the average of the measured values from a reference value (bias or systematic error), which we described using the deviation of the mean, and the median, from the true height, i.e. zero. Precision refers to the deviation of individual measurements from the average (noise or random error), which we described using the mean, median and 95% quantile of absolute error (AE) and the root mean square error (RMSE), all with the median as reference. Accuracy refers to the combination of precision and trueness, i.e. the deviation of individual measurements from the true value, which we described using the same parameters as for precision, but with the true height, i.e. zero, as reference.

To reduce temporal auto-correlation in the high-frequency data for the statistical analyses, we subsampled the tracking data to a minimum interval of 5 min. As positions at the beginning of high-frequency blocks and short stationary periods were overrepresented in the subsampled data and these had higher than average vertical error, we removed the first minute of every high-frequency block and stationary periods consisting of < 5 subsequent positions before subsampling to prevent bias.

To statistically compare vertical accuracy on the three levels across methods and tag models, we applied hierarchical bootstrapping (Ren et al., 2010). We chose this non-parametric method to estimate confidence intervals because the distributions of the height data had very long tails (see Results), which prevented the use of parametric methods like linear models (residual distributions remained unsatisfactory after log or Box-Cox-transformation of the response variable). For each of the 26 combinations of method and tag model, we resampled at the first hierarchical level (individual tags) with replacement, and then without replacement at the second hierarchical level (individual height data within each resampled tag) following Ren et al. (2010). In this way, 1,000 bootstrap replicates were constructed for each combination for six parameters of interest, i.e. mean and median error with true height as reference (trueness), mean and median absolute error with median height as reference (precision), and mean and median absolute error with true height as reference (accuracy). We used the mean and the range between the 2.5% and 97.5% quantiles across the replicates as estimate and confidence interval. We considered differences between groups to be significant when the confidence intervals did not overlap.

3.3.5. Visual inspections of high-frequency tracking data

To assess the credibility of height profiles in high-frequency tracks across stationary and flight positions, and to identify potential error patterns, we carried out visual inspections of individual high-frequency tracks. A graph of height a.g.l. over time was produced for every track of at least 100 consecutive high-frequency positions (n = 9,993 high-frequency tracks).

3.3.6. Effect of error on flight height distributions and proportion of positions at collision risk height range based on simulations

To assess the effect of error on flight height distributions and derived flight parameters relevant for conservation, we performed simulations by adding different levels of bias or noise to two example flight height distributions from high-frequency GPS data, from Red Kites in Grand Est (tag model OT-25) and from Marsh Harriers in Groningen (tag models 4C.L and 6C.L; Table A3.1.1). As an example of a derived parameter, we used the proportion of positions at the height range of wind turbine rotors, which is a commonly used input parameter in collision risk assessments (Band et al., 2007; T. Schaub et al., 2020). We applied 50-200 m a.g.l. as collision risk height range (CRHR), representing the height range of the rotors of most modern wind turbines. Concerning the proportion of positions within the CRHR, the two example datasets represented the extremes among our study species, with 37.4% of positions within the CRHR in the Red Kites data, compared to 4.2% in the Marsh Harrier data (distribution modes around 22 and 1 m a.g.l., respectively; Appendix 3.3: Figure A3.3.6). Note that the flight height data used here are not free of error, but it is sufficiently small (see Results) not to be problematic for this illustrative purpose.

To clearly separate the effect of precision (noise) and trueness (bias), we applied both types of error separately. For bias, we applied both the mean error found for each combination of tag model and method in this study based on stationary positions on the ground (26 values; Table A3.2.1), and a theoretical range of bias between -20 and 20 m with increments of 1 m. These levels of bias were added to the flight positions as a constant.

Regarding noise, first, we applied the empirical error distributions found in the 10 tag models, with the median per combination of tag model and method as reference ("precision"), on the two flight height distributions. We added an error randomly drawn from the error distributions to each flight position. Secondly, we applied theoretical error distributions to illustrate the effect of gradually increasing error. We applied exponential distributions for the AE $F(x) = \lambda e^{-\lambda x}$, with rate parameter $\lambda = \frac{1}{\bar{x}}$ where $\bar{x}$ (i.e. mean AE), was varied between 1 and 40 m (increments of 1 m), and normal distributions with standard deviation varying between 1 and 50 m (increments of 1 m), corresponding to mean AE of 0.8-39.9 m. The range of mean AE for the theoretical distributions was chosen so that it covered the range of mean AE in relation to the median in the empirical distributions (1.3-29.5 m; see Results), with some extension towards higher values which could be present in GPS tag model not studied here. Note that the exponential error distributions generally matched the empirical error distributions better than the normal distributions. For each flight position, we added or subtracted a randomly drawn value from the exponential or normal error distributions (random choice of algebraic sign in the exponential distributions).

For both empirical and theoretical error distributions, we plotted the relative increase of the proportion of positions within the CRHR, compared to the baseline where no additional error is applied, against the mean absolute error of the error distributions.

3.4. Results

3.4.1. Estimation of vertical accuracy based on stationary periods

Overall, the distributions of error around true height from stationary positions on the ground showed a clear mode (Figure 3.1). The medians of the recorded height a.g.l. were close to zero in the GPS data (-3.8 to 4.3 m for GPS), while barometric height data had a reduced trueness, with median height a.g.l, between -15.0 to -4.9 m (Figure 3.2; Appendix 3.2: Table A3.2.1). Trueness did not differ significantly between low- and high-frequency sampling within GPS or barometric data in most tag models (Figure 3.2).

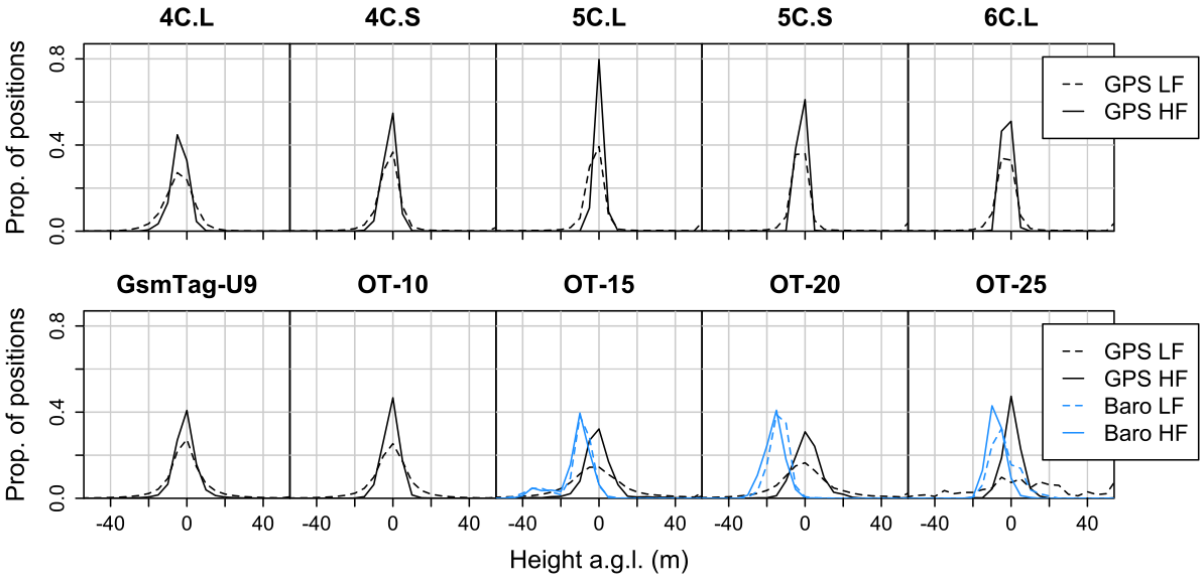

Figure 3.1: Distributions of the recorded height above ground level from stationary positions on the ground for each tag model and method. The lines connect the proportions of positions per height class of 5 m (central class centred around zero). Height data < -50 and > 50 m a.g.l. not shown. Prop. = proportion, LF = low frequency, HF = high frequency.

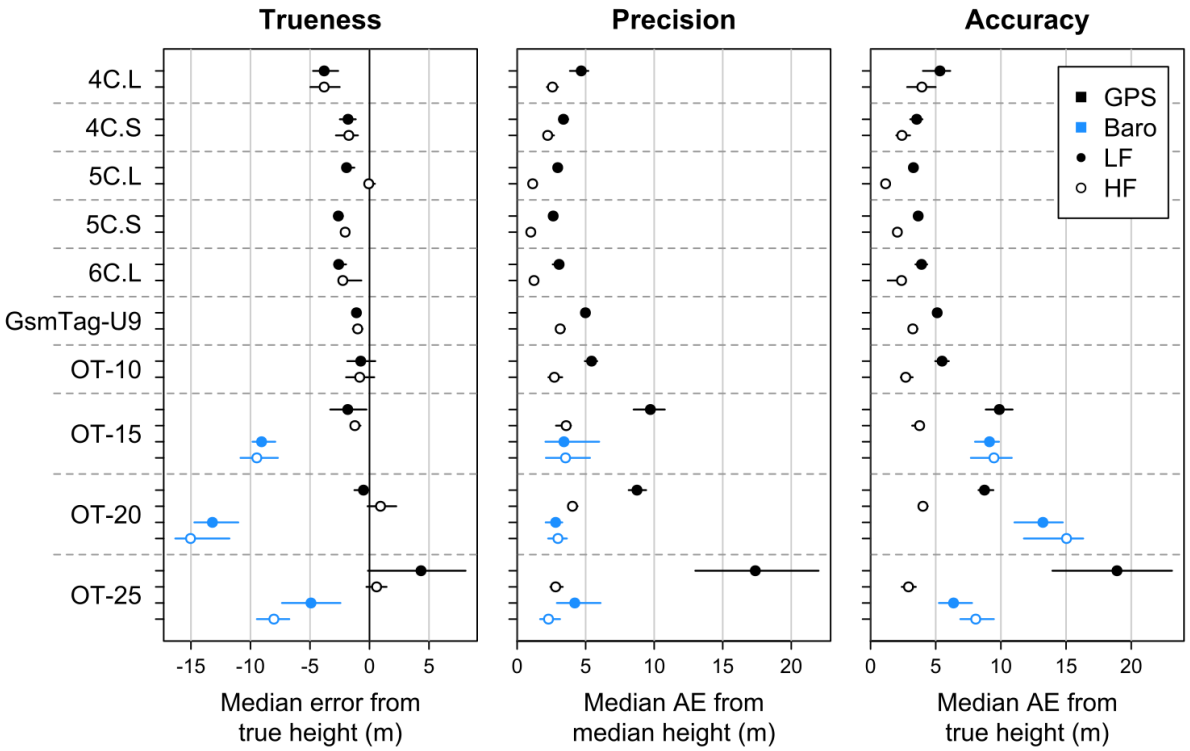

Figure 3.2: Estimates and 95% confidence intervals for trueness, precision and accuracy for each combination of GPS tag model and method based on hierarchical bootstrapping. Parameters used: median error with true height as reference (equivalent to median height a.g.l.; trueness), median absolute error with median height as reference (precision), median absolute error with true height as reference (accuracy). a.g.l. = above ground level; AE = absolute error.

By contrast, there was a much higher variation in precision (error around median height) in low-frequency GPS data between tag models, with median AE ranging from 2.6 to 17.4 m (mean across tag models ± SD 6.3 ± 4.6), compared to high-frequency GPS data (range of median AE 1.0-4.0 m; mean 2.4 ± 1.0) and to both low- and high-frequency barometric data (range of median AE 2.8-4.2 [mean 3.5 ± 0.7] and 2.3-3.5 m [mean 2.9 ± 0.6], respectively). Most importantly, in low-frequency GPS data, the median AE around the median was on average 2.6 times larger than in high-frequency GPS data (median 2.3; range 1.5-6.2). In barometric data, regardless the sampling frequency, precision was similar to high-frequency GPS data or slightly higher (Figure 3.2; Appendix 3.2: Table A3.2.1). Large outliers with absolute height above median > 50 m occurred regularly in low-frequency GPS data (on average 6.6% of positions; range 0.3-17.4%), whereas these were much scarcer in high-frequency GPS data (mean 0.4%; range 0.0-1.5%), and nearly absent in barometric data (mean 0.1%; range 0.0-0.2%; Table A3.2.3). In every tag model, the mean AE was higher than the median AE, especially in low-frequency GPS data, reflecting the long tails of the AE distributions. Therefore, differences between low- and high-frequency GPS data increased when considering mean instead of median AE (mean AE in low-frequency data on average 8.1 times larger than in high-frequency data; median 3.8; range 2.0-20.0; Appendix 3.3: Figure A3.3.1).

Also regarding overall accuracy, low-frequency GPS data had larger errors (with true height as reference) than high-frequency GPS data in all tag models. Median AE ranged from 3.3 to 18.9 m in low-frequency GPS data (mean 6.8 ± 4.8 m), and from 1.2 to 4.0 in high-frequency data (mean 2.9 ± 0.9 m; median AE on average 2.4 times larger in low-frequency data; median 1.9; range 1.4-6.5). Mean AE ranged from 7.4 to 29.9 m in low-frequency GPS data (mean 18.9 ± 18.9 m), and from 1.5 to 7.0 in high-frequency data (mean 3.9 ± 1.7 m; mean AE on average 6.6 times larger in low-frequency data; median 3.4; range 1.6-19.0; Table A3.2.1). The difference between high- and low-frequency GPS data was significant in all cases (except for one tag model for median AE; Figure 3.2, Figure A3.3.1). In barometric data, accuracy did not differ between high- and low-frequency data in any tag model (Figure 3.2, Figure A3.3.1). Median AE varied between 6.4 and 15.0 m (mean 10.2 ± 3.3 m) and mean AE between 6.8 and 15.2 m (mean 11.3 ± 3.2 m). The results for barometric height data in comparison to high- and low-frequency GPS data were mixed among tag models, with barometric data being less accurate (based on median AE) than low-frequency GPS in OT-20, similarly accurate than low-frequency GPS in OT-15 and intermediate between low- and high-frequency GPS in OT-25 (Figure 3.2).

3.4.2. Difference between GPS and barometric height

For stationary positions, regardless of sampling frequency, the difference between GPS and barometric height was on average larger than zero (range of median difference: 4.9 to 16.4 m; Figure 3.3, Appendix 3.2: Table A3.2.4), i.e. barometric height was on average lower than GPS height. However, the median difference was smaller or even slightly negative for flight positions (range of median difference: -1.1 to 7.6 m; Figure 3.3). The median difference also changed with (barometric) height a.g.l. in low-frequency data, becoming negative in positions > 0-40 m a.g.l. in two of the three tag models, indicating that barometric height was on average higher than GPS height (Figure 3.4; see Figure A3.3.2-4 for graphs showing the entire height range and data from the other two tag models). In absolute terms, the difference between GPS and barometric height data was smallest in high-frequency flight positions (range of median absolute difference: 4.6-8.1 m; compared to 8.0-16.5 m in stationary high-frequency data and 11.6-21.6 m in low-frequency data; Table A3.2.4).

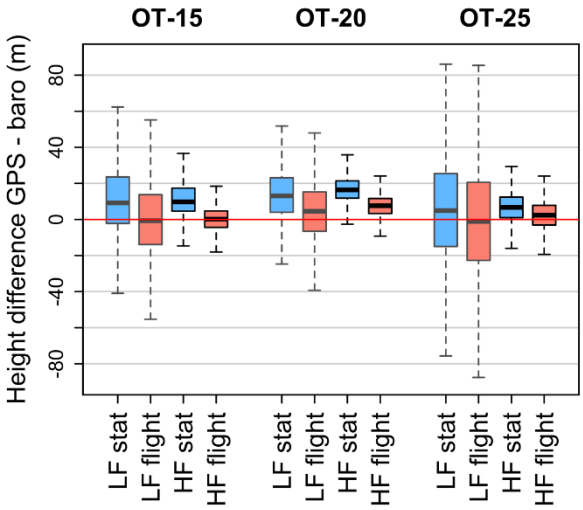

Figure 3.3: Difference between GPS and barometric height for three tag models (OT-15, OT-20 and OT-25) for high- and low-frequency sampling (LF/HF) and stationary ("stat") and flight positions ("flight"). Thick horizontal lines indicate medians and boxes the ranges between the 1st and the 3rd quartiles; whiskers extend to the most extreme data point at a distance of no more than 1.5 times the interquartile range from the box; data points outside of whiskers were omitted. See Appendix 3.2: Table A3.2.4 for sample sizes.

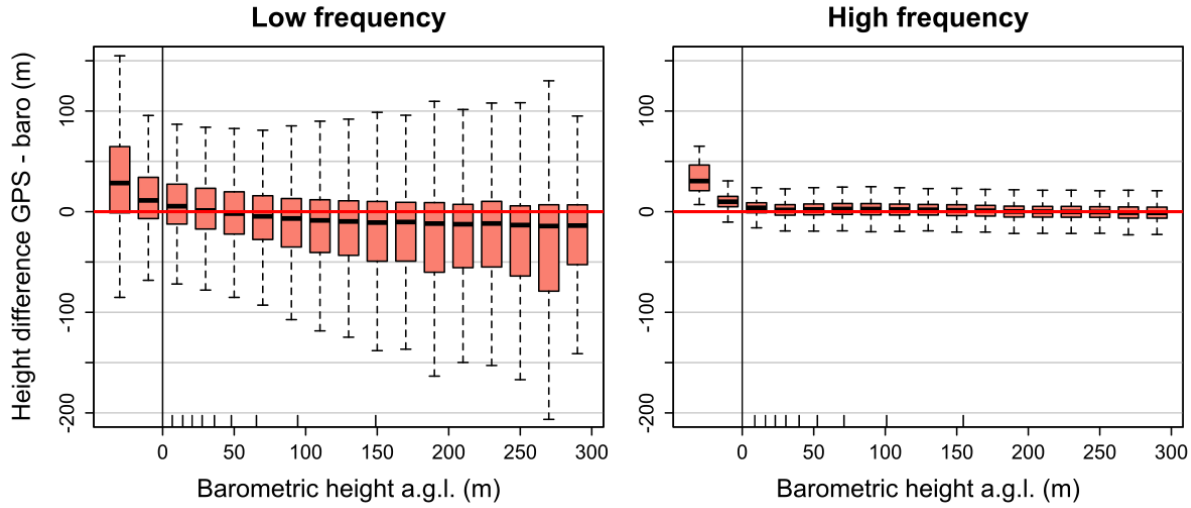

Figure 3.4: Difference between GPS and barometric height in relation to height above ground level (a.g.l.; range -40 and 300 m) for OT-25 GPS tags deployed on Red Kites in low- and high-frequency sampling (bins of 20 m). Only flight positions were considered. Thick horizontal lines indicate medians and boxes the ranges between the 1st and the 3rd quartiles; whiskers extend to the most extreme data point at a distance of no more than 1.5 times the interquartile range from the box; data points outside of whiskers were omitted. Sample size: 126,278 positions for low-frequency; 1,032,956 for high-frequency. Tick marks above the x-axis indicate deciles.

In line with the differences found between GPS and barometric height data in flight, the flight height distributions based on barometric data appeared to be shifted by a few metres compared to those from high-frequency GPS data in two of the tag models, whereas the shapes of the distributions were similar (Figure 3.5, Figure A3.3.7). By contrast, in

low-frequency GPS data, the flight height distributions differed remarkably from those of the three other methods by being flattened out, showing a less pronounced peak.

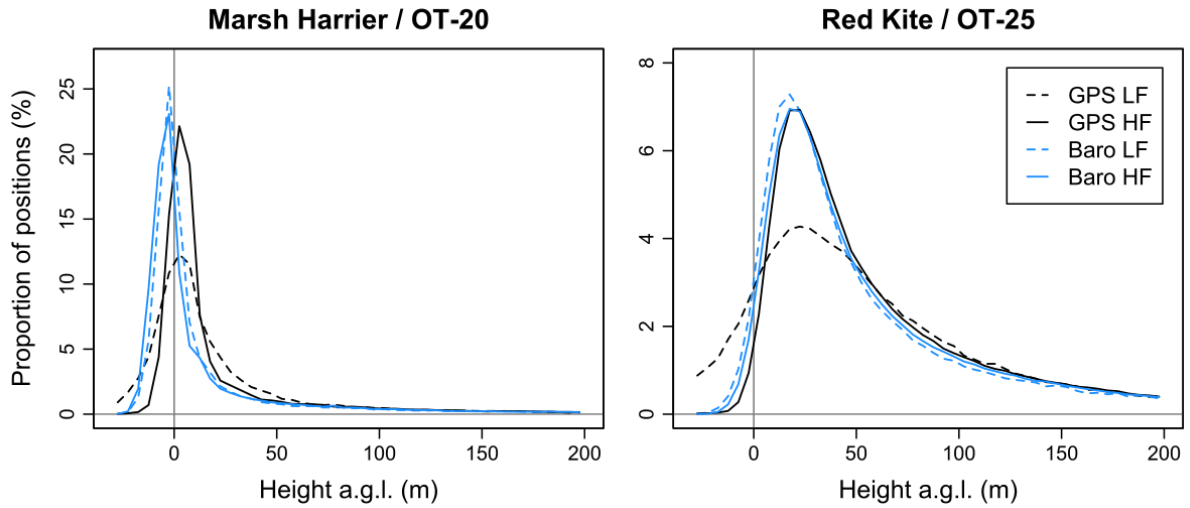

Figure 3.5: Flight height distributions of Marsh Harriers and Red Kites based on either GPS or barometric height data from OT-20 and OT-25 GPS tags collected using either low- (LF) or high-frequency (HF) sampling (height classes of 5 m). Note different scales of the y-axis between panels. Height data < -30 m and > 200 m above ground level (a.g.l.) not shown.

3.4.3. Description of high-frequency tracking data including recurrent error patterns

Overall, high-frequency tracks from all tag models showed realistic flight movements, in line with flight patterns expected for our study species. Thermal ascent flights were easily discernible by zig-zag patterns in the horizontal plane, and commonly alternated with descending gliding flights (Figure 3.6b). The height sequences of barometric height and GPS height were generally very close to each other (Figure 3.6c; Appendix 3.3: Figure A3.3.5).

Nevertheless, we identified three recurrent error patterns in GPS height data from high-frequency tracks, with variable frequency across the three tag manufacturers. First, GPS height often showed a quick increase or decrease at the beginning of a high-frequency bout. When barometric data were available, this frequently coincided with a conspicuous offset of the GPS height compared to the barometric height which disappeared usually within 30-60 seconds (Figure 3.6c, Figure A3.3.5c-d). Secondly, gradual drifting of GPS height during stationary periods was observed in *Ornitela* tags, mainly at a scale < 30 m (Figure 3.6c, Figure A3.3.5b). Thirdly, height data from *Milsar* tags included "spikes", i.e. individual and easily discernible outliers, normally at a scale < 50 m (typically 20-50 spikes per hour; Figure 3.6d).

The pattern of changes in the difference between GPS and barometric height in relation to movement (stationary vs. flight) was also observed during the visual inspection of high-

frequency tracks, with abrupt changes coinciding with the moments of take-off and landing (Figure A3.3.5d).

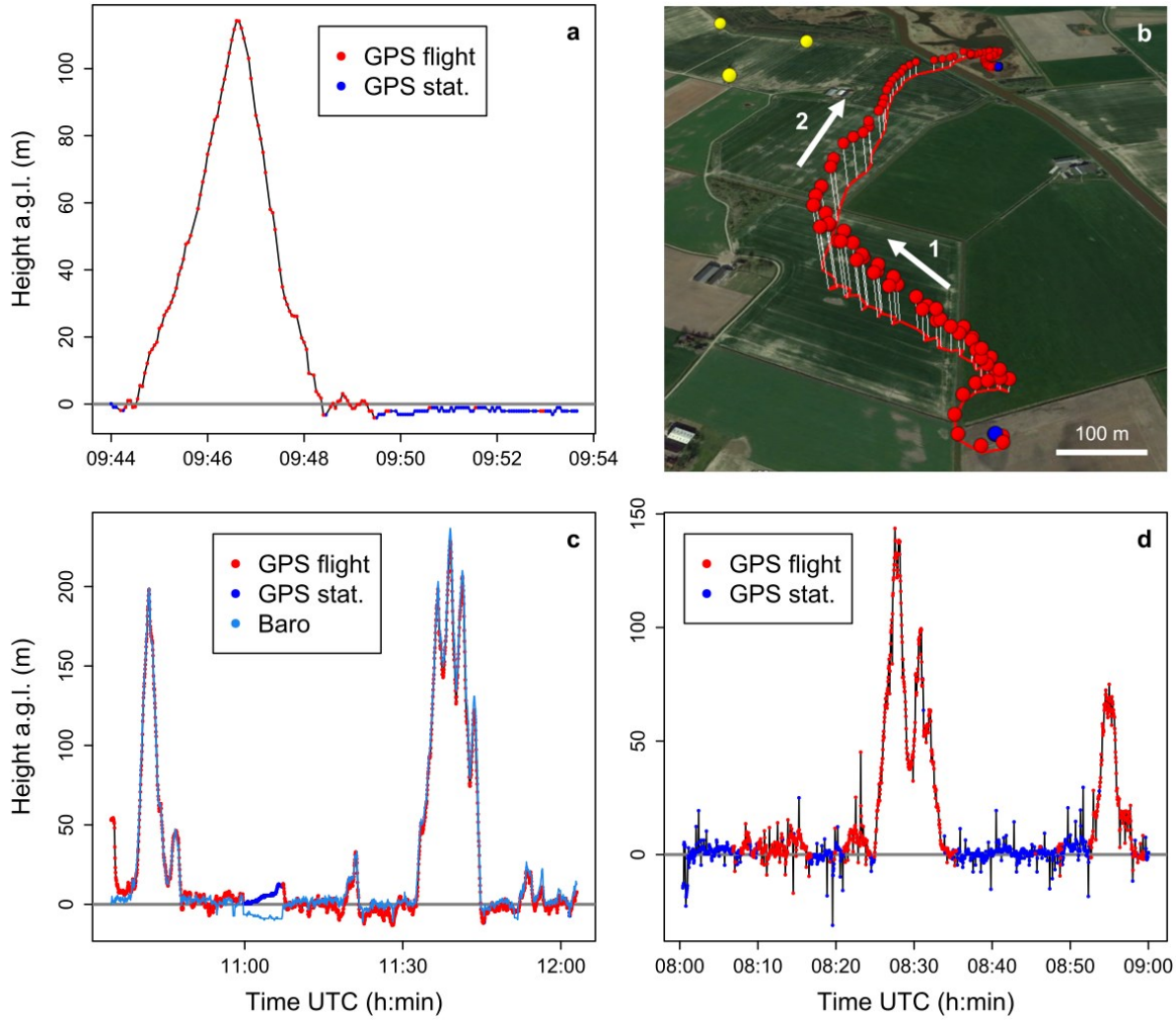

Figure 3.6: Typical examples of height profiles of high-frequency tracks: **a**) example showing realistic height profile in high-frequency sampling (thermal ascent flight from ground level to ca. 110 m a.g.l., descending gliding flight back to approximate ground level; Marsh Harrier Groningen, tag model *UvA-BiTS 6C.L*); **b**) 3D representation of the same track showing zig-zag pattern during thermal ascent (1) and straight descending gliding flight (2); yellow points: wind turbines; satellite image: *Google Earth*; **c**) example showing closeness between GPS and barometric height, accuracy time lag in GPS height data in the first minute of the sequence (quickly decreasing GPS height) and drift of GPS height in stationary periods (Marsh Harrier Flevoland, *Ornitela OT-15*); **d**) example showing "spikes" in GPS height data from *Milsar* tags (Hen Harrier Champagne, *Milsar GsmTag-U9*). Note different time scales on the x-axis between panels (**a-b**: 10 min, **c**: 90 min, **d**: 60 min). a.g.l. = above ground level; stat. = stationary.

3.4.4. Effect of error on flight height distributions and proportion of positions at collision risk height range based on simulations

When applying additional bias to flight height data of Red Kites and Marsh Harriers, the effect on the proportion of positions within the CRHR was similar in both species (Figure 3.7). The levels of bias found in the different GPS tag models in this study in stationary positions lead to a relative change of the proportion at risk height of -22.1% to +8.3% in Red Kites, and -24.2% to +9.0% in Marsh Harriers.

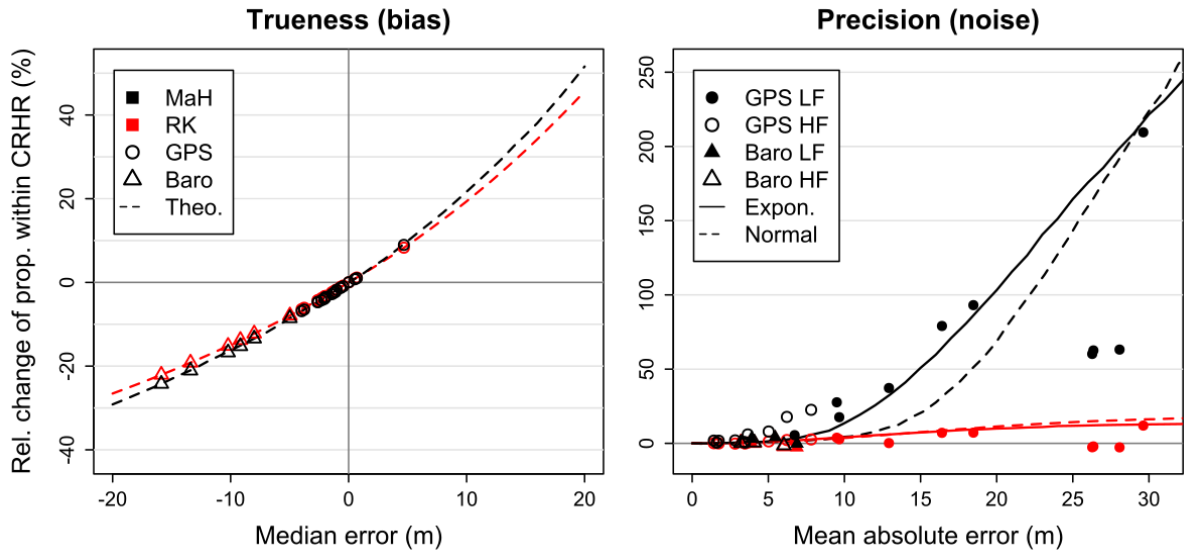

Figure 3.7: Relative change of the proportion of positions within the collision risk height range (50-200 m) in Marsh Harriers (black) and Red Kites (red) when applying different degrees of bias (trueness) or noise (precision) to the height data. Points represent empirical error distributions found in different GPS tag models in either GPS or barometric height data from either low-frequency or high-frequency sampling. Lines represent gradually increasing bias for trueness and increasing noise based on theoretical error distributions (exponential or normal) for precision. Expon. = exponential, MaH = Marsh Harrier, RK = Red Kite, Baro = barometric, LF = low-frequency, HF = high-frequency.

When applying additional noise, the flight height distributions were flattened out with less pronounced peaks (Figure A3.3.6), similarly to the empirical flight height distributions based on low-frequency GPS data (Figure 3.5). The proportion of positions within the CRHR generally increased with increasing additional noise (Figure 3.7). The effect of noise depended on the flight height distribution of the considered species. In Marsh Harriers (steep flight height distribution with low mode; Figure A3.3.6), the proportion of positions within the CRHR was overestimated by > 50% in six out of ten applied empirical error distributions from low-frequency GPS data, with a maximum of 209.5% (Figure 3.7). By contrast, in Red Kites showing a flatter flight height distribution with mode closer to

the CRHR compared to Marsh Harriers, the proportion within the CRHR was only overestimated by up to 12.0%.

3.5. Discussion

Based on a data set consisting of ca. 11 million GPS positions collected using 194 tags of 10 GPS models from three manufacturers, we found substantial differences in accuracy between different methods of collecting height data (low-frequency GPS, high-frequency GPS, low-frequency barometric, high-frequency barometric). In GPS data, the vertical error consisted mainly of noise rather than bias, whereas the barometric data mainly suffered from bias, with relatively little noise. Notably, overall accuracy was improved in high-frequency (continuous-mode) compared to low-frequency (discrete-mode) GPS height data. In barometric data, vertical accuracy was intermediate in stationary positions, but likely the bias was smaller in flight.

Importantly, using simulations based on our empirical data, we showed that the degree of error found in low-frequency GPS data can significantly bias the outcomes of practical applications of the data in some conditions. More specifically, noise in the height data can lead to a significant increase of the proportion of positions within the collision risk height range (CRHR). This would in turn lead to an important overestimation of wind turbine collision mortality when implemented in collision risk models (Masden et al., 2021). In other words, this confirmed that the low accuracy in low-frequency GPS data can be a genuine problem in the study of collision risk of birds with wind turbines and other vertical human infrastructures. By contrast, the effect of the remaining error in high-frequency GPS data and barometric data on the proportion of positions within the CRHR was small.

3.5.1. Accuracy in GPS height

We found that GPS height data were more accurate in the high-frequency (continuous) mode than in the standard low-frequency (discrete) mode in all the considered tag models. This can be explained by an increased number of satellites used for the GPS fixes in the high-frequency mode (about twice as many satellites used per fix compared to the low-frequency mode; mean ± SD 12.4 ± 3.3 vs. 6.5 ± 2.0; Appendix 3.3: Figure A3.3.8). The notable differences which we found in the accuracy of GPS height data between tag models, especially in low-frequency GPS data (range of mean AE 7.4-29.9 m), might partly be due to technical differences in the GPS modules used in the tags, like the application of additional global navigation satellite systems (GNSS) in addition to GPS (e.g. GPS + GLONASS in *Ornitela* tags as opposed to GPS only in *Milsar* tags) or different internal settings (for example regarding time-to-fix). The year of data collection could also affect the positional accuracy of GPS data, as over the years, more satellites have been added to the orbit. However, in our case, there has only been a slight increase of the number of satellites over the years (Figure A3.3.8).

There is also a large variation among results on vertical accuracy of GPS tags reported in earlier studies, and our results generally fell within these ranges. In low-frequency sampling, Bouten et al. (2013) reported a mean AE in relation to true height of 20.8-26.3 m with 10-min intervals and 4.0 m with 1 min intervals, while Péron et al. (2020) indicated a mean AE of 27 m with 1-min intervals, Acácio et al. (2022) of 9.7 m with 60 min and 5.0 m with 1-min intervals and Heuck et al. (2019) a 95% quantile of AE of 33 m (compared to 20-161 m in our data; Table A3.2.2). Note that we did not consider differences in accuracy between different intervals in low-frequency GPS tracking here, as opposed to some of the studies cited. Regarding high-frequency GPS data, reference data are scarce, but Bouten et al. (2013) reported mean AE of 1.4-2.8 m with 6-s intervals (compared to 1.5-7.0 m in our data) and Thaxter et al. (2018) whisker ranges of 11-14 m with 10 s intervals (compared to 8-33 m in our data; Table A3.2.2).

Visual inspection of height profiles of high-frequency tracks indicated some recurrent error patterns in the high-frequency GPS height data (accuracy time lag at the beginning of high-frequency sequences, spikes, drift in stationary periods). However, these concerned only a relatively small proportion of positions, or stationary positions only. The error arising from the accuracy time lag and spikes could be reduced with relatively simple methods. For example, applying a moving average with a window of nine data points to the high-frequency GPS data of *Milsar GsmTag-U9* tags reduced the 95% quantile of AE from 13.1 to 10.7 m (Appendix 3.4). The accuracy time lag has been also reported in earlier studies, where it was found to last 10-35 s (Corman & Garthe, 2014; Grünkorn & Welcker, 2019). This problem can be solved by removing the first part of high-frequency sequences (Appendix 3.4). The finding of increasing accuracy within the first portion of high-frequency GPS sequences is in opposition to the suggestion that there could be a constant initial error that is maintained during the entire high-frequency sequence (Péron et al., 2020).

3.5.2. Accuracy in barometric height and pathways for improvement

Our results on vertical accuracy in barometric height data were mixed. On the one hand, in stationary positions, barometric height had a substantial bias compared to true height. On the other hand, the closeness of GPS and barometric height in high-frequency data (Figure 3.4, Figure 3.6) and the similarity between flight height distributions obtained from high-frequency GPS and barometric data (Figure 3.5) suggest that the accuracy of barometric height data for flight positions is relatively high, and that it indeed represents an improvement compared to low-frequency GPS data.

It has been described earlier that the vertical error in barometric height data consists to a large extent of a bias related to weather conditions and calibration, as opposed to the error dominated by random noise in the GPS height data (Heuck, Sommerhage, et al., 2019; Péron et al., 2020). This implies also the absence of extreme outliers in the barometric height data (this study, Heuck, Sommerhage, et al., 2019). As in our data, the bias

in barometric height data from stationary positions reported by Heuck et al. (2019) was negative (median of -22.6 m). Regarding the precision in barometric height data, Heuck et al. (2019) reported a 95% quantile of AE in relation to median height of only 1.3 m in barometric data in a stationary experiment (tags not deployed on birds), compared to 9.5 - 26.5 m in our data. With drone experiments, Lato et al. (Lato et al., 2022) found a mean vertical error of only 1.6 m in barometric data and Péron et al. (2020) reported a RMSE of 22 m between barometric and GPS height for low-frequency data. The latter is also considerably lower than the RMSE between the two types of data in our study (43 -92 m). These differences could be explained by the longer time span during which our data were collected, implying a wider range of weather conditions in which air pressure was measured. Moreover, we cannot exclude that the increased error in barometric height data in our study resulted from the fact that we evaluated accuracy in a field setting, with tags deployed on free-living birds. For example, there might be effects of heat radiation of the birds, moisture or dirt on the pressure readings.

An important aspect of our results which has, to our knowledge, not been described earlier is that the difference between GPS height and barometric height differed systematically between stationary and flight positions. Possibly, the difference could be due to an effect of movement on the air pressure measurement, which could be related to differences in wind speed and temperature between moving and stationary states, or the fact that often the tag is partially covered by feathers when the birds are stationary, possibly impairing the measurements. The difference between stationary and flight positions implies that a correction of the barometric height data based on stationary tests (Heuck, Sommerhage, et al., 2019) might not be optimal for flight positions. Moreover, the difference between GPS height and barometric height changed along the height gradient in low-frequency data, with barometric height on average exceeding GPS height for recorded barometric heights > 0-40 m a.g.l. This could be caused by an altitudinal bias in the barometric height data. However, if this was the case, we would expect this pattern to be also present in high-frequency data. We could not exactly retrace how the altitudinal pattern arose, but the comparison of flight height distributions obtained from the different methods (Figure 3.7) suggested that the distributions based on barometric data both from low- and high-frequency sampling were shifted by an approximately constant offset compared to high-frequency GPS data, at least within the height range relevant for wind turbine collision risk (below 300 m). Therefore, a correction offset based on the mean difference between GPS height and barometric height in flight positions could be a way of aligning barometric and GPS height data. However, mean GPS height during flight might not be free of bias either (Lato et al., 2022). Experiments with drones might help to verify if this correction approach is indeed effective, but note that also in such experiments, obtaining reference data for true height in flight is not trivial (but see Lato et al., 2022). The correction should optimally be conducted for each tag separately, as we obtained indications that the bias in barometric data differs between individual tags (unpublished data), similarly to Heuck et al. (2019). It should be noted that even though the accuracy in barometric height data might be improved with further corrections, our results also suggest that a bias of a few metres, which probably remained in the barometric height data without corrections,

might not have major implications for the proportion of positions within the collision risk height range, as opposed to extensive noise as in low-frequency GPS height data (Figure 3.7).

3.5.3. Sources of error

The aim of this study was to assess the overall vertical accuracy occurring in a practical field setting. However, we do want to stress that the accuracy we described here in fact represent a combination of different sources of error, not only related to the height measurement itself, but also to the digital elevation model (DEM) and to the identification of stationary periods on the ground (Table 3.1).

Table 3.1: Overview of the sources of error in GPS and barometric height data, either regarding the determination of height above ground itself or regarding the identification of stationary periods on the ground on which we based our assessment of vertical accuracy.

Source of error	GPS height	Barometric height
Determination of height above ground		
- GPS height above geoid/ellipsoid	X	
- Air pressure measurement		X
- Weather data		X
- Simplifications in barometric height formula		X
- Horizontal GPS position	X	X
- Digital elevation model	X	X
Identification of stationary periods on the ground		
- GPS speed	X	X
- Classification of stationary/flight positions	X	X
- Habitat classification	X	X

Moreover, the total error in our study also includes error in the identification of stationary periods on the ground (e.g. occasional erroneous classification of flight positions as stationary; Table 3.1). Therefore, we expect that the true vertical error itself is somewhat smaller than indicated here. In addition, it has been reported that horizontal and vertical accuracy in GPS data is higher when tags are moving (Zheng et al., 2014; Grünkorn & Welcker, 2019). This suggests that our estimation of accuracy based on stationary positions is conservative when transferred to flight positions.

At several stages of our analysis, we came across problems of obtaining raw data from the GPS tags. For example, the raw height above ellipsoid data were only available for one out of three manufacturers, and in the case of another manufacturer, height above geoid was truncated at zero, precluding negative values. These limitations potentially bias error assessments as conducted here, but can also have implications for analyses of flight height. Therefore, we want to call on manufacturers to make raw data (unprocessed

height above ellipsoid for GPS and raw pressure measurements for barometers) available throughout, in line with Péron et al. (2020).

The large differences in vertical accuracy across tag models, especially in low-frequency GPS data, and the need for correction of the barometric height data as found here, underline the importance of testing the accuracy of GPS tags. Assessing accuracy using data from tags already deployed on birds, as done here, has the advantages that it can be applied a posteriori and that it integrates the in situ conditions of data collection. However, it requires the possibility to identify periods during which the true height of the birds is approximately known, like stationary periods on the ground (this study) or on the sea surface (Thaxter et al., 2018), which is not possible for every species. This approach is also restricted to non-flight positions. Un-deployed tags can be tested with stationary experiments (Bouten et al., 2013; Heuck, Sommerhage, et al., 2019; Péron et al., 2020), experiments where tags are moved horizontally (Grünkorn & Welcker, 2019), or using drones (Lato et al., 2022). Approaches based on stationary data have the disadvantage that results may not be fully applicable to flight data (see above). Approaches with moving tags have the disadvantage that the true height is difficult to determine, but drones with laser altimeter represent a promising new method to solve this issue (Lato et al., 2022).

3.5.4. Effect of error on proportion of positions within the collision risk height range

Using simulations, we showed that both bias and noise in the height data can lead to a bias in the proportion of positions within the collision risk height range (CRHR). However, the potential effect of noise was much larger than the effect of bias (up to +210% with noise compared to up to -24% with bias). Moreover, the effect of noise differed strongly between the two considered species, with a strong overestimation of the proportion within the CRHR in Marsh Harriers at the highest levels of noise, but only a small overestimation in Red Kites. This can be explained by differences both in the shape of the flight height distributions and in the location of the mode in relation to the CRHR in the two species, with a very steep distribution with a mode located relatively far from the CRHR in Marsh Harriers and a broader distribution with the mode being closer to the CRHR in Red Kites. It is important to note that extensive noise could not only lead to an overestimation of the proportion of positions within the CRHR, but also to an underestimation, most probably in cases where the mode of the flight height distribution falls within the CRHR (e.g. larger soaring birds like Short-toed Eagle *Circaetus gallicus*, unpublished data). This would in turn lead to an underestimation of wind turbine collision risk.

We would like to stress that low-frequency GPS data does not necessarily produce erroneous outcomes. In our empirical flight height data, the difference in the proportion of positions within the CRHR between high-frequency and low-frequency GPS data was surprisingly small in some tag model-species combinations (Appendix 3.2: Table A3.2.5). The effect of noise on the results will depend on 1) the level of noise in the data (which we showed to vary between tag models); 2) the true flight height distribution (e.g. Marsh

Harrier vs. Red Kite); and 3) the question for which the data are applied (e.g. definition of the CRHR). However, in practice, neither the exact level of noise nor the true flight height distribution are normally known, making it difficult to predict the effect of noise on the outcomes.

3.5.5. Pros and cons of high-frequency GPS tracking and barometric altimetry

Our study showed that the use of high-frequency GPS tracking results in the highest vertical accuracy amongst the considered methods. Additionally, this method provides the advantage of an increased horizontal accuracy (Bouten et al., 2013; Table 3.2). Moreover, the high temporal resolution enables the use of high-frequency GPS tracking data for detailed analyses of 3D flight trajectories with many potential applications, e.g. regarding habitat use and foraging behaviour (Schlaich et al., 2015) or the use of thermal uplifts (Harel et al., 2016; Duriez et al., 2018). In particular, the study of wind turbine avoidance by birds requires high positional accuracy both in the horizontal and vertical dimension, and reliable information on this aspect is urgently needed to improve the predictions of mortality from wind turbine collisions (Chamberlain et al., 2006). High-frequency GPS tracking could play an important role to fill this knowledge gap (Thaxter et al., 2018; T. Schaub et al., 2020).

Table 3.2: Advantages and disadvantages of high-frequency GPS tracking and barometric altimetry, compared to standard low-frequency GPS tracking.

	High-frequency GPS tracking	**Barometric altimetry**
Advantages		
Increased vertical accuracy	X	X
Increased horizontal accuracy	X	
Potential for detailed trajectory analyses	X	
Disadvantages		
High battery demand	X	
- Intensive management of tag settings required	X	
- Sampling only during restricted time periods	X	
- Sampling bias towards periods of good solar charging conditions	X	
Weather data required		X
Reduced accuracy in unstable weather conditions		X
Increase of tag weight		X

The main disadvantage of high-frequency GPS tracking is the high battery demand, which implies that this type of data can only be collected during restricted time periods.

The collection of high-frequency GPS data depends on solar charging conditions, which poses the risk of a sampling bias by an underrepresentation of circumstances with poor solar charging, for example in relation to time of day, weather, season or sex (und errepresentation of females due to reduced movement during the breeding season). However, whenever representative results on the vertical niche of a bird species are required, it is important to sample across the aforementioned variables in an unbiased way. Note that the extent of the problem of battery demand and sampling bias might depend on the behaviour of the study species (e.g. depending on time spent flying and habitat) and the climatic conditions in the study area (e.g. less problematic in tropical areas).

The application of high-frequency GPS tracking has been facilitated by the possibility of remotely modifying tag settings, mainly through the GSM network in recent tag models. However, to date, the monitoring of battery voltage levels and the activation of the high-frequency mode often have to be performed manually, which requires a considerable time investment on a daily basis and might discourage researchers from applying high-frequency settings. Note that the automatic initiation of the high-frequency mode when battery voltage reaches a defined threshold is already an available option in some manufacturers at present, but this potentially leads to a strong bias towards good solar charging conditions. In this respect, it would be a considerable step forward if tag manufacturers could provide more complex programming options for tag settings (for example, when a defined voltage threshold is reached, scheduling a one-hour sequence of high-frequency sampling for a random time on the next day). Another example of a promising avenue in this context is automatic flight detection, i.e. automatic application of high-frequency tracking when the bird is in flight, and low-frequency tracking when the bird is stationary, which is already available in some tag models (Harel et al., 2016; Grünkorn & Welcker, 2019), but not yet fully efficient for all bird species (unpublished data).

Barometric data have the advantage of reduced battery demand compared to high-frequency GPS data (Table 3.2). In fact, barometric measurements are recorded alongside every GPS fix with a negligible increase in battery consumption. This makes it much easier to obtain flight height data without the aforementioned sampling biases. A disadvantage of barometric altimetry is the additional weight of the pressure sensor. For example, the lightest GPS tag with pressure sensor of the manufacturer *Ornitela* currently weighs 20 g, preventing its use on smaller species such as Montagu's and Hen Harrier.

3.5.6. Conclusions

The recent advancements of the GPS tracking technology have opened many opportunities for the study of animal movements. However, it has remained challenging to obtain accurate flight height data from GPS tags. At the same time, this data is urgently needed to accurately predict the collision risk of birds with wind turbines and identify effective mitigation measures. Based on a field assessment using data from GPS tags deployed on free-living birds, we confirmed that GPS height data from standard low-frequency GPS tracking is associated with substantial error, blurring flight height distributions and potentially leading to an important bias in parameters relevant for bird conservation.

Barometric altimetry may provide more accurate height data, but there is the risk of a systematic error which is difficult to resolve fully. Dedicated experiments are needed, especially to elucidate the behaviour of barometric height in relation to movement (stationary vs. flying), to derive an effective correction method for barometric height data. Most importantly, we showed that high-frequency (continuous-mode) GPS tracking substantially improves vertical accuracy compared to low-frequency (discrete-mode) GPS tracking. It can be seen as a complementary approach to statistical modelling techniques accounting for the vertical error (Ross-Smith et al., 2016; Péron et al., 2020). Moreover, it has the additional advantage that it enables detailed 3D trajectory analyses, notably with respect to wind turbine avoidance. However, care should be taken to collect the high-frequency data in an unbiased, representative way.

3.6. Declarations

3.6.1. Ethics approval and consent to participate

GPS tracking was approved by the responsible authorities CRBPO (personal projects 633 and 987), Wageningen University & Research (project 2017.D-0045.004), University of Groningen (permits 5869B and 6429B) and LAVES Niedersachsen (permit 33.12-42502-04-14/1550), and was performed following all relevant guidelines.

3.6.2. Availability of data and materials

The datasets used during the current study are available from the corresponding author on reasonable request.

3.6.3. Competing interests

The authors declares that they have no competing interests.

3.6.4. Funding

TS' PhD position was co-funded by ENGIE and ANRT (Cifre grant 2020/0448). GPS tags and fieldwork were funded by Natural England (Montagu's and Hen Harriers Champagne), ENGIE Green, CNR, EDPR, Boralex (Red Kites Grand Est), Dutch Province of Flevoland and Dutch Ministry of Agriculture, Nature and Food Quality (Marsh Harriers Flevoland), Dutch Province of Groningen, Dutch Ministry of Agriculture, Nature and Food Quality, Prins Bernhard Cultuurfonds and B.V. Oldambt (Montagu's, Hen and Marsh Harriers Groningen).

3.6.5. Authors' contributions

TS, AMil, RB, SL, AMio and RK did fieldwork. TS, AMil, CZ and RK conceptualised the study. TS performed data processing and data analysis, with support from AMil and JC. TS and RK wrote the first draft. All authors contributed to subsequent drafts and approved the final manuscript.

3.6.6. Acknowledgements

We would like to thank everyone involved in fieldwork, notably Jean-Luc Bourrioux, Pascal Albert, Jérôme Isambert, Arthur Keller, Christelle Scheid, Julien Rougé, Marine Felten, Lucas and Eric Graja, La Volerie des Aigles, Parc Animalier de Sainte-Croix, Werkgroep Roofvogels Noordoostpolder, Kjell Janssens, Almut Schlaich, Madeleine Postma, Sylvia de Vries and Ben Koks; Ramunas Zydelis (*Ornitela*) and Paweł Otulak (*Milsar*) for support with the GPS tags; Willem Bouten for support with the *UvA-BiTS* system and helpful discussions; Bart Nolet, Chris Thaxter, Simon Chamaillé-Jammes, Agathe Leriche and Anne Prieur-Vernat for helpful comments and advice; Christophe Baehr and Bart van Stratum for help with weather data and barometric calculations; and two anonymous reviewers for valuable comments which improved the manuscript. The UvA-BiTS infrastructure was facilitated by Infrastructures for EScience, developed with the support of the Netherlands eScience Centre (NLeSC) and LifeWatch, and conducted on the Dutch National E-Infrastructure with support from the SURF Foundation.

4. Informed selection of wind turbine dimensions mitigates the collision risk of birds of prey

Tonio Schaub, Raymond H. G. Klaassen, Caroline De Zutter, Pascal Albert, Olivier Bedotti, Jean-Luc Bourrioux, Ralph Buij, Joël Chadœuf, Celia Grande, Hubertus Illner, Jérôme Isambert, Kjell Janssens, Eike Julius, Simon Lee, Aymeric Mionnet, Gerard Müskens, Rainer Raab, Stef van Rijn, Judy Shamoun-Baranes, Geert Spanoghe, Benoît Van Hecke, Jonas Waldenström & Alexandre Millon

Submitted

4.1. Abstract

Wind energy development is a key component of climate change mitigation. However, flying animals may collide with wind turbines, and this additional mortality negatively impacts populations – especially in long-lived species like raptors. Collision risk could be reduced by an informed selection of turbine dimensions, but this approach is currently hampered by a lack of information on species-specific flight heights.

We used high-frequency GPS tracking, providing high positional accuracy, to study flight height in six European raptor species (275 individuals). Five species had a unimodal flight height distribution, with a mode below 25 m above ground level, while Short-toed Eagle showed a more uniform distribution with a weak mode between 120-260 m. The proportion of positions at collision risk height (32-200 m) varied significantly between species, ranging from 11% in Marsh Harrier to 54% in Red Kite.

Subsequently, we studied the effect of the ground clearance and rotor diameter of wind turbines on collision risk, using the Band collision risk model. With increasing ground clearance (from 20 to 100 m), collision risk decreased in the species with low mode (-56 to -66%), but increased in Short-toed Eagle (+38%). With increasing rotor diameter (from 50 to 160 m) at fixed ground clearance, the collision risk *per turbine* increased in all species (+151 to +558%), while the collision risk *per MW* decreased in the species with low mode (-50% to -57%).

These results confirmed that wind turbine dimensions have a substantial effect on the collision risk of raptors. As the effect varied between species, wind energy planning should consider the composition of the local bird community to optimise wind turbine dimensions. For species with a low mode of flight height, the collision risk for a given total power output can be reduced by increasing ground clearance, and using fewer turbines with larger diameter.

4.2. Introduction

Mitigating climate change and halting biodiversity loss are increasingly perceived as two interconnected challenges (Pörtner et al., 2021). A key component of the strategies to reduce greenhouse gas emissions is the development of wind energy. For example, the European Union targets a total installed wind power capacity of 510 GW by 2030 (European Commission, 2022), which requires a more than twofold increase compared to 2022 (WindEurope, 2023). However, the expansion of wind energy may impact bird populations through an increase of lethal collisions with wind turbines (Bellebaum et al., 2013; Thaxter et al., 2017), unless effective mitigation measures are put in place (Arnett & May, 2016).

A variety of mitigation measures are used to reduce the collision risk of birds with wind turbines, ranging from pre-construction measures such as informed site selection to post-construction measures like wind turbine shut-down during periods with increased collision risk or shut-down, e.g. triggered by automatic bird detection devices (Marques et al., 2014; Arnett & May, 2016). Another possible pre-construction measure is the informed selection of the wind turbine dimensions (hub height, rotor diameter), which determine the height range and the area swept by the wind turbine rotors (A. Johnston et al., 2014). This rotor height range, delimited by the lowest and highest points the rotor blades can reach ("ground clearance" and "maximum tip height"; Figure 4.1a), differs strongly between available wind turbine models. For example in onshore wind turbines constructed since 2015 in six European countries, ground clearance varied between 10-100 m, and the rotor diameter between 40-170 m (Figure 4.1). Over the past decades, there has been a clear trend towards increasing rotor diameters (Appendix 4.1: Figure A4.1.1; Serrano-González & Lacal-Arántegui, 2016), while average ground clearance has increased in some countries but remained unchanged in others (Figure A4.1.2).

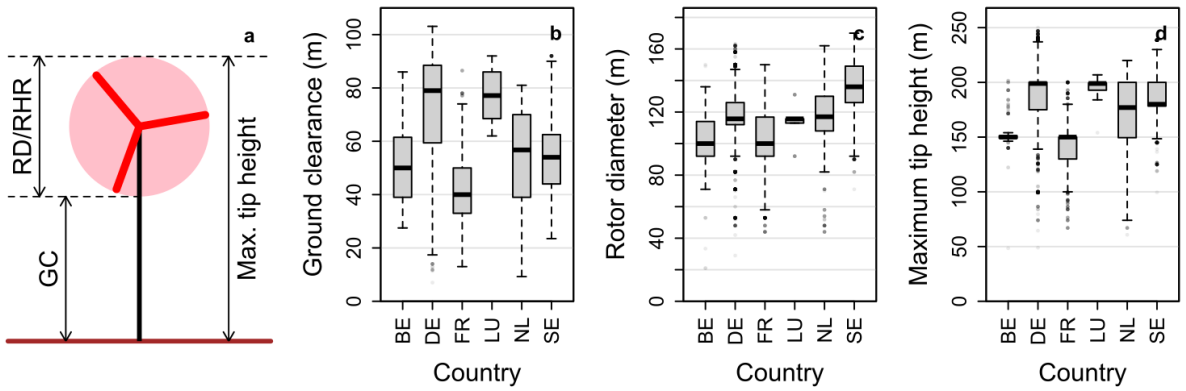

Figure 4.1: a) Illustration of the terms used in this study: GC = ground clearance, RD = rotor diameter, RHR = rotor height range. **b-d**) Ground clearance, rotor diameter and maximum tip height of wind turbines constructed between 2015 and 2023 in Belgium, Germany, France, Luxemburg, The Netherlands and Sweden (n = 12,809 for ground clearance and maximum tip height, and 14,911 for rotor diameter). Source: The Wind Power (2022, 2023).

The selection of the rotor height range of wind turbines potentially has a large effect on collision risk, as birds tend to use the vertical airspace in a non-uniform way, using certain height ranges more often than others (Ross-Smith et al., 2016; Pfeiffer & Meyburg, 2022). However, flight height distributions differ between bird species (A. Johnston et al., 2014), implying that the informed selection of wind turbine dimensions to minimise collision risk requires species-specific information on flight height.

The study of flight height of birds in the context of wind turbine collision risk has been notoriously difficult, as it requires a high level of accuracy in the height measurements. Methods like visual observations or bird-borne GPS tags generally imply large vertical errors, which require the use of complex modelling techniques to obtain unbiased flight height distributions (A. Johnston et al., 2014; Péron et al., 2020). Radar provides higher accuracy, but generally does not allow for species determination, and often only flights above a certain minimum height can be tracked (Spaar & Bruderer, 1997; Krijgsveld et al., 2009; Bruderer et al., 2018). A novel possibility to collect accurate flight height data of individual birds over extended time periods is high-frequency GPS tracking, with GPS fixes taken at intervals of a few seconds, where the GPS module remains turned on between fixes. This "continuous mode" substantially reduces the error in GPS height data to a level offering new opportunities to derive recommendations for mitigating wind turbine collision risk (mean absolute error 1-7 m; Bouten et al., 2013; T. Schaub et al., 2023).

Here, we used an extensive high-frequency GPS tracking dataset to investigate the flight height distributions of six raptor species across 15 study areas in six European countries. Raptors have been found to be particularly prone to wind turbine collisions (Thaxter et al., 2017). Moreover, they are long-lived and reproduce at low pace, making their populations particularly sensitive to increased mortality (Carrete et al., 2009; Bellebaum et al., 2013). Our study species include the Red Kite *Milvus milvus*, which has received much attention in the wind energy context in Europe as it is at the same time endemic to the continent and perceived to be one of the most collision-prone bird species (Bellebaum et al., 2013; Dürr, 2023).

Our main objective was to assess how the theoretical collision risk varied according to the ground clearance and rotor diameter of wind turbines. Our study approach was based on a stochastic adaptation of the Band collision risk model (Band, 2000; McGregor et al., 2018). In this way, we took into account the overlap of the wind turbines' rotor height range with the flight height distributions of birds ("vertical overlap"), alongside technical parameters varying according to the rotor diameter, such as rotor rotation speed. Furthermore, we considered the increase of rated power of wind turbines with larger rotor diameters, to determine whether the collision risk for a given targeted power output can be minimised using a large number of small turbines or a small number of large turbines. Finally, we assessed the consistency of the results between study areas.

4.3. Materials and methods

4.3.1. Data collection

We collected flight height data using solar-powered GPS tags deployed on 275 individuals of six raptor species (Montagu's Harrier *Circus pygargus* [MoH; n = 76], Hen Harrier *C. cyaneus* [HH; n = 51], Marsh Harrier *C. aeruginosus* [MaH; n = 29], Common Buzzard *Buteo buteo* [CB; n = 24], Red Kite [RK; n = 93] and Short-toed Eagle *Circaetus gallicus* [STE; n = 2]) in 15 study areas in France, Belgium, Luxembourg, The Netherlands, Germany and Sweden between 2009 and 2023 (Table 4.1). For the 21 species-area combinations (Appendix 4.1: Figure A4.1.1), the number of individuals varied between 2 and 48 (median: 9; Table A4.1.2).

Table 4.1: Sample size overview per species. Ind. = individuals (number of individuals with ≥ 5 h of flight data in brackets); pos. = positions.

Species	n study areas	Time period	n ind. (≥ 5 h)	n GPS pos.	Time span (h)
Montagu's Harrier	6	2009-23	76 (54)	1,906,493	1,554.2
Hen Harrier	2	2012-23	51 (21)	386,371	300.4
Marsh Harrier	4	2012-23	29 (19)	892,025	747.9
Common Buzzard	3	2021-23	24 (15)	356,742	294.9
Red Kite	5	2019-23	93 (70)	3,826,726	3,188.9
Short-toed Eagle	1	2021-23	2 (2)	47,519	39.6
Total	*21*		*275 (181)*	*7,415,876*	*6,125.9*

The majority of the dataset was composed of adult birds (n = 205) which were captured using one of the following methods: mist net with a stuffed or live predator as lure, nest-trap, catching pole or whoosh-net with carrion as bait. One STE was tagged before its release from a bird rescue centre. Nestlings were captured on the nest before fledging (n = 70; only RK, HH and MaH; Appendix 4.1: Table A4.1.2). Eleven different GPS tag models from the manufacturers *Milsar*, *Ornitela* and *UvA-BiTS* (Bouten et al., 2013) were mounted as backpacks using a thoracic cross-strap harness (Anderson et al., 2020) made from Teflon ribbon. Tags weighed 9.7-26.3 g, representing 1.4-6.5% of individual body weight (median: 2.9%; mean: 3.2%; SD: 1.0%). GPS tagging was approved by the responsible authorities in each country (see Appendix 4.3). Generally, there were no indications of significant adverse tag effects: the tagged birds fulfilled their annual cycle and reproduced as expected, with the exception of two adult HH (one male, one female) which deserted their nest after capture (but note that the chicks did nevertheless fledge in both cases with the support of the remaining adult). The tags transferred the recorded data remotely, either using the GSM network (*Milsar, Ornitela*) or local antennas (*Milsar, UvA-BiTS*).

Throughout this study, we exclusively relied on high-frequency GPS tracking data, with the GPS module operating in continuous mode (i.e. it remained turned on between successive fixes). This type of tracking data provides considerably more accurate height data than GPS data in standard mode, with mean absolute error of 1-7 m, as opposed to 4-30 m in standard mode (Bouten et al., 2013; T. Schaub et al., 2023). High-frequency data were collected using a GPS interval of 3 s in *Ornitela* and *UvA-BiTS* tags, and 2-3 s in *Milsar* tags. High-frequency data were collected mostly during manually set blocks of 1-4 hours per day, and to a lesser extent using automatic geofences around areas of interest such as wind farms. Due to the energy demand of the continuous GPS mode, collection of high-frequency data was only possible when battery voltage of the tags was high. Conversely, limited amounts of high-frequency data were harvested when solar yield was low, for example during winter, longer spells of overcast weather and incubation periods of females. However, by manually setting the periods of high-frequency data collection, as opposed to automated approaches directly based on battery voltage, we unlinked data collection from the immediate charging conditions as much as possible, which ensured a relatively even sampling across the course of the day and different weather conditions.

The dataset was restricted to the 15 defined study areas (Appendix 4.1: Figure A4.1.4), representing the breeding areas. CB were year-round residents within the study areas, while all tagged MoH, MaH and STE (trans-Saharan migrants) and most tagged HH and RK (partial migrants) left the study areas outside the breeding season. As a consequence of the migratory behaviour and the above-mentioned battery restrictions, our dataset was largely focused on the breeding season (93% from March-August; Figure A4.1.5).

All six study species typically forage in open habitats. MoH, HH and MaH nest on the ground in agricultural fields, reedbeds, shrubland or woodland clearings, while CB, RK and STE nest in trees, generally close to the woodland edge (del Hoyo et al., 1994). The study areas were generally dominated by agricultural or semi-natural open habitat with a varying proportion of woodland. The topography varied from flat polder landscapes to hilly terrain and low mountains (range of SD of elevation above sea level [a.s.l.] per study area: 1.5 m [Noordoostpolder/NL] to 85.2 m [Luxembourg]; range of median elevation: -5 m [Noordoostpolder/NL] to 379 m [Haute-Marne/FR]; Table A4.1.1).

4.3.2. Data processing

All data processing and analyses were performed in *R* 4.0.3 (R Core Team, 2020). The dataset was restricted to flight positions only, based on the instantaneous GPS ground speed recorded alongside each GPS location. The distribution of speed values typically shows two modes; one representing stationary and one representing flight positions. We used the location of the minimum between the two modes (Kölzsch, 2022) as a threshold, which we determined visually in histogram plots (centre of bin with minimum number of positions; bin width 0.5 m s^{-1}). The speed threshold was determined for each combination of species and tag manufacturer and varied between 0.75 m s^{-1} (harriers) and 2.25 m s^{-1} (Short-toed Eagle).

The GPS altitude obtained from the tags was height above mean sea level, which we transformed into height above ground level (termed height a.g.l. hereafter) by applying the *Shuttle Radar Topography Mission* global digital elevation model with a resolution of 30 m (NASA JPL, 2013). Despite the high accuracy in the height data, negative heights a.g.l. were recorded to some extent, especially in the harrier species predominantly flying at low height. To avoid introducing biases, these negative height data were kept in the dataset (Péron et al., 2020). See Appendix 4.1 for additional information on the processing of the GPS height data.

The final dataset encompassed 7,415,876 in-flight GPS positions, i.e. 6,126 h of recorded flight movements (timespan calculated as sum of the time intervals to the previous GPS position). The timespan per species was 1,554 h (MoH), 300 h (HH), 748 h (MaH), 295 h (CB), 3,189 h (RK) and 40 h (STE; Table 4.1). Per individual, the timespan varied between < 0.1 and 200.4 h (median: 10.7 h; mean: 22.3 h). For all parts of the analysis where individual differences were considered, individuals with < 5 h of flight data (n = 94) were omitted (Table 4.1).

4.3.3. Comparison of flight height distributions

To compare flight height distributions, we derived the following five parameters per species, species-area combination and individual bird: mode (centre of the 5 m bin with the highest proportion of positions), proportion of mode (proportion of positions in the bin of the mode), median, interquartile range and the proportion within the "general collision risk height range". The latter was defined as the range of 32-200 m a.g.l., corresponding to the smallest height range which included the rotor height ranges of 75% of wind turbines constructed in the six study countries since 2015 (see section 4.3.4). We reported parameters of the flight height distributions per species or species-area combination as estimates (all individuals lumped), alongside the first and third quartile of the individual values to indicate individual variation.

Due to difficulties to fit parametric models to the flight height distribution parameters, we applied non-parametric Kruskal-Wallis rank-sum tests (*R* function *kruskal.test*). For each of the five distribution parameters, the differences between species and among study areas within species were tested. For the between-species tests, a significance level of 0.05 was used; for the within-species tests (five tests per distribution parameter; STE excluded as data were only available from one study area), we applied a Bonferroni-correction to account for multiple testing (significance level of 0.01). For the between-species comparisons, we applied Dunn's tests with Bonferroni correction as post-hoc tests (function *dunn_test*, *R* package *rstatix*).

4.3.4. Wind turbine data

For information on available wind turbine models and wind turbines installed in the six study countries, we relied on the databases provided by The Wind Power (2022,

2023). For later use in the collision risk index (see below), we built Generalized Additive Models (GAM) for the relationships of mean rotation speed (revolutions per minute), blade width and rated power with rotor diameter (see Appendix 4.1 for details).

For the analysis of the effect of wind turbine dimensions on collision risk, we set up a range of hypothetical wind turbine models by combining ground clearances of 10-120 m (increments of 5 m) and rotor diameters of 40-170 m (increments of 10 m; 322 combinations in total), covering a reasonable breadth of turbine dimensions of onshore wind turbines constructed in the six study countries since 2015 (Figure 4.1).

4.3.5. Collision risk index

To assess the effect of wind turbine dimensions on relative collision risk we applied an "all other things being equal" approach, i.e. while ground clearance and rotor diameter were varied for a wind turbine at a given location, bird behaviour was assumed to be equal. For each combination of hypothetical wind turbine models (described above) and study species, we derived a collision risk index (CRI) based on the Band collision risk model (CRM; Band, 2000), estimating the expected number of collisions given a range of bird- and wind-turbine-related input parameters. In this way, our CRI did not only integrate differences in vertical overlap between wind turbine models, but also differences in technical characteristics such as rotation speed and blade width, which are correlated with rotor diameter (Appendix 4.1: Figure A4.1.3). The Band CRM consists of two stages: Stage I estimates the expected number of rotor crossings N_{cross}, largely determined by bird density, vertical overlap and avoidance rate. Stage II estimates the collision probability per rotor crossing P_{coll}, based on rotation speed, blade width and flight speed, amongst others. The expected number of collisions are obtained using the formula $N_{coll} = N_{cross} \times P_{coll}$.

We defined the CRI for a given combination of wind turbine dimensions as the expected number of collisions per year for one turbine in an area with a bird density of 0.1 flying individuals per km^2, assuming the default avoidance rate of 98% (SNH, 2018). Note that the choice of these two parameters affected the absolute CRI value, but not the relative change in CRI between wind turbine models, our focus of interest. The following input parameters were modified according to the wind turbine model: ground clearance, rotor diameter, flight speed (mean instantaneous ground speed calculated across all GPS positions within the given rotor height range; Figure A4.1.6), rotation speed and blade width. The latter two were assumed to only vary with rotor diameter. The CRM calculations were performed using the function *band_crm* from the *R* package *stochLAB* (Caneco et al., 2022). See Appendix 4.1 for additional details and an overview of the input parameters used.

To obtain confidence intervals, we adapted the "stochastic collision risk model" (sCRM; McGregor et al., 2018; Caneco et al., 2022) to fit our study question. Stochasticity was only included for those parameters which could affect the relative difference of collision risk between wind turbine models, i.e. flight height distribution for the effect of ground clearance, and flight height distribution, rotation speed and blade width for the effect of rotor diameter. First, 500 bootstrap replicates of the flight height distributions were

constructed for each species using hierarchical bootstrapping (sampling with replacement at the level of individual birds). Per bootstrap replicate, a CRM was built for each wind turbine model. Rotation speed and blade width were derived as a function of the rotor diameter using the GAM described above. For analysing the effect of ground clearance, the mean predicted value for the given rotor diameter was used; for the effect of rotor diameter, we used a random draw from the posterior distribution of the GAM for each of the stochastic replicates (see Appendix 4.1 for details).

As the rated power of a wind turbine typically increases with the rotor diameter (Figure A4.1.3), we also computed the CRI per unit of power for each hypothetical turbine model. For each of the 500 stochastic replicates per turbine model, one power value was sampled from the posterior distribution of the GAM for the given rotor diameter. The CRI per power allows comparing situations where the same total power output is achieved using wind turbines of different diameters, implying different numbers of turbines. As turbine density is negatively correlated with rotor diameter for technical reasons (larger rotor diameter requiring larger distances between neighbouring turbines), the choice between fewer larger or more smaller turbines is a realistic situation whenever a wind farm is planned in a limited designated area.

To separate the effect of ground clearance and rotor diameter on collision risk, we varied ground clearance at fixed rotor diameter (scenario 1) and vice versa (scenario 2). Additionally, we varied rotor diameter at fixed maximum tip height (scenario 3), implying simultaneous variation of diameter and ground clearance. Primarily, we used the medians across wind turbines constructed since 2015 in the six countries as fixed values for diameter and ground clearance (120 and 60 m, respectively). For maximum tip height, we applied 150 m as this represents a common statutory limit in France and Belgium (Figure 4.1d).

4.4. Results

4.4.1. Flight height distributions

We found between-species differences in the flight height distributions for all the parameters tested (Appendix 4.2: Table A4.2.1). The species split up in two groups, MoH, HH and MaH on the one hand and CB, RK and STE on the other hand, with significant differences only occurring between the groups (Table A4.2.2). In MoH, HH, MaH, CB and RK, the distributions were clearly unimodal (Figure 4.2). The mode was located at the lowest height in the three species of harriers (2.5 m; Q1-Q3: 2.5-2.5), followed by CB (7.5 m; 7.5-7.5) and RK (22.5 m; 17.5-27.5). In STE, the flight height distribution deviated from the other species, being relatively uniform (Q1: 115 m; Q3: 320 m; Table A4.2.3) with an indistinct mode varying between 127.5-252.5 m in the two tracked individuals. Also, medians and interquartile ranges were lowest in the harriers and highest in STE (Figure 4.2, Table 4.2). The proportion of positions within the "general rotor height range" (32-200 m)

was higher in RK (54.2 %; 48.9-59.5), STE (47.7%; 36.3-52.8) and CB (46.1%; 42.5-51.2) than in HH (20.6%; 13.0-26.2), MoH (12.1%; 8.8-14.2) and MaH (11.4%; 10.4-16.1; Figure 4.2).

Table 4.2: Parameters of flight height distributions per species. Estimate: value across all data; range in brackets: first and third quantile of values per individual (except for STE with only two individuals, where minimum and maximum are indicated). Spec. = species; MoH = Montagu's Harrier, HH = Hen Harrier, MaH = Marsh Harrier, CB = Common Buzzard, RK = Red Kite, STE = Short-toed Eagle; prop. = proportion, IQR = inter-quartile range.

Spec.	Mode (m)	Mode prop. (%)	Median (m)	IQR (m)	Prop. 32-200 m (%)
MoH	2.5 (2.5-2.5)	36.9 (30.4-44.7)	4.0 (2.2-6.4)	11.6 (7.0-16.9)	12.1 (8.8-14.2)
HH	2.5 (2.5-2.5)	24.1 (20.9-29.2)	7.2 (4.0-10)	32.6 (16.6-47)	20.6 (13.0-26.2)
MaH	2.5 (2.5-2.5)	34.4 (23.4-34.2)	3.0 (3.0-7.5)	11.0 (11.0-27.5)	11.4 (10.4-16.1)
CB	7.5 (7.5-7.5)	9.4 (7.7-11.1)	37.4 (36.0-41.8)	82.0 (77.5-95.5)	46.1 (42.5-51.2)
RK	22.5 (17.5-27.5)	6.1 (4.7-7.5)	51.3 (44.4-73.3)	89.9 (65.8-132.5)	54.2 (48.9-59.5)
STE	127.5 (127.5-252.5)	2.0 (1.3-2.6)	187.9 (155.2-287.9)	204.3 (126.0-266.0)	47.7 (28.1-61.1)

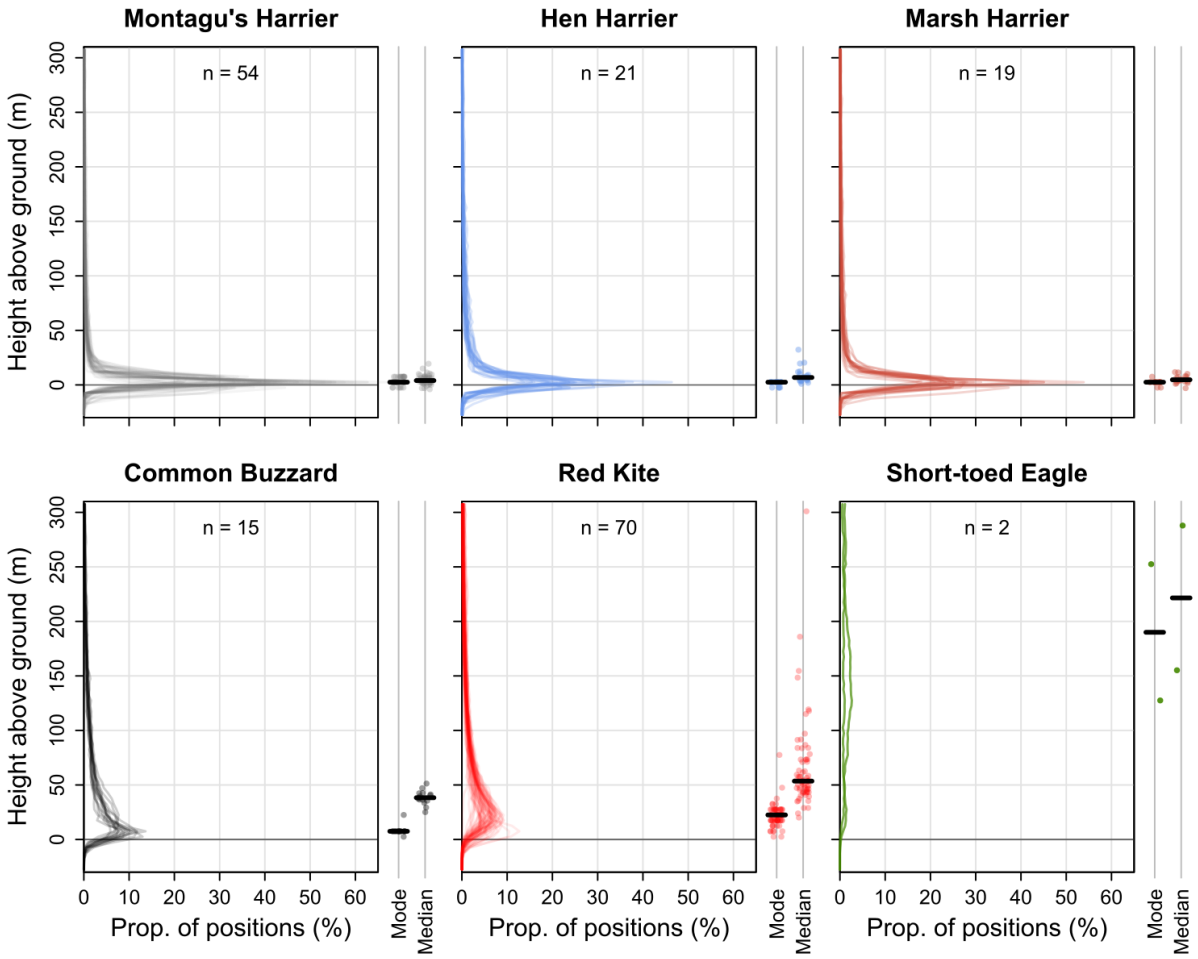

Figure 4.2: Flight height distributions per species and individual in height bins of 5 m. The distributions of modes and medians per individual are indicated right of the panels (thick horizontal line indicating medians across individuals). Prop. = proportion.

The variation in the flight height distributions between study areas was generally smaller than the variation between species (Figure 4.3; Appendix 4.2: Figure A4.2.1-2). Significant between-area differences were only found regarding mode, proportion of mode, median and inter-quartile range in MoH, though with a small effect size (e.g. mode at 7.5 m in Aumelas as opposed to 2.5 m in the other five study areas); density at mode in MaH (e.g. 47.5% in Groningen as opposed to 22.8-26.3% in the three other areas); and regarding proportion of mode and median in RK (e.g. median at 93.2 m in East NL as opposed to 48.4-56.4 m in the four other areas; Table A4.2.1; Figure A4.2.2). Importantly, there was no significant difference between sites in the proportion of positions within the general rotor height range for any species.

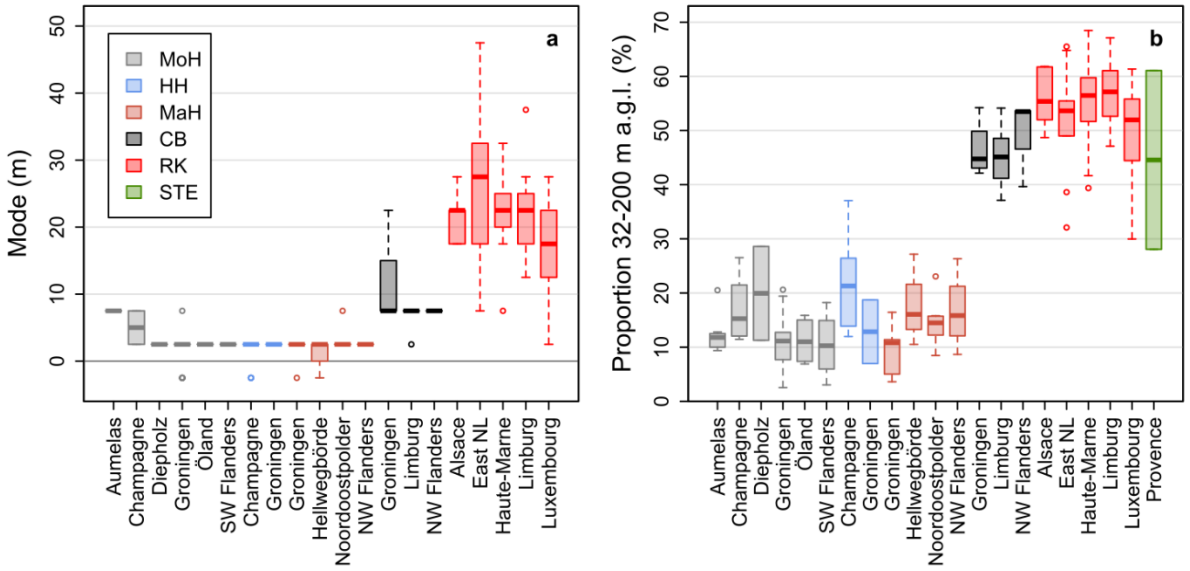

Figure 4.3: Mode of flight height distributions (**a**) and proportion of positions within the general rotor height range (32-200 m a.g.l.; **b**) for six raptor species, per study area (n = 181 individuals; 2-29 per area). In **a**, one RK (study area East NL) and the two STE fell outside the applied y-axis range (modes of 77.5 m, 127.5 and 252.5 m, respectively). See Table 4.2 for species abbreviations.

4.4.2. Effect of wind turbine dimensions on collision risk

The collision risk index (CRI) per wind turbine varied considerably between hypothetical turbine models in all species, the highest CRI (means across stochastic replicates) being 12.1-13.5 times higher than the lowest. Also regarding the CRI per power, there was large variation between turbine models in the five species with low mode of flight height (MoH, HH, MaH, CB and RK; termed "low-mode species" hereafter; highest CRI per power 12.1-17.0 times higher than lowest), while variation was relatively small in STE (highest 1.5 times higher than lowest). In relative terms, the effect of wind turbine dimensions was similar for the low-mode species, whereas STE showed a distinctly diverging pattern throughout (Figure 4.4-5, Figure 4.7). In absolute terms, the CRI differed considerably between the low-mode species (Figure 4.6), in line with the observed differences in the proportion of positions within the general collision risk height range (Figure 4.3).

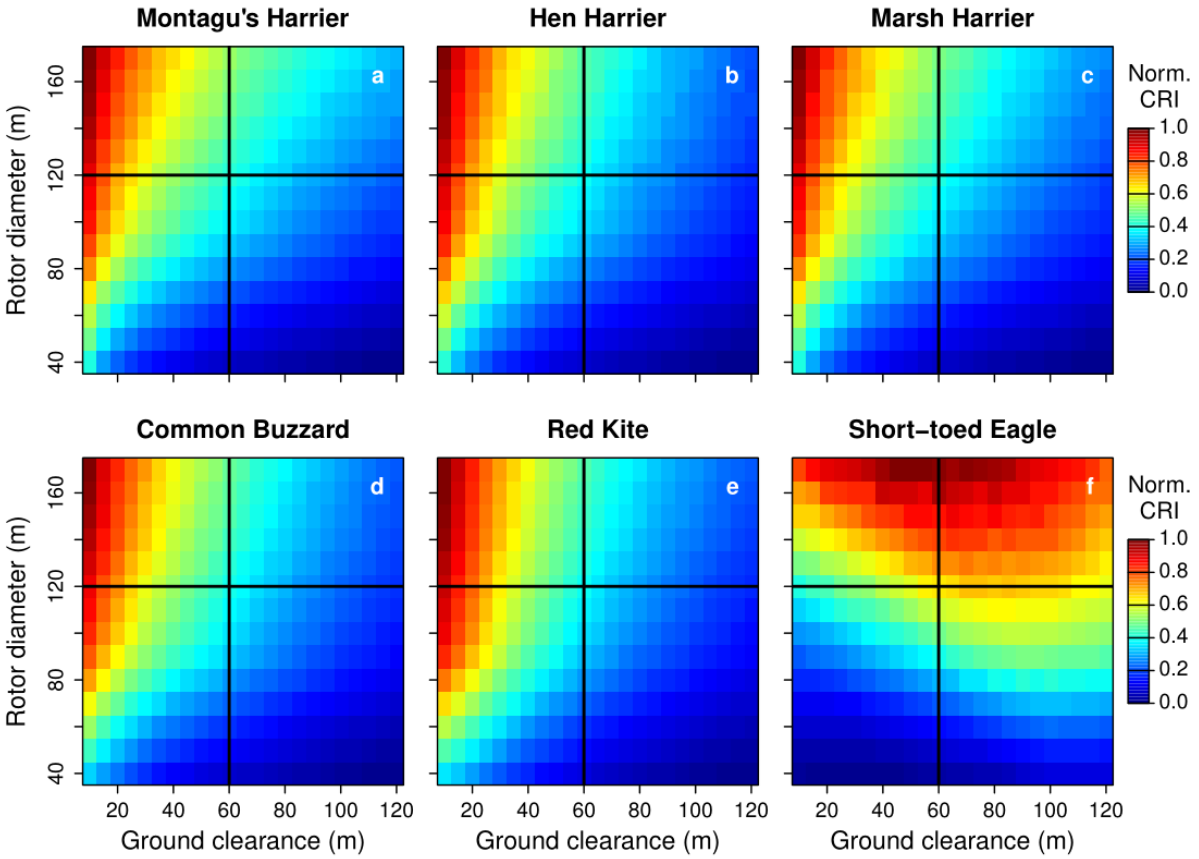

Figure 4.4: Effect of ground clearance and rotor diameter of wind turbines on collision risk. Colours indicate the collision risk index, normalised to a scale from 0 to 1 per panel. Thick black lines indicate cross-sections considered in Figure 4.6-7.

4.4.2.1. Ground clearance

With increasing ground clearance at fixed rotor diameter (scenario 1), the CRI per turbine decreased in the five low-mode species for all levels of rotor diameter (Figure 4.4). In STE, CRI increased with increasing ground clearance at small rotor diameters (below ca. 80 m), whereas it had a maximum around 50-90 m at larger diameters (Figure 4.4f). Confidence intervals for the effect of ground clearance were narrow in the low-mode species, but much wider in STE (Figure 4.6a). For a turbine with 120 m diameter, the relative change in CRI from 20 to 100 m ground clearance was significant in all species (-56 to -66% in the low-mode species, +38% in STE; Figure 4.7; see Table A4.2.4 for confidence intervals and additional pairwise combinations). In STE, the choice of the fixed level for the rotor diameter affected the effect of ground clearance, with a reduced effect with increased diameter (Table A4.2.4).

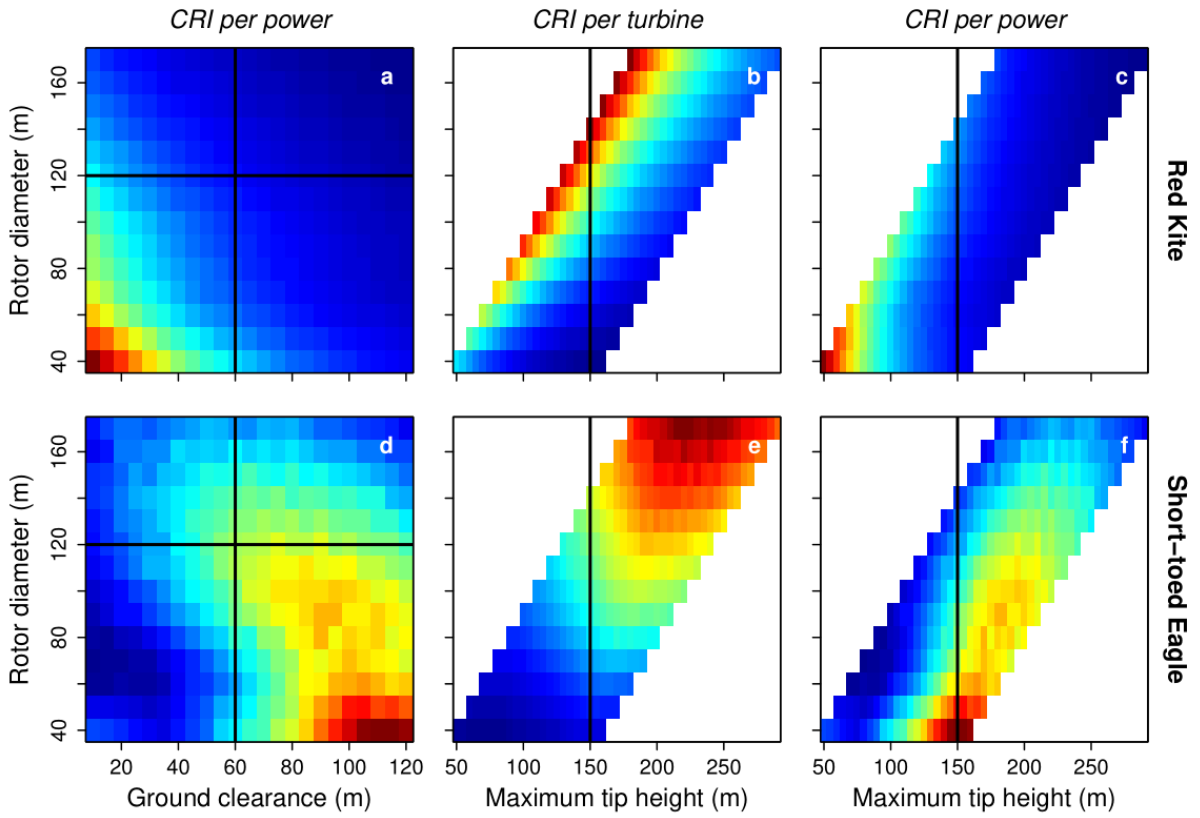

Figure 4.5: Effect of ground clearance, rotor diameter and maximum tip height of wind turbines on collision risk for species with low (Red Kite) or high mode of flight height (Short-toed Eagle). Colours indicate the collision risk index (CRI) per turbine (**b**, **e**) or per rated power (**a**, **c**, **d**, **f**), normalised to a scale from 0 to 1 per panel (see Figure 4.4 for colour scale). NA values (white) arise from impossible combinations of maximum tip height and rotor diameter. Thick black lines indicate cross-sections considered in Figure 4.6-7.

4.4.2.2. Rotor diameter

The effect of rotor diameter on collision risk at fixed ground clearance (scenario 2) was influenced by two opposite trends: on the one hand, the number of rotor crossings (stage I of Band CRM) increased strongly with increasing diameter; on the other hand, the probability of colliding per rotor crossing (stage II of Band CRM) decreased (Appendix 4.2: Figure A4.2.3), mainly as a consequence of reduced rotation speed (Appendix 4.1: Figure A4.1.3). The resulting CRI per turbine increased with increasing diameter in all six species for all levels of ground clearance (Figure 4.4; e.g. increase by 151-558% when increasing the diameter from 50 to 160 m at a ground clearance of 60 m; Table A4.2.4).

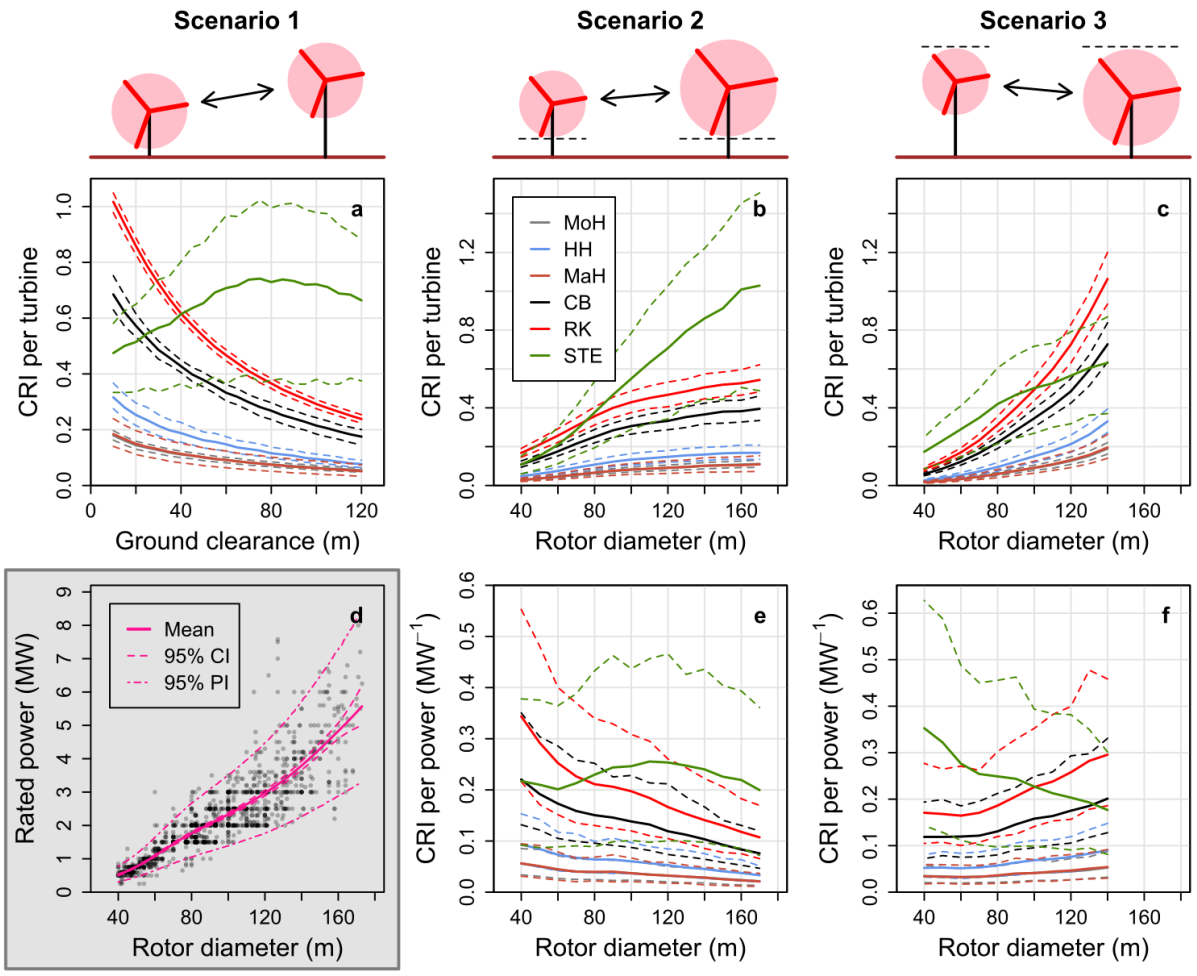

Figure 4.6: Effect of ground clearance and rotor diameter of wind turbines on collision risk (cross-sections from Figure 4.4-5). Panels refer to wind turbines with 120 m diameter (**a**), 60 m ground clearance (**b, e**) or maximum tip height of 150 m (**c, f**). Thick lines indicate means and dashed lines 95% confidence intervals (CI). Note that lines for MoH and MaH lie on top of each other. **d**) Relationship of rated power with rotor diameter for onshore wind turbines. Points: individual wind turbine models (n = 1,360); lines: predictions from a Generalized Additive Model. CRI = collision risk index; PI = prediction interval. See Table 4.2 for species abbreviations.

The mean rated power increased with increasing diameter, from 0.8 MW for 50 m to 4.8 MW for 160 m (Figure 4.6d). Consequently, the CRI per power decreased with increasing diameter in the low-mode species for all levels of ground clearance (Figure 4.5a). In STE, this was also the case when ground clearance was large (above ca. 90 m). With smaller ground clearance, CRI per power in STE was highest at diameters of 90-140 m (Figure 4.5b). Regarding the effect of rotor diameter on CRI per power, the confidence intervals were wide in all species (Figure 4.6e), reflecting the large variation in rated power for a given rotor diameter (e.g. 95% prediction interval of 1.8-4.5 MW for a 120 m diameter; Figure 4.6d). Nevertheless, for a turbine with 60 m ground clearance, the relative change in CRI per power between a diameter of 50 and 160 m was significant in all low-mode species (-50 to -57 %), while it was not for STE (Figure 4.7; Table A4.2.4).

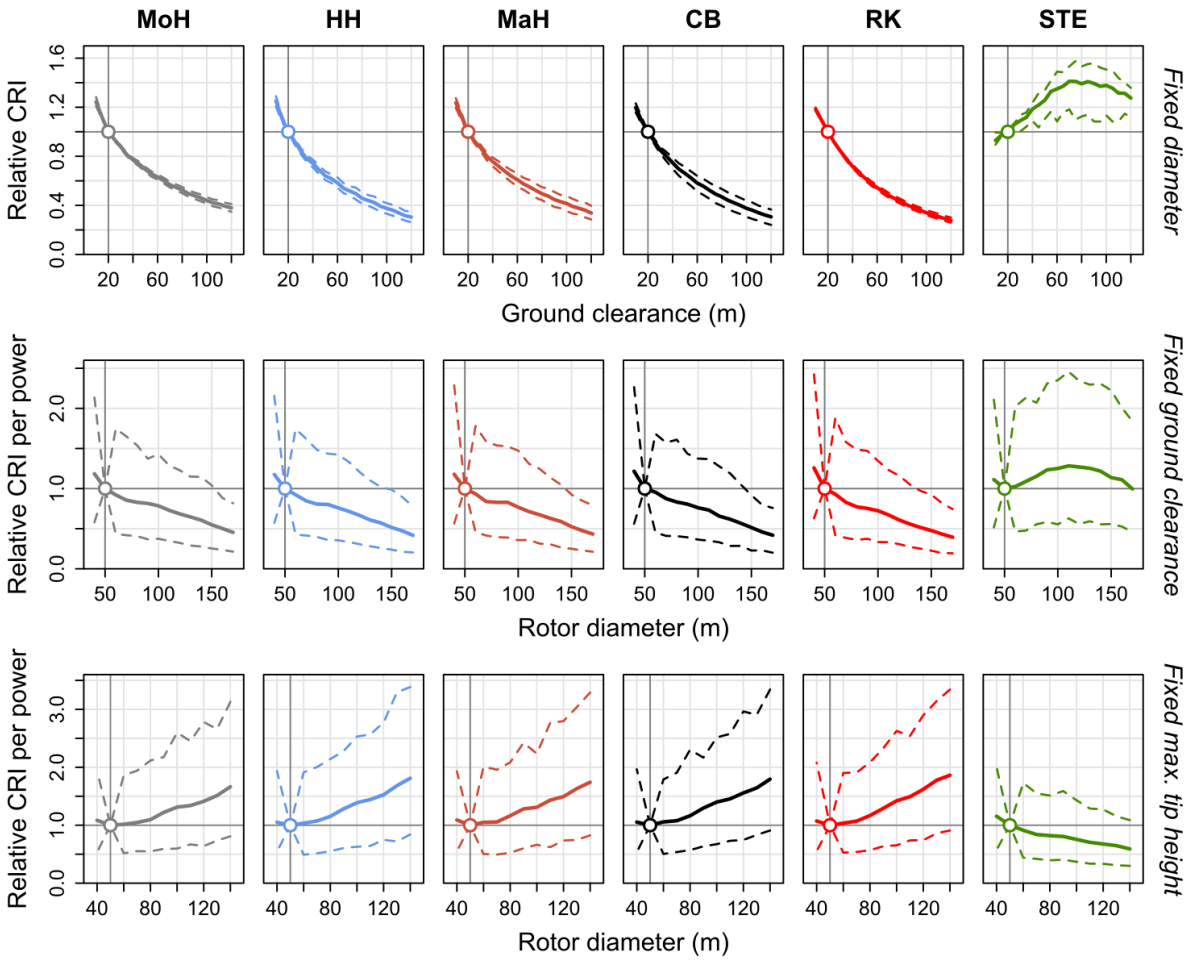

Figure 4.7: Effect of ground clearance and rotor diameter of wind turbines on collision risk relative to a reference level (thick vertical line). Panels show either collision risk index per turbine (first row) or per rated power (second and third row), and refer to wind turbines with 120 m diameter (first row), 60 m ground clearance (second row) or maximum tip height of 150 m (third row). Thick lines indicate means and dashed lines 95% confidence intervals. See Table 4.2 for species abbreviations.

With increasing rotor diameter at fixed maximum tip height (scenario 3), the CRI per turbine increased in all species for all levels of maximum tip height (Figure 4.5b, e). In the low-mode species, this increase was stronger than in the fixed ground clearance case (scenario 2; Figure 4.6b, c), reflecting that an increased rotor diameter at fixed maximum tip height implies a decreased ground clearance. The CRI per power increased with increasing diameter in the low-mode species, while it decreased in STE (Figure 4.5c, f). For CRI per power, confidence intervals were again large (Figure 4.6f). The relative change in CRI per power between a diameter of 50 and 130 m for a turbine with 150 m maximum tip height was close to significant in both the low-mode species (+51 to +78 %) and STE (-35 %; Figure 4.7; see Table A4.2.4 for confidence intervals). The effects of ground clearance and rotor diameter on CRI were similar across study areas for each species (Appendix 2: Figure A4.2.4-6).

4.5. Discussion

4.5.1. Flight height distributions

High-frequency GPS tracking allowed us to describe the flight height distributions of six raptor species during the breeding season. Based on the mode of the flight height distributions, the six species were separated into two groups: Montagu's Harrier (Mo H), Hen Harrier (HH), Marsh Harrier (MaH), Common Buzzard (CB) and Red Kite (RK) showed clearly unimodal distributions with a mode at low height (below 30 m a.g.l.), while Short-toed Eagle (STE) showed a more uniform distribution with a weak mode at 120-260 m. These differences are related to the species' behaviour, with harriers hunting while flying low above the vegetation, CB and RK more often soaring at higher height, but predominantly foraging at heights below 50 m, and STE regularly searching for prey from 100 m and above (del Hoyo et al., 1994).

In CB, RK and STE, the proportion of flights within the rotor height range of most modern wind turbines (32-200 m) was considerably higher than in the harriers (46-54% vs. 11-21%). This could be seen as an indication of a generally higher wind turbine collision risk in the first group. However, the overall collision risk per species also depends on other aspects of flight behaviour besides the flight height distribution, such as the proportion of time spent in flight (e.g. 6% in CB vs. 45% in MoH for breeding males; own data, not shown) and the wind turbine avoidance rate (SNH, 2018).

The flight height distributions found here generally matched the results of earlier studies on the same species (Wilson et al., 2015; Grajetzky & Nehls, 2017; Pfeiffer & Meyburg, 2022). However, it is difficult to compare results between studies due to differences in tracking methods and the parameters reported (e.g. Shamoun-Baranes et al., 2006). Amongst the large number of recent GPS-tracking studies on birds, only surprisingly few studies reported the exact shape of the flight height distributions including the mode (cf. Tikkanen, Rytkönen, et al., 2018; Pfeiffer & Meyburg, 2022), which is however essential to assess the effect of wind turbine dimensions on collision risk, as demonstrated here.

Within species, flight height has been shown to vary according to a range of factors such as weather conditions, time of day, season, habitat, topography, flight type (e.g. soaring vs. flapping), sex and age of the birds (e.g. Shamoun-Baranes et al., 2006; Buij et al., 2022; Pfeiffer & Meyburg, 2022; Vignali et al., 2022; van Erp et al., 2023). These effects were beyond the scope of our study, as we were primarily interested in the overall flight height distributions across longer time periods with a representative mix of weather conditions and flight behaviours, to derive conclusions concerning the effect of wind turbine dimensions on collision risk. However, it is important to note that the flight height distributions presented here are only representative of the birds' local movements during the breeding season. We expect different distributions during migration, presumably with a larger proportion of time at greater heights (Spaar & Bruderer, 1997) and a less pronounced mode, which in turn might alter the effect of wind turbine dimensions.

It is noteworthy that we found only little variation in flight height distributions between study areas. The average flight height distributions across weather conditions or habitats during the breeding season can thus be seen as a basic characteristic of a species associated with its morphology and ecology. One exception was the East NL study area, where RK showed a less pronounced mode and higher median flight height than in the other four study areas. However, this difference did not qualitatively alter the effect of wind turbine dimensions on collision risk. We suspect that this difference arose from a higher proportion of non-breeding individuals (Appendix 4.1: Table A4.1.2).

Our study included data from only two individual STE. However, we are confident that the large differences between the flight height distributions of STE and the other five study species are genuine, as we generally found small individual variation in the shape of flight height distributions. Moreover, data from three additional GPS-tagged STE from other areas confirmed the relatively uniform flight height distribution (own data, not shown).

4.5.2. Wind turbine dimensions indeed affect collision risk

For the five low-mode species, we found that collision risk decreased with greater ground clearance. The collision risk per power decreased with larger rotor diameter if ground clearance was fixed, but tended to increase at fixed maximum tip height. STE showed the opposite trend in these three scenarios, as a consequence of the higher mode compared to the other five species. From data available on other species, it can be presumed that flight height distributions with low mode are relatively common, aside from migratory and commuting flights. Low modes (< 30 m) have been found in other birds of prey such as White-tailed Eagle *Haliaeetus albicilla* (Buij et al., 2022), Golden Eagle *Aquila chrysaetos* (A. Hemery, pers. comm.) and Eagle Owl *Bubo bubo* (Grünkorn & Welcker, 2019), and a range of seabirds (A. Johnston et al., 2014; Ross-Smith et al., 2016). Distributions with high mode as in STE were found in vultures (R. Buij, pers. comm.; O. Duriez, pers. comm.; note the phylogenetical closeness of STE and vultures of the Aegypiinae subfamily; Lerner & Mindell, 2005). During migratory and commuting flights, higher modes and therefore an increase of collision risk with greater ground clearance at fixed rotor diameter, and with greater rotor diameter at fixed ground clearance, are to be expected for many species (Krijgsveld et al., 2009; Stumpf et al., 2011).

We made the assumption that the degree to which the birds avoid wind turbines is independent of the wind turbine dimensions. In practice, this is not necessarily the case, but reliable data on the effect of wind turbine dimensions on avoidance are not yet available, due to the intrinsic difficulty of measuring avoidance in the field and obtaining sufficient sample size to test differences between wind turbine models. Differences in avoidance could influence both the effect of rotor diameter and ground clearance on collision risk. For example, the size and rotation speed of turbines could affect detectability by birds (Blary et al., 2023), and different behaviours such as foraging or display flights shown within different height ranges could make birds more or less susceptible to wind turbine collisions (Hoover & Morrison, 2005). Studies based on carcass searches are an

alternative to assess the effect of wind turbine dimensions on collision risk without relying on information on avoidance rates, but these have other methodological and practical difficulties, such as large uncertainty of fatality estimates (Smallwood, 2013; Thaxter et al., 2017) and the difficulty to collect fatality data using standardised methodology on a country- or continent-wide scale. Earlier studies based on carcass searches confirm our results on the effect of rotor diameter, indicating an increased number of collisions per turbine, but a reduced number of collisions per power, with increased rated power of wind turbines across a wide range of bird species (Thaxter et al., 2017), and in raptors in particular (Smallwood, 2013). To our knowledge, the effect of ground clearance has not been assessed based on carcass search studies to date. This would be a valuable pathway for future research.

4.5.3. Practical implications: higher is (often) better

The large effects of ground clearance and rotor diameter on collision risk found here offer opportunities for reducing collision risk, which are applicable to the installation of new wind farms as well as the repowering of existing turbines. Installing wind turbines with higher ground clearance is likely to benefit a range of bird species (species with a low mode of flight height). Larger rotor diameters increase the collision risk per turbine, but reduce the collision risk per power for species with low mode if ground clearance is not simultaneously reduced. This implies that the total collision risk can be mitigated by using fewer large-diameter turbines instead of more small-diameter turbines.

These general conclusions don't apply to species with a high mode of flight height, and possibly don't hold in a migration context. In other words, there is no "one-size-fits-all" approach and careful consideration of the community of bird (and bat) species present in the given area of interest at different times of the year (breeding, migration, winter) is indispensable to determine which wind turbine design minimises collision risk across species and seasons.

During the planning process of a wind farm, the choice of a turbine model is complex, depending on local wind conditions, legal regulations, model availability and economical aspects. The collision risk index proposed here can be used as an additional layer to compare alternative wind farm designs involving (different numbers of) wind turbines of different models and optimise the planned wind farm both economically and ecologically. Aside from the ecological effects, higher ground clearance at fixed rotor diameter has the disadvantages of higher material and transport costs and increased visibility and noise pollution for humans. Currently, higher ground clearances are often inhibited by legal regulations on maximum tip height. In such cases, high ground clearance can only be achieved using a small rotor diameter, which might not be economically viable. These regulations appear to be especially strict in Belgium and France, where maximum tip height is often limited to 150 m or less (Figure 4.1). We recommend that these regulations are reviewed given our findings on the potential of higher ground clearances to reduce collision risk for a range of bird species.

4.6. Acknowledgments

We would like to thank everyone involved in the local GPS tracking projects, amongst others A. Keller, C. Montégu, L. Boldt, A. Schlaich, B. Koks, J. Rougé and Werkgroep Roofvogels Noordoostpolder (see Appendix 4.3 for a full list of involved persons and organisations); Boralex, EDPR, Soler, natur&ëmwelt a.s.b.l. and SICONA for allowing data use for this study; all farmers and landowners who gave permission to access their land for fieldwork; R. Zydelis (*Ornitela*), P. Otulak (*Milsar*) and W. Bouten (*UvA-BiTS*) for support with the GPS tags; and B. Nolet, C. Thaxter, S. Chamaillé-Jammes and A. Leriche for helpful comments and advice. TS' PhD position was co-funded by ANRT and ENGIE (Cifre grant 2020/0448). See Appendix 4.3 for information on funding for the local GPS tracking projects.

4.7. Author contributions

TS, RK, CDZ and AMil conceptualised the study. TS, RK, PA, JLB, RB, CG, HI, JI, KJ, EJ, SL, AMio, GM, RR, SR, GS, BVH, KW and AMil organised the local GPS tracking projects and did fieldwork. TS performed data processing and data analysis with support from RK, JC and AMil. TS and AMil wrote the first draft. All authors contributed to subsequent drafts and approved the final manuscript.

4.8. Conflicts of interest

This study was partly funded by the energy company ENGIE (TS's PhD position and part of the GPS tracking work). However, the scientific orientation of the PhD project was directed by the partner universities (Aix-Marseille University and University of Groningen), and academic freedom in publishing the results was guaranteed by a partnership agreement. We certify that the results were not influenced by the company's economic interests.

5. Sensitivity to wind turbine collisions: Large differences in time spent flying, proportion of flights at risk height and distance from nest among raptor species

Tonio Schaub, Raymond H. G. Klaassen, Caroline De Zutter, Pascal Albert, Jean-Luc Bourrioux, Ralph Buij, Joël Chadœuf, Celia Grande, Hubertus Illner, Kjell Janssens, Arthur Keller, Simon Lee, Aymeric Mionnet, Gerard Müskens, Stef van Rijn, Judy Shamoun-Baranes, Geert Spanoghe, Benoît Van Hecke, Jonas Waldenström & Alexandre Millon

In preparation

5.1. Abstract

Wind energy development leads to an increased mortality of birds due to collisions with wind turbines, especially in raptors. Detailed information on the flight behaviour of different species is essential to assess sensitivity to wind turbine collisions ir respective of current exposure, improve collision risk predictions, and identify effective mitigation measures.

In this comparative study, we assessed the sensitivity to wind turbine collisions of breeding birds of six raptor species – Montagu's Harrier (MoH), Hen Harrier, Marsh Harrier, Common Buzzard (CB), Red Kite (RK) and Short-toed Eagle (STE) – based on the time spent in flight, the proportion of flights at risk height and the distance travelled from the nest location. We used GPS-tracking data collected in 15 study areas in six European countries, comprising 280 individuals, 74501 individual tracking days and 5786 h of high-frequency flight tracks, providing accurate flight height data.

The average time spent in flight ranged from 0.5 (CB) to 3.4 h d^{-1} (MoH) in females and from 1.0 (CB) to 7.4 h d^{-1} (MoH) in males. The proportion of flights at risk height (32-200 m above ground level) varied between 12.4% (MoH) and 56.4% (RK). In both aspects, variation between study areas was small. The largest total amount of time at risk height per year was found in RK (1.7-7.4 times more than in the other species).

The mean 90% quantile of distance from nest ranged from 0.7 km (CB) to 9.8 km (STE) in females, and from 1.0 km (CB) to 5.6 km (MoH) in males (no data from male STE available), with considerable individual variation. With increasing distance from nest, the estimated time spent at risk height per km^2 decreased in all species, albeit with a species-specific slope.

Our results indicate that basic characteristics of flight behaviour could explain substantial differences in the sensitivity to wind turbine collisions among raptor species, and suggest a particularly high sensitivity in Red Kites. The collision risk for breeding birds can be substantially reduced by increasing the distance between wind turbines and nest sites.

5.2. Introduction

Wind energy is expanding globally, representing a major component of the decarbonisation of energy production. The global wind energy capacity was expected to surpass 1.000 GW in 2023, a more than 40-fold increase since 2000 (GWEC, 2023). To achieve the objective of net-zero emissions in 2050, an estimated ca. 8-fold increase of the global wind energy capacity is required (IEA, 2021). This expansion, however, should not come at the expense of biodiversity (Pörtner et al., 2021). One negative impact of wind energy is an increased mortality of birds due to collisions with wind turbines (Bellebaum et al., 2013; Schuster et al., 2015). Given the current pace of wind energy expansion, there is an urgent need to improve estimations of collision risk, identify effective mitigation measures and eventually reduce the number of collisions.

Conceptually, the risk an anthropogenic threat poses to a species can be divided into two components: sensitivity, i.e. the "intrinsic aspects of a species' biology that determine its capability to withstand a given threat" (also termed hazard), and exposure, i.e. the "intensity of threat acting against the species" (Dickinson et al., 2014; p. 1), mainly determined by geographic location (Dickinson et al., 2014; May et al., 2015). This division is particularly valuable as it allows comparison between species with different current levels of exposure, including species which are not yet exposed to the threat in their distribution range, but might be affected in the future. Hence, information on species-specific sensitivity is essential for informing collision risk mitigation when developing wind energy projects.

One of the main approaches to investigate wind turbine collision risk in birds has been to record collision fatalities based on carcass searches around wind turbines (Smallwood, 2013; Thaxter et al., 2017). However, this approach does not allow to distinguish between sensitivity and exposure, as the collision rates are the product of both components. For example, high collision rates in farmland bird species could be unrelated to high sensitivity, but instead result from high exposure, as most wind turbines are installed in agricultural areas (Thaxter et al., 2017). Moreover, results from carcass searches are prone to biases related to carcass persistence, carcass detectability and variation in search protocols (Huso et al., 2017).

An alternative approach which does allow to distinguish sensitivity and exposure is to study the birds' flight behaviour and estimate the expected collision rate using theoretical collision risk models (Masden & Cook, 2016; Vasilakis et al., 2016; T. Schaub et al., 2020). These models include different aspects of flight behaviour, morphological traits and wind turbine characteristics and thus provide mechanistic insights on how collision risk arises (Band et al., 2007; Masden & Cook, 2016). They also provide the ability to conduct scenario studies for planned wind farms, for example regarding the location and spatial configuration of wind farms and the turbine models used (Vasilakis et al., 2016; T. Schaub et al., 2020).

Within the framework of collision risk models, different aspects of the birds' flight behaviour affect the expected number of wind turbine collisions in a given area of interest (footprint of an installed or planned wind farm; Figure 5.1): the extent to which birds are

present in the area (expressed as bird density or time spent within the area), the proportion of time spent in flight, the proportion of flights at collision risk height, flight speed and avoidance rate (Band et al., 2007; T. Schaub et al., 2020; Masden et al., 2021). These aspects vary between species due to differences in ecology and behaviour. For example, reported values for the average amount of time spent in flight per day among birds of prey (in the broad sense; McClure et al., 2019) vary by more than a factor of 30, with 15 min in Eagle Owls *Bubo bubo*, a sit-and-wait predator (Grünkorn & Welcker, 2019) and 8.2 h in Montagu's Harriers *Circus pygargus*, which perform extended foraging flights to capture prey (T. Schaub et al., 2020), and. Also regarding the proportion of flights at collision risk height, important inter-specific differences have been found, e.g. 2-49% among raptor species in southern Africa (McClure et al., 2021). Such differences could partly explain the variation in the observed number of wind turbine collisions between species or species groups (Thaxter et al., 2017; Dürr, 2023). Hence, information on species-specific flight behaviour contribute to improving our understanding of interspecific differences in collision risk. However, this information is not yet available for many species.

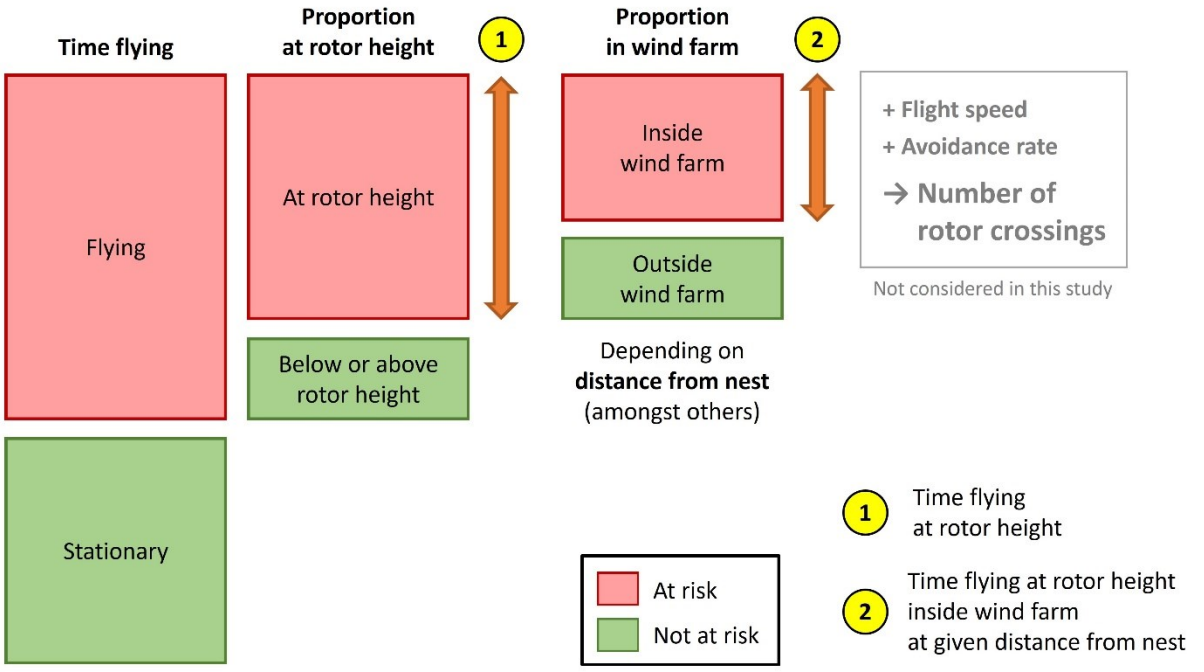

Figure 5.1: Scheme of the conceptual approach adopted in this study. Numbers 1 and 2 indicate the two sensitivity indices calculated. The number of rotor crossings is a main component of collision risk in the Band Collision Risk Model (besides the probability of colliding per rotor crossing; Band et al., 2007). The size of the different compartments is not based on actual data.

The proportion of time that a given bird spends inside the area of a (planned) wind farm will depend on factors such as habitat suitability and topography (Tikkanen, Rytkönen, et al., 2018). In addition, the distance from the nest location may play an important role during the breeding season (Mammen et al., 2017; T. Schaub et al., 2020), as the activity of breeding birds is commonly concentrated around the nest, and food for the chicks has to be transported to the nest regularly (central-place foraging; Bell, 1990).

Therefore, the distances travelled from the nest location by breeding birds can be used to characterise the general "spatial sensitivity" of birds to wind turbine collisions and provide indications for recommended distances that should be kept between wind turbines and known nest locations (LAG VSW, 2014).

In this comparative study, we analysed the sensitivity to collisions with wind turbines in six species of birds of prey, a species group found to be particularly prone to wind turbine collisions (Thaxter et al., 2017; Perold et al., 2020), in 15 study areas in Europe based on three aspects of flight behaviour: 1) the time spent in flight, 2) the proportion of flights at collision risk height and 3) the distance travelled from the nest location, using GPS-tracking. Based on the first two aspects, we estimated the time spent at collision risk height per year per species and sex (Figure 5.1), serving as a general indication of the species-specific sensitivity to wind turbine collisions. In addition, we assessed the relationship of the intensity of area use with distance from nest (Figure 5.1) and determined 50% and 90% quantiles of distance from nest per species and sex, providing an indication for the spatial sensitivity. To assess if the results can be transferred between regions, we assessed the differences between study areas throughout.

5.3. Materials and methods

5.3.1. Data collection

GPS-tracking data of breeding birds of six raptor species were collected using solar-powered GPS tags deployed on 280 individuals (Montagu's Harrier *Circus pygargus* [MoH; n = 101], Hen Harrier *C. cyaneus* [HH; n = 54], Marsh Harrier *C. aeruginosus* [MaH; n = 31], Common Buzzard *Buteo buteo* [CB; n = 31], Red Kite [RK; n = 61] and Short-toed Eagle *Circaetus gallicus* [STE; n = 2]) in 15 study areas in France, Belgium, Luxembourg, The Netherlands, Germany and Sweden between 2009 and 2023 (Appendix 5.1: Figure A5.1.1, Table A5.1.1). Most individuals were captured as adults (n = 268); 12 individuals (8 HH, 1 MaH and 3 RK) were tagged as nestlings and tracked until adulthood. See Appendix 5.1 for details on bird captures. Twelve different GPS tag models (Table A5.1.1) from the manufacturers *Milsar*, *Ornitela* and *UvA-BiTS* (Bouten et al., 2013) were mounted as backpacks using a thoracic cross-strap harness (Anderson et al., 2020) made from Teflon ribbon. Tags weighed 9.7-26.3 g (1.4-6.5% of individual body weight; median: 3.1%), and 12.2-30.4 g including harness (1.6-7.7% of body weight; median: 3.8%). GPS tagging was approved by the responsible authorities in each country (see Appendix 5.3).

In spring and summer, the basic setting for the GPS fix interval was 5 min (MoH, MaH, RK, STE) or 15 min (CB and most HH) during daytime, and 1-4 h at night. Based on the expected daily flight activity pattern per species, the daytime setting covered twilight periods in MoH, HH, MaH, CB (until solar depression angle of 6°) and RK (until 4°), while sunrise and sunset were used as limits for STE (0°). During autumn and winter, periods

of bad weather, and incubation periods in females, the fix interval was increased to 1-12 h to preserve battery voltage.

In addition to this basic data collection scheme ("low-frequency data"), "high-frequency data" were collected using an interval of 3 s in *Ornitela* and *UvA-BiTS* tags and 2-3 s in *Milsar* tags (GPS operating in continuous mode) to obtain more accurate flight height data (Bouten et al., 2013; T. Schaub et al., 2023). These were collected mostly during manually set blocks of 1-4 hours per day, and to a lesser extent using automatic geofences around areas of interest such as wind farms. Due to the high energy demand of the tags when in continuous GPS mode, high-frequency data were mainly available from spring and summer (94.8% of positions from March-August; Appendix 5.1: Figure A5.1.2; Table A5.1.1). By manually setting the periods of high-frequency data collection, we unlinked data collection from the immediate charging conditions as much as possible, which ensured a relatively even sampling across the course of the day and different weather conditions.

The study was restricted to breeding birds, with breeding status assigned per calendar year (data retained from individual years ["bird-years"] during which at least one breeding attempt was made). Information on breeding attempts (nest location, timing and breeding success) were collected based on field observations (including the ringing of chicks to determine the hatching date) or based on data from the GPS tags (mainly in females; GPS positions and accelerometer data). To determine the approximate dates of egg-laying and fledging of chicks, generic values for the length of incubation and nestling periods were applied per species (Appendix 5.1: Table A5.1.2).

The dataset was restricted to 15 defined study areas (Appendix 5.1: Figure A5.1.1), which are used for breeding by the study species. CB were year-round residents within the study areas, while all tagged MoH, MaH and STE (trans-Saharan migrants) and most tagged HH and RK (partial migrants) left the study areas outside the breeding season.

5.3.2. Data processing and analysis

All data processing and analyses were performed in *R* 4.3.1 (R Core Team, 2023). Data were restricted to daytime (except for a methodological validation exercise concerning the proportion of positions classified as being in flight during night, see below), applying solar depression angles of 6° (MoH, HH, MaH, CB), 4° (RK) and 0° (STE; in line with the limits for daytime settings, see above) as limits using the *crepuscule* function (R package suntools; Bivand & Luque, 2023). For the three studied aspects of flight behaviour, different datasets were prepared (Appendix 5.1: Table A5.1.4-6).

5.3.2.1. Time spent in flight

To obtain a dataset with more homogeneous GPS fix intervals for the analysis of the time spent in flight, the GPS tracking data were subsampled to a minimum interval of 15 min. To account for interspecific differences in the time spent in the study areas per year, we considered three different time periods. Period A covered the whole calendar year

(implying a different length of the stay in the study areas per species); period B was the period when all species were present in the study areas, defined as 1 May to 8 August (day of the year 121-220; 100 days); and period C was the period with active nests, which was determined per individual year as the time between 1) seven days before the estimated date of the onset of egg-laying and 2) seven days after the estimated fledging date of the first chick, or, if applicable, the estimated date of nest failure. Note that for periods A and B, data after nest failure were retained within the dataset.

We distinguished between in-flight and stationary GPS positions using the GPS-based ground speed measurements provided along every position. The distribution of speed values typically shows two modes associated with stationary and flight positions, respectively. We used the location of the minimum between the two modes as a threshold, which we determined visually in histogram plots (centre of bin [bin width 0.5 m s^{-1}] with minimum number of positions). The speed threshold was determined separately for low-frequency and high-frequency data for each combination of species and tag manufacturer. It varied between 1.25 and 3.75 m s^{-1} in low-frequency data, and between 0.75 and 2.25 m s^{-1} in high-frequency data (Table A5.1.3). We explored the effect of the different thresholds on the resulting proportion of positions classified as being in flight by applying both the minimum and the maximum threshold values to all species-manufacturer combinations. This showed that the overall differences between species were conserved whatever the applied threshold (Appendix 5.1: Figure A5.1.3)

All six study species are known to be diurnal, normally not flying during night. Hence, to provide an indication for the degree of misclassification, we assessed the proportion of positions classified as being in flight during night. This proportion was generally small (50% of individuals below 0.3%; 90% below 2.2%), but it reached up to 37.5% in some individuals (Figure A5.1.3). Manual inspection of the data suggested that the highest proportions were due to unusually large error in the speed data in the concerned tags (undiscernible minimum between modes in distribution of ground speed), thus we removed individuals with > 10% of flight positions during night for this part of the analysis (n = 11 MoH males; 3 with *Milsar* tags [study area Aumelas], 8 with *UvA-BiTS* tags [study area Groningen]). Eventually, the dataset for time period A comprised 271 individuals, 524 individual years and 3,302,242 GPS positions (see Appendix 5.1: Table A5.1.4 for periods B-C).

Our objective was to obtain the mean time spent in flight per day across the three time periods mentioned above. To correct for uneven seasonal sampling, amongst others due to seasonal variation in the GPS fix interval (see above), the calendar year was split into ten-day periods (TDP). For each combination of TDP, individual and year, the proportion of flight positions during daytime was determined, only considering individual TDP with ≥ 30 GPS positions (n = 7487). The time spent in flight per day was derived by multiplying the proportion of positions in flight during daytime with the average day length in the given TDP at the location of the given individual (applying the solar depression angles mentioned above). We then calculated the mean across individual years per TDP per combination of species and sex (Figure 5.2; only considering TDP with data from ≥ 2 individuals years). Finally, to obtain the overall average, the mean across the means per TDP was

calculated. The same approach was applied for each combination of species, sex and study area with ≥ 10 individual TDP with ≥ 30 GPS positions.

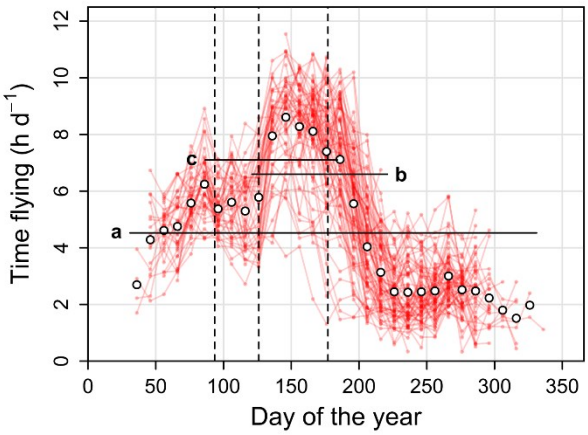

Figure 5.2: Illustration of the applied approach to derive the mean time spent in flight per day corrected for uneven seasonal sampling (example for male Red Kites). Red points and lines represent data per ten-day period for individual years ("bird-years"; n = 74; from 32 individuals). White points: means across individual years per ten-day period; vertical dashed lines: median laying, hatching and fledging dates; horizontal black lines: corrected means for three time periods (a; whole year, b; period of shared presence in the breeding area, i.e. May-August; c: period with active nests [determined per individual year]).

To obtain confidence intervals, we used hierarchical bootstrapping by resampling 1000 times among individual years with replacement. The 2.5% and 97.5% quantiles of the resulting 1000 replicates of the corrected mean time spent in flight were used as limits of the 95% confidence interval. We considered groups (species-sex or species-sex-area combinations) to be significantly different if their 95% confidence intervals did not overlap. Due to the small sample size (number of individual years) for some species-sex-area combinations, the confidence intervals at this level should only be taken as indications. We used bootstrapping instead of mixed modelling because a) the dataset was unbalanced in different regards (e.g. data from only one sex in some species and species-area combinations); b) the non-linear seasonal pattern of time spent in flight was difficult to include in mixed models, as it was species- and sex-specific (Appendix 5.2: Figure A5.2.1-2); and c) bootstrapping allowed to derive combined confidence intervals when multiplying the outcomes on the three considered aspects of flight behaviour (see below).

5.3.2.2. Proportion of flights at risk height

As low-frequency GPS height data are subject to large error which may lead to biases (Péron et al., 2020; T. Schaub et al., 2023), we relied exclusively on the more accurate high-frequency data to determine the proportion of flights at risk height. Furthermore, the data were restricted to flight positions and to individuals with at least 5 h of recorded flights; the resulting dataset comprised 162 individuals and 7,013,897 in-flight GPS positions, i.e. 5,786.1 h of recorded flights (Appendix 5.1: Table A5.1.5). As collision risk height

range, we applied 32-200 m above ground level (a.g.l.), encompassing the rotors 75% of wind turbines installed in the six study countries since 2015 (determined based on The Wind Power, 2022, 2023). The GPS altitude obtained from the tags was height above mean sea level, which we transformed into height a.g.l. by applying the *Shuttle Radar Topography Mission* global digital elevation model with a resolution of 30 m (NASA JPL, 2013). See Appendix 5.1 for additional information on the processing of the GPS height data. To obtain confidence intervals for the proportion of flights at risk height per species and species-area combinations, we used hierarchical bootstrapping by resampling 1000 times among individuals with replacement. Note that for this part of the analysis, we did not distinguish between sexes, as only limited high-frequency data was available from females.

5.3.2.3. Time spent at risk height

The total time spent at risk height within the study areas per species-sex combination ("1" in Figure 5.1) was calculated for the whole calendar year (period A) and for the period of shared presence (period C, see above), by multiplying the average time spent in flight per day T_F with the proportion of flights at risk height P_{RH} and the length of the time period in days (for period A: average number of days present within the study areas per year T_P, determined per species based on the GPS tracking data [see Appendix 5.1 for details]; for period C: 100 d). To obtain confidence intervals for the average time spent at risk height, the bootstrap replicates for the input parameters (see above) were combined (for period A: T_{Fi} x P_{RHi} x T_{Pi}; for period C: T_{Fi} x P_{RHi} x 100) and 2.5% and 97.5% quantiles were calculated on the resulting 1000 combined replicates.

5.3.2.4. Distance from nest

To assess the spatial distribution of flight movements around the nest location, we analysed the distance of flight positions from the nests. The dataset was subsampled to a minimum interval of 15 min (see above) and restricted to the period with active nests (period C; see above) and to completely recorded successful breeding seasons. The latter were defined based on the number of TDP with ≥ 30 GPS positions while the given nest was active, using thresholds ranging from 7 TDP in MoH and HH to 13 TDP in STE (Appendix 5.1: Table A5.1.2). As two male MaH had two successful nests in one year, the analysis was performed on the level of combinations of individual year and nest. The dataset comprised 169 individual year-nest combinations from 111 individuals and 767,208 GPS positions, thereof 230,943 in-flight positions (Table A5.1.6). The distance from nest was calculated for each in-flight GPS position using the function *distGeo* (R package geosphere; Hijmans, 2022).

GPS intervals were not always homogeneous across the breeding season (e.g. due to a reduced number of positions collected during the incubation and early nestling phases in females). To correct for this potential bias, we first determined the average time spent in flight per day for each TDP as in the analysis of time spent in flight (see above). Subsequently, we resampled the in-flight GPS positions within every individual TDP to achieve

the number of flight positions expected with a 15-min interval given the time spent in flight for the TDP in question. The set of resampled GPS positions for each individual year-nest combination was used to derive 50% and 90% quantiles of distance from nest, and the proportion of positions in concentric distance bands of 0.5 km around the nest location. To obtain confidence intervals for the 50% and 90% quantiles, bootstrapping was used by resampling among the individual year-nest combinations with replacement.

To estimate the intensity of space use as a function of distance from nest, we divided the proportion of positions per distance band of 0.5 km by the area size per distance band (area linearly increasing with distance; e.g. 0.8 km^2 for 0.0-0.5 km and 16.5 km^2 for 5.0-5.5 km). Furthermore, the proportion of positions per area for each distance band was multiplied by the average time spent in flight per day and the proportion of flights at risk height to obtain the time spent at risk height per area as a function of distance from nest ("2" in Figure 5.1).

5.4. Results

5.4.1. Time spent in flight

The mean time spent in flight across the calendar year was higher in males than in females in all five species with data available from both sexes (males flying on average 1.5-2.2 times more than females; Figure 5.3a, d; Table A5.2.1). Time spent in flight per day varied greatly between species, ranging from 0.5 (CB) to 3.4 (MoH) h in females and from 1.0 (CB) to 7.4 (MoH) h in males (Figure 5.3; Table 5.1). When considering only the period of shared presence in the breeding areas (May-August) or periods with active nests, the differences between species stayed substantial, although the ranking of species was somewhat modified (e.g. second place for RK males [7.1 h d^{-1}] together with MaH [6.5 h d^{-1}] behind MoH [8.2 h d^{-1}] with active nests; Table A5.2.1). There was only little variation in time spent in flight between study areas (Figure 5.4a, b; Table A5.2.2).

5.4.2. Proportion of flights at risk height

The proportion of flight positions at collision risk height (32-200 m a.g.l.) varied between 12.4% (MoH) and 56.4% (RK; Figure 5.3b). Most pairwise comparisons between species were significant (Table 5.1), but note the large CI in STE (Figure 5.3b; Table A5.2.3). Again, variation between study areas was small relative to the variation between species (Table 5.1; Figure 5.4c; but note significant differences between some study areas in MoH and RK; Table A5.2.4).

5.4.3. Time spent at risk height

As a result of the found differences in time spent flying, proportion at risk height and the number of days spent in the breeding area (Figure 5.3e; Table A5.2.5), the time spent at risk height within the breeding areas across the whole calendar year varied significantly between species (Figure 5.3c, f; Table A5.2.6). It was highest in RK, both in females (342 h y^{-1}; 1.7-7.4 times more than in the other species) and males (609 h y^{-1}; 3.5-6.0 times more than in the other species). STE had the second highest mean in females (202 h y^{-1}), but note the large confidence interval (125-308 h y^{-1}). When restricting the comparison to the period of shared presence in the breeding areas (May-August), RK still stood out compared to MoH, HH, MaH and CB (3.8-6.4 times more in RK females; 3.6-4.6 times more in RK males; Figure A5.2.3; Table A5.2.6).

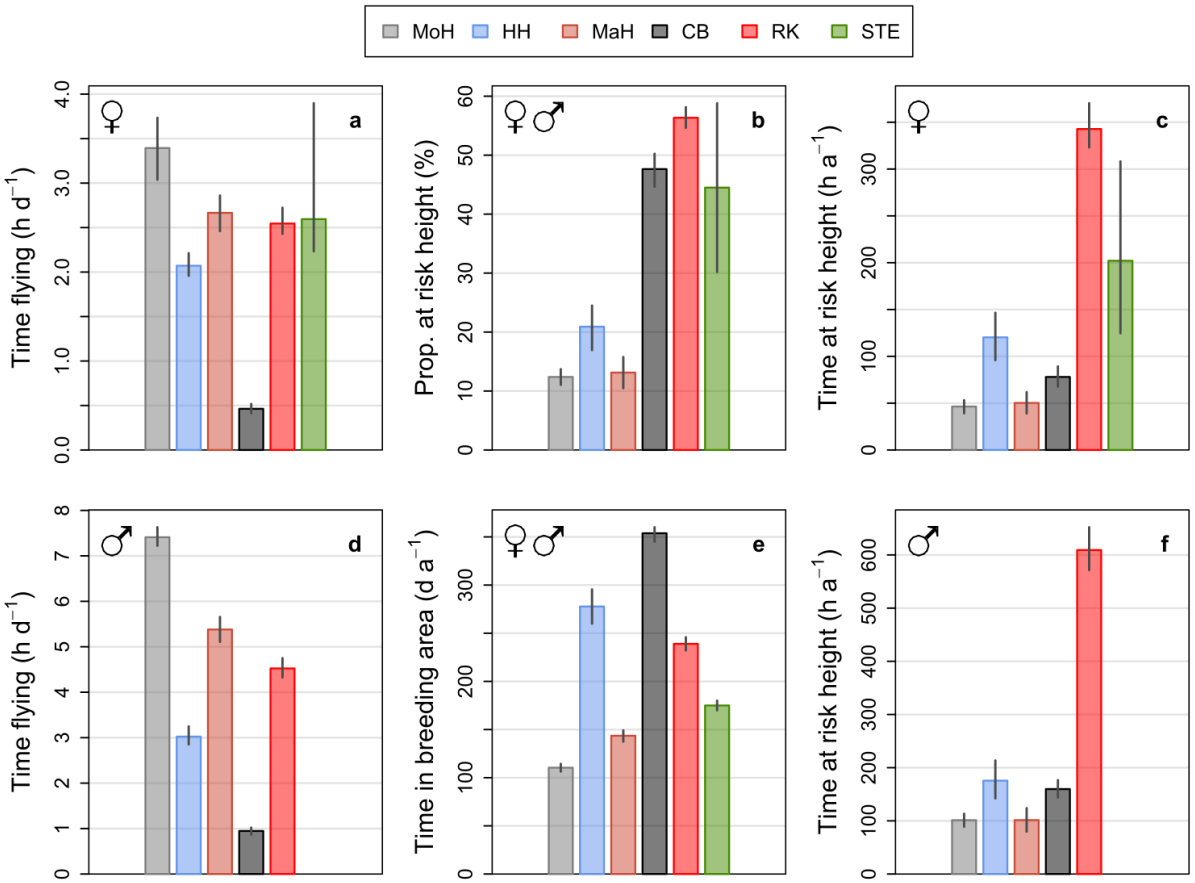

Figure 5.3: Time spent in flight per day (**a**, **d**), proportion of flight positions at risk height (**b**), time spent within the breeding area (**e**) and time spent at risk height within the breeding area per year (i.e. the product of the three previous aspects; **c**, **f**) for six raptor species (means and 95% confidence intervals from bootstrapping). Note different y-axis scales between females and males. Sexes were lumped in **b** and **e**. See Appendix 5.2: Table A5.2.1, Table A5.2.3 and Table A5.2.5-6 for sample sizes, and Figure A5.2.3 for corresponding results for the period of shared presence in the breeding area (May-August). a = year.

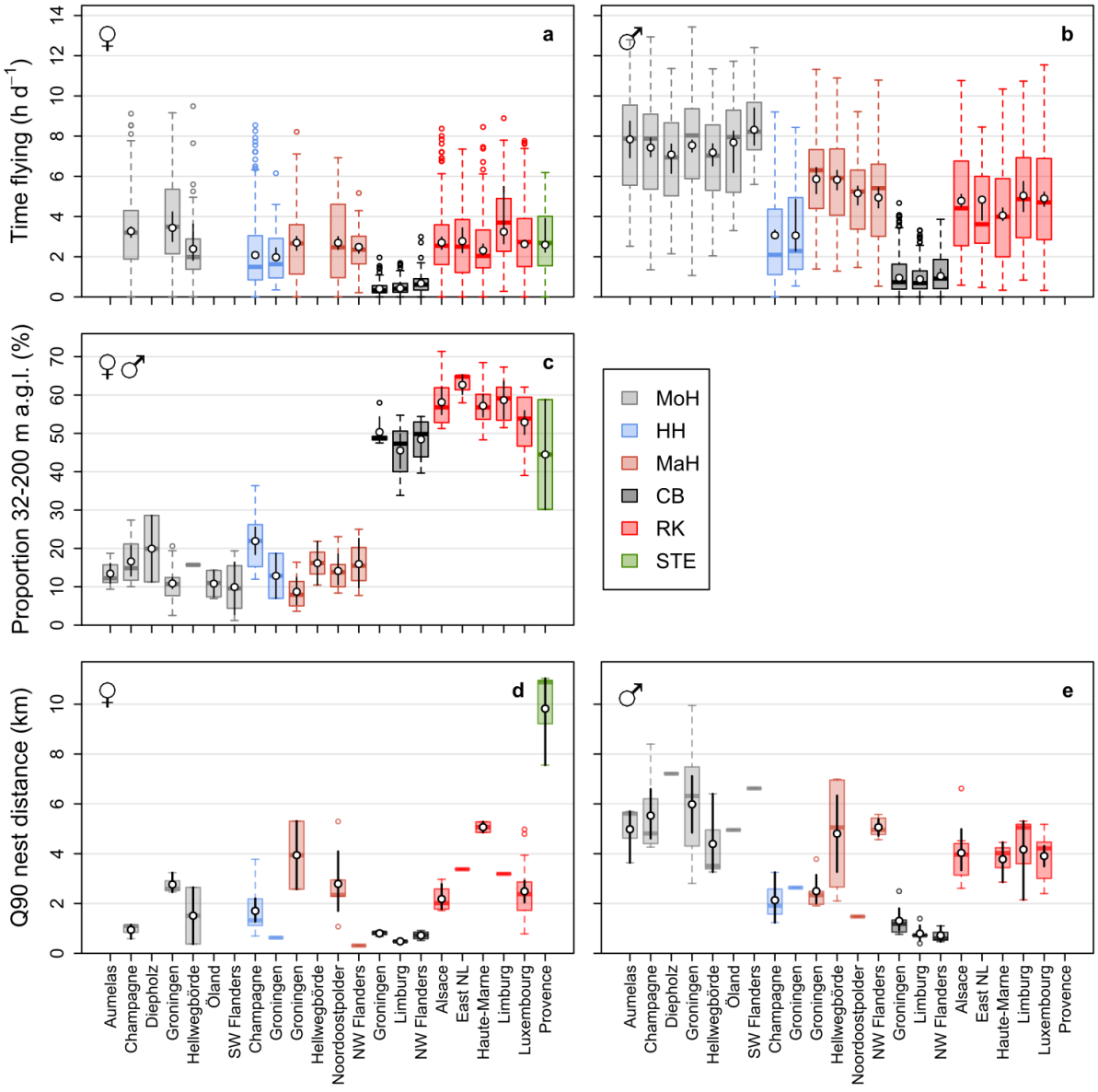

Figure 5.4: Variation between study areas in three aspects of flight behaviour for breeding birds of six raptor species. **a** & **b**) Time spent in flight per day during the whole calendar year ("period A"); boxplots: data per individual ten-day periods (hence including seasonal variation); overlaid points: means for the whole year corrected for unbalanced seasonal sampling. **c**) Proportion of flight positions at risk height (females and males lumped); boxplots: data per individual. **d** & **e**) 90% quantile of distance from nest for complete successful breeding seasons; boxplots: data per combination of individual year and nest. In all panels, overlaid points and vertical black lines indicate means and 95% confidence intervals from bootstrapping. See Appendix 5.2: Table A5.2.2, Table A5.2.4 and Table A5.2.8 for sample sizes. MoH = Montagu's Harrier, HH = Hen Harrier, MaH = Marsh Harrier, CB = Common Buzzard, RK = Red Kite, STE = Short-toed Eagle.

Table 5.1: Proportion of significant pairwise comparisons between species, and between study areas within species, in relation to the total number of pairs for different aspects of flight behaviour. For time flying and nest distance, only pairwise comparisons within sexes were considered (sex not considered for proportion at risk height). Prop. = proportion.

Aspect	Between species	Between areas (within species)
Time flying		
Whole year	21 / 25	5 / 64
Shared presence	17 / 25	-
Active nests	15 / 25	-
Prop. at risk height	12 / 15	3 / 35
Time at risk height		
Whole year	21 / 25	-
Shared presence	13 / 25	-
Nest distance		
Median	15 / 25	7 / 28
Q90	18 / 25	7 / 28

5.4.4. Distance from nest

Both the 50% and 90% quantiles of distance from nest were smaller in females than in males (Figure 5.5; e.g. 1.8 vs. 5.6 km for the mean 90% quantile for female and male MoH), but the difference was not significant in all cases for the 90% quantile (HH, MaH and CB; Table A5.2.7). Individual variation was large (e.g. 90% quantile ranging between 2.8 and 9.9 km in MoH males), resulting in relatively wide confidence intervals (Figure 5.5; Table A5.2.7). In females, the mean 90% quantile varied between 0.7 km (CB) and 9.8 km (STE); and in males between 1.0 (CB) and 5.6 km (MoH). There was more variation between study areas than for the other two studied aspects of flight behaviour (Table 5.1; Figure 5.4d, e; Figure A5.2.4; Table A5.2.8).

Overall, the proportion of positions in distance bands of 0.5 km decreased with increasing distance from nest, while the slopes differed between species and sexes (Figure A5.2.5; see Figure A5.2.6-7 for individual variation). When considering the proportion of positions per km^2, the decrease with distance was even more pronounced, especially between the 0.0-0.5 km and the 0.5-1.0 km distance band (e.g. 98.6% km^{-2} in the first compared to 8.2% km^{-2} in the second band in CB females; Figure A5.2.5).

Consequently, the time at risk height per km^2 also decreased with increasing distance from nest in all species and in both sexes, while the ranking of species changed along the distance scale (Figure 5.6). In females, between 0-2.5 km, the amount of time at risk height per km^2 was greatest in RK, while above 2.5 km, it was greatest in STE. In males, RK had the highest value in all distance bands until 6.5 km, with MoH taking over at higher distances. CB males spent on average nearly as much time at risk height as RK in the smallest distance band (0.0-0.5 km), but much less at higher distances (e.g. time at risk height 9.3 times larger in RK than in CB at 1-1.5 km, and 21.8 times larger at 1.5-2 km; Figure 5.6).

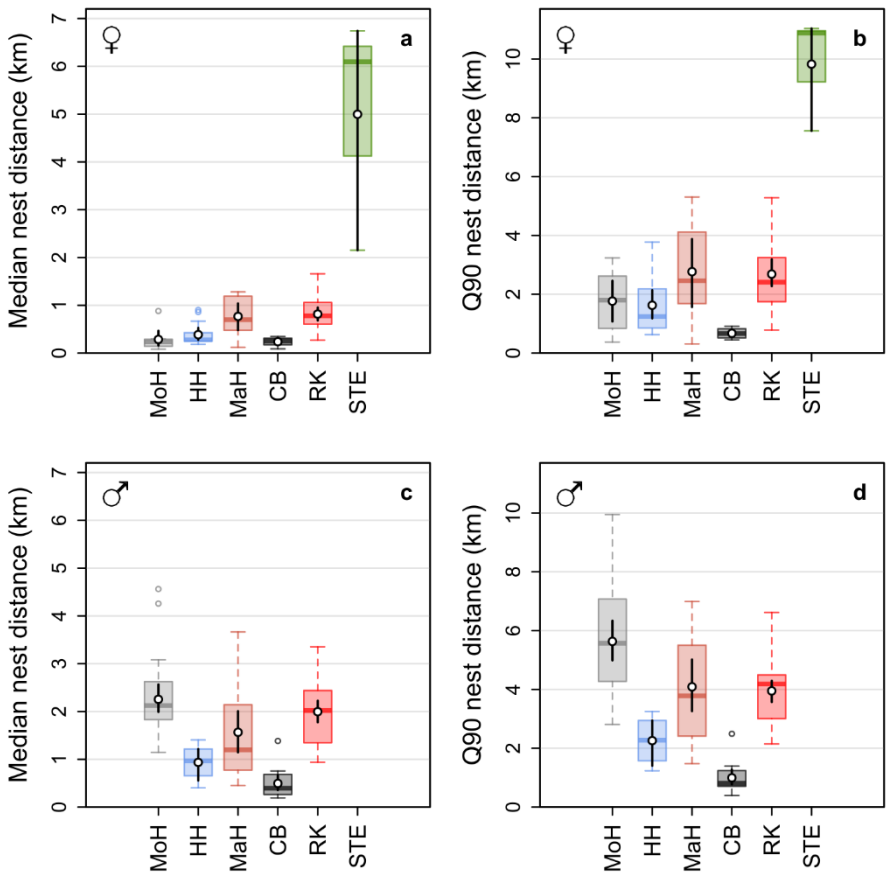

Figure 5.5: Median (**a**, **c**) and 90% quantile (Q90; **b**, **d**) of distance from nest for complete successful breeding seasons. Overlaid white points represent means (black bars: confidence intervals from bootstrapping). MoH = Montagu's Harrier, HH = Hen Harrier, MaH = Marsh Harrier, CB = Common Buzzard, RK = Red Kite, STE = Short-toed Eagle. See Appendix 5.2: Table A5.2.7 for sample sizes.

5.5. Discussion

Our study of flight behaviour in six raptor species based on extensive GPS-tracking data, including high-frequency data providing high vertical accuracy, illustrated how variation in the time spent in flight, the proportion of flights at risk height (i.e. within the height range of wind turbine rotors) and the distances travelled from the nest site translates into interspecific and spatial variation in the sensitivity to wind turbines collisions. This approach is valuable as it improves the understanding of wind turbine collision risk and allows to compare the species-specific sensitivity irrespective of current exposure, which may ultimately help to reconcile wind energy development with bird conservation.

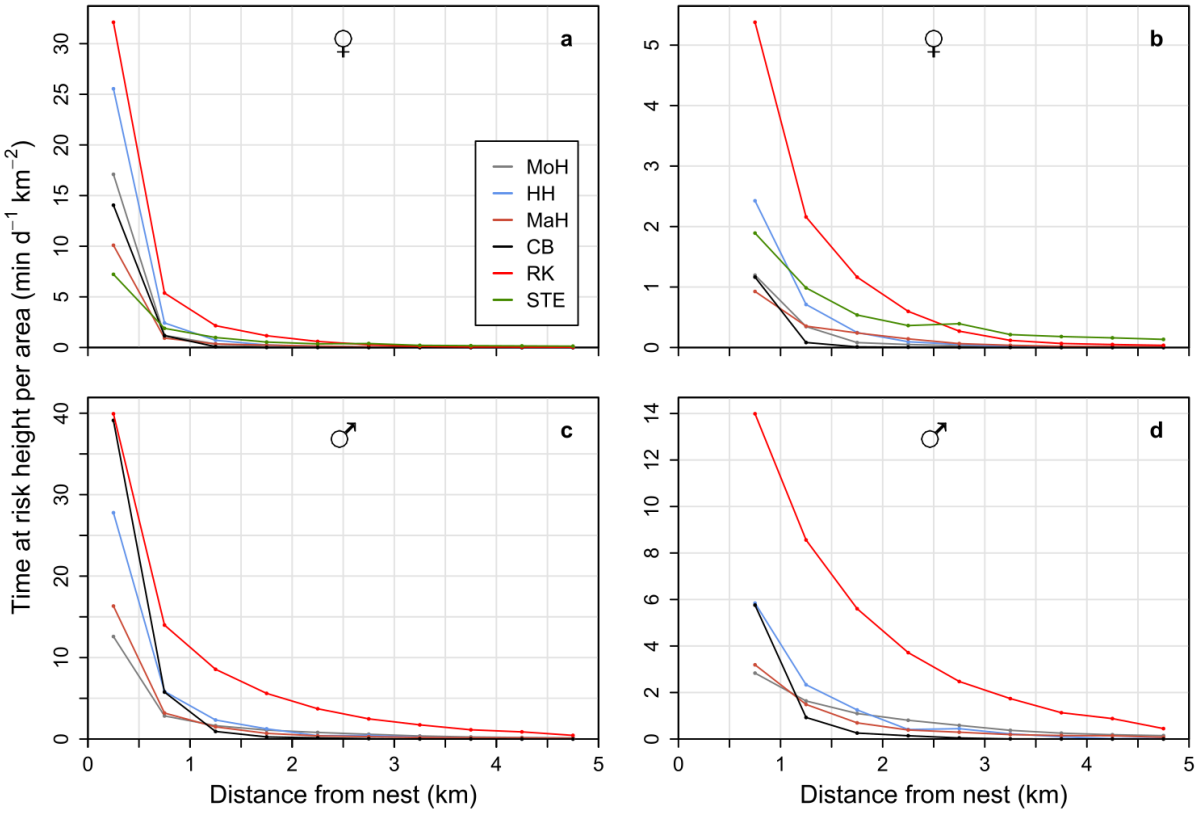

Figure 5.6: Time spent at risk height (32-200 m a.g.l.) per km² as a function of distance from nest for complete successful breeding seasons (distance bins of 0.5 km; means across individual breeding seasons). Panels **b** and **d** are zoomed-in versions of **a** and **c** with shortened y-axis (distance bin 0.0-0.5 km excluded). Note different y-axis scales between females and males.

5.5.1. Sensitivity based on time spent flying and proportion of flights at risk height

We found that both the time spent in flight and the proportion of flights at risk height varied considerably between species, with profound effects on the sensitivity to wind turbine collisions. The comparison between species highlighted that sensitivity is determined by the interaction of both aspects: for example, the sensitivity (time spent at risk height per year) for both MoH and CB was relatively low. However, in MoH, this was the result of flying much in combination with a low proportion of flights at risk height, whereas CB flew little, but with a high proportion at risk height. By contrast, RK were found to both fly relatively much and often at risk height, resulting in a notably high relative sensitivity. This matches the general perception of RK being a particularly collision-prone species. For example, RK are the species with the second-highest number of reported fatalities in Germany (Dürr, 2023) and the number of fatalities divided by the national population size (Gedeon et al., 2014) is about 7 times higher in RK than in CB (but note that this comparison does not involve corrections for potential biases related to e.g. geographical distribution of search effort or differences in reporting probability between species).

Overall, the time spent in flight and the proportion of flights at risk height varied more between species than between study areas. This implies that these aspects of flight behaviour can be considered as (more or less) fixed characteristics of the species, closely related to their ecology and behaviour. Thus, it generally appears possible to transfer the results between areas in the species studied here. This is helpful when wind farms are developed in areas from which no data is available. However, this might not apply to areas with very different landscape characteristics (topography, land use, climate etc.) compared to the study areas considered here. Moreover, our results only apply to the stay in the breeding areas. It would thus be valuable to apply a year-round perspective on the time spent in flight and the proportion of flights at risk height in future studies, including the migration period and the stay on the wintering grounds.

Besides interspecific variation, our results show large differences in time spent in flight between sexes in all five species for which data on both sexes were available, with males flying about twice as much as females when considering the whole period of presence in the study areas (range of 1.5-2.2 among species). This is in line with the fact that in all five species, the duties of incubation and brooding are predominantly fulfilled by the females, while the males hunt and supply prey (del Hoyo et al., 1994). As a consequence of the larger amount of time spent in flight, we found a higher sensitivity to wind turbine collisions in males than in females. However, it has to be noted that these differences could change when sex-specific variation in the proportion of flights at risk height are considered, which was not possible here. For example, a higher proportion of flights at risk height in female MaH compared to males was reported in earlier studies (Grande, 2017; Buij et al., 2022), whereas no sex-specific differences in mean flight height were found in RK (Pfeiffer & Meyburg, 2022). For MoH, there are indications of a higher collision risk in males than in females based on carcass searches (Bouzin, 2013). Moreover, time spent in flight can be expected to vary according to factors like season (e.g. highest flight activity during the nestling phase; Appendix 5.2: Figure A5.2.1-2), time of day or weather, but these were beyond the scope of this study.

It also should be noted that our approach does not provide a complete account of sensitivity to wind turbine collisions. Additional factors might modify the ranking of species, such as avoidance behaviour, morphology (e.g. bird size), population size and population dynamics (higher population effects of increased mortality in species with low pace of reproduction; Diffendorfer et al., 2021). Avoidance behaviour on different spatial scales is assumed to vary between species (SNH, 2018), but clear evidence from data is lacking, especially for the smaller spatial scales. Note that avoidance behaviour also includes aspects like visual capacity or manoeuvrability, which have been identified as important aspects of avian sensitivity to wind turbine collisions (May, 2015). Concerning RK, it has been suggested that the high perceived sensitivity (see above) was due to a lack of avoidance behaviour (Hötker, 2017), but recent studies have shown a substantial degree of wind turbine avoidance in RK (Mercker et al., 2023; Reichenbach et al., 2023). Here, we show that a high sensitivity in RK compared to other raptor species could "simply" result from basic aspects of flight behaviour, i.e. time spent in flight and proportion of flights at risk height.

5.5.2. Spatial sensitivity

We found that the proportion of time spent in a given area, and consequently the sensitivity to wind turbines collisions, decreased with increasing distance from nest in all species. Similar results have been obtained in earlier studies (Eichhorn et al., 2012; Rasran et al., 2017; Tikkanen, Rytkönen, et al., 2018; T. Schaub et al., 2020). With our comparative approach, we could show that the ranking of species changed over distance. For example, despite of a much lower overall amount of time spent in flight, CB males were on average nearly as sensitive to collisions as RK males at lowest distance from the nest (0-500 m; but much less sensitive at larger distances). This illustrates how the interplay of the three considered aspects of flight behaviour shapes sensitivity to wind turbine collisions. Note that we did not account for a potential effect of distance from nest on the proportion of flights at risk height, which would be a valuable improvement for future studies. For example, certain flight behaviour could predominantly be performed in the vicinity of the nest site (e.g. display or guarding flights), which could affect the proportion at risk height.

Regarding distance from nest (50% and 90% quantiles), our results showed more variation between study areas and individuals than for the two other aspects of flight behaviour. It can be expected that this variation is due to factors like habitat suitability (including prey density), spatial distribution of suitable habitats, spatial configuration of individual territories, individual preferences etc. Also in seabirds, a considerable amount of regional and individual variation in foraging distances from the breeding colony was found (Cleasby et al., 2023).

5.5.3. Implications for management

In this study, we provided a framework to assess the sensitivity of bird species to wind turbine collisions irrespective of current exposure based on basic aspects of flight behaviour and space use. If the sensitivity of different species is known, species can be prioritised during wind energy planning, regarding site selection and the mitigation measures to apply. However, this approach does not yet provide a complete account of sensitivity, as for example avoidance rate, population size and population dynamics were not considered. This would be a valuable pathway for future studies.

Concerning the site selection for wind energy projects, our results lead to the conclusion that an increasing distance between wind turbines and nest sites (or key breeding areas) reduces collision risk of breeding birds, and that especially wind turbines at close vicinity of nests should be avoided. The distance quantiles we provided can serve as first indications for the distances to keep for each species; the 90% quantile could be applied to be "on the safe side". However, defining a threshold is not straightforward: as sensitivity differs between species, it appears sensible to apply different quantiles as a threshold (e.g. larger quantile for species with high sensitivity such as RK). Ideally, a threshold should be based on a complete assessment of sensitivity (see above), amongst others accounting for the species-specific population dynamics (e.g. larger threshold for slowly

reproducing species with higher population effects of additional mortality). It should also be noted that distance from nest only gives a first indication of the expected intensity of use of a given area of interest, as other factors such as habitat type also play an important role (Tikkanen, Rytkönen, et al., 2018; Heuck, Herrmann, et al., 2019). For example, high habitat quality can lead to an intensity of use which is higher than expected based on distance from nests alone. These additional aspects should be considered within the environmental impact assessments for planned wind energy projects.

5.6. Acknowledgments

We would like to thank everyone involved in the local GPS tracking projects, amongst others J. Isambert, C. Montégu, L. Boldt, A. Schlaich, B. Koks, J. Rougé and Werkgroep Roofvogels Noordoostpolder (see Appendix 5.3 for a full list of involved persons and organisations); Boralex, EDPR, Soler, natur&ëmwelt, SICONA, CSD Ingénieurs and Collectief Groningen West for allowing data use for this study; all farmers and landowners who gave permission to access their land for fieldwork; R. Zydelis (Ornitela), P. Otulak (Milsar) and W. Bouten (UvA-BiTS) for support with the GPS tags; and B. Nolet, C. Thaxter, S. Chamaillé-Jammes and A. Leriche for helpful comments and advice. TS' PhD position was co-funded by ANRT and ENGIE (Cifre grant 2020/0448). See Appendix 5.3 for information on funding for the local GPS tracking projects.

5.7. Author contributions

TS, RK, CDZ and AMil conceptualised the study. TS, RK, PA, JLB, RB, CG, HI, JI, KJ, SL, AMio, GM, SR, GS, BVH, KW and AMil organised the local GPS tracking projects and did fieldwork. TS performed data processing and data analysis. TS, RK and AMil wrote the first draft. All authors contributed to subsequent drafts and approved the final manuscript.

5.8. Conflicts of interest

This study was partly funded by the energy company ENGIE (TS's PhD position and part of the GPS tracking work). However, the scientific orientation of the PhD project was directed by the partner universities (Aix-Marseille University and University of Groningen), and academic freedom in publishing the results was guaranteed by a partnership agreement. We certify that the results were not influenced by the company's economic interests.

6. Synthesis and general discussion

The transition to renewable energy sources is a major component of the strategies to mitigate anthropogenic climate change (IEA, 2021). However, renewable energy facilities such as wind farms, solar farms and hydropower plants pose threats to biodiversity and could therefore reinforce the global biodiversity crisis (Pörtner et al., 2021). To reconciliate the energy transition with biodiversity conservation, the development of renewable energy facilities needs to be accompanied by appropriate mitigation measures. Wind energy development in particular involves direct mortality of flying animals (birds, bats and insects) by collisions with wind turbines (Perrow, 2017). An array of mitigation measures for this conflict have been proposed (Marques et al., 2014; Arnett & May, 2016), but their effectiveness to reduce collision risk for the various concerned species remains to be proven.

In this PhD thesis, I studied the wind turbine collision risk of birds of prey of the order Accipitriformes. These are commonly perceived as particularly vulnerable to wind turbine collisions: first, raptors generally exhibit high collision rates (De Lucas & Perrow, 2017; Thaxter et al., 2017) and secondly, they are long-lived with low reproductive rates, implying potentially large impacts of an increased mortality on population growth (Carrete et al., 2009; Bellebaum et al., 2013). I adopted a mechanistic approach based on flight behaviour, which was conceptually divided into different aspects such as the time spent in flight and the frequency distribution of flight height. These aspects were studied comparatively in six European raptor species using individual-based GPS tracking. The main objectives were to

1) improve the understanding of wind turbine collision risk in birds of prey (relative sensitivity of the six study species to wind turbine collisions, interplay of different aspects of flight behaviour) and
2) assess the effectiveness of selected mitigation measures (selection of wind turbine dimensions, site selection accounting for distance to nest locations).

6.1. Main results from this thesis

6.1.1. Accuracy of height data from GPS tags

Information on the flight height of birds is vital to assess their collision risk with wind turbines. However, collecting accurate flight height data has proved challenging. Therefore, in **chapter 3**, we assessed two methods which could improve the accuracy of height data obtained from GPS tags:

1) high-frequency GPS tracking with fix intervals of 2-3 s, where the GPS remains turned on between fixes ("continuous mode"; as opposed to standard low-frequency GPS tracking with fix intervals ≥ 5 min) and,
2) barometric altimetry using air pressure loggers integrated in the GPS tags.

In the high-frequency GPS data, the random error (noise) in the height data was substantially reduced compared to the low-frequency GPS data, resulting in an increased overall vertical accuracy. Also in the barometric height data, noise was reduced, but there was increased systematic error (bias), resulting in an intermediate overall accuracy between low- and high-frequency GPS data.

Simulations showed that the extensive noise found in the low-frequency GPS data may have pronounced effects on the shape of the flight height distribution (flattening out peaked distributions) and the proportion of positions within the collision risk height range, whereas the remaining vertical error in barometric and high-frequency GPS data only led to small biases. We discussed that high-frequency GPS tracking, besides providing the highest vertical accuracy, has the additional advantages of increased horizontal accuracy and high temporal resolution, allowing detailed analyses of flight trajectories in 3D, for example regarding wind turbine avoidance (Figure 6.1). Despite the risk of a systematic bias, barometric altimetry could be an alternative approach to obtain relatively accurate flight height data, especially when battery charging of tags is limited. The accuracy in barometric height data might be further improved by more advanced calibration methods.

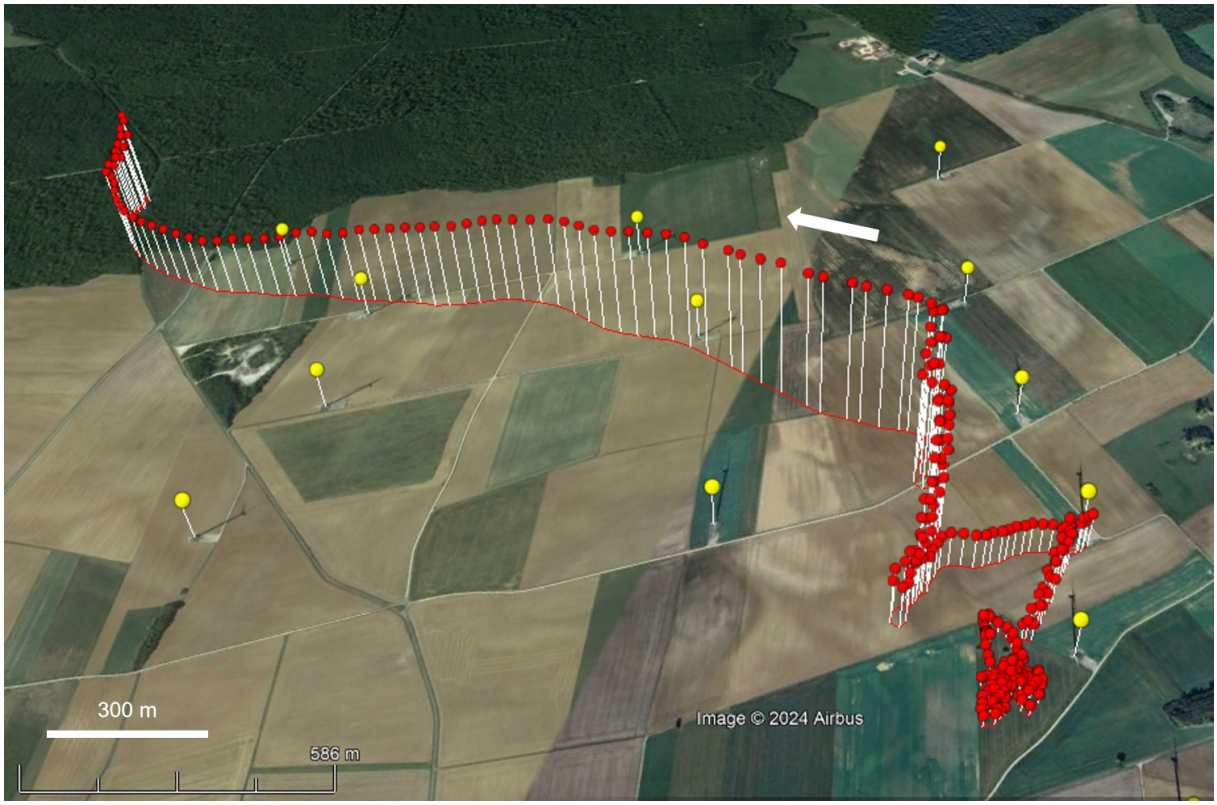

Figure 6.1: Example of a flight trajectory of a Red Kite within a wind farm (study area Haute-Marne/FR) recorded with high-frequency GPS tracking (fix interval 3 s; max. flight height: 414 m a.g.l.). Yellow points: wind turbine hubs (100 m a.g.l.; rotor diameter 92 m); white arrow: direction of flight. Map: *Google Earth*.

6.1.2. Flight height distributions and effect of wind turbine dimensions on collision risk

In **chapter 4**, we determined the flight height distributions of the six study species during their stay in the breeding areas, and used them to assess the effect of wind turbine dimensions (ground clearance and rotor diameter) on collision risk. As highest accuracy in the height data was required to correctly determine the shape of the flight height distribution (as shown in chapter 3), this analysis was exclusively based on high-frequency GPS data. We found that five out of six species had clearly unimodal flight height distributions with a mode below 25 m above ground level. Consequently, for these species, the theoretical collision risk decreased substantially with increasing ground clearance of wind turbines. Moreover, with increasing rotor diameter at fixed ground clearance, the collision risk per MW decreased. By contrast, a more uniform flight height distribution with a weak mode between 120-260 m was found in Short-toed Eagles. This resulted in opposite outcomes regarding the effect of wind turbine dimensions on collision risk compared to the other five species (increased risk with increasing ground clearance, stable risk per MW with increasing rotor diameter at fixed ground clearance).

These findings indicated that the selection of wind turbine dimensions affects the collision risk of raptors. As the effect varied between species, wind energy planning should

consider which bird species occur locally to optimise wind turbine dimensions. For species with a low mode of flight height (i.e. presumably the majority of bird species), increasing ground clearance mitigates collision risk, and installing wind turbines with particularly low ground clearance is unadvisable (Figure 6.2). Moreover, for these species, the collision risk for a given total power output can be reduced by using fewer turbines with larger diameter instead of more turbines with smaller diameter (if ground clearance is constant).

Figure 6.2: Examples of recently installed wind turbines with particularly low ground clearance. Left: Ground clearance 11 m, diameter 138 m, 4.2 MW, installed in 2023 (in comparison to older turbine with higher ground clearance [45 m] and smaller rotor diameter [40 m; 0.5 MW] in the background). North Rhine-Westphalia, Germany. Right: Ground clearance 18.5 m, diameter 131 m, 3.6 MW, installed in 2022. Drenthe, the Netherlands. Photos: H. Illner, H. J. Ottens.

6.1.3. Species-specific sensitivity to wind turbine collisions

Chapter 5 was dedicated to the sensitivity of the six study species to wind turbine collisions based on three aspects of flight behaviour, i.e. the time spent in flight, the proportion of flights at risk height and the distance travelled from the nest location. For all three aspects, we found considerable variation between species and sexes. The average time spent in flight during the stay in the breeding areas ranged from 0.5 (Common Buzzard) to 3.4 h d^{-1} (Montagu's Harrier) in females and from 1.0 (Common Buzzard) to 7.4 h d^{-1} (Montagu's Harrier) in males. The proportion of flights at collision risk height varied between 12.4% (Montagu's Harrier) and 56.4% (Red Kite). In both aspects, variation between study areas was relatively small, implying that the results could be transferred to areas where no tracking data were collected. The largest total amount of time at risk height per year was found in Red Kites (1.7-7.4 times more than in the five other species). These results indicated that basic characteristics of flight behaviour could explain

substantial differences in the sensitivity to wind turbine collisions among raptor species, and confirmed a particularly high sensitivity in Red Kites.

The average 90% quantile of distance from nest ranged from 0.7 km (Common Buzzard) to 9.8 km (Short-toed Eagles) in females, and from 1.0 km (Common Buzzard) to 5.6 km (Montagu's Harrier) in males (Figure 6.3; note that no data were available from male Short-toed Eagles), but variation between individuals (and possibly between study areas) was considerable. With increasing distance from nest, the expected time spent at risk height per km^2 decreased in all species, while the ranking of species changed over distance (e.g. Common Buzzard nearly as sensitive as Red Kite at 0-500 m from the nest in males). These results lead to the conclusions that installing wind turbines in the vicinity of nest locations should be avoided, and that possible threshold distances need to be species-specific.

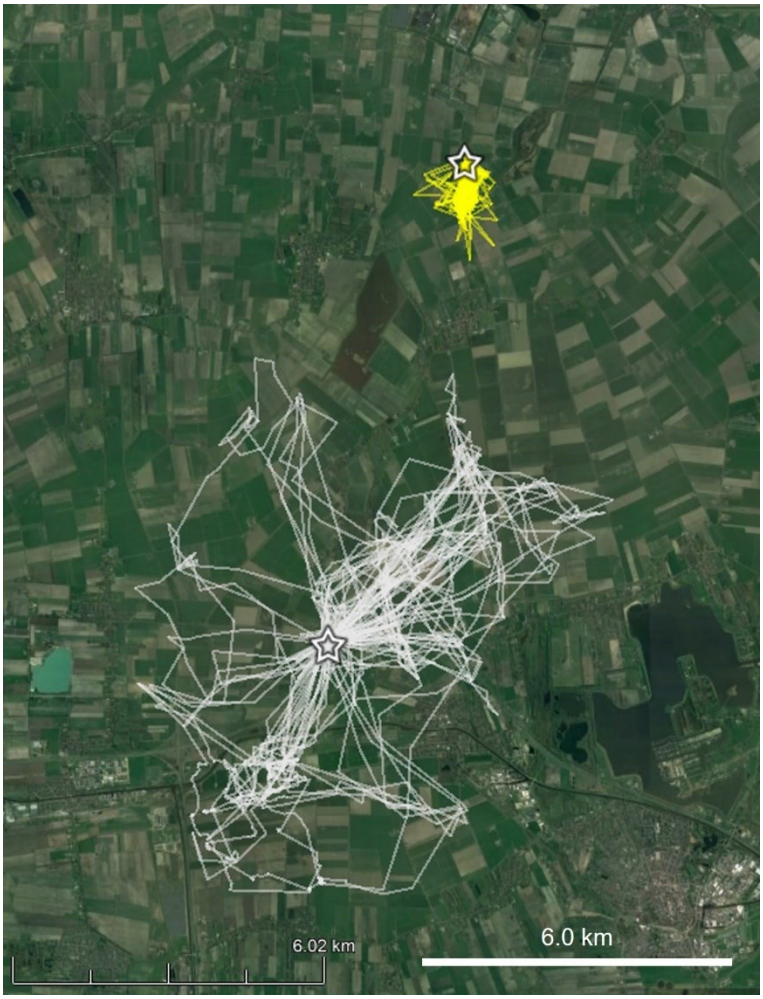

Figure 6.3: Example home ranges of a male Montagu's Harrier (white) and a male Common Buzzard (yellow) in the study area Groningen (NL) in 2023, illustrating the found interspecific differences regarding the distances travelled from the nest location (stars). For both individuals, the locations during the 1st week after the hatching of young are indicated. Map: *Google Earth*.

6.2. Implications for mitigation measures

A variety of measures to mitigate wind turbine collision risk have been proposed (Marques et al., 2014; May, 2017), acting on different aspects of flight behaviour (Table 6.1). Out of these, two were studied in this thesis, i.e. informed selection of wind turbine dimensions (ground clearance, rotor diameter) and informed site selection (spatial planning) based on the distance from nest locations of concerned species. For both measures, the results from this thesis indicated a large mitigation potential. For example, the collision risk per MW varied by more than a factor of 10 among the considered combinations of wind turbine dimensions in five out of six species. Moreover, with both measures the mitigation of collision risk can potentially be achieved without energy production losses. This is in contrast to shutdown (curtailment) schemes (Table 6.1) which are per definition associated with (possibly substantial) production losses.

Table 6.1: Possible measures to mitigate wind turbine collision risk in birds, assigned to the aspect of flight behaviour on which they act (red: studied in this PhD thesis). Pre-defined shutdown refers to the shutdown of wind turbines in pre-defined conditions with high collision risk, e.g. based on season or weather. Note that shutdown based on real-time detection of approaching birds (McClure et al., 2018) is not included in the scheme.

Time in flight	Time at rotor height	Time in wind farm	Avoidance behaviour
• Pre-defined shutdown	• Informed selection of wind turbine dimensions • Pre-defined shutdown	• Spatial planning (e.g. based on distance from nests) • Habitat management • Pre-defined shutdown	• Increased visibility of turbines • Deterrent systems

In this thesis, I did not attempt to define thresholds regarding both wind turbine dimensions and distance from nests (e.g. minimum ground clearance or minimum distance to nests to be kept when installing wind farms). Defining such thresholds is difficult due to the gradual nature of the relationships (e.g. collision risk gradually decreasing with increasing ground clearance). Moreover, to determine meaningful species-specific thresholds, absolute collision rates and effects on populations would need to be known (see section 6.3). Eventually, defining thresholds is a political-societal decision on the acceptable number of bird collisions and the acceptable degree of population decline, in light of the major benefits of wind energy for the energy transition and reduction of greenhouse gas emissions.

Regarding the effect of wind turbine dimensions on collision risk, we found that increasing the ground clearance of wind turbines at fixed rotor diameter, and using fewer turbines with larger rotor diameter at fixed ground clearance, reduced the collision risk per MW for five out of six study species, whereas the opposite was true for Short-toed Eagles. These results highlight a major complexity with respect to mitigation measures:

their effectiveness is species-specific, and the effects may even be opposite for different species. This implies that if species with such opposite responses occur in the same area, trade-offs between benefits for some species and costs for others have to be made. In this context, the identification of sensitive species based on flight behaviour (this thesis, chapter 5), life-history traits, conservation status and other traits (Gauld et al., 2022) helps to prioritise between species. For making these trade-offs in the best possible way, it is crucial to complete the body of knowledge for the various concerned species. It should be a research priority to collect accurate flight height data for as many species as possible, so that flight height distributions and the effect of wind turbine dimensions on collision risk can be assessed broadly.

Besides birds, decisions on wind turbine dimensions and siting must also consider bats, another group of flying animals affected by wind turbine collisions, possibly more severely than birds (Barclay et al., 2017; Thaxter et al., 2017). Concerning wind turbine dimensions, different studies have shown contrasting effects of turbine dimensions on the collision rates of birds and bats. For example, Barclay et al. (2007) found a strong increase in collisions of (migrating) bats with tower height based on carcass search data, but no effect on birds (without distinguishing between species). Thaxter et al. (2017) found that collision rates per MW decreased with increasing rated power of wind turbines in birds and bats, but in bats, it increased again at the highest power (up to 2.5 MW), although with a wide confidence interval. Note that ground clearance or tower height were not taken into account in the latter study. Based on acoustic monitoring, Leroux *et al.* (2023) found that bat activity was negatively affected by rotor diameter, leading to the recommendation of avoiding larger rotor diameters to minimise habitat loss. However, the increase of power capacity with increasing rotor diameter was not taken into account in this analysis. In general, the possibilities to track bats with GPS tags to obtain accurate flight height data and assess flight height distributions are restricted due to the small body size (but see Roeleke et al., 2016).

6.3. Strengths and limitations of the mechanistic approach based on flight behaviour

This thesis illustrates several strengths of the approach to assess wind turbine collision risk based on flight behaviour in combination with collision risk models, as compared to the second main approach based on carcass searches. First, as collision risk models encompass a range of input variables both concerning the flight behaviour of the study species and the technical characteristics of wind turbines, they offer a great flexibility of theoretical analyses (scenario studies) by varying individual input variables while keeping the other variables constant. In this thesis, this allowed to estimate the effect of ground clearance and rotor diameter on collision risk (chapter 4), assuming constant flight behaviour and exposure (bird density close to wind turbines). Such analyses are much more difficult to make based on carcass search data, as in general, multiple factors vary between

wind farms and individual wind turbines at a time, for example wind turbine dimensions (often both rotor diameter and ground clearance), other technical characteristics such as rotation speed and especially the species-specific density bird species in the surroundings (which is often not precisely known). Hence, large sample sizes are required to disentangle the multitude of factors.

Secondly, the division into multiple input variables improves the understanding of wind turbine collision risk by providing mechanistic insights. In this thesis, I showed how the interplay of different aspects of flight behaviour affected the species-specific sensitivity to wind turbine collisions. For example, in certain species, a large amount of time spent in flight was balanced out by a small proportion of flights at risk height (Montagu's Harrier, Marsh Harrier), or vice versa, a large proportion of flights at risk height was balanced out by a low amount of time spent in flight (Common Buzzard). By contrast, in Red Kites, high values in both aspects added up to a particularly high relative sensitivity (chapter 5). Moreover, the interplay of different technical characteristics of wind turbines was illustrated. For example, a larger rotor diameter implies an increased risk volume and hence an increased collision risk, but this increase is buffered by a reduced rotation speed which in turn reduces collision risk (chapter 4).

Thirdly, it was possible to determine the species-specific sensitivity to wind turbine collisions irrespective of current exposure (chapter 5). Therefore, this approach can also be applied for species which are not yet exposed to wind farms in their distribution range, which is not possible using carcass search data. Fourthly, the value of the approach based on flight behaviour relative to carcass searches also arises from practical shortcomings of the latter approach: although carcass searches have been performed at various wind farms in Europe (partly as a mandatory requirement within the construction permission), the methodology is not well standardised and the central collection of carcass search data falls short. In particular, auxiliary data concerning search effort, carcass detectability and carcass persistence are often unavailable or incomplete. However, these are indispensable for correctly estimating collision rates and avoiding biases (e.g. carcass detectability related to size of the bird; Huso et al., 2017).

The main limitation of the approach based on flight behaviour applied here was that we could not provide absolute rates of wind turbine collisions, i.e. the number of collisions per unit of time for a given area. Estimations of collision rates are necessary to evaluate the impact of wind farm collisions on bird populations, i.e. the strength of the caused population decrease (Bellebaum et al., 2013; Duriez et al., 2022), which is generally the main value of interest in conservation biology (May et al., 2019). In principle, collision risk models allow to calculate collision rates based on data on flight behaviour (Figure 6.4).

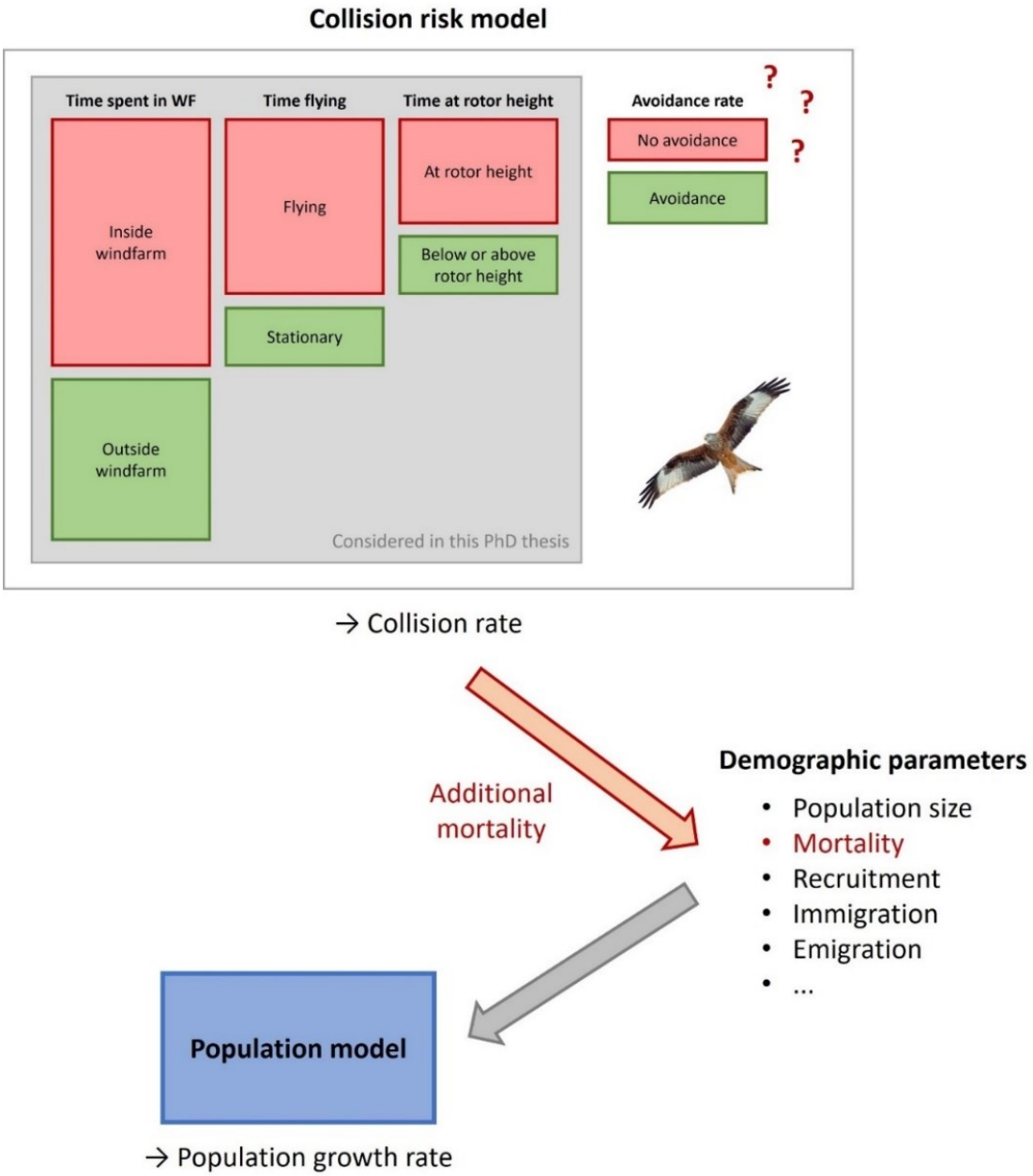

Figure 6.4: Schematic representation of the aspects of flight behaviour considered in this PhD thesis (grey box), and the required additional steps to obtain estimates of the population effects of the additional mortality through wind turbine collisions.

However, deriving absolute collision rates from collision risk models requires information on species-specific wind turbine avoidance rates on different spatial scales (Chamberlain et al., 2006; note that in chapter 4, we did apply collision risk models, but with a default avoidance rate for all study species). Avoidance behaviour, especially on the smaller spatial scales (meso- and micro-scale; Cook et al., 2014), is notoriously difficult to study and thus, reliable data are still largely lacking. In recent years, progress has been made to quantify wind turbine avoidance for some (larger) bird species using GPS tracking, amongst others thanks to the high positional accuracy provided by high-frequency GPS tracking (T. Schaub et al., 2020; Santos et al., 2021; D. T. Johnston et al., 2022; Fielding et al., 2022). However, these studies only provided a partial account of avoidance

(macro- and meso-scale), as micro-scale avoidance was omitted, i.e. last-second avoidance of the approaching rotor blade (Cook et al., 2014; May, 2015). This last part of avoidance behaviour is virtually impossible to study using GPS tracking even with the highest spatio-temporal resolution, as also the exact three-dimensional position of the individual rotor blades needs to be known at high temporal resolution. Turbine-mounted automatic camera systems might come a step closer to quantifying micro-scale avoidance (Skov et al., 2018; Reichenbach et al., 2023). Nevertheless, it should be noted that also besides the issue of unknown avoidance rates, it is problematic that collision risk models as a whole (with the underlying assumptions and simplifications; e.g. Christie & Urquhart, 2015) have not been thoroughly validated with respect to the predicted absolute number of collisions yet. It is therefore questionable if collision risk models will be able to provide accurate estimations of absolute collision rates in the near future.

In conclusion, the two main approaches hitherto applied to assess wind turbine collision risk can best be considered as two complementary approaches. The approach based on flight behaviour in combination with collision risk models is powerful for *relative* considerations (e.g. comparing different scenarios of wind energy development), while carcass searches allow to estimate *absolute* collision rates, if correction procedures are applied (Huso et al., 2017).

6.4. Direct study of wind turbine collisions based on GPS tracking

Besides the two main approaches to assess wind turbine collision risk discussed above, an additional option is to determine bird mortality from collisions directly using tracking devices. The recent development of GPS-GSM tracking devices (as used for the majority of tagged birds in this thesis) has extended the possibilities for this approach, as these tags both allow to track the birds' movements at high temporal resolution with high positional accuracy, and to record mortality events (see section 6.5). The downside of this approach is that a very large sample size of tagged birds, associated with major financial investments and fieldwork efforts, is required to achieve representative results. One current example is the LIFE EUROKITE project, gathering GPS tracking and mortality data of > 2000 Red Kites across Europe (www.life-eurokite.eu).

An additional issue is that the raw mortality data may easily be misleading: when upscaling from the individual mortality data to the population level, it is indispensable to account for the exposure of the studied individual birds to wind turbines. As wind turbine exposure may vary importantly between regions and individuals (see section 2.5), the sample of tagged individuals, and consequently the found wind turbine mortality rate, may not be representative for a given geographical area (e.g. region or country). A promising approach would be to relate the timespan which the tagged birds spent in the vicinity of wind turbines to the number of recorded collisions to obtain a measure of collision probability, which could then be scaled to the population level based on exposure time.

This collision probability could also be compared between species or between wind farms with different characteristics (e.g. turbine dimensions).

6.5. Box: Recorded collision fatalities in the dataset used in this thesis

Out of 136 mortality events of GPS-tagged birds from the dataset used in this thesis (with known exact location of death), five were due to a wind turbine collision (one Common Buzzard and four Red Kites; Table 6.2; Figure 6.5). Additionally, two non-lethal collisions were recorded, out of which one (Short-toed Eagle) was confirmed in the field (bird eventually died after release from bird rehabilitation centre). The second case (Red Kite) was presumed only based on the GPS-tracking data (no ground-truthing; Table 6.2).

Deliberately, I did not determine mortality rates here, as this would most probably be misleading: first, the small sample size of recorded mortality events per species may induce biases. Secondly, accounting for the exposure of the tagged birds to wind turbines is crucial (see above), which would require a specific analysis on its own. Certainly, wind turbine exposure differed between species within the dataset, implying that mortality rates without accounting for wind turbine exposure do not reflect the species-specific sensitivity.

Figure 6.5: Left: Carcass of a Red Kite (adult female) which collided with a wind turbine in Germany (Rhineland-Palatinate) on 9 October 2022. The bird was GPS-tagged in the Netherlands in 2021. Photo: Warner Jan de Wilde. Right: GPS positions of the same individual. Map: *Google Earth*.

Table 6.2: Overview of the wind turbine collisions of GPS-tagged birds within the dataset used in this thesis. Coll. = collision; MoH = Montagu's Harrier, HH = Hen Harrier, MaH = Marsh Harrier, CB = Common Buzzard, RK = Red Kite, STE = Short-toed Eagle; CY = calendar year; F = female, M = male, U = unknown sex.

Species	Country tagging and coll.	Date coll.	Age at coll.	Sex	Remarks
Lethal collisions					
CB	NL -> NL	2021-09-14	Adult	F	
RK	NL -> DE	2019-07-29	1CY	U	
RK	LU -> ES	2022-04-07	3CY	U	
RK	LU -> BE	2022-04-09	3CY	U	
RK	NL -> DE	2022-10-09	Adult	F	
Non-lethal collisions*					
RK	FR -> FR	2021-07-19	Adult	M	Presumed non-lethal collision: bird immobile in wood during ca. 50 h after being grounded at 100 m of wind turbine during 1.5 h; bird survived at least until following spring
STE	FR -> ES	2023-09-13	2CY	M	Confirmed non-lethal* collision, injured bird nursed in rehabilitation centre during three weeks, died five days after release

* Note that the collision of the 2CY STE would certainly have been lethal in the end if the injured bird wasn't brought to a bird rehabilitation centre shortly after the collision had taken place, which was only possible thanks to information from the GPS tag.

6.6. Year-round perspective on collision risk

In this thesis, the analyses were restricted to the breeding areas of the study species and therefore excluded the migration and winter period in the migratory species, i.e. all study species except Common Buzzard (Hen Harrier, Marsh Harrier and Red Kite being partial migrants; Figure 6.6). However, for a complete picture on wind turbine collision risk, a year-round perspective is required. Here, it is again helpful to apply the concept of risk = sensitivity x exposure. The sensitivity to wind turbine collision could vary between breeding, migration and winter periods due to differences in flight behaviour. For example, the time flying per day might be highest during spring migration (pressure to quickly reach the breeding area) and lowest in winter (no need to provide food for the offspring; e.g. low flight activity in winter seen in the resident male Common Buzzards in the raw data from this thesis; Figure A5.2.2). Also the proportion of flights at collision risk height could vary between the different periods of the annual cycle, for example with an increased proportion during migration, or an increased proportion during breeding (e.g. due to display flights at high height; Arroyo et al., 2013). Both the time flying and the proportion at risk height could be studied year-round using GPS tracking (e.g. based on the

dataset used in this thesis), which would be a valuable pathway for future studies. However, for birds wintering at higher latitudes (e.g. NL, Germany, France), data collection during winter is limited by poor solar charging with the GPS tags currently available: in these cases, GPS positions can often only be recorded at a low frequency (even < 10 per month), and collecting high-frequency GPS data to obtain accurate height data is virtually impossible. Then, the use of barometric altimetry (barely consuming battery), or state-space models to post-process the height data (see above), could be a solution to obtain (relatively) accurate estimates of the time spent at risk height.

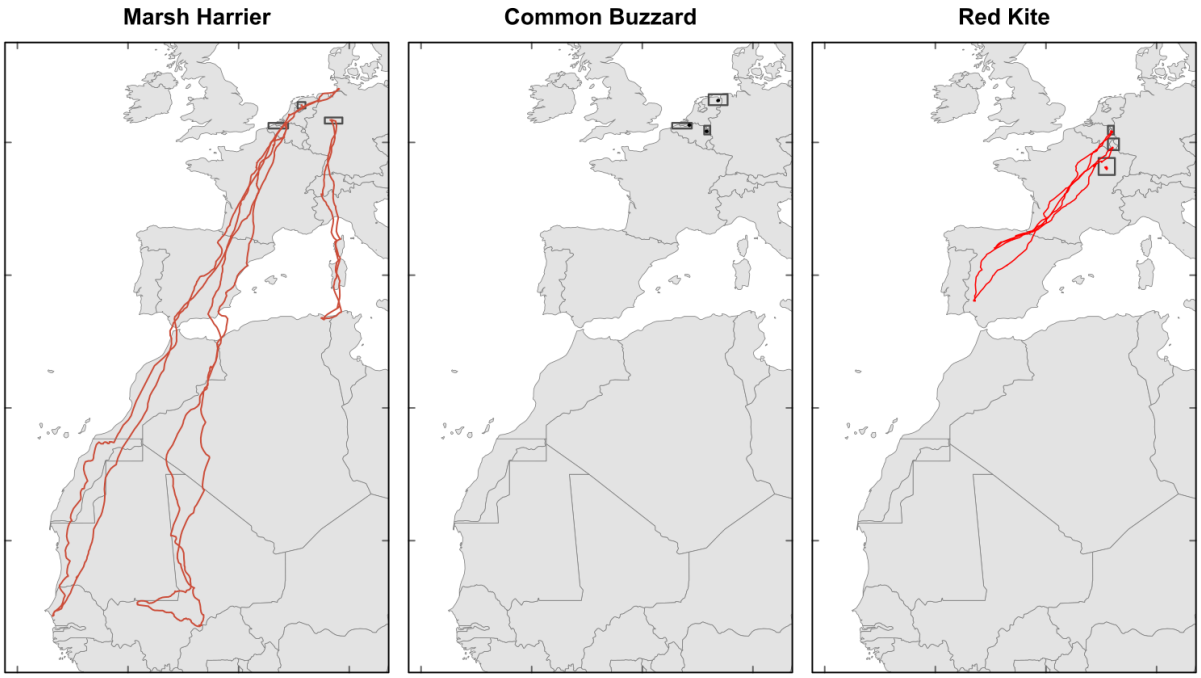

Figure 6.6: Examples of year-round tracks of Marsh Harriers, Common Buzzards and Red Kites (three individuals per species; one calendar year per individual). All three Common Buzzards and one Red Kite were resident within the study areas (rectangles). Tick marks: increments of 10° longitude and latitude.

The exposure to wind turbines (time spent in the vicinity of wind turbines) may also differ importantly across the annual cycle, depending on the density of wind turbines in the areas where the birds breed and winter, and through which they migrate (Assandri et al., 2024). This might vary strongly between species, subpopulations and individuals (depending on the location of the individual breeding territory, migration route and wintering area). For the species wintering in sub-Saharan Africa (in this study: Montagu's Harrier, Marsh Harrier [Figure 6.6] and Short-toed Eagle), there is (currently) nearly no exposure to wind turbines during winter. However, for the species wintering in Europe (e.g. in Spain as in Hen Harrier and Red Kite [Figure 6.6]), exposure to wind turbines during winter could on average be similar as, or higher than, during the breeding season. To verify these hypotheses, it would be valuable to quantify the year-round variation of exposure to wind turbines using GPS-tracking data in migratory species. However, due to the

individual variation, a large number of tracked individuals would be necessary to obtain representative population averages.

When comparing wind turbine collision risk between the different periods of the annual cycle, the interplay of daily collision risk (daily mortality rate) and period length needs to be considered (Klaassen, Hake, et al., 2014). For example, as migration periods are generally much shorter than breeding and winter periods, a higher daily rate of mortality due to wind turbine collisions during migration might not lead to an higher overall mortality for the migration period.

Appendix 3.1: Supplementary details on methods (chapter 3)

Data collection

Adults were captured using the following techniques: mist net with stuffed or live predator as lure, nest trap, catching pole or whoosh-net with carrion as bait. Nestlings were captured on the nest before fledging. Bird captures and tag deployment were performed with all necessary permissions. See Figure A3.1.1 for the location of the study areas.

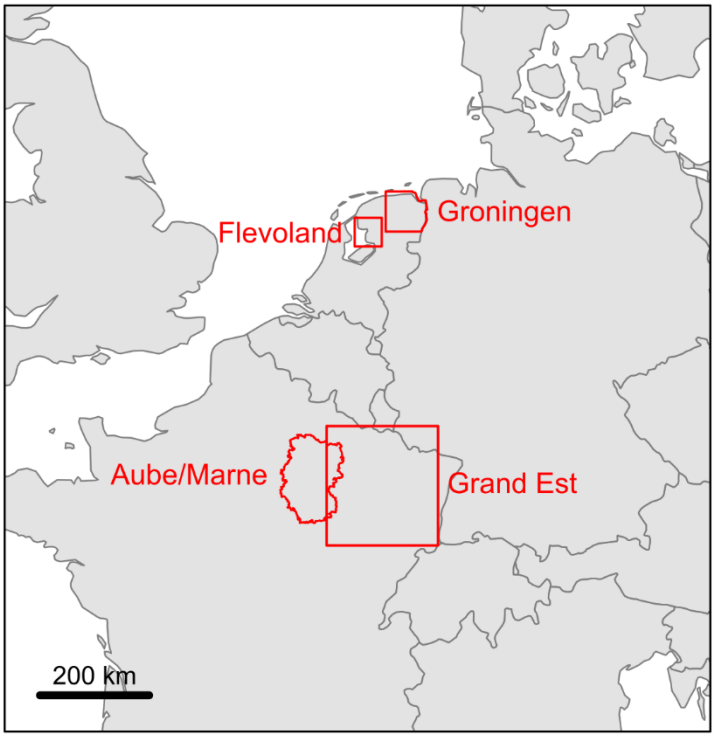

Figure A3.1.1: Location of the four study areas, and the boundaries applied. Background map created using the *R* package *maps* (Brownrigg et al., 2018).

Some of the tag models were used in different versions in our study (with or without elevated solar panel [*Ornitela*], with different GSM network connectivity [*Ornitela*], with or without external antenna for communication with antenna system [*UvA-BiTS*]; Table A3.1.1), but these were lumped for the analyses as we did not expect differences in the vertical accuracy between tag model versions.

General data processing

The data were constrained to the four study areas, partly defined by rectangular bounding boxes and partly by administrative borders (Figure A3.1.1). The latter were used where topographic data for the habitat classification were available for administrative units. 1st December 2022 was applied as the common end datum for the different data sets. However, barometric height data could only be used until the end of September 2022 because the ERA5 weather data (see section Height data processing) were only available until then. The basic data processing was performed in the program *R* version 4.0.3 (R Core Team, 2020). using the packages *dplyr* (Wickham et al., 2022), *sp* (E. J. Pebesma & Bivand, 2005), *sf* (E. Pebesma, 2018) and *raster* (Hijmans, 2015).

As *Milsar* tags deployed in 2019 recorded erroneous height data during high-frequency sampling due to a firmware issue, high-frequency data from these tags were removed (n = 56,300). In two OT-25 tags deployed on Red Kites the pressure sensor failed permanently at a given moment in time; moreover, in two OT-15 and four OT-20 tags, in several instances the pressure measurements remained temporarily static during high-frequency blocks. The barometric height data for these positions were removed (n = 382,436 and 7,555 for the two cases, respectively).

To determine the antimode in the distribution of GPS speed values for distinguishing between stationary and flight positions function *locmodes* from the *R* package *multimode* (Ameijeiras-Alonso et al., 2021) was used (Kölzsch, 2022). To allow determination of the antimode, the highest 0.1% of speed values were removed, although these data points remained within the general data set.

Subsampling was performed using a self-written function in *R*. As a minimum interval between positions, 5 min was used. Because GPS intervals are somewhat irregular (the actual interval can sometimes be smaller than 5 min when 5 min is the set interval in the tag settings), we included a tolerance of 30 s.

Table A3.1.1: Overview of GPS tracking data sets used in this study. The number of GPS and barometric height measurements per tag model include stationary and flight positions. Ind. = individuals; LF = low-frequency sampling; HF = high-frequency sampling, baro = barometric. MoH = Montagu's Harrier, HH = Hen Harrier, MaH = Marsh Harrier, RK = Red Kite.

Manufac-turer	Model	Model versions	Species	Area	Period	n tags	n ind.	n GPS LF	n GPS HF	n baro LF	n baro HF
UvA-BiTS	4C.L	4CWL	MaH	Groningen	2012-16	2	2	704,150	645,431	0	0
UvA-BiTS	4C.L	4CWL	MoH	Groningen	2012-14	5	5	264,091	525,395	0	0
UvA-BiTS	4C.S	4CWS	HH	Groningen	2012-15	3	3	122,734	360,594	0	0
UvA-BiTS	4C.S	4CWS	MoH	Groningen	2009-14	24	24	4,715	15,614	0	0
UvA-BiTS	5C.L	5CDL, 5CWL	HH	Groningen	2014-15	1	1	60,778	173,344	0	0
UvA-BiTS	5C.L	5CDL, 5CWL	MoH	Groningen	2014-17	5	5	147,056	428,558	146,360	421,740
UvA-BiTS	5C.S	5CDS, 5CWS	MoH	Groningen	2015-20	10	9	125,994	272,912	125,994	270,099
UvA-BiTS	6C.L	6CDL, 6CWL	MaH	Groningen	2014-21	3	3	587,953	2,647,694	467,952	2,178,229
Milsar	GsmTag-U9	GsmTag-U9	HH	Champagne	2019-22	74	84	68,878	76,938	0	0
Milsar	GsmTag-U9	GsmTag-U9	MoH	Champagne	2020-22	11	11	35,108	60,776	0	0
Ornitela	OT-10	OT-10-3GC, OT-10-3GC-C19, OT-E10-3GC, OT-E10-3GC-C19, OT-E10-4GC	HH	Champagne	2021-22	15	16	89,724	81,045	0	0
Ornitela	OT-10	OT-10-3GC-C19	MoH	Champagne	2021-21	2	2	349,356	1219,773	0	0
Ornitela	OT-10	OT-10-3GC	MoH	Groningen	2021-22	3	5	21,499	0	0	0
Ornitela	OT-15	OT-15B-3GC-C21	MaH	Flevoland	2019-22	4	5	33,010	172,075	0	0
Ornitela	OT-20	OT-20B-3GC-C21	MaH	Flevoland	2019-22	7	7	103,654	304,556	0	0
Ornitela	OT-25	OT-E25B-4GC	RK	Grand Est	2021-22	26	28	163,069	911,170	0	0
Total					*2009-22*	*194*	*204*	*2,881,769*	*7,895,875*	*740,306*	*2,870,068*

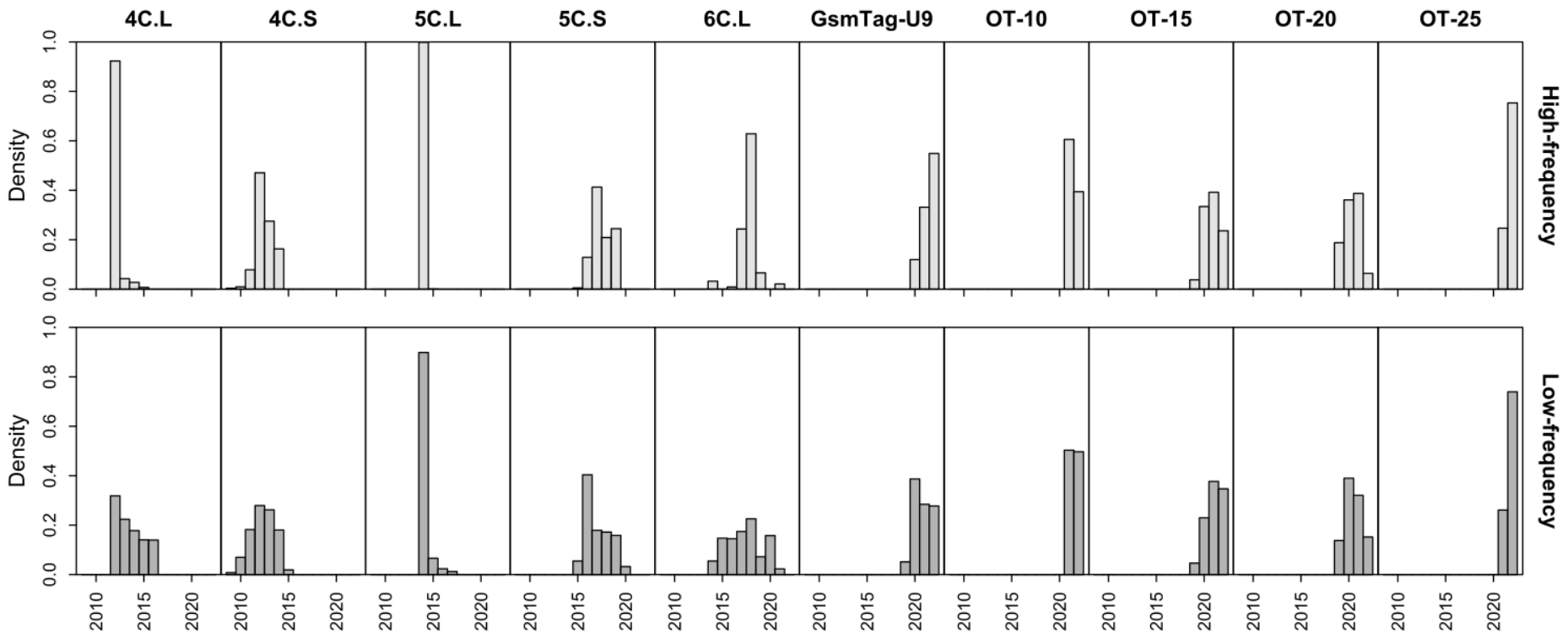

Figure A3.1.2: Distribution of the high- and low-frequency tracking data across years per GPS tag model. Histogram bins represent years between 2009 and 2022.

Height data processing

The calculation of barometric height based on the pressure measurements of the tags was performed using the barometric formula describing the relationship of air pressure with height above a reference level under different meteorological conditions $P = P_0 * (1 + \frac{L}{T_0} * z)^{-\frac{g}{LR_0}}$ (ISO, 1975; Equation 1), where P is the measured pressure at height z above the reference height level, P_0 is the pressure at reference height, L is the temperature lapse rate, T_0 is the temperature at reference height, g is the standard acceleration of free fall (9.81 m s^{-1}), and R_0 is the specific gas constant (287.05 J K^{-1} kg^{-1}). The data provided by the tags had already internally been transformed into height above sea level (a.s.l.) using the inversion of Equation 1, but using the values of the standard atmosphere P_0 = 1013.15 hPa, L = -0.0065 K m^{-1}, and T_0 = 288.15 K. In some tags, the manufacturer erroneously applied T_0 = 287.15 K (R. Zydelis, pers. comm.). To improve the height estimation by integrating actual weather data in the formula, we first transformed the height a.s.l. obtained from the tags into the original pressure measurements using Equation 1. Secondly, we applied the inversion of Equation 1 to calculate height using weather data from the global weather model ECMWF ERA5 with a temporal resolution of 1 h and a spatial resolution of 15' (Hersbach et al., 2018a, 2018b). The tracking data were annotated with ERA5 data using the Environmental-Data Automated Track Annotation System (Env-Data) provided by Movebank (Dodge et al., 2013), which included an interpolation of the ERA5 data to the timestamp and horizontal position of each GPS position. We used "Surface Air Pressure" and "Temperature (2 m above Ground)" provided by ERA5 as P_0 and T_0, thereby using the surface level of ERA5 as reference level. To obtain as estimation of L, we calculated the temperature gradient between the model surface and a higher pressure level for which the temperature could be retrieved from ERA5 (950 hPa for Red Kite data from Grand Est, 975 hPa for Marsh Harrier data from Flevoland). The geometric height a.s.l. of both the model surface and the pressure level were calculated based on the geopotential φ provided by ERA5 for these levels, using the equations $H = \frac{\varphi}{g}$ (Equation 2) and $h = \frac{r*H}{r-H}$ (Equation 3) where H is the geopotential height, φ is the geopotential, h is geometric height a.s.l. and r is the nominal earth's radius, i.e. 6,356,766 m (ISO, 1975). (Note that there is barely any difference between geometric and geopotential height at the altitude ranges considered here.) The pressure levels were on average 286.4 m (Grand Est) and 355.7 m (Flevoland) above the ERA5 surface level. Note that due to the spatial resolution of the ERA5 model of 15', the ERA5 surface is a coarse approximation of the earth's surface. Therefore, we did not use the height of the tracking data above the ERA5 surface directly as height above ground level (a.g.l.), but first calculated height a.s.l. by adding the height of the model surface a.s.l., and then applied a digital elevation model with higher spatial resolution.

The geoid model used in ERA5 was EGM96, as for the GPS tracking data. However, the EU-DEM digital elevation model was based on another geoid model (EEG2008). Therefore, we assessed the difference between EGM96 and EEG2008 by comparing the geoid

height above ellipsoid from both geoid models across all positions of our GPS tracking dataset. EGM96 raster data with spatial resolution of 15' were downloaded through (Agisoft, n.d.); EEG2008 raster data with resolution of 10' x 15' through (International Service for the Geoid, n.d.). As the difference between the two geoid models was small (mean absolute difference 0.12 m, maximum 0.65 m), we refrained from applying further corrections of the data.

Identification of stationary positions on the ground

For the three species of harriers which are known to sit on the ground most of the time when being stationary, we used the digital national topographic maps *BD TOPO* for France (IGN, n.d.) and *TOP10NL* for the Netherlands (PDOK, n.d.). We applied the topographic data from the mean year of the available tracking data per study area (pooled across species), i.e. 2021 for Champagne, 2021 for Flevoland and 2015 for Groningen, with the exception of the *BD TOPO* hedgerow layer for Champagne which was only available for 2022. The spatial overlay was performed using functions from the *R* package *sf* (E. Pebesma, 2018).

Visual checks of the classification results with satellite images on a sample basis indicated only few instances of misclassification, all referring to positions erroneously classified as "non-ground positions" (parcels of land where forest had been converted to agricultural land, which was not yet updated in the topographic data). This does not have major implications for our results, as we base our analysis on "ground positions" only.

For Red Kites, we classified the perching habitat manually by visual inspection of satellite pictures. This procedure was applied to a subset of the data (data from 2021). The visual inspection was performed using satellite images accessed using the *R* packages *OpenStreetMap* (Fellows, 2016) and *plotKML* (Hengl et al., 2015), and the program *Google Earth*.

Table A3.1.2: Overview of layers and object types used from the national topographic maps *BD TOPO* (France) and *TOP10NL* (Netherlands). English translations of the names of layers and object types are indicated in brackets. To all the listed objects a buffer of 50 m was applied to identify GPS positions on or close to vertical structures (see Methods).

Data set	Layer	Object type	Geometry type
BD TOPO	"zone_de_vegetation" (vegetation zone)	All	Polygon
BD TOPO	"batiment" (building)	All	Polygon
BD TOPO	"haie" (hedgerow)	All	Line
BD TOPO	"pylone" (pylon)	All	Point
TOP10NL	"Inrichtingselement" (structural element)	All	Line/point
TOP10NL	"Gebouw" (building)	All	Polygon/point
TOP10NL	"Terrein" (terrain)	"bebouwd gebied" (built-up area), "boomgaard" (orchard), "boomkwekerij" (tree nursery), "bos: gemengd bos" (mixed forest), "bos: griend" (osier bed), "bos: loofbos" (deciduous forest), "bos: naaldbos" (conifer forest), "dodenakker met bos" (cemetery with forest), "fruitkwekerij" (fruit orchard), "populieren" (poplar trees)	Polygon

Appendix 3.2: Supplementary results – Tables (chapter 3)

Table A3.2.1: Means and 95% confidence intervals for trueness, precision and accuracy for each combination of tag model and method based on hierarchical bootstrapping. Parameters used: mean and median error from true height (equivalent to mean and median height a.g.l.; trueness), mean and median absolute error with median height as reference (precision), mean and median absolute error with true height as reference (accuracy).

Tag model	Method	N tags	N positions	Trueness (mean)			Trueness (median)			Precision (mean)			Precision (median)			Accuracy (mean)			Accuracy (median)		
4C.L	GPS LF	7	67,136	-4.5	-4.0	-2.7	-4.7	-3.8	-2.6	5.5	6.5	7.3	3.9	4.7	5.2	6.0	7.4	8.4	4.0	5.3	6.1
4C.L	GPS HF	7	772	-5.4	-4.1	-2.6	-5.0	-3.8	-2.5	2.8	3.2	3.4	2.2	2.6	3.0	3.5	4.7	5.8	2.8	3.9	5.0
4C.S	GPS LF	27	239,866	-2.2	-0.3	1.8	-2.5	-1.8	-1.2	9.4	13.1	16.8	3.1	3.4	3.7	9.8	13.4	17.0	3.1	3.5	4.0
4C.S	GPS HF	22	6,333	-3.1	-2.1	-1.2	-2.8	-1.7	-1.0	2.4	2.8	3.2	1.9	2.2	2.7	2.6	3.2	3.9	2.0	2.4	3.0
5C.L	GPS LF	6	35,465	-0.4	3.6	6.7	-2.3	-1.9	-1.3	27.4	28.7	32.8	2.8	3.0	3.0	27.8	29.1	33.3	3.0	3.3	3.5
5C.L	GPS HF	4	900	-0.3	-0.2	0.3	-0.2	-0.1	0.5	1.0	1.5	1.6	0.8	1.1	1.3	1.1	1.5	1.6	1.0	1.2	1.3
5C.S	GPS LF	10	60,162	-0.8	-0.2	0.5	-3.0	-2.6	-2.2	19.3	26.3	32.6	2.4	2.6	2.8	20.0	27.0	33.3	3.4	3.7	3.9
5C.S	GPS HF	8	1,706	-2.4	-2.1	-1.9	-2.3	-2.0	-2.0	1.1	1.3	1.5	0.8	1.0	1.1	2.1	2.3	2.5	2.0	2.1	2.3
6C.L	GPS LF	3	116,133	-0.7	0.6	5.0	-3.0	-2.6	-2.0	24.1	27.0	32.8	2.6	3.1	3.4	24.7	27.6	33.1	3.4	3.9	4.3
6C.L	GPS HF	3	5,642	-2.4	-2.2	-0.7	-2.5	-2.2	-0.7	1.5	1.6	1.7	1.0	1.2	1.3	1.6	2.6	2.6	1.3	2.4	2.6
GsmTag-U9	GPS LF	84	670,570	-0.2	0.1	0.4	-1.4	-1.1	-0.8	9.1	9.5	9.8	4.8	5.0	5.2	9.2	9.5	10.0	5.0	5.1	5.3
GsmTag-U9	GPS HF	43	5,945	-1.2	-0.8	-0.4	-1.4	-1.0	-0.6	4.2	4.7	5.3	2.9	3.1	3.5	4.2	4.8	5.3	3.0	3.2	3.6
OT-10	GPS LF	20	136,990	-1.2	-0.1	0.9	-1.9	-0.7	0.5	8.4	9.7	11.1	4.9	5.4	5.8	8.4	9.7	11.2	5.0	5.5	6.0
OT-10	GPS HF	19	3,596	-2.2	-1.2	0.0	-2.0	-0.8	0.4	2.9	3.4	4.0	2.3	2.7	3.3	2.9	3.5	4.2	2.3	2.7	3.2
OT-15	GPS LF	4	105,932	0.4	1.3	3.5	-3.3	-1.8	-0.3	15.9	18.6	21.1	8.5	9.7	10.8	16.1	18.8	21.1	8.8	9.9	10.9
OT-15	GPS HF	4	2,828	0.0	1.0	1.2	-1.6	-1.2	-0.8	3.7	6.9	7.8	2.8	3.6	3.9	3.8	7.0	8.0	3.2	3.8	4.0
OT-15	Baro LF	4	105,399	-14.7	-11.5	-8.5	-9.8	-9.1	-7.9	3.1	6.8	11.7	2.1	3.4	6.0	9.4	12.5	16.0	8.0	9.1	9.9
OT-15	Baro HF	4	2,796	-12.9	-11.4	-9.5	-10.8	-9.5	-7.7	2.7	5.6	8.9	2.1	3.5	5.3	9.5	11.4	13.0	7.7	9.5	10.8
OT-20	GPS LF	7	93,899	1.1	2.0	2.9	-1.3	-0.5	-0.1	15.1	16.7	18.6	8.1	8.7	9.4	15.2	16.7	18.6	8.3	8.7	9.4
OT-20	GPS HF	7	1,827	0.1	1.6	2.4	-0.2	0.9	2.3	4.7	5.5	5.9	3.8	4.0	4.4	4.8	5.6	6.0	3.7	4.0	4.4
OT-20	Baro LF	7	93,899	-14.3	-13.2	-11.1	-14.7	-13.2	-11.0	2.8	3.7	4.3	2.1	2.8	3.3	11.4	13.7	14.9	11.0	13.2	14.7
OT-20	Baro HF	7	1,811	-16.5	-15.2	-12.2	-16.3	-15.0	-11.8	2.7	3.7	4.4	2.3	3.0	3.6	12.2	15.2	16.6	11.8	15.0	16.3
OT-25	GPS LF	11	691	1.9	5.8	11.1	-0.1	4.3	8.1	25.6	29.5	32.9	13.0	17.4	22.0	25.8	29.9	33.4	14.0	18.9	23.1
OT-25	GPS HF	11	400	-0.3	0.6	1.7	-0.3	0.6	1.4	3.3	3.8	4.1	2.4	2.8	3.3	3.4	3.8	4.2	2.4	2.9	3.5
OT-25	Baro LF	10	658	-5.4	-3.5	-1.4	-7.4	-4.9	-2.4	4.3	5.4	6.7	2.9	4.2	6.1	5.8	6.8	8.0	5.2	6.4	7.8
OT-25	Baro HF	10	381	-9.3	-7.9	-6.2	-9.5	-8.0	-6.7	2.6	3.2	3.8	1.7	2.3	3.1	6.8	8.2	9.4	6.9	8.1	9.5

Table A3.2.2: Parameters of vertical error distributions for each combination of GPS tag model and method (1). Shown values refer to the error from true height in stationary positions on the ground, when true height was zero. LQ = lower quartile, UQ = upper quartile, IQR = inter-quartile range, lower whisker = minimum point falling within LQ-1.5*IQR, upper whisker = maximum point falling within UQ+1.5*IQR, LF = low-frequency, HF = high-frequency.

Model	Method	N tags	N positions					Trueness						Precision		
				Min.	2.5% error	Lower whisker	LQ	Mean	Median	UQ	Upper whisker	97.5% error	Max.	IQR	Whisker range	95% range
4C.L	GPS LF	7	67,652	-408.8	-23.3	-23.4	-9.0	-4.1	-4.0	0.6	15.1	12.1	921.8	9.6	38.5	35.5
4C.L	GPS HF	7	71,212	-63.0	-14.1	-14.0	-6.2	-3.8	-3.8	-1.0	6.8	3.2	275.5	5.2	20.7	17.3
4C.S	GPS LF	27	249,652	-1,092.9	-33.7	-15.5	-5.4	-0.3	-1.9	1.3	11.4	44.9	34,809.3	6.7	26.9	78.6
4C.S	GPS HF	22	498,791	-638.0	-9.0	-10.0	-3.7	-1.5	-1.4	0.5	6.9	3.9	599.8	4.2	16.9	12.9
5C.L	GPS LF	6	35,963	-1,097.4	-127.7	-13.9	-5.0	3.6	-2.0	1.0	9.9	193.6	8,628.9	6.0	23.9	321.2
5C.L	GPS HF	4	74,248	-229.1	-4.0	-5.1	-1.4	0.1	0.0	1.1	4.7	3.7	565.5	2.5	9.8	7.7
5C.S	GPS LF	10	61,037	-1,097.0	-139.9	-13.0	-5.2	-0.3	-2.6	0.0	7.8	169.8	6,239.5	5.2	20.8	309.6
5C.S	GPS HF	8	138,232	-298.0	-5.0	-6.0	-3.0	-1.9	-2.0	-1.0	2.0	1.3	362.5	2.0	8.0	6.2
6C.L	GPS LF	3	119,677	-1,080.8	-135.0	-15.0	-5.8	0.4	-2.6	0.4	9.7	151.2	25,097.9	6.2	24.7	286.1
6C.L	GPS HF	3	512,302	-542.0	-6.0	-7.3	-3.5	-2.2	-2.3	-1.0	2.7	2.2	612.6	2.5	10.0	8.1
GsmTag-U9	GPS LF	84	677,019	-197.5	-29.3	-20.9	-5.9	0.1	-1.1	4.1	19.1	31.1	9,172.9	10.0	40.0	60.4
GsmTag-U9	GPS HF	44	565,618	-161.6	-13.4	-13.1	-4.0	-0.4	-1.0	2.1	11.2	13.7	1,391.7	6.1	24.3	27.1
OT-10	GPS LF	20	138,600	-1,173.6	-29.1	-22.6	-6.2	-0.1	-0.7	4.7	21.1	27.3	10,618.4	10.9	43.7	56.4
OT-10	GPS HF	19	326,551	-400.0	-10.3	-11.8	-3.6	-0.9	-0.7	1.8	10.0	6.9	742.6	5.4	21.8	17.2
OT-15	GPS LF	4	108,386	-1,467.3	-50.6	-40.4	-11.3	1.1	-2.1	8.1	37.2	70.9	6,636.5	19.4	77.6	121.5
OT-15	GPS HF	4	241,008	-129.1	-17.8	-15.8	-4.5	1.4	-1.3	3.0	14.2	29.3	3,206.2	7.6	30.1	47.1
OT-15	Baro LF	4	107,845	-57.7	-38.5	-22.7	-12.8	-11.5	-9.2	-6.2	3.7	0.5	844.9	6.6	26.4	39.1
OT-15	Baro HF	4	238,294	-54.6	-35.9	-24.5	-14.0	-12.2	-10.2	-7.0	3.6	-0.4	383.0	7.0	28.1	35.5
OT-20	GPS LF	7	96,852	-1,548.5	-43.6	-34.8	-8.8	2.0	-0.5	8.6	34.6	60.7	4,976.9	17.3	69.4	104.3
OT-20	GPS HF	7	177,002	-89.1	-11.6	-15.9	-3.4	1.7	0.7	4.9	17.2	19.7	419.6	8.3	33.1	31.3
OT-20	Baro LF	7	96,852	-41.8	-23.5	-25.5	-16.6	-13.4	-13.4	-10.6	-1.6	-4.9	786.3	6.0	23.9	18.6
OT-20	Baro HF	7	175,700	-34.3	-26.4	-28.7	-19.2	-16.0	-15.9	-12.8	-3.3	-6.5	403.5	6.4	25.4	19.9
OT-25	GPS LF	11	697	-184.0	-81.6	-63.4	-12.3	5.7	4.7	22.5	74.2	110.3	636.2	34.8	137.7	191.9
OT-25	GPS HF	11	31,251	-34.5	-9.1	-10.3	-2.3	0.6	0.5	3.1	11.2	11.0	70.2	5.4	21.4	20.1
OT-25	Baro LF	10	662	-22.2	-13.9	-18.6	-8.4	-3.6	-5.0	0.3	13.3	14.0	22.0	8.7	31.9	27.9
OT-25	Baro HF	10	30,004	-41.3	-16.2	-17.5	-10.6	-7.9	-8.0	-6.0	0.8	1.2	12.9	4.6	18.3	17.4

Table A3.2.3: Parameters of vertical error distributions for each combination of GPS tag model and method (2). Shown values refer to the absolute error (AE) with either median height (precision) or true height (accuracy) as reference in stationary positions on the ground, when true height was zero. Prop. = proportion, RMSE = root mean square error, LF = low-frequency, HF = high-frequency.

Model	Method	N tags	N positions	Precision (median height as ref.)					Accuracy (zero as reference)				
				Mean AE	Median AE	95% AE	Prop. AE > 50 m (%)	RMSE	Mean AE	Median AE	95% AE	Prop. AE > 50 m (%)	RMSE
4C.L	GPS LF	7	67,652	6.7	4.9	18.0	0.3	14.2	7.7	5.6	20.4	0.3	14.8
4C.L	GPS HF	7	71,212	3.4	2.8	8.9	0.1	5.3	4.7	3.9	12.0	0.1	6.6
4C.S	GPS LF	27	249,652	12.9	3.4	38.7	4.3	142.9	13.2	3.6	38.6	4.2	142.9
4C.S	GPS HF	22	498,791	2.8	2.1	6.6	0.2	7.6	3.1	2.2	7.9	0.2	7.8
5C.L	GPS LF	6	35,963	28.1	3.0	162.0	9.7	127.7	28.4	3.3	161.0	9.7	127.6
5C.L	GPS HF	4	74,248	1.7	1.2	3.8	0.1	6.4	1.7	1.2	3.8	0.1	6.4
5C.S	GPS LF	10	61,037	26.3	2.6	154.4	9.6	101.6	27.0	3.6	154.7	9.6	101.5
5C.S	GPS HF	8	138,232	1.4	1.0	3.2	0.1	5.5	2.4	2.0	4.7	0.1	5.8
6C.L	GPS LF	3	119,677	26.4	3.1	143.4	9.4	159.7	27.0	4.0	143.0	9.4	159.7
6C.L	GPS HF	3	512,302	1.6	1.2	4.1	0.0	4.1	2.6	2.4	5.3	0.0	4.7
GsmTag-U9	GPS LF	84	677,019	9.5	5.0	30.1	1.8	46.5	9.6	5.1	30.1	1.8	46.5
GsmTag-U9	GPS HF	44	565,618	5.0	3.0	13.5	0.5	13.8	5.1	3.2	13.5	0.5	13.8
OT-10	GPS LF	20	138,600	9.7	5.5	28.2	1.4	65.0	9.7	5.5	28.2	1.4	65.0
OT-10	GPS HF	19	326,551	3.5	2.7	8.9	0.1	6.4	3.5	2.7	9.2	0.1	6.4
OT-15	GPS LF	4	108,386	18.5	9.7	58.7	6.6	56.1	18.6	9.7	58.7	6.7	56.1
OT-15	GPS HF	4	241,008	7.8	3.9	22.5	1.5	28.5	7.9	4.0	22.7	1.5	28.4
OT-15	Baro LF	4	107,845	6.9	3.2	26.5	0.2	15.4	12.5	9.2	35.6	0.2	19.1
OT-15	Baro HF	4	238,294	6.0	3.5	23.3	0.0	9.8	12.4	10.2	33.6	0.0	15.5
OT-20	GPS LF	7	96,852	16.4	8.7	51.9	5.4	49.9	16.4	8.6	51.8	5.3	49.9
OT-20	GPS HF	7	177,002	6.2	4.1	15.2	0.8	12.8	6.3	4.3	15.5	0.8	12.9
OT-20	Baro LF	7	96,852	3.9	3.0	9.5	0.2	8.6	13.9	13.4	21.7	0.1	16.0
OT-20	Baro HF	7	175,700	4.1	3.2	10.1	0.0	5.9	16.1	15.9	25.0	0.0	17.1
OT-25	GPS LF	11	697	29.6	17.8	101.9	17.4	48.4	29.9	19.4	100.9	18.4	48.7
OT-25	GPS HF	11	31,251	3.7	2.7	10.1	0.3	5.7	3.7	2.6	10.0	0.3	5.7
OT-25	Baro LF	10	662	5.5	4.1	14.4	0.0	7.2	6.8	6.3	13.9	0.0	7.9
OT-25	Baro HF	10	30,004	3.2	2.2	8.7	0.0	4.4	8.2	8.0	14.4	0.0	9.0

Table A3.2.4: Difference between GPS and barometric height for the three GPS tag models (OT-15, OT-20 and OT-25), in high- and low-frequency sampling and for stationary ("sit") and flight positions ("move"). RMS = root mean square, LF = low-frequency, HF = high-frequency.

				Difference				Absolute difference			RMS difference
Model	**Data type**	**N tags**	**N positions**	**Mean**	**Median**	**2.5%**	**97.5%**	Mean	Median	95%	
OT-15	LF sit	4	110,201	13.0	9.2	-41.7	83.4	23.1	14.2	64.4	66.2
OT-15	LF move	4	36,155	-1.0	-0.7	-106.5	88.2	27.1	13.8	96.5	61.8
OT-15	HF sit	4	247,223	13.5	9.8	-8.7	43.9	15.0	10.2	36.4	32.1
OT-15	HF move	4	174,517	1.5	0.1	-14.9	27.7	7.5	4.6	22.9	16.7
OT-20	LF sit	7	99,684	15.5	13.1	-30.9	74.9	21.9	15.1	59.9	60.7
OT-20	LF move	7	26,310	4.0	4.6	-74.4	74.6	21.7	11.6	74.5	42.9
OT-20	HF sit	7	178,273	17.7	16.4	1.2	38.9	18.0	16.5	33.5	22.3
OT-20	HF move	7	91,826	7.3	7.6	-9.0	20.2	8.8	8.1	18.1	11.7
OT-25	LF sit	26	335,530	6.5	4.9	-100.3	113.9	35.9	20.6	107.7	91.9
OT-25	LF move	26	132,422	-1.5	-1.1	-133.3	118.8	39.0	21.6	126.1	82.2
OT-25	HF sit	26	1,091,803	6.8	6.7	-15.6	27.6	10.0	8.0	24.3	14.5
OT-25	HF move	26	1,086,392	2.4	2.4	-14.5	19.6	7.2	5.7	17.8	12.0

Table A3.2.5: Proportion of positions within the collision risk height range (CRHR; 50-200 m) for combinations in different methods per combination of GPS tag model, species and study area. HF = high-frequency, LF = low-frequency, baro = barometric, H. = Harrier. Rel. increase indicates the relative increase of the proportion within the CRHR between GPS LF and GPS HF.

			GPS HF		GPS LF			Baro HF		Baro LF	
Tag model	**Species**	**Study area**	**N positions**	**Prop. CRHR (%)**	**N positions**	**Prop. CRHR (%)**	**Rel. increase (%)**	**N positions**	**Prop. CRHR (%)**	**N positions**	**Prop. CRHR (%)**
4C.L	Marsh H.	Groningen	44,928	**3.2**	25,651	**4.6**	**+44.3**	0	**-**	0	**-**
4C.L	Montagu's H.	Groningen	19,807	**5.7**	7,934	**9.2**	**+60.7**	0	**-**	0	**-**
4C.S	Hen H.	Groningen	32,772	**12.1**	18,496	**11.3**	**-6.6**	0	**-**	0	**-**
4C.S	Montagu's H.	Groningen	754,687	**9.5**	164,790	**8.3**	**-13.0**	0	**-**	0	**-**
5C.L	Hen H.	Groningen	0	**-**	2,798	**8.2**	**-**	0	**-**	0	**-**
5C.L	Montagu's H.	Groningen	97,662	**8.5**	15,607	**8.8**	**+4.0**	0	**-**	0	**-**
5C.S	Montagu's H.	Groningen	159,691	**6.2**	41,082	**7.4**	**+20.9**	0	**-**	0	**-**
6C.L	Marsh H.	Groningen	362,427	**4.4**	38,264	**8.2**	**+87.4**	0	**-**	0	**-**
GsmTag-U9	Hen H.	Champagne	222,014	**16.7**	125,458	**10.8**	**-35.3**	0	**-**	0	**-**
GsmTag-U9	Montagu's H.	Champagne	273,351	**11.3**	94,296	**9.5**	**-16.3**	0	**-**	0	**-**
OT-10	Hen H.	Champagne	85,252	**11.7**	16,943	**9.7**	**-17.0**	0	**-**	0	**-**
OT-10	Montagu's H.	Champagne	4,379	**9.2**	922	**6.5**	**-29.6**	0	**-**	0	**-**
OT-10	Montagu's H.	Groningen	102,444	**8.7**	24,018	**8.5**	**-2.3**	0	**-**	0	**-**
OT-15	Marsh H.	Flevoland	178,523	**7.6**	36,313	**9.9**	**+29.5**	174,517	**7.0**	36,159	**7.4**
OT-20	Marsh H.	Flevoland	93,205	**12.2**	26,310	**12.6**	**+3.7**	91,826	**10.9**	26,310	**10.0**
OT-25	Red Kite	Grand Est	1,329,191	**37.4**	162,112	**37.9**	**+1.4**	1,086,410	**34.6**	132,422	**32.1**

Appendix 3.3: Supplementary results – Figures (chapter 3)

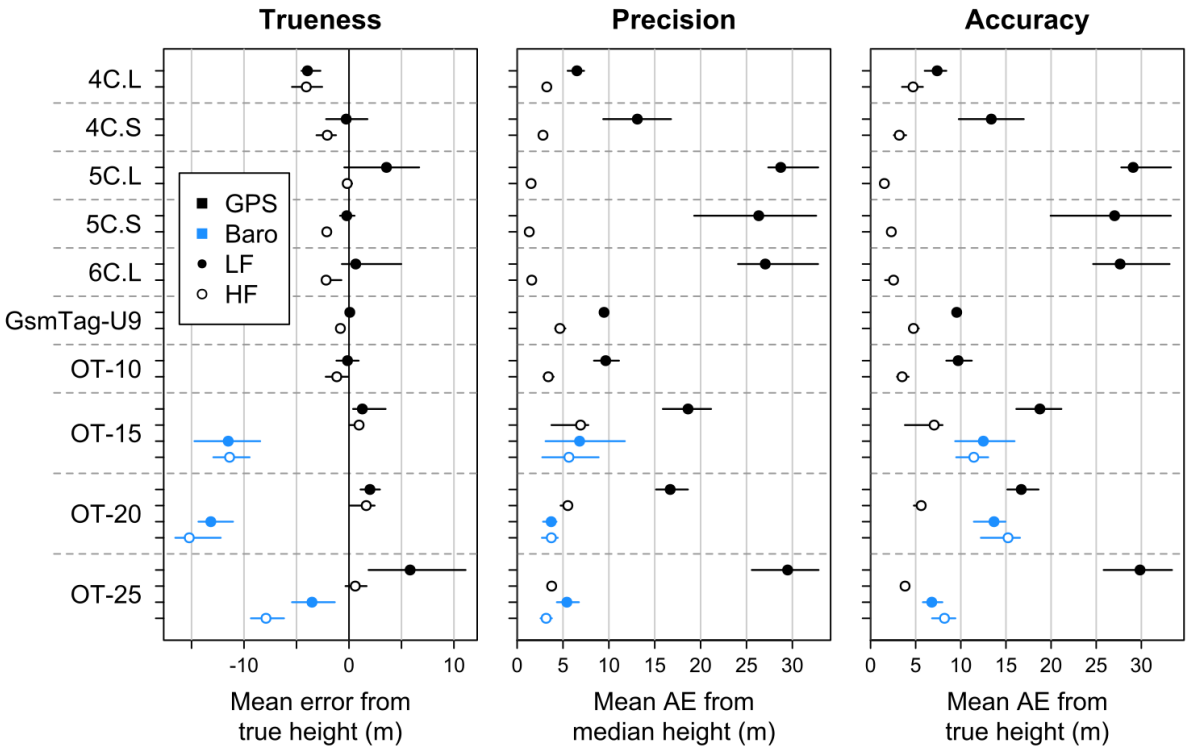

Figure A3.3.1: Estimates and 95% confidence intervals for trueness, precision and accuracy for each combination of GPS tag model and method based on hierarchical bootstrapping. Parameters used: mean error with true height as reference (equivalent to mean height a.g.l.; trueness), mean absolute error with median height as reference (precision), mean absolute error with true height as reference (accuracy). a.g.l. = above ground level; AE = absolute error.

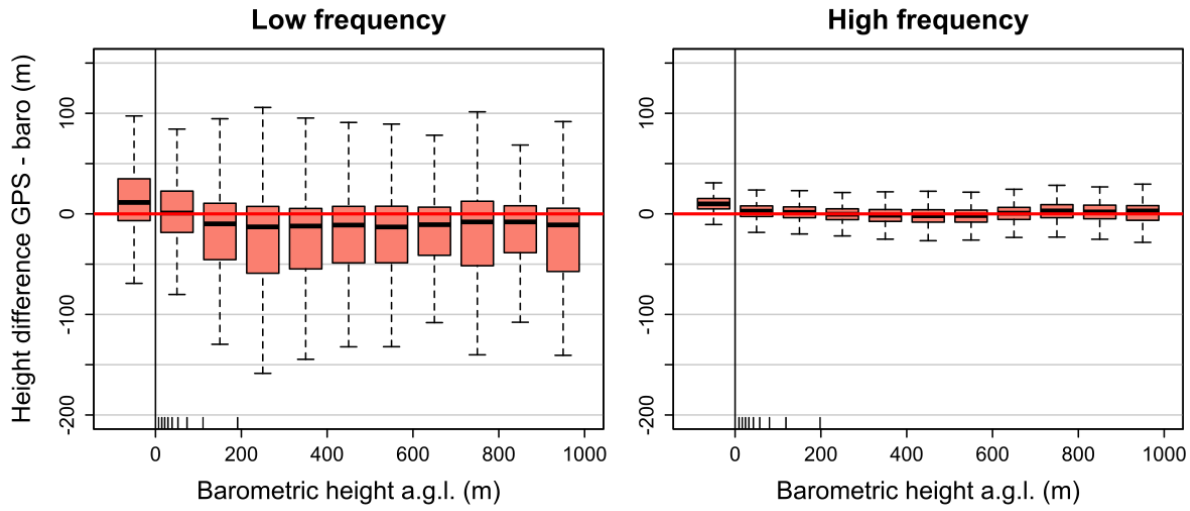

Figure A3.3.2: Difference between GPS and barometric height in relation to height above ground level (a.g.l.; range -100 and 1,000 m) for OT-25 GPS tags deployed on Red Kites in low- and high-frequency sampling (bins of 100 m). Only flight positions were considered. Thick horizontal lines indicate medians and boxes the ranges between the 1st and the 3rd quartiles; whiskers extend to the most extreme data point at a distance of no more than 1.5 times the interquartile range from the box; data points outside of whiskers were omitted. Sample size: 132,346 and 1,085,096 positions. Tick marks above the x-axis indicate deciles.

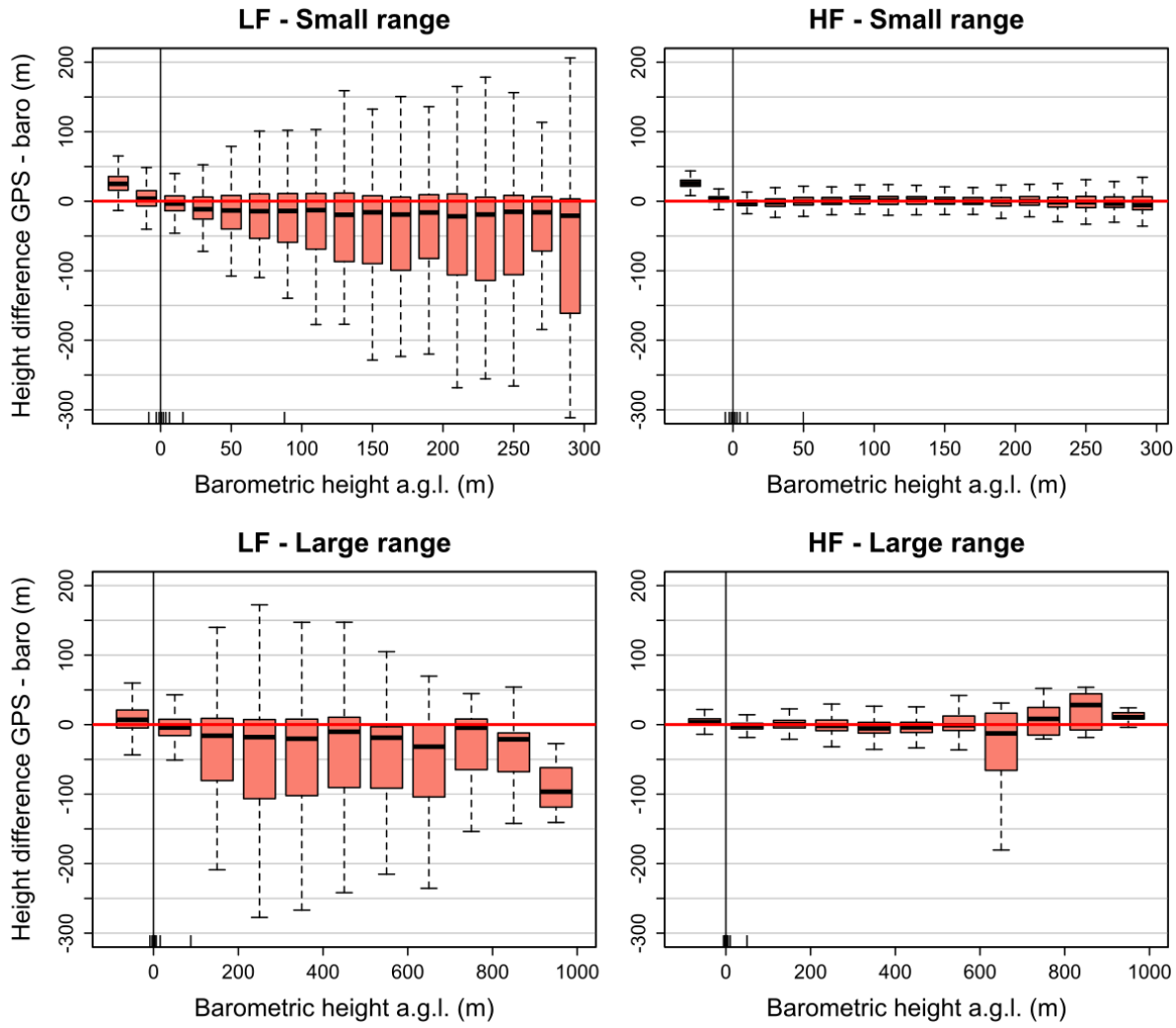

Figure A3.3.3: Difference between GPS and barometric height in relation to height above ground level (a.g.l.) for OT-15 GPS tags deployed on Marsh Harriers in low- (LF) and high-frequency (HF) sampling, in the range of -40 to 300 m a.g.l. (bins of 20 m; upper row) and -100 to 1,000 m a.g.l. (bins of 100 m; lower row). Only flight positions were considered. Thick horizontal lines indicate medians and boxes the ranges between the 1st and the 3rd quartiles; whiskers extend to the most extreme data point at a distance of no more than 1.5 times the interquartile range from the box; data points outside of whiskers were omitted. Sample sizes: 35,092; 171,779; 36,158; and 174,517 positions. Tick marks above the x-axis indicate deciles. Note decreasing sample size with increasing height.

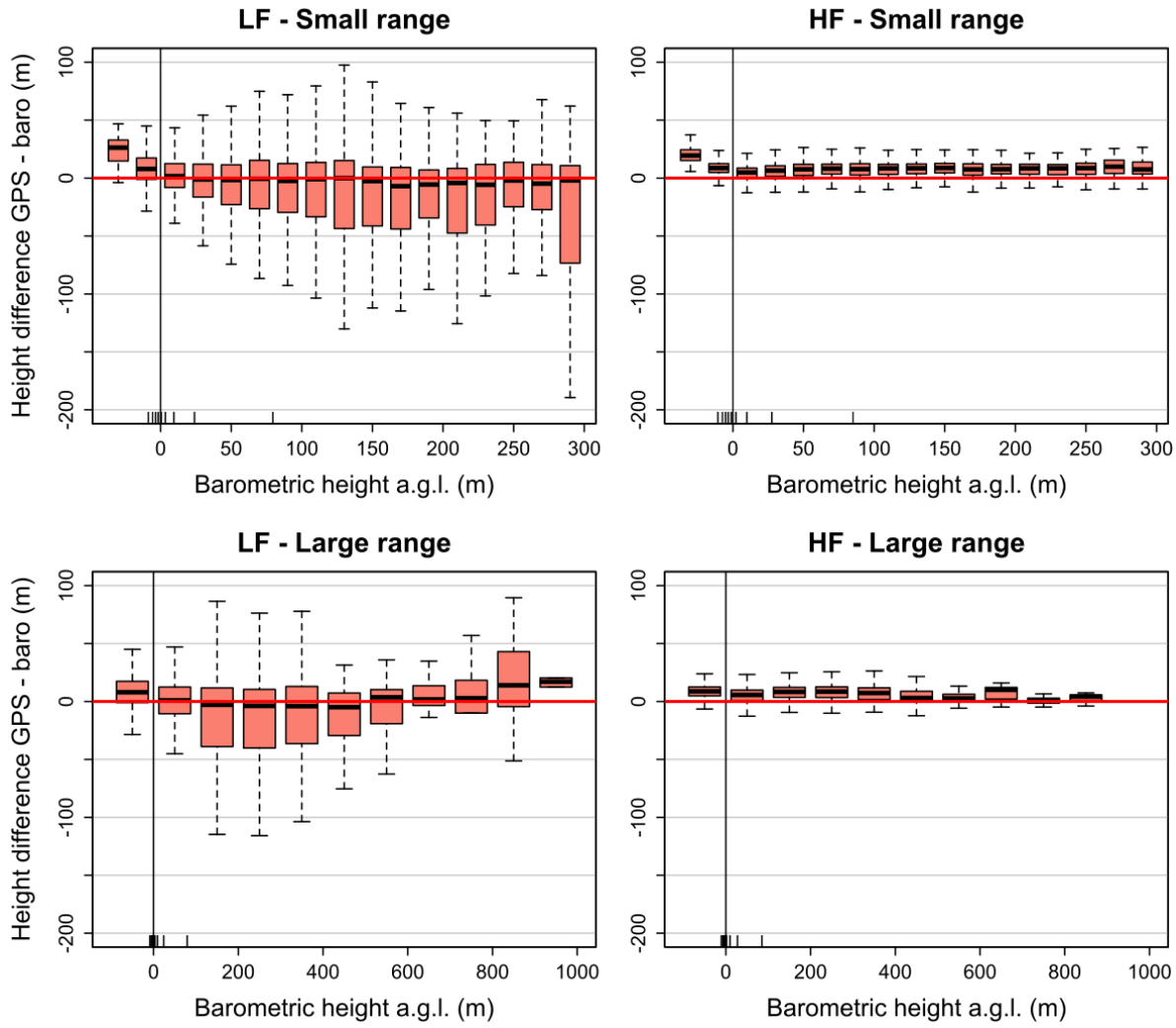

Figure 3.3.4: Difference between GPS and barometric height in relation to height above ground level (a.g.l.) for OT-20 GPS tags deployed on Marsh Harriers in low- (LF) and high-frequency (HF) sampling, in the range of -40 to 300 m a.g.l. (bins of 20 m; upper row) and -100 to 1,000 m a.g.l. (bins of 100 m; lower row). Only flight positions were considered. Thick horizontal lines indicate medians and boxes the ranges between the 1st and the 3rd quartiles; whiskers extend to the most extreme data point at a distance of no more than 1.5 times the interquartile range from the box; data points outside of whiskers were omitted. Sample sizes: 25,850; 90,200; 26,303; and 91,826 positions. Tick marks above the x-axis indicate deciles. Note decreasing sample size with increasing height.

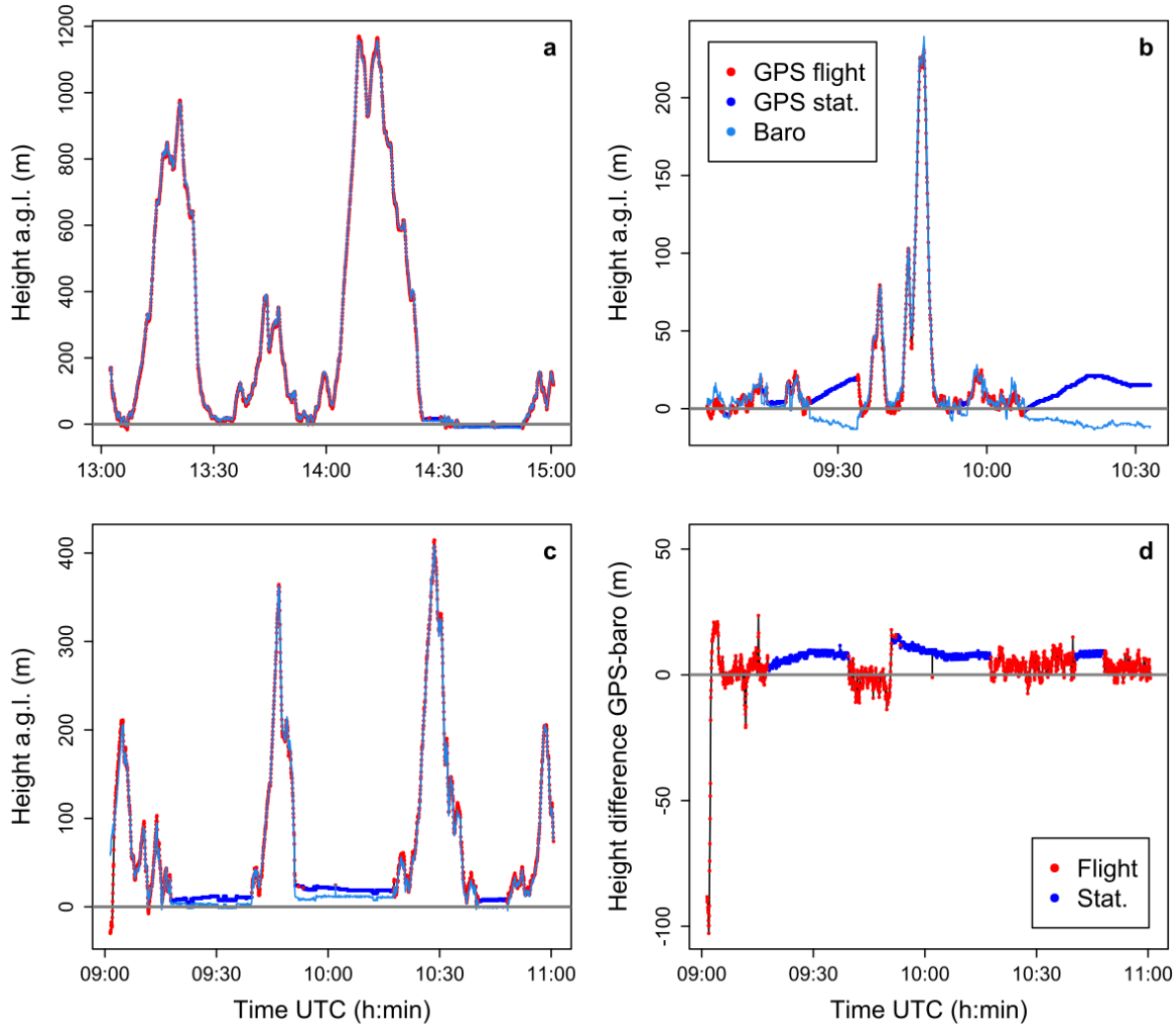

Figure A3.3.5: Additional examples of height profiles of high-frequency tracks: **a**) example showing closeness between GPS and barometric height (up to c. 1160 m a.g.l.; Red Kite Grand Est, tag model *Ornitela OT-25*); **b**) example showing drift of GPS height in stationary periods (Marsh Harrier Flevoland, *Ornitela OT-15*); **c**) example showing accuracy time lag in GPS height data in first minute of the sequence (quickly increasing GPS height; Red Kite Grand Est, *Ornitela OT-25*); **d**) difference between GPS and barometric height for the track from **c** indicating differences between stationary and flight positions. Note different time scales on the x-axis between panels (**a**, **c**, **d**: 120 min, **b**: 90 min). Legend in **b** applies also to **a** and **c**. a.g.l. = above ground level; stat. = stationary.

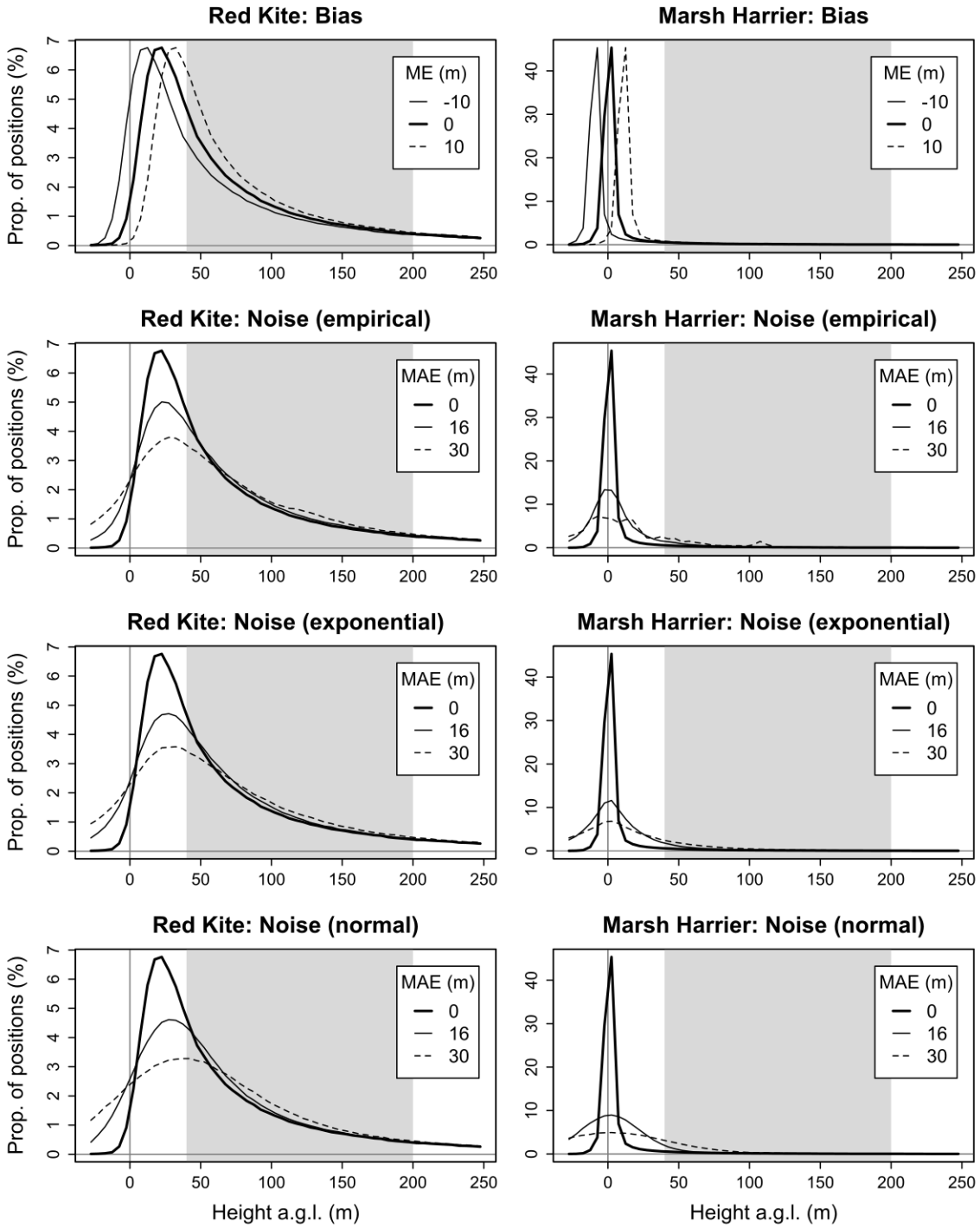

Figure A3.3.6: Flight height distributions of Red Kites and Marsh Harriers from high-frequency GPS tracking data (n = 1,329,191 and 407,355 positions; in height classes of 5 m), before and after application of different levels of additional bias or noise (two example levels shown per panel). Regarding noise, either empirical or theoretical (exponential or normal) error distributions were applied, the two applied levels of noise representing error distributions found in tag models *OT-20* (MAE 16.4 m) and *OT-25* (MAE 29.9 m) in this study (Table A3.2.3). Grey polygons represent the collision risk height range of 50-200 m a.g.l. Note different scales of the y-axis between the left and right column of panels. ME = median error; MAE = mean absolute error. Heights < -30 m and > 250 m not shown.

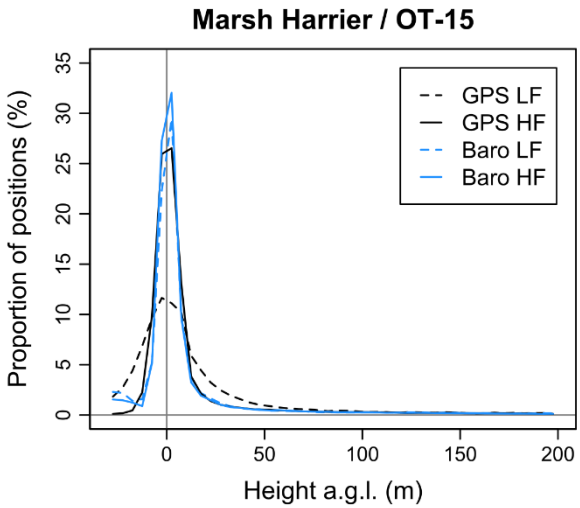

Figure A3.3.7: Flight height distributions of Marsh Harriers based on either GPS or barometric height data from *OT-15* GPS tags collected using either low- (LF) or high-frequency (HF) sampling (height classes of 5 m). Height data < -30 m and > 200 m above ground level (a.g.l.) not shown.

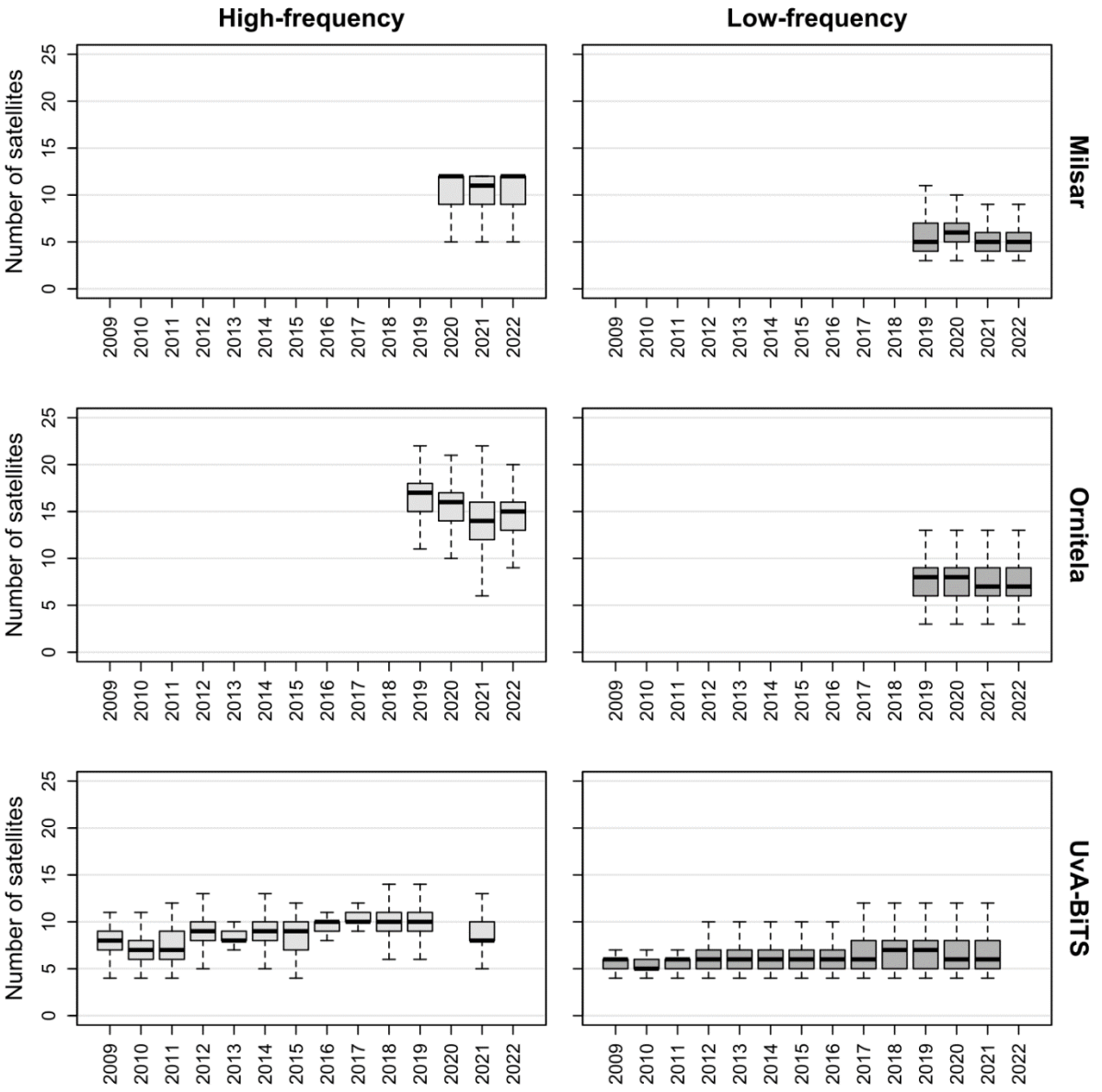

Figure A3.3.8: Number of satellites used for GPS fixes across years. Thick horizontal lines indicate medians and boxes the ranges between the 1st and the 3rd quartiles; whiskers extend to the most extreme data point at a distance of no more than 1.5 times the interquartile range from the box; data points outside of whiskers were omitted (overall maximum: 40). Sample sizes from left to right and top to bottom: 1,163,815; 903,528; 3,898,750; 1,049,230; 2,140,144; 697,374.

Appendix 3.4: Additional treatment of high-frequency GPS data (chapter 3)

Methods

We tested two treatments to reduce the vertical error associated with recurrent error patterns detected in the high-frequency (continuous-mode) GPS data. First, to reduce the error associated with "spikes", we applied a moving average to the high-frequency GPS data from *Milsar GsmTag-U9* tags. The data was restricted to sequences of at least 10 consecutive high-frequency positions. The moving average was applied on n = 3, 5 or 9 positions centred around the focal position with equal weight (Figure A3.4.1), using a function based on the *R* function *filter*. To compare the error in the treated data with the original height data, the original data was also restricted to the same set of data points for which the moving average were available (no moving average available for the first and last (n-1)/2 data points for every sequence).

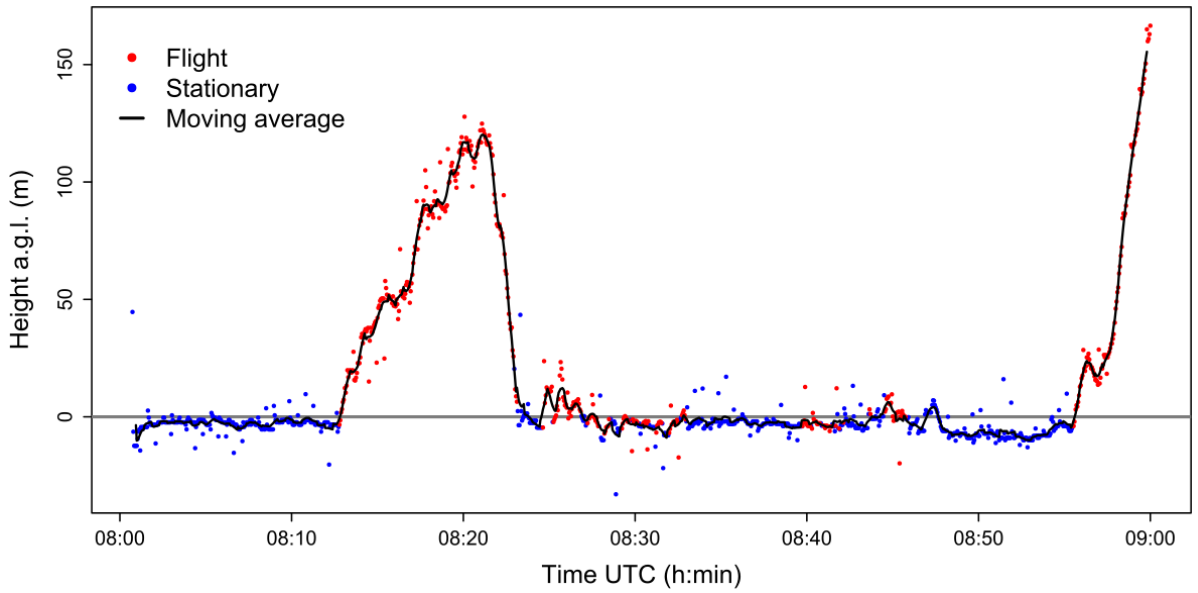

Figure A3.4.1: Example height profile of a high-frequency GPS track (1 h) from a *Milsar GsmTag-U9* tag to which a moving average was applied. Points: raw GPS height data; black line: moving average with a window of nine data points.

Secondly, to reduce the vertical error associated with the accuracy time lag at the start of high-frequency sequences, we removed the first 60 s of high-frequency sequences in the data of all tag models. For both treatments, we compared the accuracy relative to true height in the periods where the birds were stationary on the ground before and after the treatment.

Results

The error parameters all decreased after the moving average treatment compared to the original data (Table A3.4.1). The effect was larger with increasing number of adjacent positions included in the moving average. For example, applying a moving average with a window of nine data points to the high-frequency data of *Milsar GsmTag-U9* tags reduced the mean absolute error from 4.9 to 4.3 m and the 95% quantile of absolute error from 13.1 to 10.7 m.

The removal of the first minute of high-frequency sequences only led to a small increase in overall accuracy (Table A3.4.1). For example, the mean absolute error with true height as the reference decreased from 13.5 to 12.7 m in *GsmTag-U9* tags. Partly, the effect on the occurrence of extreme outliers was more substantial. For example, the proportion of positions with absolute error > 50 m decreased from 0.11% to 0.06% after the treatment in *5C.S* tags.

Table A3.4.1: Vertical accuracy based on stationary positions on the ground before and after additional treatment of high-frequency GPS tracking data (accuracy parameters with true height as reference). Moving averages (MA) across either three, five or nine adjacent positions were applied. AE = absolute error, prop. = proportion.

			Accuracy before treatment				Accuracy after treatment			
Method	**Tag model**	**N tags**	**N positions**	**Mean AE**	**95% AE**	**Prop. AE > 50 m (%)**	**N positions**	**Mean AE**	**95% AE**	**Prop. AE > 50 m (%)**
MA 3	GsmTag-U9	44	559,939	4.99	13.24	0.45	559,939	4.71	11.92	0.39
MA 5	GsmTag-U9	44	557,702	4.97	13.19	0.45	557,702	4.54	11.36	0.37
MA 9	GsmTag-U9	44	553,252	4.95	13.08	0.44	553,252	4.33	10.70	0.35
Remove first minute of sequence	GsmTag-U9	44	565,618	5.12	13.53	0.51	538,600	4.84	12.72	0.40
	OT-10	19	326,551	3.53	9.19	0.06	309,413	3.45	8.99	0.04
	OT-15	4	241,008	7.92	22.66	1.50	231,372	7.69	21.29	1.43
	OT-20	7	177,002	6.25	15.53	0.80	170,854	6.12	15.12	0.73
	OT-25	11	31,251	3.68	10.00	0.26	30,651	3.60	9.73	0.21
	4C.L	7	71,212	4.69	11.97	0.05	57,632	4.57	11.67	0.06
	4C.S	22	498,791	3.08	7.93	0.15	431,806	3.06	7.91	0.13
	5C.L	4	74,248	1.74	3.82	0.12	61,212	1.69	3.74	0.11
	5C.S	8	138,232	2.38	4.69	0.11	117,035	2.28	4.65	0.06
	6C.L	3	512,302	2.62	5.30	0.05	422,098	2.55	5.16	0.01

Appendix 4.1: Additional materials and methods (chapter 4)

Wind turbine data

For information about available wind turbine models and wind turbines installed in the study countries, we used the wind energy databases provided by The Wind Power (The Wind Power, 2022, 2023). We restricted the databases to onshore wind turbine models and onshore wind farms in the six study countries. Regarding the installed wind farms, information on wind turbine dimensions (diameter, ground clearance), commissioning year and number of wind turbines were available for 85% of all wind farms (combined fill rate for the four variables; n = 16,059 wind farms).

We used the wind turbine models database to estimate the relationship between the rated power and the rotor diameter. The database was restricted to diameters between 40 and 173 m (note that the database included only two models with larger diameters). Duplicated models were removed. With the remaining 1,360 models, a Generalized Additive Model (GAM) with the rated power as response and the rotor diameter as predictor variable (smooth term) was fitted using the function *gam* from the *R* package *mgcv* (Wood, 2017) applying a gamma error distribution with log-link. The parameter for the smooth term *k* ("dimension of the basis used to represent the smooth term") was set to 8 to prevent overfitting. 50% and 95% prediction intervals were derived by simulating from the posterior distribution of the GAM using the function *simulate* from the *R* package *gratia* (Simpson, 2023). Model assumptions were checked using diagnostic plots. The adjusted R^2 was 0.774, with 85% of deviance explained (Figure A4.1.3a).

Based on the same database, we also estimated the relationship between rotor diameter and mean rotation speed (revolutions per minute). Mean rotation speed was calculated as the mean of minimum rotation speed (cut-in speed) and maximum rotation speed (nominal speed), which were available for 408 wind turbine models. Note that this is a simplified approach, as in practice, the mean rotation speed of a wind turbine depends on the local wind conditions. As for the rated power, a GAM was fitted using a gamma error distribution with log-link. The adjusted R^2 was 0.83, with 83% of deviance explained. Besides rotation speed, we were also interested in the relationship of tip speed with rotor diameter; mean tip speed was calculated as the rotor circumference multiplied by the mean rotation speed (Figure A4.1.3c-d).

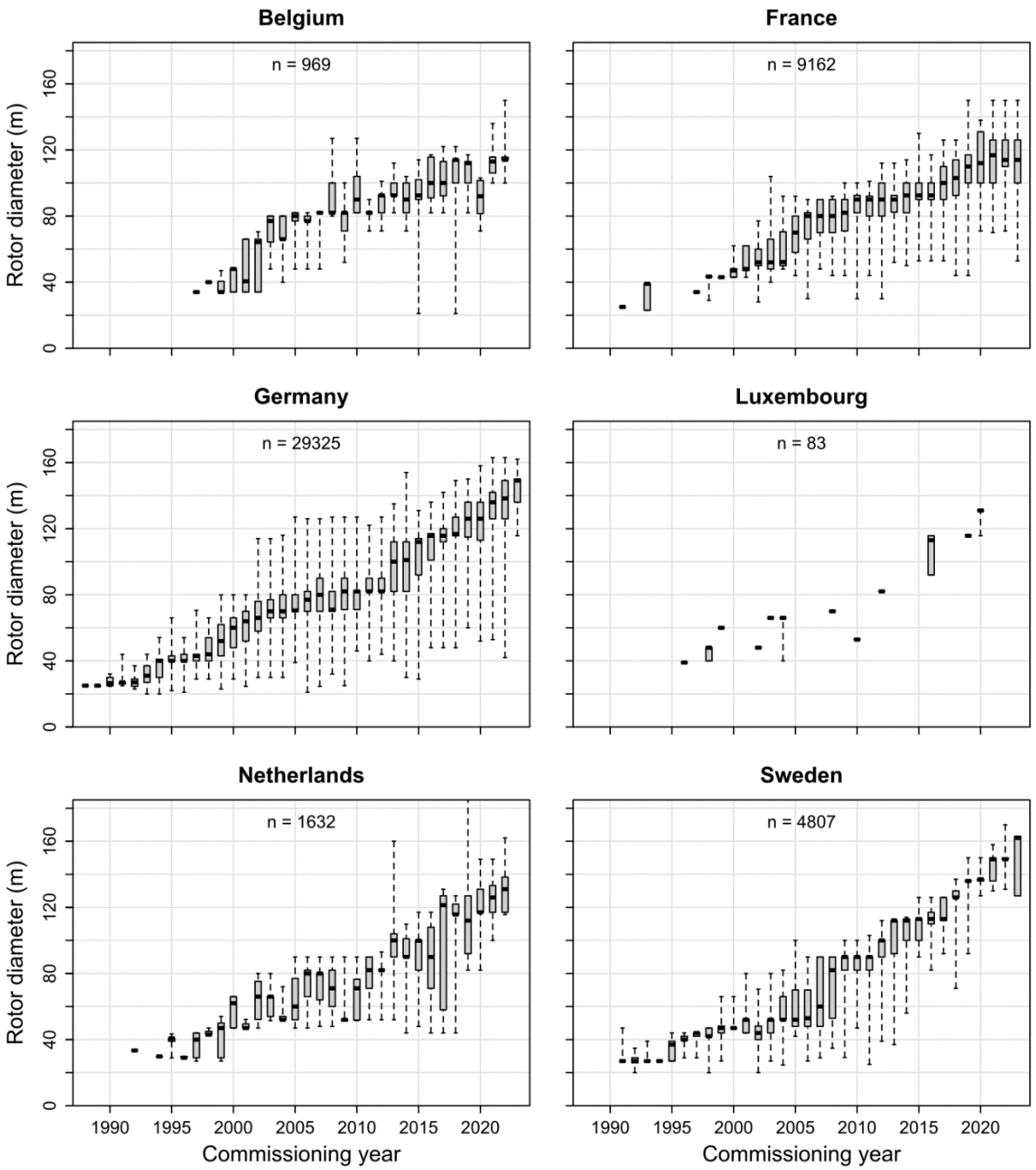

Figure A4.1.1: Trend of rotor diameter of commissioned wind turbines across years (1987-2023) in the six study countries. Whiskers extend to the data extremes. One wind turbine with diameter of 220 m not shown (Netherlands). Data source: The Wind Power (2022, 2023).

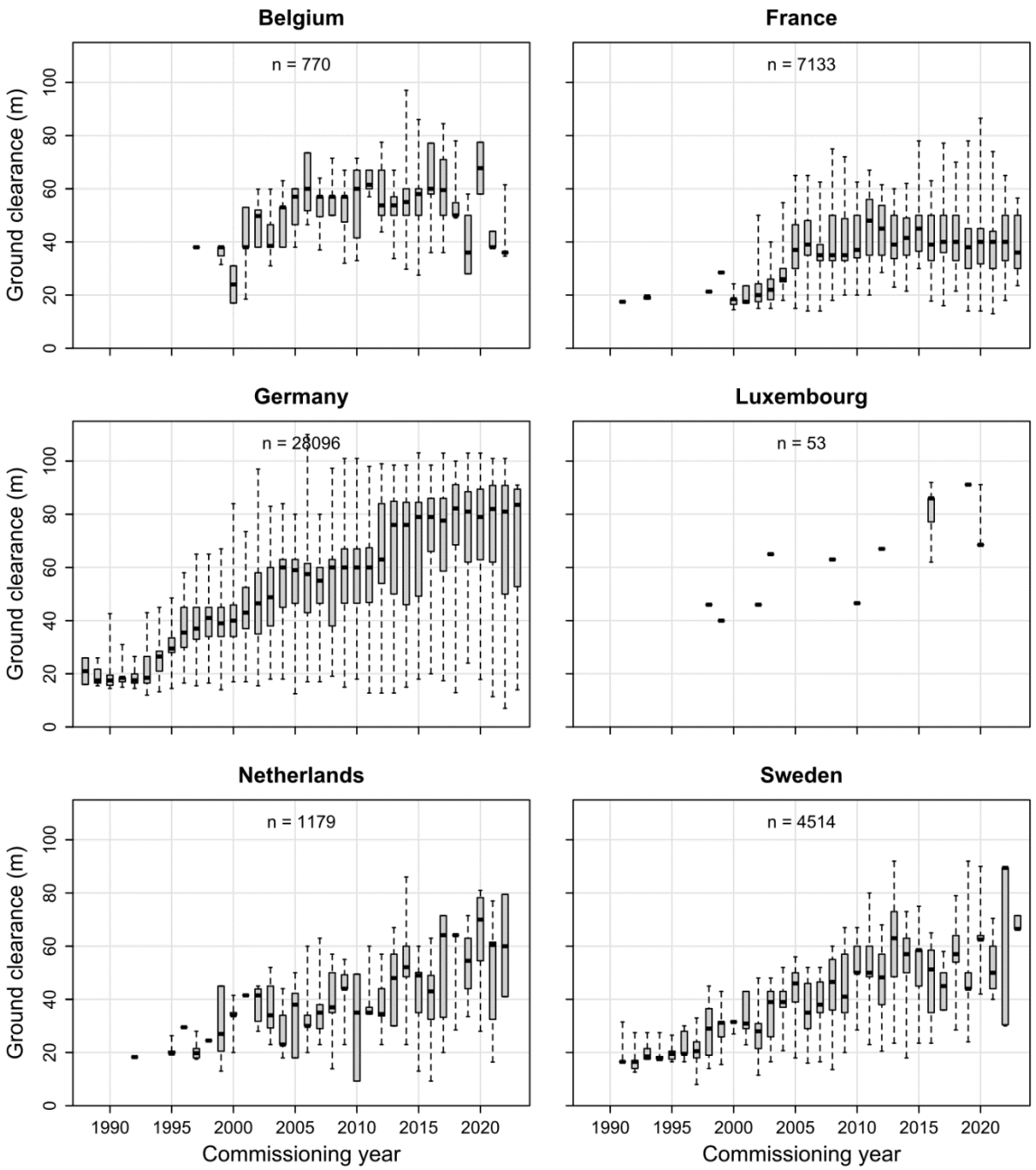

Figure A4.1.2: Trend of ground clearance of commissioned wind turbines across years (1987-2023) in the six study countries. Whiskers extend to the data extremes. Data source: The Wind Power (2022, 2023).

As information on the blade width was not available in the The Wind Power database, we manually collated blade width data for 59 wind turbine models based on information provided by the manufacturers. To assess the relationship between rotor diameter and maximum blade width, a GAM was fitted using a gamma error distribution with log-link. The adjusted R^2 was 0.94, with 94% of deviance explained (Figure A4.1.3b).

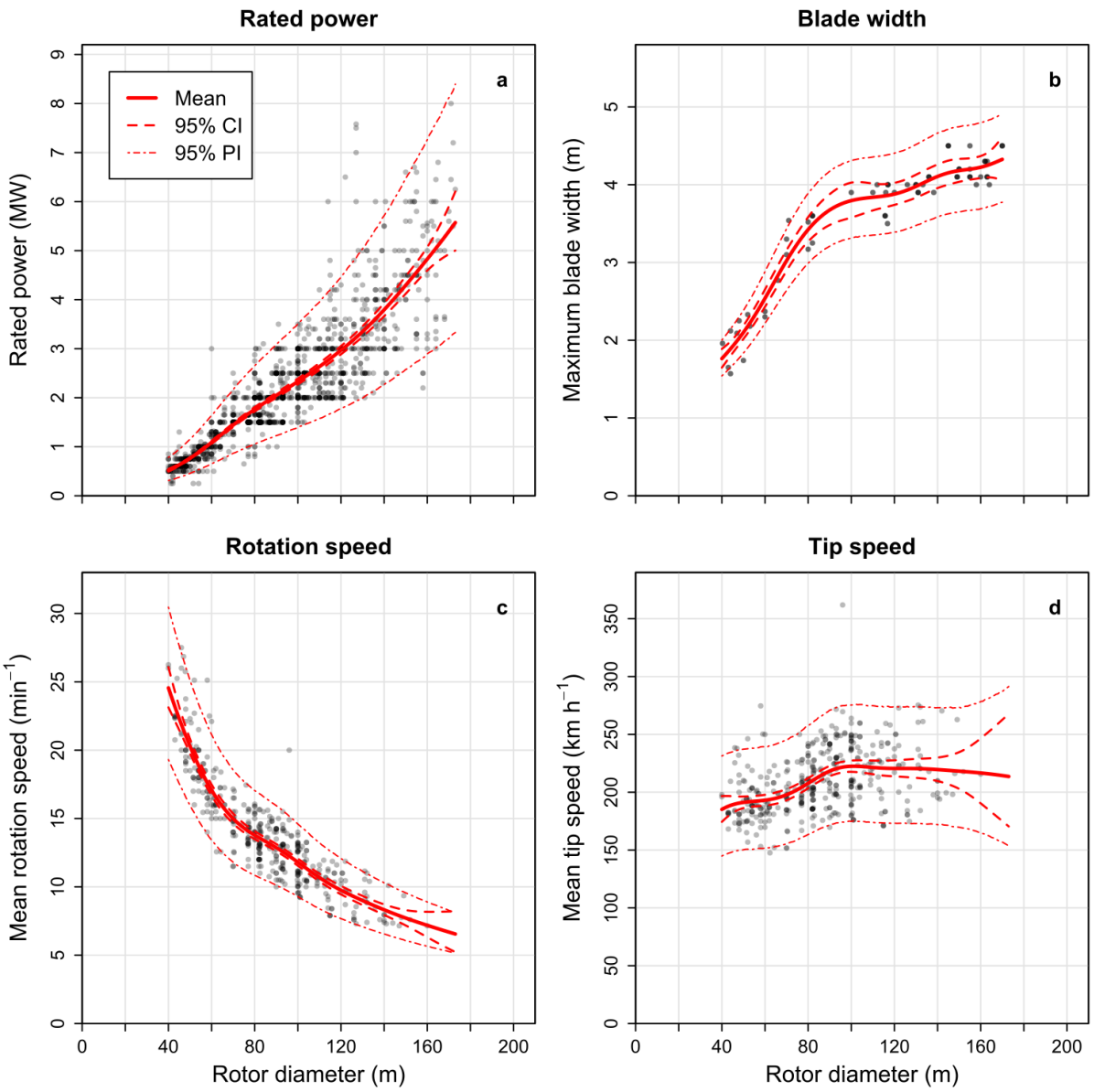

Figure A4.1.3: Relationship of different technical characteristics with rotor diameter in onshore wind turbines. Points: individual wind turbine models (n = 1,360 [**a**]; 59 [**b**]; 415 [**c**, **d**]). Lines: predictions from Generalized Additive Models. CI = confidence interval; PI = prediction interval.

Study areas

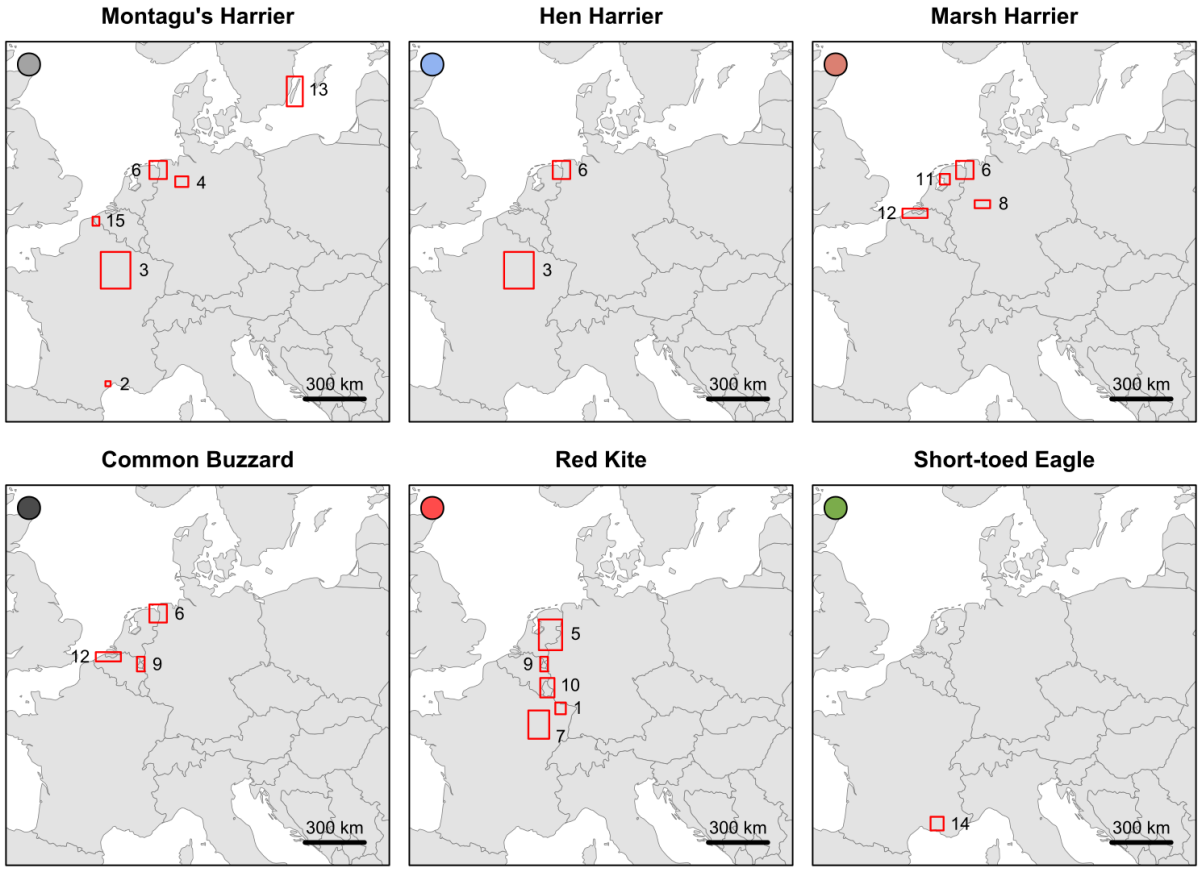

Figure A4.1.4: Location of the study areas per species within Europe. 1) Alsace (FR/DE), 2) Aumelas (FR), 3) Champagne (FR), 4) Diepholz (DE), 5) East NL (NL/DE), 6) Groningen (NL/DE), 7) Haute-Marne (FR), 8) Hellwegbörde (DE), 9) Limburg (NL/BE/DE), 10) Luxembourg (LU/BE/DE), 11) Noordoostpolder (NL), 12) NW Flanders (BE/NL), 13) Öland (SE), 14) Provence (FR), 15) SW Flanders (BE/FR). Background map created using the *R* package *maps* (Brownrigg et al., 2018).

Table A4.1.1: Overview of terrain elevation and ruggedness per study area. Elevation characteristics were based on the birds' GPS positions within the study areas. Areas are ordered by increasing terrain ruggedness (SD of elevation). MoH = Montagu's Harrier, HH = Hen Harrier, MaH = Marsh Harrier, CB = Common Buzzard, RK = Red Kite, STE = Short-toed Eagle.

				Elevation a.m.s.l. (m)			
Area	**Country**	**Species**	**N positions**	**Median**	**Min.**	**Max.**	**SD**
Noordoostpolder	NL	MaH	266,177	-5	-10	14	1.53
Groningen	NL/DE	MoH, HH, MaH, CB	1,674,790	-3	-10	18	1.96
NW Flanders	BE/NL	MaH, CB	228,510	0	-23	47	2.98
Öland	SE	MoH	130,638	8	-2	50	6.21
Diepholz	DE	MoH	43,605	45	26	84	6.30
SW Flanders	BE/FR	MoH	61,209	-1	-7	100	13.27
Hellwegbörde	DE	MaH	95,768	100	60	238	16.79
East NL	NL/DE	RK	205,849	12	-12	99	17.08
Alsace	FR/DE	RK	1,074,242	263	195	384	41.18
Champagne	FR	MoH, HH	649,373	136	53	366	41.75
Haute-Marne	FR	RK	524,053	379	206	521	42.51
Limburg	NL/BE/DE	CB, RK	614,604	149	18	390	55.20
Aumelas	FR	MoH	259,723	234	17	341	56.10
Provence	FR	STE	47,519	163	43	374	61.35
Luxembourg	LUX/BE/DE	RK	1,539,816	354	136	571	85.17

Collection and processing of GPS tracking data

The high-frequency data were collected using a GPS interval setting of 3 s in *Ornitela* and *UvA-BiTS* tags and 1 s in *Milsar* tags. With the set interval of 1 s, *Milsar* tags collected GPS fixes at intervals of 2-3 s in practice. These GPS fix intervals were below the manufacturer-specific time thresholds for the continuous GPS mode (< 7 s for *Ornitela*, < 8 s for Milsar, < 16 s for *UvA-BiTS*).

The GPS height data obtained from the tags was height above mean sea level (termed height a.m.s.l. hereafter), i.e. height above geoid. All three manufacturers indicated that the EGM96 geoid model was used. However, for the *Ornitela* tags, it was possible to also obtain the raw height data above the WGS84 ellipsoid initially determined by the GPS module before application of a geoid model. We noticed that the geoid model applied in these tags was biased compared to EGM96 by several meters in some study areas. Therefore, to obtain corrected height a.m.s.l. data, we used the height above ellipsoid data and applied the EGM96 geoid model with resolution of 0.25° (Agisoft, n.d.). The mean offset compared to the initial height a.m.s.l. using this procedure varied between -1.5 m and +5.0 m according to the study area. For *Milsar* and *UvA-BiTS*, it was not possible to obtain the height above ellipsoid data to apply the same approach.

In *Milsar* tags, GPS height data were internally and therefore irreversibly truncated at sea level, whereas no internal lower limit was applied in the data from the other two

manufacturers. However, as the ground level in all areas with *Milsar* data was above sea level, the truncation had no major implications for the aspects of the flight distributions we were interested in.

As the accuracy of GPS positions in the continuous mode usually increases after the first GPS positions taken (Corman & Garthe, 2014; Pfeiffer & Meyburg, 2022; T. Schaub et al., 2023), we removed the first minute of each bout of high-frequency data. We noted that the height data of *Milsar* tags in the high-frequency mode was characterised by frequent "spikes", i.e. single outliers with deviating height (T. Schaub et al., 2023). Therefore, we treated the *Milsar* data with a moving average based on 5 positions centred around the focal position with equal weight.

The *Shuttle Radar Topography Mission* (SRTM) global digital elevation model with a resolution of 30 m (NASA JPL, 2013) was downloaded through search.earthdata.nasa.gov (2023-04-12 & 2023-05-23).

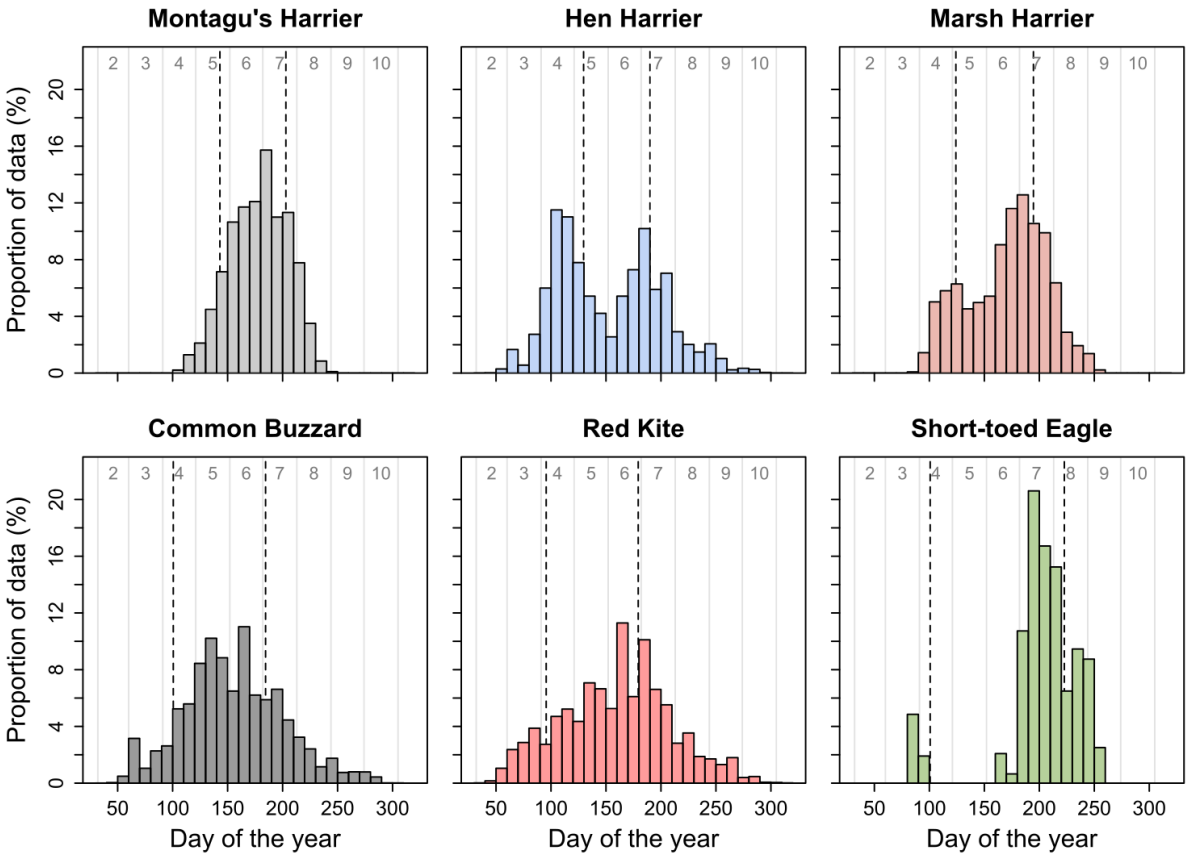

Figure A4.1.5: Distribution of the GPS tracking data across the calendar year per species in ten-day periods. Grey numbers and vertical lines indicate months. Dashed vertical lines indicate mean dates of egg-laying and fledging of chicks for the GPS-tagged birds. The data gap in STE between day 100 and 160 is due to the incubation period.

Table A4.1.2: Sample size overview per species-area combination. Prop. NB indicates the proportion of data from non-breeding birds in the dataset (based on time span; breeding status determined by calendar year). GPS tag models starting with "OT" are from manufacturer *Ornitela*; models with four-character code (e.g. "4CWL") are from *UvA-BiTS*; model GsmTag-U9 is from *Milsar*. Ind. = individuals, juv. = juvenile (tagged as nestling), pos. = GPS positions. MoH = Montagu's Harrier, HH = Hen Harrier, MaH = Marsh Harrier, CB = Common Buzzard, RK = Red Kite, STE = Short-toed Eagle.

Species	Study area	Data period	N ind. (≥ 5 h)	N ind. juv.	N pos.	Time span (h)	Prop. NB (%)	GPS tag models
MoH	Aumelas (FR)	2021-23	8 (7)	0	259,723	187.6	1.5	GsmTag-U9
MoH	Champagne (FR)	2020-23	13 (8)	0	288,905	207.0	5.4	GsmTag-U9, OT-10-3GC-C19
MoH	Diepholz (DE)	2020-21	3 (2)	0	43,605	34.8	0.0	GsmTag-U9
MoH	Groningen (NL/DE)	2009-23	42 (29)	0	1,122,413	979.7	0.7	4CWL, 4CWS, 5CDL, 5CDS, 5CWL, 5CWS, OT-10-3GC
MoH	Öland (SE)	2020-23	5 (4)	0	130,638	94.0	5.1	GsmTag-U9
MoH	SW Flanders (BE/FR)	2021-23	5 (4)	0	61,209	51.0	12.4	OT-10-3GC
HH	Champagne (FR)	2020-23	48 (19)	20	360,468	278.0	15.9	GsmTag-U9, OT-10-3GC, OT-10-3GC-C19, OT-E10-3GC, OT-E10-3GC-C19, OT-E10-4GC
HH	Groningen (NL/DE)	2012-14	3 (2)	0	25,903	22.4	0.0	4CWS
MaH	Groningen (NL/DE)	2012-21	7 (5)	0	371,690	317.7	0.0	4CWL, 6CWL
MaH	Hellwegbörde (DE)	2021-23	4 (3)	0	95,768	79.8	0.0	OT-15-3GC
MaH	Noordoostpolder (NL)	2019-23	12 (7)	4	266,177	218.5	5.4	OT-15B-3GC-C21, OT-20B-3GC-C21
MaH	NW Flanders (BE/NL)	2021-23	6 (4)	0	158,390	132.0	1.7	OT-15-3GC, OT-15-3GCT
CB	Groningen (NL/DE)	2021-23	10 (4)	0	154,784	128.6	2.7	OT-E25B-4GC-C3
CB	Limburg (NL/BE/DE)	2021-23	9 (8)	0	131,838	109.8	10.3	OT-E25B-4GC-C3
CB	NW Flanders (BE/NL)	2021-23	5 (3)	0	70,120	56.4	0.0	OT-E25B-4GC-C3
RK	Alsace (FR/DE)	2021-23	10 (10)	0	1,074,242	895.2	1.8	OT-E25B-4GC
RK	East NL (NL/DE)	2019-23	17 (10)	15	205,849	171.5	64.2	OT-E25B-3GC, OT-E25B-3GC-C7, OT-E25B-4GC
RK	Haute-Marne (FR)	2021-23	18 (15)	6	524,053	436.7	1.5	OT-E25B-4GC
RK	Limburg (NL/BE/DE)	2019-23	10 (8)	6	482,766	402.3	46.2	OT-E25B-3GC, OT-E25B-3GC-C7, OT-E25B-4GC
RK	Luxembourg (LU/BE/DE)	2019-23	38 (27)	19	1,539,816	1,283.2	7.9	OT-20B-3GC, OT-E25-3GC-C7, OT-E25B-3GC, OT-E25B-3GC-C7, OT-E25B-4GC, OT-E27B-3GC
STE	Provence (FR)	2021-23	2 (2)	0	47,519	39.6	0.0	OT-E25B-3GC

Collision risk index

For the biometric input parameters of the Band collision risk model (CRM), i.e. body length and wingspan, we applied the mean of the range indicated for each species in Ferguson-Lees & Christie (2001; Table A4.1.3). Rotation speed (revolutions per minute) and blade width were derived as a function of the rotor diameter using the GAM described above (section Wind turbine data). For analysing the effect of ground clearance, the predicted value for the given rotor diameter was used; for the effect of rotor diameter, we used a random draw from the posterior distribution of the GAM for each of the stochastic replicates using the function *simulate* from the *R* package *gratia* (Simpson, 2023). For flight speed, we used the instantaneous ground speed provided by the GPS tags alongside the 3D positions (mean ground speed across all GPS positions within the rotor height range of the given wind turbine model; Figure A4.1.6). We used the "extended" version of the Band CRM which takes into account the flight height distribution instead of assuming a uniform distribution of flights within the rotor height range (Band, 2012; Caneco et al., 2022). The flight height distributions were supplied as proportions per 1-m height band, as required by the *band_crm* function. The bootstrapping of the flight height distributions was performed on the level of the individual birds, excluding individuals with < 5 h of flight data. See Table A4.1.4 for an overview of all input parameters used in the CRM.

Table A4.1.3: Biometric input parameters for the Band collision risk model per study species (Ferguson-Lees & Christie, 2001). MoH = Montagu's Harrier, HH = Hen Harrier, MaH = Marsh Harrier, CB = Common Buzzard, RK = Red Kite, STE = Short-toed Eagle.

Parameter	MoH	HH	MaH	CB	RK	STE
Body length (m)	0.44	0.46	0.48	0.46	0.66	0.66
Wingspan (m)	1.13	1.11	1.30	1.23	1.57	1.77

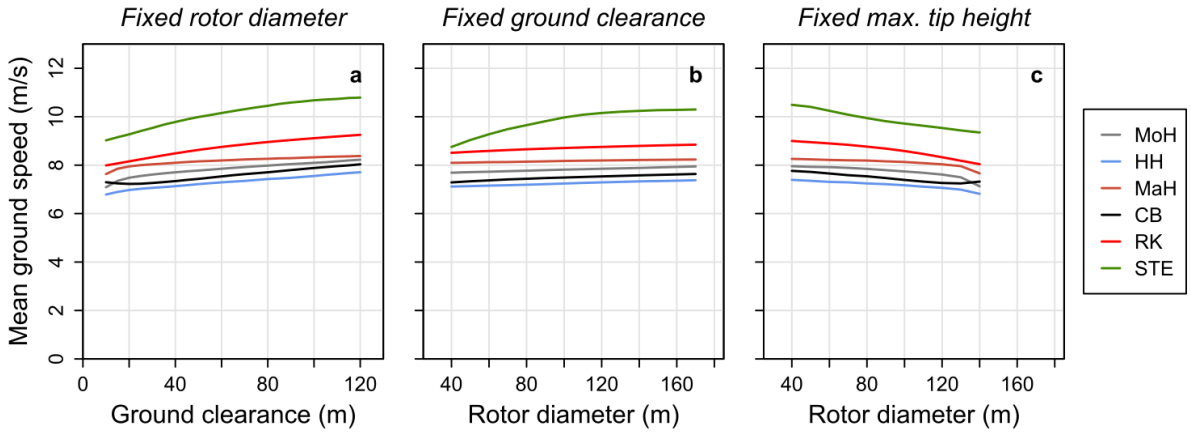

Figure A4.1.6: Mean flight speed (ground speed) within the rotor height ranges of wind turbines with varying dimensions. Panels refer to wind turbines with 120 m diameter (**a**), 60 m ground clearance (**b**) or maximum tip height of 150 m (**c**).

Per wind turbine model, the mean across the 500 stochastic replicates was used as estimate of the collision risk index, and the 2.5 and 97.5% quantiles as limits of the 95% confidence interval. To explore the underlying relationships of the CRM outcomes, we divided them into the two fundamental stages of the Band CRM, i.e. the number of rotor crossings N_{cross} (stage I) and the collision probability per rotor crossing P_{coll} (stage II). P_{coll} was calculated using the function *get_avg_prob_collision* from the *stochLAB* package (Caneco et al., 2022); no stochasticity was considered at this stage. N_{cross} was calculated by dividing the number of collisions N_{coll} (output from function *band_crm*; mean across stochastic replicates, see main text) by P_{coll} for each combination of wind turbine model and study species.

To obtain confidence intervals for the relative difference in the collision risk index for pairwise comparisons of wind turbine models (e.g. 20 m vs. 100 m ground clearance), mean and 2.5 and 97.5% quantiles were calculated across the relative difference values obtained for the pair of turbine models using the same bootstrap replicate for the flight height distribution.

We explored differences in the effect of ground clearance and rotor diameter on collision risk between study areas, by calculating the CRI for each hypothetical wind turbine model and each species-area combination. Flight height distributions per study area were used (lumping data across individuals; Appendix 4.2: Figure A4.2.1), while for the other CRM input parameters, we used generic data as in the version of the CRI on the species level (Table A4.1.4). No stochasticity was included.

Table A4.1.4: Input parameters for Band collision risk models built with the *R* function *band_crm*. RHR = rotor height range; GAM = Generalized Additive Model; GC = ground clearance; RD = rotor diameter.

Parameter of *band_crm* function	Explanation	Value	Stochasticity
model_options	Model options	'3' (extended model with generic flight height distribution)	no
flight_speed	Bird flying speed	Mean of instantaneous ground speed of GPS positions within RHR (Figure A4.1.6)	no
body_lt	Length of the bird	Value from literature per species (Table A4.1.3)	no
wing_span	Wingspan of the bird	Value from literature per species (Table A4.1.3)	no
flight_type	Flight type ('flapping' or 'gliding')	'gliding'	no
avoid_rt_ext	Avoidance rate for the extended model	0.98	no
noct_activity	Nocturnal flight activity level	0 (for all months)	no
dens_month	Estimates of daytime in-flight bird densities per month within the windfarm footprint	0.1 km^{-2} (for all months)	no
prop_upwind	Proportion of flights upwind	0.5	no
gen_fhd	Flight height distributions of the species	Based on GPS tracking data	GC, RD
rotor_speed	Operational rotation speed	Function of rotor diameter (based on GAM; Figure A4.1.3c)	RD
rotor_radius	Radius of the rotor	According to definition of wind turbine model	no
blade_width	Maximum blade width	Function of rotor diameter (based on GAM; Figure A4.1.3b)	RD
blade_pitch	Average blade pitch angle (angle between blade surface and rotor plane)	0.09 rad (5°)	no
n_blades	Number of blades in rotor	3	no
hub_height	Height of the rotor hub	According to definition of wind turbine model	no
chord_prof	Chord taper profile of the rotor blade	chord_prof_5MW (default; profile of a 5-MW turbine)	no
n_turbines	Number of turbines in the wind farm	1	no
turb_oper_month	Proportion of time during which turbines are operational per month	0.8 (for all months)	no
wf_width	Approximate longitudinal width of the wind farm	5 km	no
wf_latitude	Latitude of the centroid of the windfarm	51°	no
tidal_offset	Tidal offset (difference between highest astronomical tide and mean sea level)	0	no
lrg_arr_corr	Large array correction	FALSE	no
yinc, xinc	Increments along the y-axis and x-axis for numerical integration across segments of the rotor circle (proportion of rotor radius)	0.05 (default)	no

Appendix 4.2: Additional results (chapter 4)

Table A4.2.1: Results from Kruskal-Wallis rank-sum tests on differences in parameters of flight height distributions between species and between study areas within species. No within-species tests were performed for Short-toed Eagle (data only from one study area). Significant tests are indicated in bold (significance levels of 0.05 for between-species tests and 0.01 within-species tests). Range indicates the minimum and maximum of values per species (between-species test), or across the individuals of the given species (within-species tests), in the raw data as an approximate indication of effect size. See Table A4.2.2 for post-hoc tests for the between-species level. MoH = Montagu's Harrier, HH = Hen Harrier, MaH = Marsh Harrier, CB = Common Buzzard, RK = Red Kite.

Parameter/level	Spec.	N groups	N ind.	χ2	d.f.	P value	Range
Mode (m)							
Between-species	**All**	**6**	**181**	**138.7**	**5**	**<0.001**	**2.5-127.5**
Within-species	**MoH**	**6**	**54**	**29.5**	**5**	**<0.001**	**2.5-7.5**
Within-species	HH	2	21	0.5	1	0.482	2.5-2.5
Within-species	MaH	4	19	3.8	3	0.281	2.5-2.5
Within-species	CB	3	15	2.6	2	0.269	7.5-7.5
Within-species	RK	5	70	6.2	4	0.185	17.5-27.5
Prop. of mode (%)							
Between-species	**All**	**6**	**181**	**146.4**	**5**	**<0.001**	**2.0-36.9**
Within-species	**MoH**	**6**	**54**	**28.7**	**5**	**<0.001**	**25.4-44.5**
Within-species	HH	2	21	5.2	1	0.023	23.0-39.7
Within-species	**MaH**	**4**	**19**	**11.9**	**3**	**0.008**	**22.8-47.5**
Within-species	CB	3	15	1.9	2	0.395	8.1-10.0
Within-species	**RK**	**5**	**70**	**19.9**	**4**	**0.001**	**3.6-6.9**
Median (m)							
Between-species	**All**	**6**	**181**	**141.8**	**5**	**<0.001**	**3.0-187.9**
Within-species	**MoH**	**6**	**54**	**31.5**	**5**	**<0.001**	**2.5-8**
Within-species	HH	2	21	3.2	1	0.072	3.0-7.6
Within-species	MaH	4	19	7.5	3	0.057	1.0-7.1
Within-species	CB	3	15	1.0	2	0.592	35.3-39.1
Within-species	**RK**	**5**	**70**	**16.4**	**4**	**0.003**	**48.4-93.2**
IQR (m)							
Between-species	**All**	**6**	**181**	**115.7**	**5**	**<0.001**	**11-204.3**
Within-species	**MoH**	**6**	**54**	**17.9**	**5**	**0.003**	**6.1-25.4**
Within-species	HH	2	21	2.1	1	0.151	18-33.8
Within-species	MaH	4	19	10.3	3	0.016	6.0-33.0
Within-species	CB	3	15	0.5	2	0.791	80.7-85.0
Within-species	RK	5	70	12.4	4	0.014	78.2-174.0
Prop. 32-200 m (%)							
Between-species	**All**	**6**	**181**	**141**	**5**	**<0.001**	**11.4-54.2**
Within-species	MoH	6	54	8.1	5	0.148	9.7-16.1
Within-species	HH	2	21	1.4	1	0.231	16.4-20.9
Within-species	MaH	4	19	3.0	3	0.395	7.1-17.5
Within-species	CB	3	15	0.5	2	0.763	44.4-48.7
Within-species	RK	5	70	6.7	4	0.150	51.6-56.9

Table A4.2.2: Results from Dunn tests on differences in parameters of flight height distributions between species (post-hoc tests for Kruskal-Wallis tests, see Table A4.2.1). "N ind." indicates the number of individuals for each of the two species of the given pair. Significant pair-wise comparisons are indicated in bold. Adj. = adjusted, MoH = Montagu's Harrier, HH = Hen Harrier, MaH = Marsh Harrier, CB = Common Buzzard, RK = Red Kite, STE = Short-toed Eagle.

Parameter	Species pair	N ind. 1	N ind. 2	z value	P value (adj.)
Mode (m)	MoH : HH	54	21	-1.14	1.000
	MoH : MaH	54	19	-0.63	1.000
	MoH : CB	**54**	**15**	**3.02**	**0.038**
	MoH : RK	**54**	**70**	**9.40**	**<0.001**
	MoH : STE	**54**	**2**	**3.44**	**0.009**
	HH : MaH	21	19	0.39	1.000
	HH : CB	**21**	**15**	**3.47**	**0.008**
	HH : RK	**21**	**70**	**8.02**	**<0.001**
	HH : STE	**21**	**2**	**3.75**	**0.003**
	MaH : CB	**19**	**15**	**3.04**	**0.036**
	MaH : RK	**19**	**70**	**7.23**	**<0.001**
	MaH : STE	**19**	**2**	**3.56**	**0.006**
	CB : RK	15	70	2.89	0.058
	CB : STE	15	2	2.12	0.506
	RK : STE	70	2	1.08	1.000
Prop. of mode (%)	MoH : HH	54	21	-2.33	0.296
	MoH : MaH	54	19	-1.43	1.000
	MoH : CB	**54**	**15**	**-4.93**	**<0.001**
	MoH : RK	**54**	**70**	**-11.17**	**<0.001**
	MoH : STE	**54**	**2**	**-3.78**	**0.002**
	HH : MaH	21	19	0.69	1.000
	HH : CB	21	15	-2.48	0.197
	HH : RK	**21**	**70**	**-5.72**	**<0.001**
	HH : STE	21	2	-2.87	0.062
	MaH : CB	**19**	**15**	**-3.06**	**0.033**
	MaH : RK	**19**	**70**	**-6.35**	**<0.001**
	MaH : STE	**19**	**2**	**-3.15**	**0.025**
	CB : RK	15	70	-2.06	0.597
	CB : STE	15	2	-1.70	1.000
	RK : STE	70	2	-0.97	1.000
Median	MoH : HH	54	21	1.40	1.000
	MoH : MaH	54	19	0.39	1.000
	MoH : CB	**54**	**15**	**4.55**	**<0.001**
	MoH : RK	**54**	**70**	**10.55**	**<0.001**
	MoH : STE	**54**	**2**	**3.62**	**0.004**
	HH : MaH	21	19	-0.81	1.000
	HH : CB	21	15	2.86	0.063
	HH : RK	**21**	**70**	**6.23**	**<0.001**
	HH : STE	**21**	**2**	**3.04**	**0.035**
	MaH : CB	**19**	**15**	**3.55**	**0.006**
	MaH : RK	**19**	**70**	**6.98**	**<0.001**
	MaH : STE	**19**	**2**	**3.37**	**0.011**
	CB : RK	15	70	2.04	0.615
	CB : STE	15	2	1.70	1.000
	RK : STE	70	2	0.98	1.000

Table A4.2.2 (continued)

Parameter	Species pair	N ind. 1	N ind. 2	z value	P value (adj.)
IQR (m)	MoH : HH	54	21	2.91	0.054
	MoH : MaH	54	19	1.14	1.000
	MoH : CB	**54**	**15**	**5.63**	**<0.001**
	MoH : RK	**54**	**70**	**9.74**	**<0.001**
	MoH : STE	**54**	**2**	**3.45**	**0.009**
	HH : MaH	21	19	-1.41	1.000
	HH : CB	21	15	2.65	0.122
	HH : RK	**21**	**70**	**4.08**	**0.001**
	HH : STE	21	2	2.34	0.288
	MaH : CB	**19**	**15**	**3.88**	**0.002**
	MaH : RK	**19**	**70**	**5.64**	**<0.001**
	MaH : STE	19	2	2.93	0.051
	CB : RK	15	70	0.42	1.000
	CB : STE	15	2	1.11	1.000
	RK : STE	70	2	1.00	1.000
Prop. 32-200 m (%)	MoH : HH	54	21	2.19	0.430
	MoH : MaH	54	19	0.66	1.000
	MoH : CB	**54**	**15**	**5.27**	**<0.001**
	MoH : RK	**54**	**70**	**10.83**	**<0.001**
	MoH : STE	54	2	2.41	0.241
	HH : MaH	21	19	-1.22	1.000
	HH : CB	21	15	2.88	0.059
	HH : RK	**21**	**70**	**5.62**	**<0.001**
	HH : STE	21	2	1.58	1.000
	MaH : CB	**19**	**15**	**3.94**	**0.001**
	MaH : RK	**19**	**70**	**6.90**	**<0.001**
	MaH : STE	19	2	2.09	0.543
	CB : RK	15	70	1.49	1.000
	CB : STE	15	2	0.26	1.000
	RK : STE	70	2	-0.32	1.000

Table A4.2.3: Descriptive statistics for flight height distributions per species and species-area combination. The mode was determined using bins of 5 m (centre of bin with highest proportion of positions). Proportion of mode refers to the proportion of positions in the bin of the mode. Ind. = individuals, prop. = proportion, Q1/Q3 = first/third quartile, IQR = interquartile range, SD = standard deviation. See Table A4.2.2 for species abbreviations.

Spec.	Study area	N ind.	Time span (h)	Mode (m)	Mode prop. (%)	Median (m)	Mean (m)	Q1 (m)	Q3 (m)	IQR (m)	SD (m)	Prop. 32-200 m (%)
MoH	All	76	1554.2	2.5	36.9	4.0	29.6	1.0	12.6	11.6	82.0	12.1
	Aumelas	8	187.6	7.5	28.7	8.0	30.2	4.0	15.8	11.8	77.3	12.5
	Champagne	13	207.0	2.5	25.4	7.8	49.8	3.6	27.4	23.8	109.8	15.2
	Diepholz	3	34.8	2.5	29.3	4.0	40.4	0.0	25.4	25.4	93.8	16.1
	Groningen	42	979.7	2.5	43.0	3.0	25.1	0.0	8.0	8.0	75.6	11.2
	Öland	5	94.0	2.5	37.0	3.6	22.8	0.4	12.0	11.6	65.6	12.5
	SW Flanders	5	51.0	2.5	44.5	2.5	21.9	0.4	6.5	6.1	66.5	9.7
HH	All	51	300.4	2.5	24.1	7.2	41.6	1.6	34.2	32.6	96.2	20.6
	Champagne	48	278.0	2.5	23.0	7.6	42.5	1.8	35.6	33.8	97.7	20.9
	Groningen	3	22.4	2.5	39.7	3.0	28.0	1.0	19.0	18.0	70.8	16.4
MaH	All	29	747.9	2.5	34.4	3.0	26.7	-0.3	10.7	11.0	81.4	11.4
	Groningen	7	317.7	2.5	47.5	1.0	10.1	-1.0	5.0	6.0	37.8	7.1
	Hellwegbörde	4	79.8	2.5	22.8	5.3	45.3	0.3	23.5	23.2	110.4	15.3
	Noordoostpolder	12	218.5	2.5	25.0	3.7	27.5	-1.3	12.7	14.0	78.0	12.3
	NW Flanders	6	132.0	2.5	26.3	7.1	53.1	2.1	35.1	33.0	121.6	17.5
CB	All	24	294.9	7.5	9.4	37.4	71.7	13.3	95.3	82.0	92.9	46.1
	Groningen	10	128.6	7.5	10.0	38.4	73.5	14.4	96.4	82.0	94.0	46.4
	Limburg	9	109.8	7.5	9.4	35.3	69.0	10.6	91.3	80.7	92.2	44.4
	NW Flanders	5	56.4	7.5	8.1	39.1	72.8	15.1	100.1	85.0	91.4	48.7
RK	All	93	3188.9	22.5	6.1	51.3	94.5	24.4	114.3	89.9	122.1	54.2
	Alsace	10	895.2	22.5	6.9	48.4	87.2	25.4	103.6	78.2	110.3	55.8
	East NL	17	171.5	27.5	3.6	93.2	163.3	38.9	212.9	174.0	189.6	52.7
	Haute-Marne	18	436.7	22.5	6.8	49.4	91.0	25.4	106.3	80.9	121.6	56.5
	Limburg	10	402.3	22.5	5.5	56.4	95.2	26.4	119.4	93.0	114.0	56.9
	Luxembourg	38	1283.2	17.5	6.1	48.7	91.2	21.9	112.3	90.4	118.1	51.6
STE	Provence	2	39.6	127.5	2.0	187.9	228.9	114.9	319.2	204.3	157.2	47.7

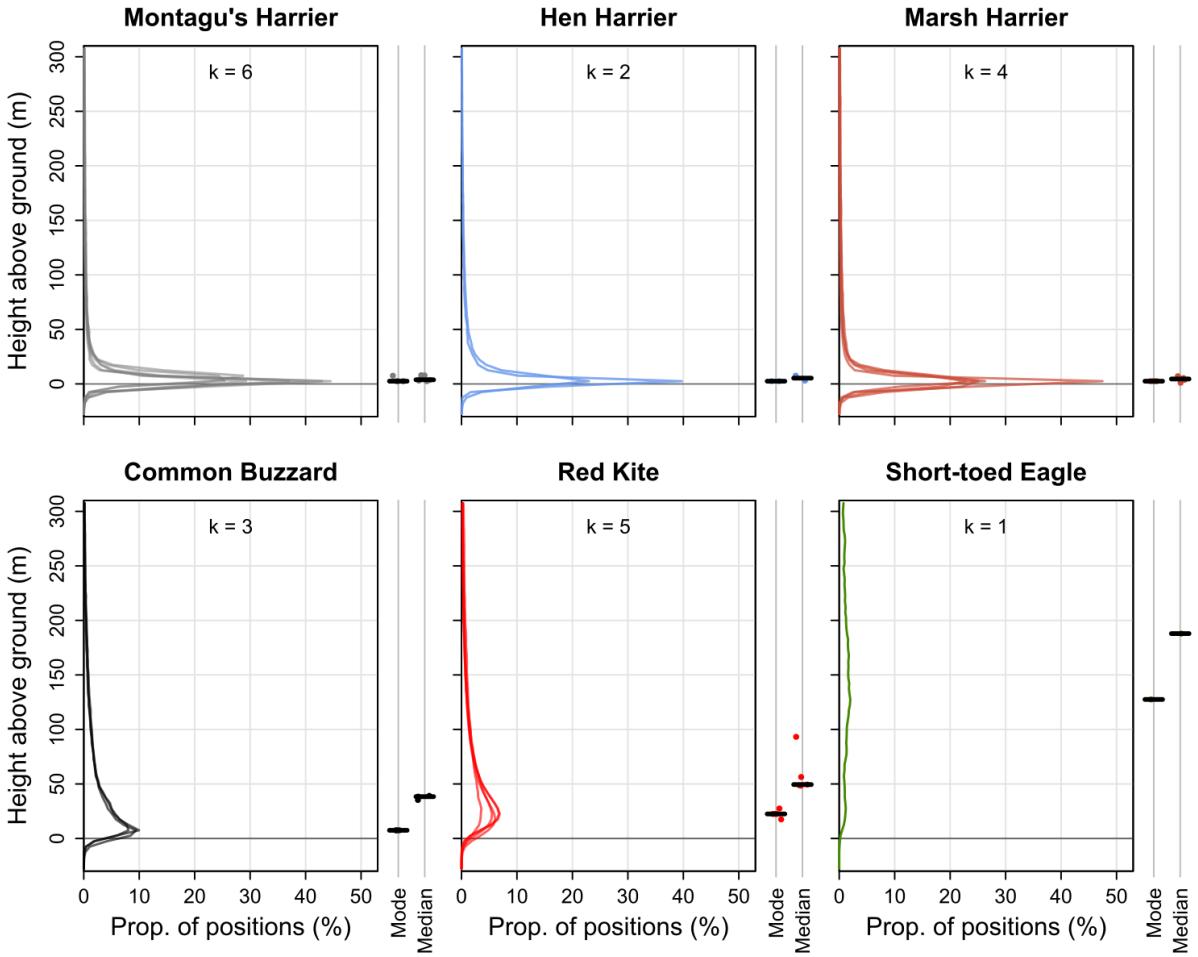

Figure A4.2.1: Flight height distributions per combination of species and study area in height bins of 5 m. The distributions of modes and medians are indicated right of the panels (thick horizontal line indicating median across study areas). Prop. = proportion; k = number of study areas.

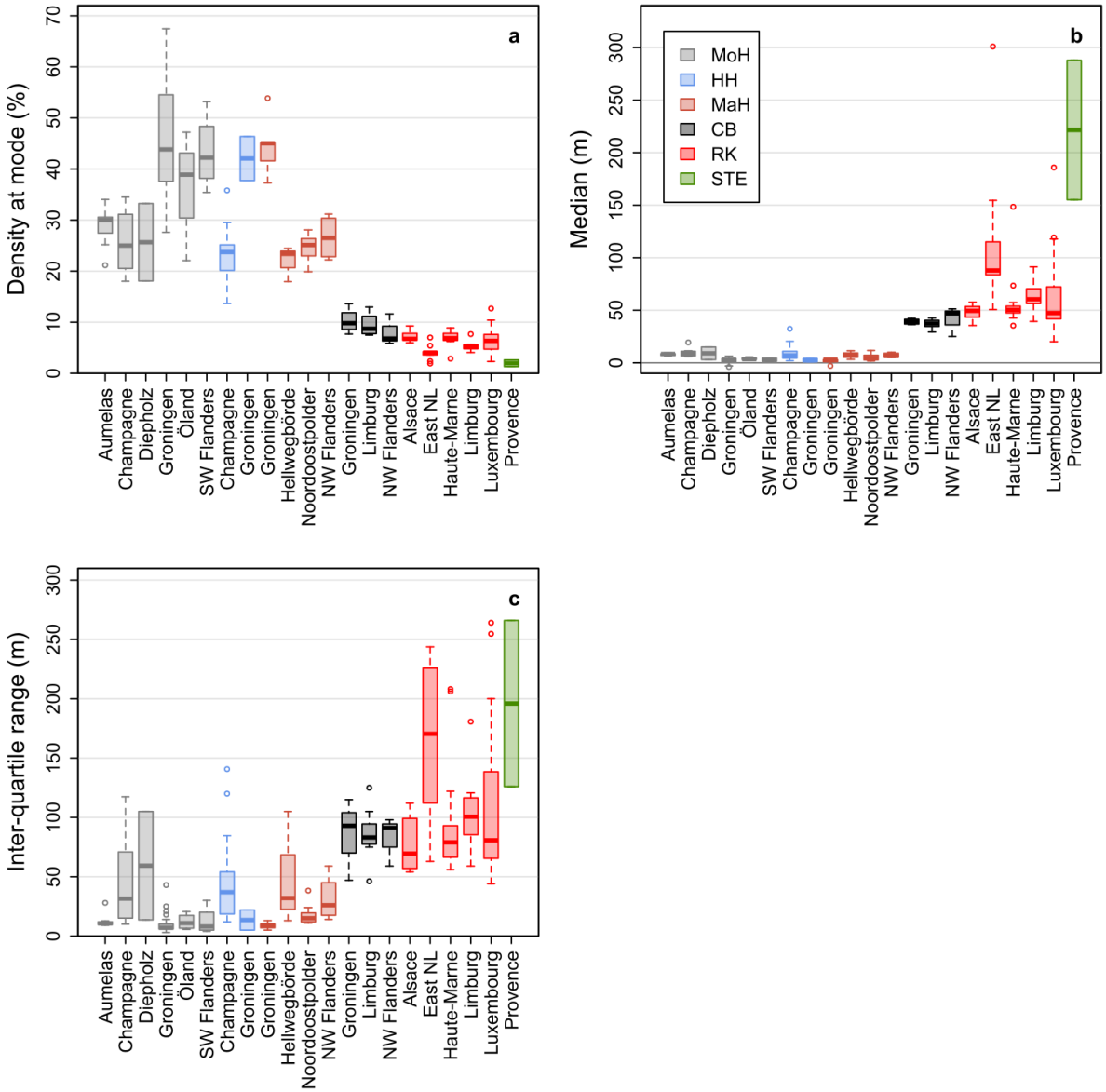

Figure A4.2.2: Proportion of mode (**a**), median (**b**) and interquartile range (**c**) of flight height distributions of six raptor species, per study area. Every data point represents one individual with ≥ 5 h of recorded flight data (n = 181; 2-29 per area). In **c**, one RK fell outside the applied y-axis range (IQR of 407 m; study area East NL). MoH = Montagu's Harrier, HH = Hen Harrier, MaH = Marsh Harrier, CB = Common Buzzard, RK = Red Kite, STE = Short-toed Eagle.

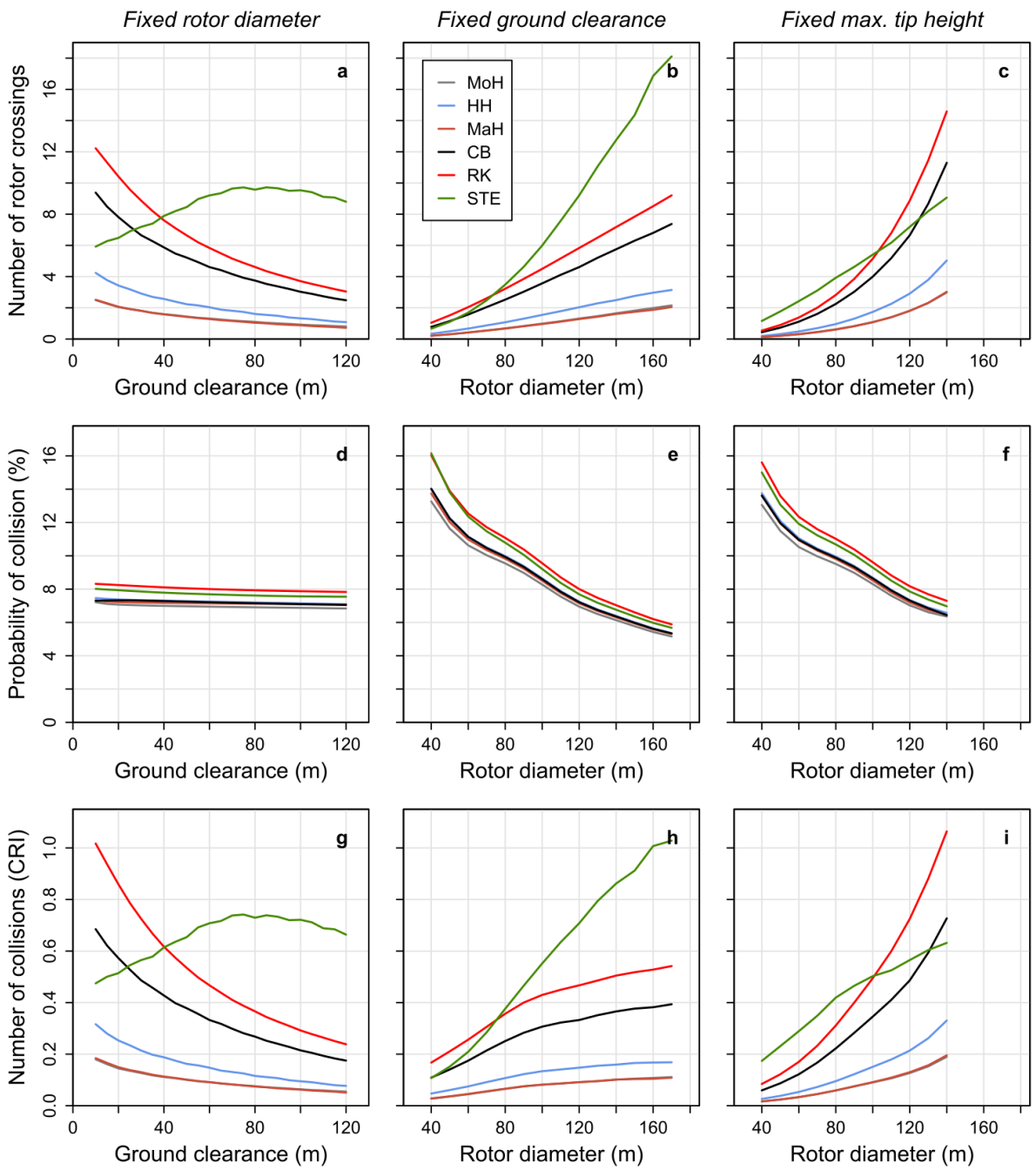

Figure A4.2.3: Effect of ground clearance and rotor diameter of wind turbines on collision risk, divided into the different stages of the Band collision risk model. First row of panels: number of rotor crossings per year (stage I); second row: collision probability per rotor crossing (stage II); third row: number of collisions per year (product of stages I and II; used as collision risk index [CRI]). Note that lines partly lie on top of each other. Wind turbine specifications as for Figure 4.6 were applied. See Figure A4.2.2 for species abbreviations.

Table A4.2.4: Relative change of the collision risk index for pairwise comparisons of different levels of ground clearance and rotor diameter of wind turbines (mean and 95% confidence interval; significant difference indicated in bold). Start value, end value and fixed level refer to different parameters depend on the scenario: 1) ground clearance varied, rotor diameter fixed; 2) rotor diameter varied, ground clearance fixed; 3) rotor diameter varied, maximum tip height fixed. For example, the first row refers to the difference between wind turbines with a ground clearance of either 20 or 10 m, both with a diameter of 120 m. Scen. = scenario, var. = variable; val. = value. See caption of Figure A4.2.1 for species abbreviations.

Scen.	Vari.	Start val. (m)	End val. (m)	Fixed level (m)	Relative change of collision risk index (%) MoH	HH	MaH	CB	RK	STE
1	CRI per turbine	20	10	120	**24 (21; 28)**	**25 (21; 29)**	**24 (19; 27)**	**20 (16; 23)**	**18 (17; 20)**	**-7 (-10; -1)**
		20	50	120	**-31 (-33; -29)**	**-36 (-39; -32)**	**-32 (-37; -28)**	**-34 (-40; -29)**	**-38 (-39; -36)**	**26 (10; 34)**
		20	80	120	**-48 (-50; -45)**	**-54 (-59; -49)**	**-51 (-56; -45)**	**-53 (-60; -47)**	**-57 (-59; -55)**	**39 (12; 53)**
		20	100	50	**-66 (-68; -63)**	**-70 (-74; -66)**	**-67 (-73; -62)**	**-68 (-75; -61)**	**-73 (-75; -71)**	**103 (17; 164)**
		20	100	120	**-56 (-59; -53)**	**-62 (-67; -58)**	**-58 (-65; -52)**	**-62 (-69; -56)**	**-66 (-68; -64)**	**38 (13; 51)**
		20	100	160	**-52 (-55; -49)**	**-62 (-66; -58)**	**-57 (-62; -51)**	**-61 (-67; -54)**	**-63 (-65; -61)**	**5 (3; 7)**
		30	50	120	**-21 (-23; -19)**	**-24 (-27; -21)**	**-22 (-26; -18)**	**-22 (-28; -18)**	**-26 (-28; -25)**	**15 (10; 18)**
		30	60	120	**-28 (-30; -26)**	**-31 (-35; -27)**	**-30 (-35; -25)**	**-32 (-38; -26)**	**-36 (-37; -34)**	**23 (8; 31)**
		60	80	120	**-17 (-19; -15)**	**-22 (-25; -17)**	**-19 (-22; -15)**	**-19 (-23; -16)**	**-22 (-23; -20)**	**3 (3; 4)**
		60	100	120	**-30 (-33; -28)**	**-36 (-40; -32)**	**-32 (-37; -27)**	**-35 (-40; -31)**	**-37 (-39; -35)**	**2 (1; 5)**
2	CRI per turbine	50	120	60	**155 (114; 201)**	**144 (99; 190)**	**150 (108; 196)**	**138 (93; 186)**	**123 (86; 161)**	**360 (274; 451)**
		50	160	20	**140 (100; 184)**	**120 (79; 169)**	**129 (86; 171)**	**132 (84; 181)**	**107 (69; 149)**	**668 (330; 1003)**
		50	160	60	**204 (157; 258)**	**179 (129; 233)**	**186 (139; 241)**	**174 (119; 238)**	**151 (111; 193)**	**558 (448; 682)**
		50	160	100	**230 (183; 286)**	**179 (132; 235)**	**204 (153; 268)**	**187 (137; 244)**	**181 (137; 238)**	**301 (237; 378)**
		90	120	60	**22 (4; 44)**	**21 (2; 42)**	**21 (3; 43)**	18 (0; 38)	17 (-2; 38)	**51 (28; 77)**
		90	160	60	**45 (24; 71)**	**38 (14; 63)**	**39 (17; 62)**	**35 (14; 63)**	**32 (12; 56)**	**117 (86; 152)**
		120	160	60	19 (0; 39)	14 (-3; 34)	15 (-2; 35)	15 (-3; 35)	13 (-5; 35)	**44 (24; 68)**
2	CRI per power	50	120	60	-32 (-68; 23)	-33 (-69; 21)	-33 (-69; 25)	-34 (-67; 28)	-39 (-69; 16)	27 (-44; 134)
		50	160	20	**-60 (-80; -25)**	**-63 (-83; -35)**	**-61 (-81; -29)**	**-61 (-83; -33)**	**-66 (-84; -35)**	27 (-50; 143)
		50	160	60	**-50 (-76; -12)**	**-53 (-79; -11)**	**-52 (-77; -15)**	**-54 (-77; -20)**	**-57 (-80; -18)**	11 (-47; 101)
		50	160	100	-45 (-74; 1)	**-53 (-77; -16)**	**-49 (-75; -3)**	**-50 (-76; -8)**	**-54 (-77; -17)**	-33 (-67; 31)
		90	120	60	-11 (-59; 67)	-12 (-56; 63)	-13 (-58; 67)	-15 (-56; 51)	-14 (-59; 52)	10 (-48; 102)
		90	160	60	-35 (-71; 19)	-38 (-68; 11)	-38 (-72; 18)	-40 (-68; 5)	-39 (-70; 13)	-4 (-57; 75)
		120	160	60	-22 (-63; 38)	-25 (-66; 38)	-24 (-64; 34)	-25 (-65; 31)	-25 (-64; 43)	-7 (-54; 80)

Table A4.2.4 (continued)

Scen.	Var.	Start val. (m)	End val. (m)	Fixed level (m)	Relative change of collision risk index (%) MoH	HH	MaH	CB	RK	STE
3	CRI per	50	130	150	**537 (438; 662)**	**589 (467; 738)**	**566 (450; 703)**	**587 (445; 727)**	**631 (514; 778)**	**169 (119; 243)**
3	turbine	90	120	150	**70 (45; 100)**	**75 (46; 105)**	**74 (48; 108)**	**72 (44; 108)**	**83 (53; 120)**	**23 (3; 47)**
3		90	130	150	**104 (71; 141)**	**115 (79; 156)**	**110 (78; 148)**	**110 (76; 150)**	**123 (86; 162)**	**33 (9; 66)**
3		90	130	200	**86 (58; 116)**	**94 (65; 129)**	**88 (56; 124)**	**94 (65; 135)**	**96 (63; 131)**	**50 (29; 77)**
3		90	140	150	**155 (115; 205)**	**171 (125; 220)**	**161 (114; 217)**	**157 (113; 209)**	**168 (125; 219)**	**38 (14; 68)**
3		90	170	200	**221 (169; 273)**	**244 (187; 317)**	**232 (169; 300)**	**250 (185; 327)**	**271 (205; 344)**	**80 (52; 115)**
3		120	140	150	**50 (26; 76)**	**56 (30; 84)**	**50 (25; 81)**	**50 (29; 78)**	**47 (22; 74)**	12 (-6; 32)
3	CRI per	50	130	150	51 (-27; 166)	68 (-28; 230)	63 (-25; 204)	64 (-17; 191)	78 (-14; 214)	-35 (-69; 15)
3	power	90	120	150	23 (-41; 133)	26 (-40; 128)	26 (-44; 136)	27 (-41; 140)	32 (-36; 141)	-11 (-59; 68)
3		90	130	150	32 (-37; 141)	38 (-31; 154)	37 (-34; 158)	34 (-31; 157)	45 (-27; 169)	-14 (-61; 66)
3		90	130	200	22 (-41; 127)	22 (-42; 116)	24 (-42; 136)	26 (-37; 138)	25 (-41; 116)	-3 (-56; 75)
3		90	140	150	46 (-29; 172)	50 (-28; 174)	46 (-33; 169)	45 (-27; 182)	52 (-23; 165)	-21 (-63; 53)
3		90	170	200	29 (-39; 135)	36 (-34; 157)	34 (-34; 147)	37 (-31; 162)	47 (-28; 167)	-28 (-67; 42)
3		120	140	150	26 (-37; 137)	25 (-43; 134)	23 (-38; 116)	23 (-42; 117)	22 (-39; 128)	-7 (-57; 70)

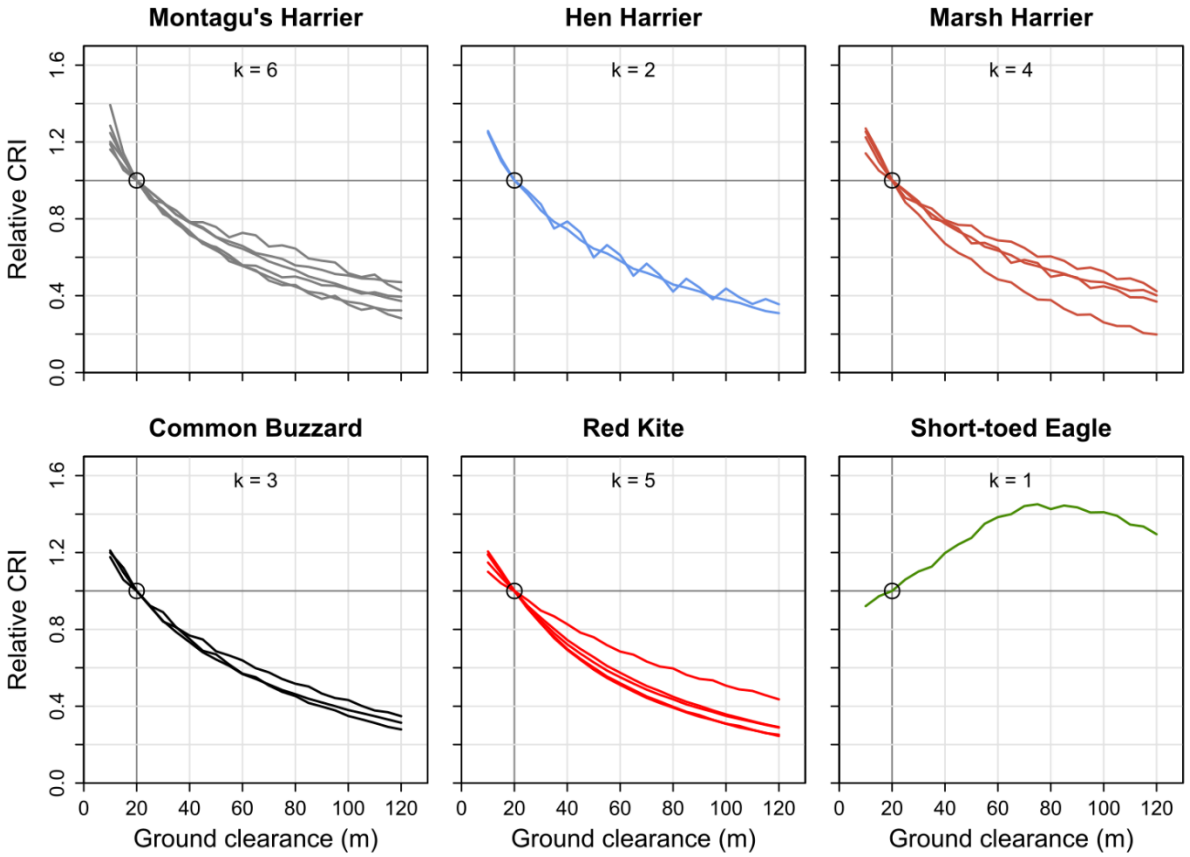

Figure A4.2.4: Effect of the ground clearance of wind turbines on the collision risk index (CRI) per study area, for wind turbines with a rotor diameter of 120 m. The CRI was expressed relative to the reference level of 20 m. Note that jagged curves are an artifact of the CRI calculation with the *band_crm* function, appearing mainly in study areas with relatively small sample size in the flight height data. k = number of study areas.

Figure A4.2.5: Effect of the rotor diameter of wind turbines on the collision risk index (CRI) per study area, for wind turbines with a ground clearance of 60 m. The CRI was expressed relative to the reference level of 50 m. k = number of study areas.

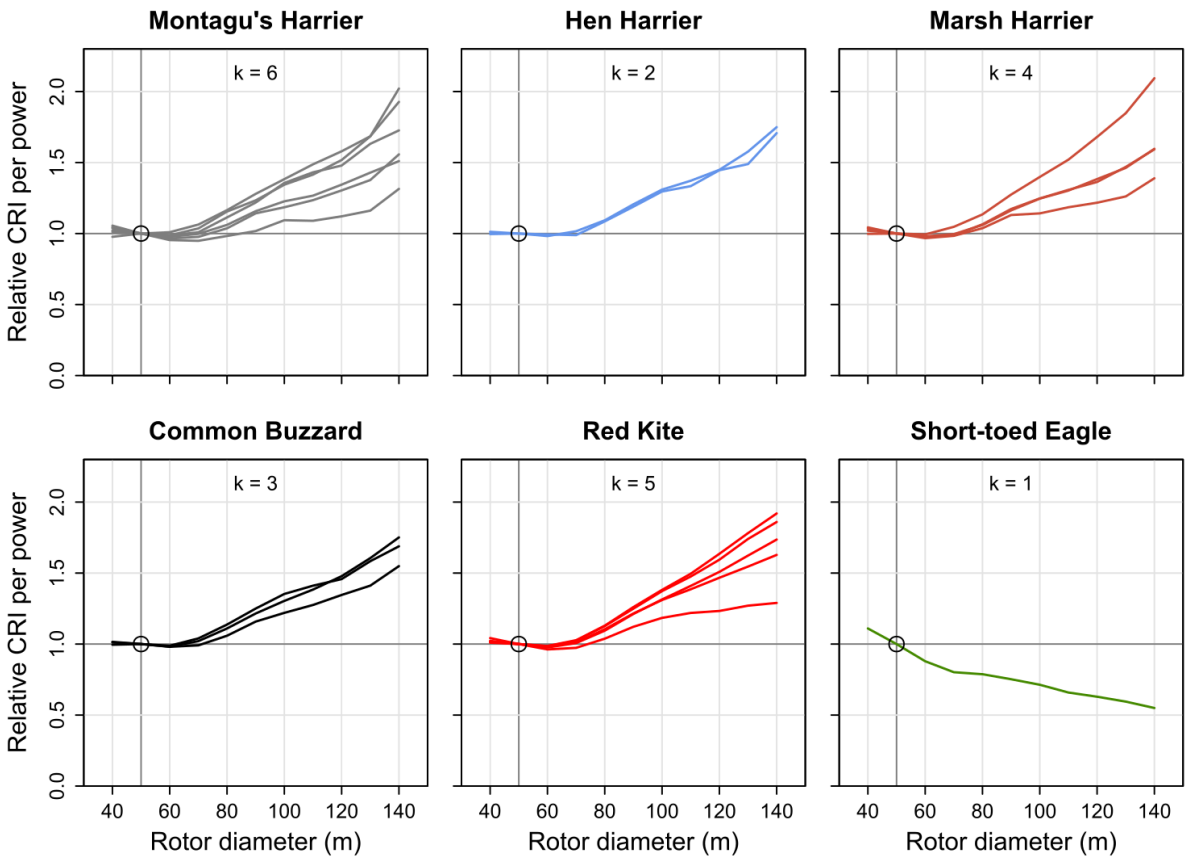

Figure A4.2.6: Effect of the rotor diameter of wind turbines on the collision risk index (CRI) per study area, for wind turbines with a maximum tip height of 150 m. The CRI was expressed relative to the reference level of 50 m. k = number of study areas.

Appendix 4.3: Information on local GPS-tracking projects (chapter 4)

Table A4.3.1: Information on local tracking projects. MoH = Montagu's Harrier, HH = Hen H., MaH = Marsh H., CB = Common Buzzard, RK = Red Kite.

Study area	Species	Involved persons (in addition to co-authors)	Funding	Permit
Alsace (FR)	RK	Arthur Keller, Sébastien Didier (LPO Alsace), Christelle Scheid (Ecofaune), Alexandre Gill (La Volerie des Aigles), Wouter Pieters and colleagues (Parc Animalier de Sainte-Croix), Alexandre Eich (Office National des Forêts)	ENGIE Green, CNR	PP 987 A. Mionnet (CRBPO)
Aumelas (FR)	MoH	Camille Montégu, Aurélie Béa (LPO Occitanie), Colin Moffa (Aix Marseille Univ), Carole Millon (GepB)	Aix Marseille Univ, Natural England	PP 633 T. Printemps (CRBPO)
Champagne (FR)	MoH, HH	José Dorey, Roland Faynot, Bernard Vacheret, Laurent Cocquyt, Gérard Crouzier, Claude Bouillon (GepB)	Aix Marseille Univ, Natural England	PP 633 T. Printemps (CRBPO)
Diepholz (DE)	MoH	Luise Boldt, Thorsten Obracay (BUND Diepholzer Moorniederung)		33.19-42502-04-18/2865 (LAVES Niedersachsen)
East NL & Limburg (NL)	RK	Arend van Dijk, Mark Zekhuis, René Janssen, Rick de Ruiter, Willem van Manen, Warner Jan de Wilde, Gijs Bouwmeester	Province of Limburg, Province of Drenthe, Werkgroep Roofvogels Nederland, Vogelbescherming Nederland, Netherlands (IJsvogelfonds), Bettie Wiegman Fonds, Vogelwerkgroep Noordwest-Achterhoek, Landschap Overijssel, Fonds 1999, Jeroen de Bruijn	IvD-light, 23 April 2009 (University of Groningen)
Groningen (NL/DE)	MoH, HH, MaH, CB	Almut Schlaich, Sylvia de Vries, Madeleine Postma, Jitty Hakkert, Toni Hoenders, Jan Ploeger, Danny Gerrets, Pien Tibbe (Dutch Montagu's Harrier Foundation); Ben Koks; René Janssen (Bionet Natuuronderzoek); Felix Jachmann, Marike Boekhoff	Province of Groningen, Dutch Ministry of Agriculture, Nature and Food Quality, Prins Bernhard Cultuurfonds, B.V. Oldambt, Dutch Montagu's Harrier Foundation. The UvA-BiTS infrastructure was facilitated by Infrastructures for EScience, developed with the support of the Netherlands eScience Centre (NLeSC) and LifeWatch, and conducted on the Dutch National E-Infrastructure with support from the SURF Foundation.	5869B, 6429B & 172544-01-001 (University of Groningen), 33.12-42502-04-14/1550 & 33.19-42502-04-16/2149 (LAVES Niedersachsen)

Table A4.3.1 (continued). MoH = Montagu's Harrier, MaH = Marsh H., CB = Common Buzzard, RK = Red Kite, STE = Short-toed Eagle.

Study area	Species	Involved persons (in addition to co-authors)	Funding	Permit
Haute-Marne (FR)	RK	Julien Rougé, Jérôme Chamoin, Patrick Demorgny (LPO Champagne-Ardenne), Lucas Graja (Fauconnerie 2000), Eric Graja (La Volerie des Templiers), Marine Felten (LOANA), Paul Supper, Benjamin Colonges	ENGIE Green, CNR, EDPR, Boralex	PP 987 A. Mionnet (CRBPO)
Hellwegbörde (DE)	MoH, MaH	Margret Bunzel-Drüke, Olaf Zimball, Patrick Hundorf (Arbeitsgemeinschaft Biologischer Umweltschutz), Thomas Laumeier (NABU-Station Münsterland)	Bezirksregierung Arnsberg	84-02.04.2017.A038 (Landesamt für Natur, Umwelt und Verbraucherschutz Nordrhein-Westfalen)
Limburg (NL)	CB		Gaiafund Zoo Kerkrade, Müskens Fauna	172544-01-001 (University of Groningen), 2017.D-0045.004 (Wageningen University & Research)
Luxembourg (LU)	RK	Katharina Klein (natur&ëmwelt a.sb.l.), Simone Schneider (SICONA)	Ministère de l'Environnement, du Climat et du Développement durable (MECDD): Fonds Environnement (SICONA-Project « Contribution du secteur communal à la mise en œuvre du 2ème Plan National concernant la Protection de la Nature dans le sud-ouest et le centre du Grand-Duché »); LIFE Eurokite; Soler	N/Réf 90832 CD/tw, N/Réf 93179 CD/gp, N/Réf 95445 CD/ne, N/Réf 102316 (Ministère de l'Environnement, du Climat et du Développement durable)
Noordoostpolder (NL)	MaH	Harold Boer, Jan Nagel, Jacques van der Ploeg and colleagues (Werkgroep Roofvogels Noordoostpolder), Nicolai Bolt (Province of Flevoland), Reinhard Vohwinkel	Province of Flevoland, Dutch Ministry of Agriculture, Nature and Food Quality in the context of WUR Knowledge Base Program KB36 Biodiversity in a Nature Inclusive Society	2017.D-0045.004 (Wageningen University & Research)
NW Flanders & SW Flanders (BE)	MaH, CB, MoH	Tanja Milotic, Peter Desmet (INBO); Natuurwerkgroep De Kerkuil	Flemish Agency for Nature and Forest, Research Foundation - Flanders (FWO) as part of the Belgian contribution to LifeWatch	INBO
Öland (SE)	MoH	Susanne Forslund, Helena Lager, Aron Edman (Kalmar County Administrative Board)	BirdLife Sweden, Kalmar County Administrative Board	01858-2020 (Linköpings djurförsöksetiska nämnd)
Provence (FR)	STE	Olivier Hameau, Alexandre Van der Yeught, Thomas Girard (LPO PACA), Alexandre Lautier (GS Sainte-Victoire), Elvin Miller	Aix Marseille Univ, LPO Provence-Alpes-Côte d'Azur	PP 1167 B. Van Hecke (CRBPO)

Appendix 5.1: Additional materials and methods (chapter 5)

Study areas

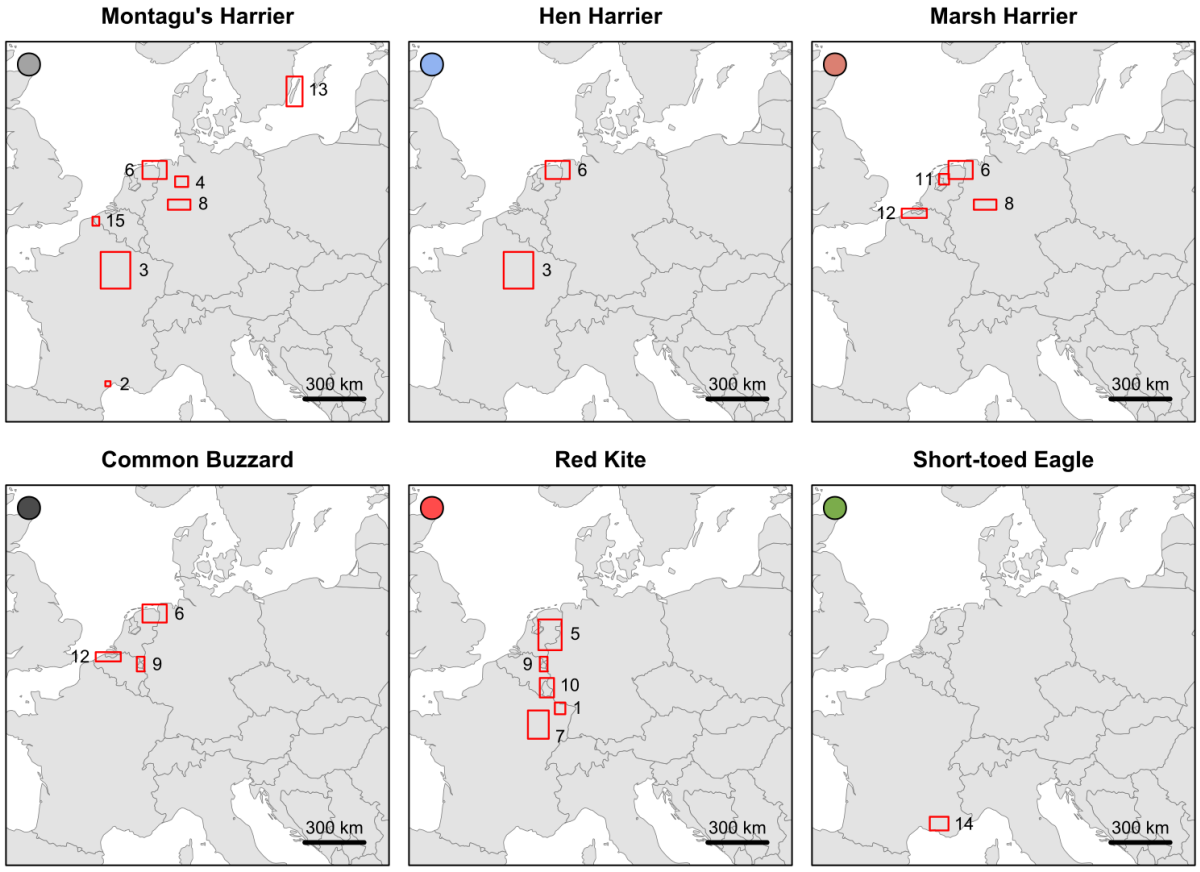

Figure A5.1.1: Location of the study areas per species within Europe. 1) Alsace (FR/DE), 2) Aumelas (FR), 3) Champagne (FR), 4) Diepholz (DE), 5) East NL (NL/DE), 6) Groningen (NL/DE), 7) Haute-Marne (FR), 8) Hellwegbörde (DE), 9) Limburg (NL/BE/DE), 10) Luxembourg (LU/BE/DE), 11) Noordoostpolder (NL), 12) NW Flanders (BE/NL), 13) Öland (SE), 14) Provence (FR), 15) SW Flanders (BE/FR). Background map created using the *R* package *maps* (Brownrigg et al., 2018).

Data collection

The majority of individuals were captured as adults (n = 268) near their nest, mostly using a mist net with a stuffed or live predator, or a stuffed conspecific, as decoy. For harriers, also nest-traps, catching poles or a whoosh-net with carrion as bait were used. For the captures, care was taken to minimise disturbance and prevent negative effects on the breeding process. However, two adult Hen Harriers (one male, one female) deserted their nest after capture (but note that the chicks did nevertheless fledge in both cases with the support of the remaining adult). One adult STE was tagged before being released from a bird rescue centre after an injury. The remaining 12 individuals were tagged as nestlings shortly before fledging.

There were no indications of pronounced adverse tag effects: the tagged birds fulfilled their annual cycle (including migrations) and reproduced as expected. Information on possible more subtle tag effects on survival or flight performance (Longarini et al., 2023) are unavailable for the study species so far. However, note that Sergio et al. (2015) showed a lack of tag effects on survival in Black Kites *Milvus migrans*.

The high-frequency data were collected using a GPS interval setting of 3 s in *Ornitela* and *UvA-BiTS* tags and 1 s in *Milsar* tags. With the set interval of 1 s, *Milsar* tags collected GPS fixes at intervals of 2-3 s in practice. These GPS fix intervals were below the manufacturer-specific time thresholds for the continuous GPS mode (< 7 s for *Ornitela*, < 8 s for Milsar, < 16 s for *UvA-BiTS*).

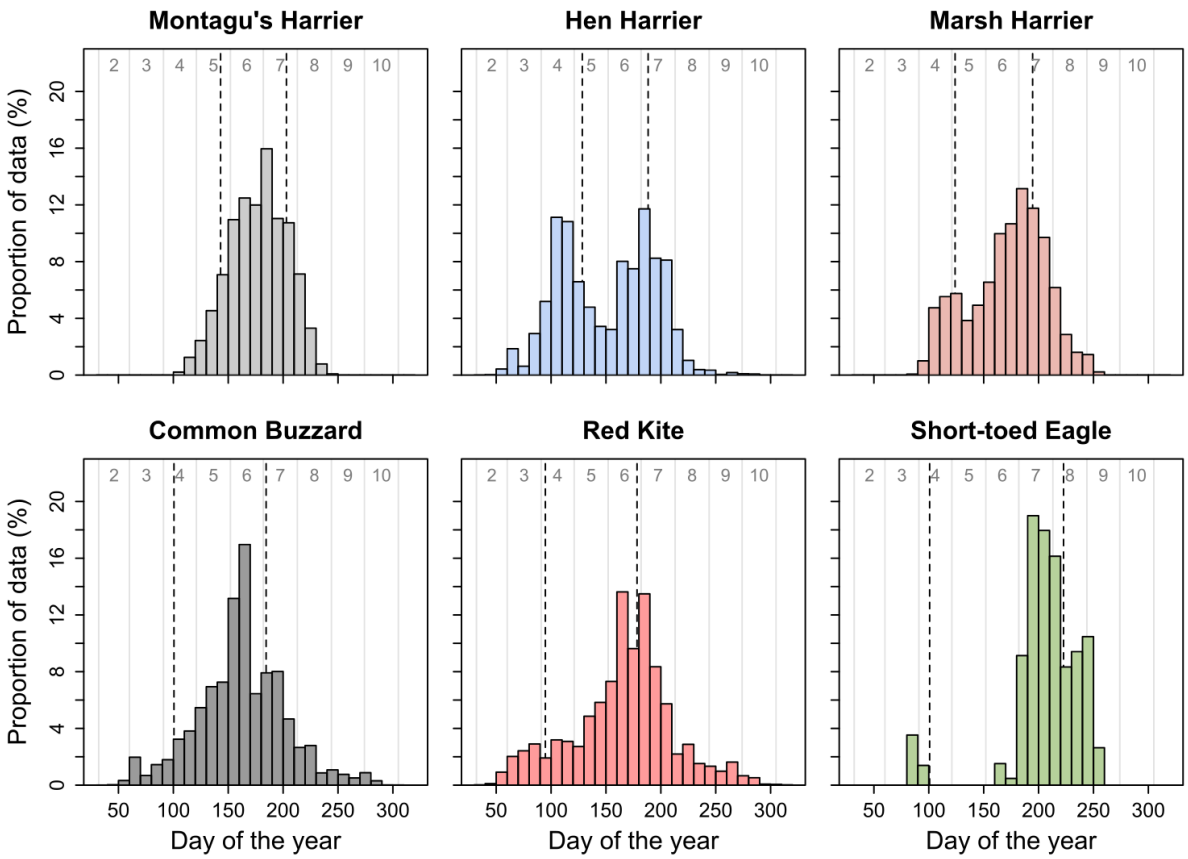

Figure A5.1.2: Distribution of the high-frequency GPS tracking data across the calendar year per species in ten-day periods. Grey numbers and vertical lines indicate months. Dashed vertical lines indicate mean dates of egg-laying and fledging of chicks for the GPS-tagged birds.

Table A5.1.1: Sample size overview per species-area combination. GPS tag models starting with "OT" are from manufacturer *Ornitela*; models with four-character code (e.g. "4CWL") are from *UvA-BiTS*; models GsmTag-U9 and GsmRadioTag-S9 are from *Milsar*. The number of individuals (N ind.) refers to the whole study; the number of GPS positions (N pos.) refers to the dataset used to analyse the time spent in flight for period A (see Table A5.1.4). Note that one female Montagu's Harrier appears in two study areas (having bred in Groningen and SW Flanders in one year each).

Species	Study area	Data period	N ind. female	N pos. female	N ind. male	N pos. male	GPS tag models (incl. variant specification)
Montagu's Harrier	Aumelas (FR)	2021-23	0	0	7	41,089	GsmTag-U9
Montagu's Harrier	Champagne (FR)	2020-23	7	52,663	7	81,377	GsmTag-U9, OT-10-3GC, OT-10-3GC-C19
Montagu's Harrier	Diepholz (DE)	2018-21	0	0	5	30,414	GsmRadioTag-S9, GsmTag-U9
Montagu's Harrier	Groningen (NL/DE)	2009-23	13	39,740	38	167,079	4CWL, 4CWS, 5CDL, 5CDS, 5CWL, 5CWS, GsmRadioTag-S9, GsmTag-U9, OT-10-3GC
Montagu's Harrier	Hellwegbörde (DE)	2017-22	3	14,859	8	48,819	GsmRadioTag-S9, GsmTag-U9, OT-10-3GC
Montagu's Harrier	Öland (SE)	2020-22	0	0	6	42,291	GsmTag-U9
Montagu's Harrier	SW Flanders (BE/FR)	2020-23	3	2,926	5	24,261	OT-10-3GC
Hen Harrier	Champagne (FR)	2019-23	37	295,273	13	110,983	GsmTag-U9, OT-10-3GC, OT-10-3GC-C19, OT-E10-3GC, OT-E10-3GC-C19, OT-E10-4GC
Hen Harrier	Groningen (NL/DE)	2012-15	1	17,554	3	28,491	4CWS, 5CDL
Marsh Harrier	Groningen (NL/DE)	2012-23	4	45,116	3	66,429	4CWL, 6CWL, OT-15-3GC
Marsh Harrier	Hellwegbörde (DE)	2019-23	1	433	8	116,003	GsmRadioTag-S9, OT-15-3GC
Marsh Harrier	Noordoostpolder (NL)	2019-23	6	58,701	3	50,199	OT-15B-3GC-C21, OT-20B-3GC-C21
Marsh Harrier	NW Flanders (BE/NL)	2020-23	1	15,975	5	53,709	OT-15-3GC, OT-15-3GCT
Common Buzzard	Groningen (NL/DE)	2021-23	4	57,747	5	133,418	OT-E25B-4GC-C3
Common Buzzard	Limburg (NL/BE/DE)	2021-23	5	107,023	8	171,306	OT-E25B-4GC-C3
Common Buzzard	NW Flanders (BE/NL)	2021-23	3	45,680	6	92,143	OT-E10-3GC "special", OT-E25B-4GC-C3
Red Kite	Alsace (FR/DE)	2021-23	4	86,760	7	174,135	OT-E25B-4GC
Red Kite	East NL (NL/DE)	2021-23	3	32,831	2	8,836	OT-E25B-3GC-C7, OT-E25B-4GC
Red Kite	Haute-Marne (FR)	2021-23	6	79,728	8	101,564	OT-E25B-4GC
Red Kite	Limburg (NL/BE/DE)	2021-23	2	26,094	3	42,123	OT-E25B-3GC-C7, OT-E25B-4GC
Red Kite	Luxembourg (LU/BE/DE)	2017-23	14	328,280	12	386,805	OT-20B-3GC, OT-E25-3GC-C7, OT-E25B-3GC, OT-E25B-3GC-C7, OT-E25B-4GC, OT-E27B-3GC
Short-toed Eagle	Provence (FR)	2021-23	2	23,385	0	0	OT-E25B-3GC
Total			*119*	*1,330,768*	*162*	*1,971,474*	

Data processing

Table A5.1.2: Applied length of incubation and nestling phases per species for estimating laying, hatching and fledging dates. Length of breeding period was determined as the sum of incubation and nestling periods plus 14 days (7 before egg-laying and 7 after fledging). MoH = Montagu's Harrier, HH = Hen Harrier, MaH = Marsh Harrier, CB = Common Buzzard, RK = Red Kite, STE = Short-toed Eagle; TDP = ten-day period. Sources: del Hoyo et al. (1994), Bauer et al. (2005), Mebs & Schmidt 2017 (2017).

Species	Length incubation phase (d)	Length nestling phase (d)	Length breeding period (d)	Minimum number of TDP
MoH	29	32	75	7
HH	30	33	77	7
MaH	33	40	87	8
CB	33	50	97	9
RK	33	51	98	9
STE	45	77	136	13

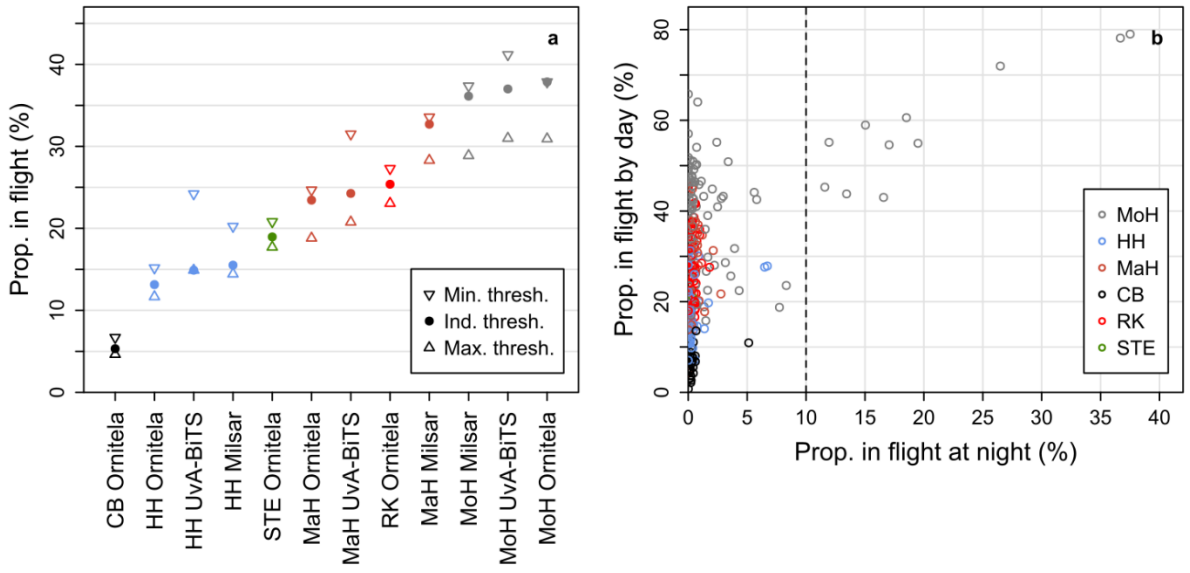

Figure A5.1.3: a) Proportion of positions in the raw low-frequency data identified as being in flight using different ground speed thresholds: the threshold determined for the given combination of species and tag manufacturer ("ind. thresh."), the minimum of thresholds per combination (1.25 m/s; MoH Ornitela; "min. thresh.") and the maximum of thresholds per combination (3.75 m/s; HH UvA-BiTS; "max. thresh."). **b**) Proportion of positions identified as being in flight by day and at night per individual. Dashed vertical line: threshold of 10% applied to remove tags with unreliable speed data.

Table A5.1.3: Thresholds of ground speed applied to distinguish between stationary and in-flight GPS positions per combination of species, tag manufacturer and data type (low-frequency [LF] and high-frequency [HF]).

Species	Manufacturer	Data type	Speed threshold ($m\ s^{-1}$)
Montagu's Harrier	Milsar	HF	0.75
Montagu's Harrier	Milsar	LF	1.75
Montagu's Harrier	Ornitela	HF	0.75
Montagu's Harrier	Ornitela	LF	1.25
Montagu's Harrier	UvA-BiTS	HF	1.25
Montagu's Harrier	UvA-BiTS	LF	2.25
Hen Harrier	Milsar	HF	0.75
Hen Harrier	Milsar	LF	3.25
Hen Harrier	Ornitela	HF	0.75
Hen Harrier	Ornitela	LF	2.75
Hen Harrier	UvA-BiTS	HF	1.25
Hen Harrier	UvA-BiTS	LF	3.75
Marsh Harrier	Milsar	HF	0.75
Marsh Harrier	Milsar	LF	1.75
Marsh Harrier	Ornitela	HF	0.75
Marsh Harrier	Ornitela	LF	1.75
Marsh Harrier	UvA-BiTS	HF	0.75
Marsh Harrier	UvA-BiTS	LF	2.75
Common Buzzard	Ornitela	HF	1.75
Common Buzzard	Ornitela	LF	2.75
Red Kite	Ornitela	HF	1.25
Red Kite	Ornitela	LF	2.25
Short-toed Eagle	Ornitela	HF	2.25
Short-toed Eagle	Ornitela	LF	2.75

Table A5.1.4: Sample size overview for the datasets used to analyse the time spent in flight per day per species-sex combination. Period A: whole calendar year; period B: period of shared presence in the breeding area, i.e. 1 May to 8 August; period C: period with active nests [determined per individual year]. Ind. = individuals, a = individual years, pos. = GPS positions, TDP = ten-day periods (with ≥ 30 GPS positions during daytime).

Species	Sex	N areas	Period A				Period B				Period C			
			N ind.	N a	N pos.	N TDP	N ind.	N a	N pos.	N TDP	N ind.	N a	N pos.	N TDP
Montagu's Harrier	f	4	25	42	110,188	286	25	42	86,919	224	25	42	50,110	161
Montagu's Harrier	m	7	67	111	435,330	862	67	111	364,346	673	64	107	244,957	490
Hen Harrier	f	2	38	67	312,827	1073	38	66	158,336	425	37	65	78,339	272
Hen Harrier	m	2	16	27	139,474	424	16	26	78,305	169	16	23	40,144	89
Marsh Harrier	f	4	12	25	120,225	267	12	25	83,567	177	12	25	61,263	146
Marsh Harrier	m	4	19	45	286,340	549	19	45	203,717	355	19	38	124,237	243
Common Buzzard	f	3	12	23	210,450	498	12	23	113,096	205	11	22	84,454	175
Common Buzzard	m	3	19	36	396,867	818	18	35	201,616	305	16	29	133,181	222
Red Kite	f	5	29	70	553,693	1,249	29	69	299,172	566	28	62	177,039	446
Red Kite	m	5	32	74	713,463	1,397	32	72	378,131	614	31	67	258,364	473
Short-toed Eagle	f	1	2	4	23,385	64	2	4	13,684	36	2	4	17,477	49
Short-toed Eagle	m	0	0	0	0	0	0	0	0	0	0	0	0	0
Total			*271*	*524*	*3,302,242*	*7,487*	*270*	*518*	*1,980,889*	*3,749*	*261*	*484*	*1,269,565*	*2,766*

The GPS height data obtained from the tags was height above mean sea level (termed height a.m.s.l. hereafter), i.e. height above geoid. All three manufacturers indicated that the EGM96 geoid model was used. However, for the *Ornitela* tags, it was possible to also obtain the raw height data above the WGS84 ellipsoid initially determined by the GPS module before application of a geoid model. We noticed that the geoid model applied in these tags was biased compared to EGM96 by several meters in some study areas. Therefore, to obtain corrected height a.m.s.l. data, we used the height above ellipsoid data and applied the EGM96 geoid model with resolution of 0.25° (Agisoft, n.d.). The mean offset compared to the initial height a.m.s.l. using this procedure varied between -1.5 m and +5.0 m according to the study area. For *Milsar* and *UvA-BiTS*, it was not possible to obtain the height above ellipsoid data to apply the same approach.

As the accuracy of GPS positions in the continuous mode usually increases after the first GPS positions taken (Corman & Garthe, 2014; Pfeiffer & Meyburg, 2022; T. Schaub et al., 2023), we removed the first minute of each bout of high-frequency data. We noted that the height data of *Milsar* tags in the high-frequency mode was characterised by frequent "spikes", i.e. single outliers with deviating height (T. Schaub et al., 2023). Therefore, we treated the *Milsar* data with a moving average based on 5 positions centred around the focal position with equal weight.

Table A5.1.5: Sample size overview for the dataset used to analyse the proportion of flights at risk height per species. Ind. = individuals, pos. = high-frequency GPS positions, TS = time span of recorded flight tracks, prop. = proportion [of time span], period B = period of shared presence in the breeding area, i.e. 1 May to 8 August.

Species	N areas	N ind.	N pos.	TS (h)	Prop. females (%)	Prop. March-August (%)	Prop. period B (%)
MoH	7	55	1,901,576	1543.4	2.7	99.9	94.6
HH	2	18	261,008	202.8	60.5	98.9	64.6
MaH	4	19	929,361	774.3	21.5	99.1	82.1
CB	3	17	506,147	419.3	6.4	96.5	79.9
RK	5	51	3,350,555	2792.0	22.5	94.1	73.7
STE	1	2	65,250	54.4	100	89.7	64.2

Table A5.1.6: Sample size overview for the dataset used to analyse the distance from nest per species-sex combination. Ind. = individuals, a = individual years, pos. = GPS positions.

Species	Sex	N areas	N ind.	N a	N nests	N pos.	N in-flight pos.
Montagu's Harrier	f	3	7	8	8	16,682	3,114
Montagu's Harrier	m	7	22	29	29	117,070	59,303
Hen Harrier	f	2	11	14	14	31,502	5,153
Hen Harrier	m	2	4	4	4	17,625	5,157
Marsh Harrier	f	3	5	8	8	33,429	5,230
Marsh Harrier	m	4	12	17	19	84,310	32,622
Common Buzzard	f	3	6	10	10	51,045	1,545
Common Buzzard	m	3	11	14	14	88,708	10,625
Red Kite	f	5	15	28	28	122,516	17,782
Red Kite	m	4	16	32	32	190,148	87,616
Short-toed Eagle	f	1	2	3	3	14,173	2,796
Short-toed Eagle	m	0	0	0	0	0	0
Total			*111*	*167*	*169*	*767,208*	*230,943*

Time spent in the study areas per year

The average number of days spent in the study areas per species was calculated based on the GPS tracking data as the difference between the mean first day of the year and the mean last day of the year with data. The first and last day with data were determined per individual year, whereby the first year of tracking per individual were omitted for the first day (as the first day in the first year represents the day of capture instead of the day of arrival in the study area), and the last year per individual for the last day (as the last day in the last year may represent the day of death or of [presumed] tag failure instead of the day of departure from the study area). To obtain confidence intervals for the average number of days present, we produced 1000 bootstrap replicates both for the first day D_F and the last day D_L per species (resampling on the level of individual years with replacement). These were combined (D_{Li} - D_{Fi}), and 2.5% and 97.5% quantiles were calculated on the resulting 1000 combined replicates. Note that we did not differentiate between sexes and study areas for this aspect.

Appendix 5.2: Additional results (chapter 5)

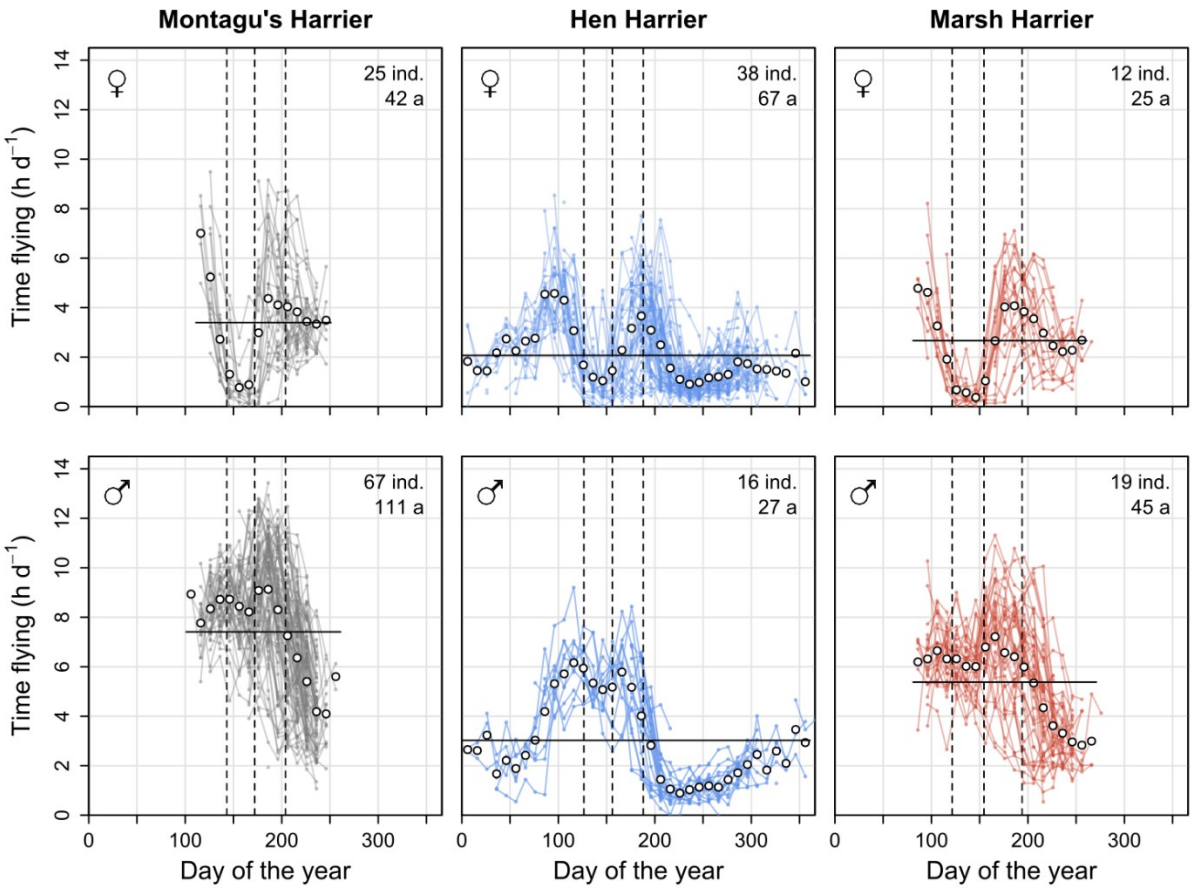

Figure A5.2.1: Seasonal variation of time spent in flight per day for breeding Montagu's Harriers, Hen Harriers and Marsh Harriers per ten-day period. Lines represent individual years. White points: means across individual years per ten-day period; horizontal black lines: means corrected for unbalanced seasonal sampling; vertical dashed lines: median laying, hatching and fledging dates; ind. = individuals; a = individual years.

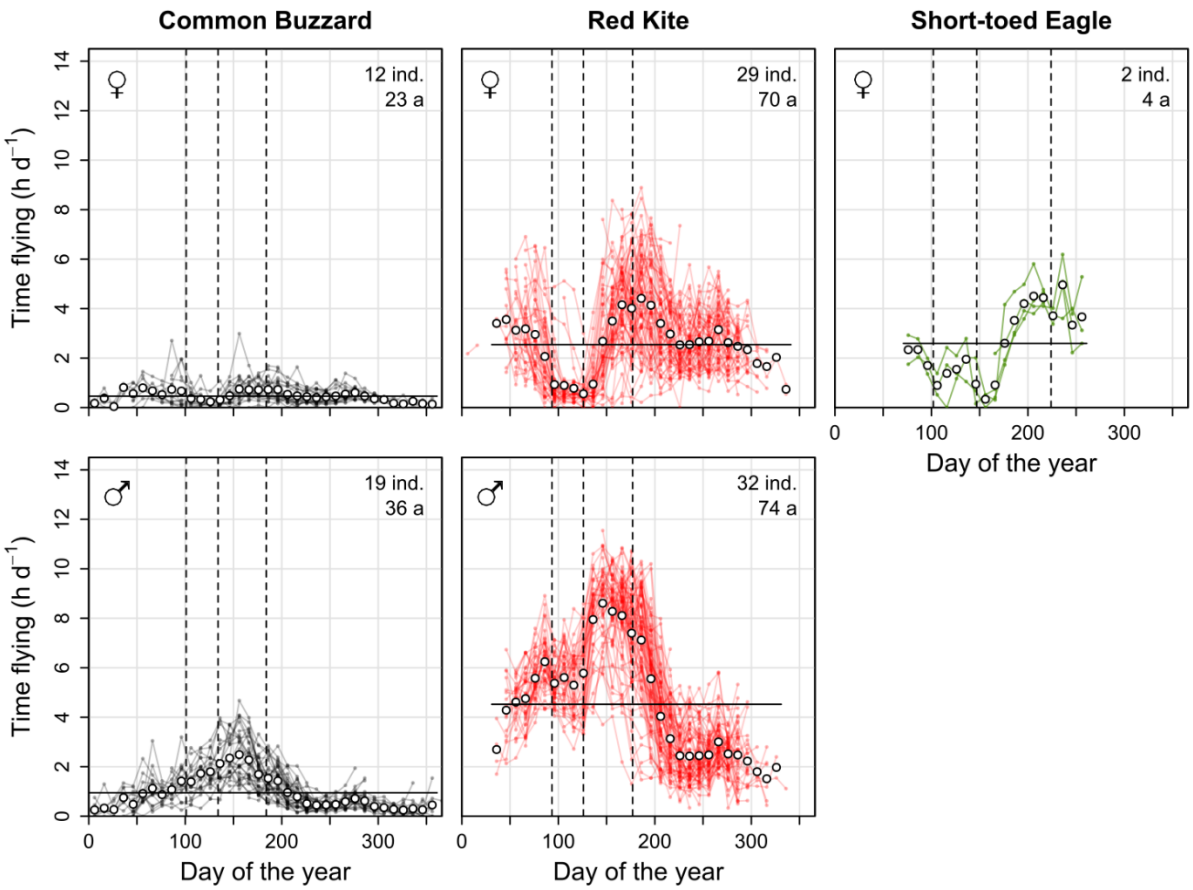

Figure A5.2.2: Seasonal variation of time spent in flight per day for breeding Common Buzzards, Red Kites and Short-toed Eagles per ten-day period. Lines represent individual years. White points: means across individual years per ten-day period; horizontal black lines: means corrected for unbalanced seasonal sampling; vertical dashed lines: median laying, hatching and fledging dates; ind. = individuals; a = individual years.

Table A5.2.1: Time spent in flight (TF) per day for breeding birds of six raptor species (means corrected for unbalanced seasonal sampling with 95% confidence intervals from bootstrapping) for three different time periods (A: whole calendar year; B: period of shared presence in the breeding area, i.e. 1 May to 8 August; C: period with active nests [determined per individual year]). MoH = Montagu's Harrier, HH = Hen Harrier, MaH = Marsh Harrier, CB = Common Buzzard, RK = Red Kite, STE = Short-toed Eagle; N ind. = number of individuals; N a = number of individual years. Letters a-c indicate significant differences between species. See Appendix 5.1: Table A5.1.4 for details on sample size.

Species	Sex	Period A (whole year)			Period B (May-August)			Period C (active nest)		
		N ind. (N a)	TF (h d^{-1})	Group	N ind. (N a)	TF (h d^{-1})	Group	N ind. (N a)	TF (h d^{-1})	Group
MoH	f	25 (42)	3.39 (3.06-3.70)	a	25 (42)	3.02 (2.64-3.47)	ab	24 (41)	2.67 (2.25-3.11)	a
HH	f	38 (67)	2.07 (1.96-2.21)	b	38 (66)	2.16 (1.99-2.35)	c	37 (65)	2.40 (2.13-2.66)	ab
MaH	f	12 (25)	2.67 (2.46-2.87)	c	12 (25)	2.38 (2.07-2.68)	bc	12 (25)	2.28 (1.94-2.46)	ab
CB	f	12 (23)	0.46 (0.41-0.52)	d	12 (23)	0.57 (0.48-0.65)	d	11 (22)	0.49 (0.38-0.61)	c
RK	f	29 (70)	2.55 (2.44-2.72)	c	29 (69)	3.08 (2.82-3.31)	a	28 (62)	1.92 (1.68-2.25)	b
STE	f	2 (4)	2.60 (2.23-3.90)	ac	2 (4)	2.50 (2.11-3.35)	abc	2 (4)	2.33 (2.02-3.45)	ab
MoH	m	67 (111)	7.41 (7.19-7.66)	a	67 (111)	8.26 (8.01-8.49)	a	64 (106)	8.23 (7.97-8.70)	a
HH	m	16 (27)	3.02 (2.85-3.25)	b	16 (26)	4.18 (3.93-4.45)	b	16 (23)	4.72 (4.41-5.58)	b
MaH	m	19 (45)	5.38 (5.10-5.69)	c	19 (45)	6.10 (5.68-6.50)	c	19 (38)	6.48 (6.04-6.87)	c
CB	m	19 (36)	0.95 (0.87-1.03)	d	18 (35)	1.74 (1.56-1.93)	d	16 (28)	1.75 (1.56-1.93)	d
RK	m	32 (74)	4.52 (4.30-4.74)	e	32 (72)	6.60 (6.30-6.91)	c	31 (67)	7.10 (6.83-7.38)	c

Table A5.2.2: Time spent in flight (TF) per day for breeding birds of six raptor species per study area (means corrected for unbalanced seasonal sampling with 95% confidence intervals from bootstrapping) during the whole calendar year (period A). MoH = Montagu's Harrier, HH = Hen Harrier, MaH = Marsh Harrier, CB = Common Buzzard, RK = Red Kite, STE = Short-toed Eagle; N ind. = number of individuals; N a = number of individual years. Letters a-b indicate significant differences between study areas for each species.

Sex	Species	Area	N ind. (N a)	TF (h d^{-1})	Group
f	MoH	Champagne	7 (13)	3.27 (2.97-3.48)	a
f	MoH	Groningen	13 (20)	3.44 (2.76-4.22)	a
f	MoH	Hellwegbörde	3 (6)	2.39 (1.83-3.62)	a
f	HH	Champagne	37 (63)	2.09 (1.97-2.22)	a
f	HH	Groningen	1 (4)	1.97 (1.79-2.44)	a
f	MaH	Groningen	4 (8)	2.70 (2.32-3.00)	a
f	MaH	Noordoostpolder	6 (14)	2.69 (2.37-3.00)	a
f	MaH	NW Flanders	1 (2)	2.49 (2.18-2.63)	a
f	CB	Groningen	4 (7)	0.41 (0.29-0.57)	a
f	CB	Limburg	5 (10)	0.43 (0.38-0.50)	a
f	CB	NW Flanders	3 (6)	0.68 (0.57-0.78)	b
f	RK	Alsace	4 (9)	2.70 (2.37-2.98)	ab
f	RK	East NL	3 (5)	2.77 (2.21-3.43)	ab
f	RK	Haute-Marne	6 (11)	2.31 (2.10-2.63)	a
f	RK	Limburg	2 (4)	3.24 (2.65-5.49)	b
f	RK	Luxembourg	14 (41)	2.63 (2.49-2.82)	ab
f	STE	Provence	2 (4)	2.60 (2.23-3.90)	-
m	MoH	Aumelas	5 (9)	7.84 (6.93-8.73)	a
m	MoH	Champagne	7 (16)	7.43 (6.98-7.91)	a
m	MoH	Diepholz	5 (8)	7.08 (6.16-7.60)	a
m	MoH	Groningen	31 (52)	7.54 (7.22-7.80)	a
m	MoH	Hellwegbörde	8 (11)	7.19 (6.53-7.62)	a
m	MoH	Öland	6 (8)	7.68 (6.19-8.24)	a
m	MoH	SW Flanders	5 (7)	8.32 (7.56-9.39)	a
m	HH	Champagne	13 (20)	3.07 (2.90-3.32)	a
m	HH	Groningen	3 (7)	3.06 (2.29-4.85)	a
m	MaH	Groningen	3 (11)	5.86 (5.14-6.44)	a
m	MaH	Hellwegbörde	8 (17)	5.83 (5.33-6.29)	a
m	MaH	Noordoostpolder	3 (7)	5.15 (4.58-5.51)	a
m	MaH	NW Flanders	5 (10)	4.94 (4.44-5.44)	a
m	CB	Groningen	5 (11)	0.95 (0.86-1.11)	a
m	CB	Limburg	8 (16)	0.88 (0.77-0.99)	a
m	CB	NW Flanders	6 (9)	1.04 (0.90-1.39)	a
m	RK	Alsace	7 (16)	4.78 (4.49-5.10)	a
m	RK	East NL	2 (2)	4.84 (3.83-4.99)	ab
m	RK	Haute-Marne	8 (13)	4.06 (3.81-4.42)	b
m	RK	Limburg	3 (5)	5.04 (4.25-5.74)	ab
m	RK	Luxembourg	12 (38)	4.90 (4.52-5.21)	a

Table A5.2.3: Proportion of flights at risk height (32-200 m a.g.l.) per species (means across values per individual bird with 95% confidence intervals from bootstrapping). N ind. = number of individuals (with at least 5 h of recorded flights); TS = total time span of recorded flights. Letters a-d indicate significant differences. See Appendix 5.1: Table A5.1.5 for details on sample size.

Species	N ind.	TS (h)	Prop. 32-200 m (%)	Group
Montagu's Harrier	55	1543.4	12.4 (11.1-13.7)	a
Hen Harrier	18	202.8	20.9 (16.9-24.5)	b
Marsh Harrier	19	774.3	13.1 (10.5-15.8)	a
Common Buzzard	17	419.3	47.6 (44.6-50.2)	c
Red Kite	51	2792.0	56.4 (54.6-58.1)	d
Short-toed Eagle	2	54.4	44.5 (30.2-58.8)	cd

Table A5.2.4: Proportion of flights at risk height (32-200 m a.g.l.) per species-area combination (means across individuals with 95% confidence intervals from bootstrapping). MoH = Montagu's Harrier, HH = Hen Harrier, MaH = Marsh Harrier, CB = Common Buzzard, RK = Red Kite, STE = Short-toed Eagle; N ind. = number of individuals (with at least 5 h of recorded flights); TS = total time span of recorded flights. Letters a-b indicate significant differences.

Species	Area	N ind.	TS (h)	Prop. 32-200 m (%)	Group
Montagu's Harrier	Aumelas	7	201.5	13.4 (11.0-16.1)	ab
	Champagne	8	203.0	16.6 (12.8-20.7)	a
	Diepholz	2	34.1	19.9 (11.3-28.6)	ab
	Groningen	29	941.3	10.9 (9.6-12.4)	b
	Hellwegbörde	1	30.4	15.7 (-)	-
	Öland	4	88.7	10.8 (7.4-14.3)	ab
	SW Flanders	4	44.4	9.9 (2.8-16.4)	ab
Hen Harrier	Champagne	16	183.5	21.9 (18.5-25.5)	a
	Groningen	2	19.2	12.9 (7.0-18.7)	a
Marsh Harrier	Groningen	6	318.6	8.7 (5.4-12.4)	a
	Hellwegbörde	3	117.0	16.2 (10.5-21.8)	a
	Noordoostpolder	6	200.2	14.1 (10.5-18.5)	a
	NW Flanders	4	138.4	15.9 (9.7-22.6)	a
Common Buzzard	Groningen	5	218.0	50.3 (48.0-54.3)	a
	Limburg	8	130.9	45.6 (40.9-49.9)	a
	NW Flanders	4	70.4	48.4 (42.6-53.0)	a
Red Kite	Alsace	11	1090.9	58.1 (54.9-61.9)	ab
	East NL	3	43.1	62.7 (60.2-65.2)	a
	Haute-Marne	14	543.3	57.2 (54.3-60.2)	b
	Limburg	5	223.9	58.7 (53.8-63.6)	ab
	Luxembourg	18	890.8	52.9 (49.7-55.9)	b
Short-toed Eagle	Provence	2	54.4	44.5 (30.2-58.8)	-

Table A5.2.5: Average number of days spent in the breeding area per year for breeding birds of six raptor species, calculated as difference between mean first day and mean last day (95% confidence intervals from bootstrapping). Letters a-f indicate significant differences.

Species	N first days (N last days)	Time in breeding area (d y^{-1})	Group
Montagu's Harrier	60 (61)	110.4 (106.3-114.3)	a
Hen Harrier	40 (40)	277.8 (259.9-295.5)	b
Marsh Harrier	39 (39)	143.6 (137.5-149.2)	c
Common Buzzard	28 (28)	353.8 (345.1-360.0)	d
Red Kite	83 (83)	239.0 (232.1-245.8)	e
Short-toed Eagle	2 (2)	175.0 (170.0-180.0)	f

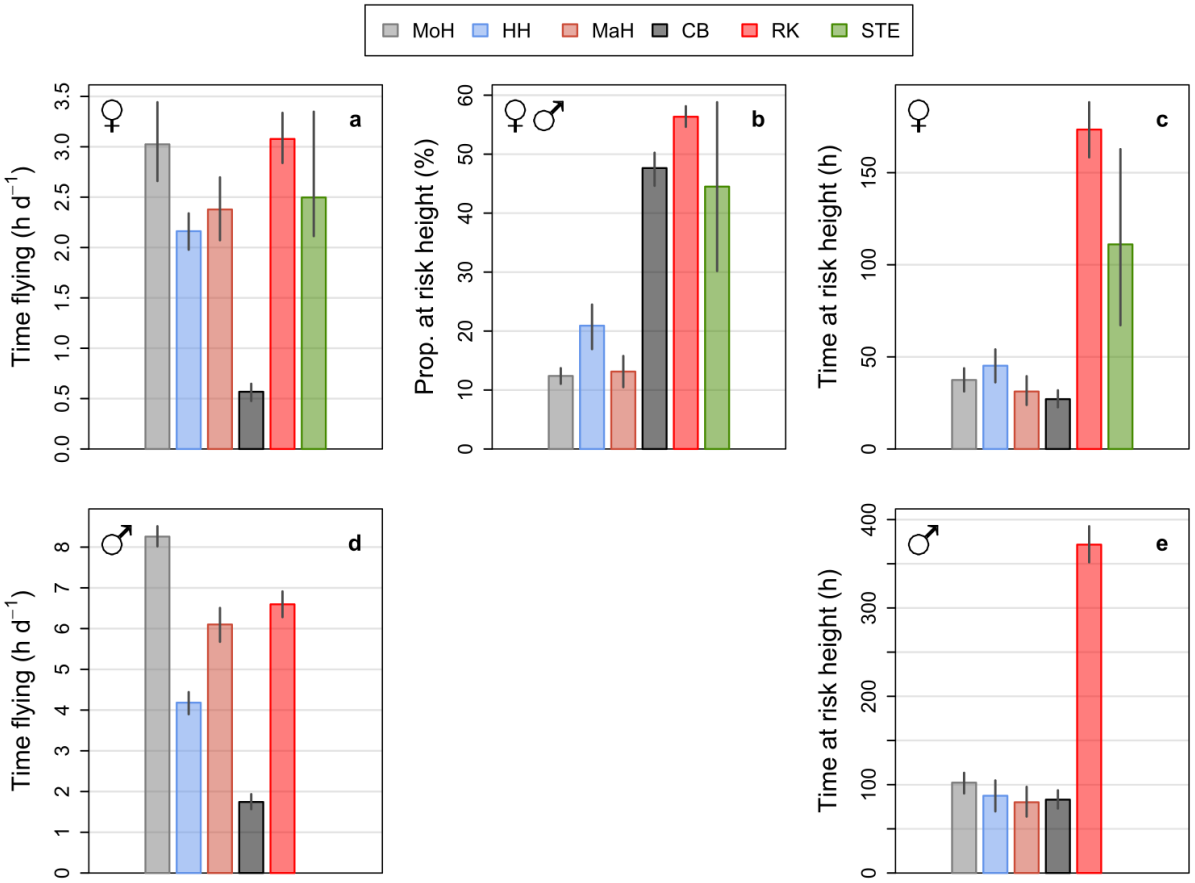

Figure A5.2.3: Time spent in flight per day (**a**, **d**), proportion of flights at risk height (**b**) and total time spent at risk height (**c**, **e**) during the period of shared presence in the breeding area (1 May to 8 August) for six raptor species (means and 95% confidence intervals from bootstrapping). Time at risk height is the product of the two other aspects and the length of the considered period (100 d). Note different y-axis scales. Sexes were merged in **b**.

Table A5.2.6: Time spent at risk height (32-200 m a.g.l.) for breeding birds of six raptor species for two different periods (A: whole calendar year; B: period of shared presence in the breeding area, i.e. 1 May to 8 August; means with 95% confidence intervals from bootstrapping). MoH = Montagu's Harrier, HH = Hen Harrier, MaH = Marsh Harrier, CB = Common Buzzard, RK = Red Kite, STE = Short-toed Eagle. Letters a-d indicate significant differences.

Sex	Species	Period A (whole year) Time at risk height (h)	Group	Period B (May-August) Time at risk height (h)	Group
f	MoH	46.4 (39.2-53.2)	a	37.5 (31.2-43.8)	ab
f	HH	120.3 (95.9-146.5)	b	45.2 (36.2-54.1)	a
f	MaH	50.2 (39.0-61.8)	a	31.2 (23.9-39.5)	ab
f	CB	78.0 (67.7-89.2)	c	27.1 (22.6-31.9)	b
f	RK	342.8 (323.1-370.3)	d	173.4 (158.3-188.3)	c
f	STE	202.1 (124.7-308.2)	b	111.1 (67.2-162.8)	c
m	MoH	101.3 (89.0-113.3)	a	102.3 (90.1-113.4)	a
m	HH	175.6 (142.3-213.5)	b	87.5 (69.8-104.8)	a
m	MaH	101.4 (79.9-123.8)	a	80.1 (63.9-97.6)	a
m	CB	159.8 (143.9-176.5)	b	83.1 (73.0-93.6)	a
m	RK	609.2 (571.5-652.1)	c	371.7 (351.6-392.5)	b

Table A5.2.7: Median and 90% quantile of distance from nest for complete successful breeding seasons per species (means across individual years [nests] with 95% confidence intervals from bootstrapping). MoH = Montagu's Harrier, HH = Hen Harrier, MaH = Marsh Harrier, CB = Common Buzzard, RK = Red Kite, STE = Short-toed Eagle. Letters a-f indicate significant differences. See Appendix 5.1: Table A5.1.6 for details on sample size.

Sex	Species	N nests	N ind.	Median distance (km)	Group	Q90 distance (km)	Group
f	MoH	8	7	0.29 (0.16-0.47)	a	1.77 (1.07-2.46)	ac
f	HH	14	11	0.39 (0.28-0.53)	ab	1.63 (1.18-2.14)	a
f	MaH	8	5	0.77 (0.48-1.04)	b	2.77 (1.57-3.88)	ac
f	CB	10	6	0.24 (0.19-0.29)	a	0.67 (0.57-0.78)	b
f	RK	28	15	0.82 (0.68-0.95)	b	2.69 (2.27-3.19)	c
f	STE	3	2	5.00 (2.15-6.74)	c	9.82 (7.56-11.04)	d
m	MoH	29	22	2.26 (1.99-2.57)	a	5.63 (4.99-6.34)	a
m	HH	4	4	0.94 (0.56-1.22)	bc	2.26 (1.41-2.94)	b
m	MaH	19	12	1.57 (1.15-2.01)	ab	4.09 (3.26-5.01)	ad
m	CB	14	11	0.50 (0.36-0.66)	c	1.00 (0.77-1.27)	c
m	RK	32	16	2.00 (1.77-2.22)	a	3.95 (3.57-4.29)	d

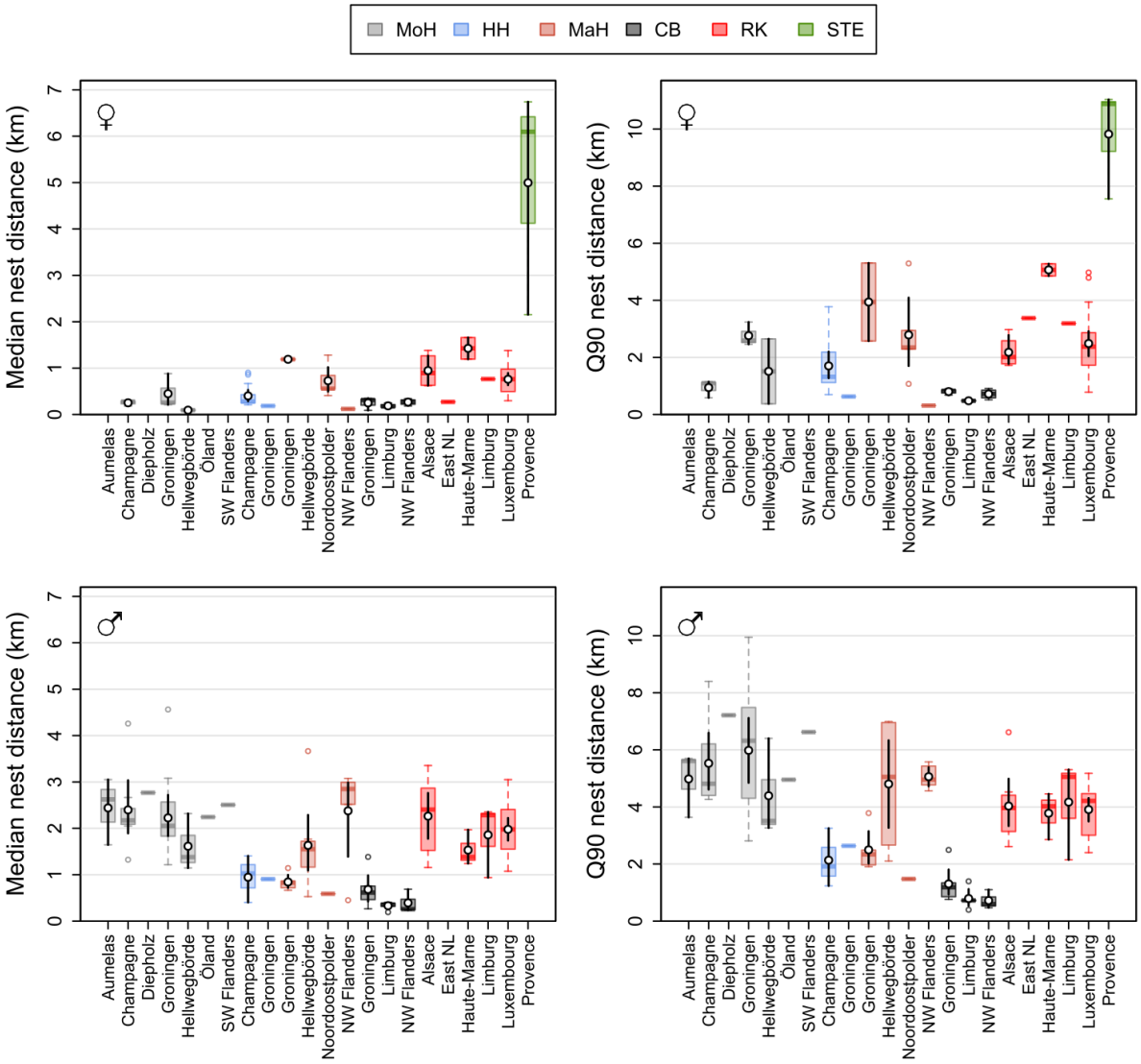

Figure A5.2.4: Median and 90% quantile of distance from nest for complete successful breeding seasons per study area (see Table A5.2.8 for sample sizes). Right column of panels is equivalent to Figure 5.4d-e. Overlaid white points and vertical black lines indicate means across individual years (nests) and 95% confidence intervals from bootstrapping. Note that data weren't available for all combinations of species, area and sex. MoH = Montagu's Harrier, HH = Hen Harrier, MaH = Marsh Harrier, CB = Common Buzzard, RK = Red Kite, STE = Short-toed Eagle.

Table A5.2.8: Median and 90% quantile of distance from nest for complete successful breeding seasons per study area (means across individual years [nests] with 95% confidence intervals from bootstrapping). MoH = Montagu's Harrier, HH = Hen Harrier, MaH = Marsh Harrier, CB = Common Buzzard, RK = Red Kite, STE = Short-toed Eagle; ind. = individuals. Letters a-b indicate significant differences between areas within combinations of species and sex.

Sex	Spe-cies	Area	N nests	N ind.	Median distance (km)	Group	Q90 distance (km)	Group
f	MoH	Champagne	3	3	0.25 (0.18-0.30)	a	0.94 (0.59-1.15)	a
f	MoH	Groningen	3	3	0.45 (0.21-0.88)	a	2.76 (2.46-3.24)	b
f	MoH	Hellwegbörde	2	1	0.09 (0.08-0.11)	b	1.51 (0.38-2.65)	ab
f	HH	Champagne	13	10	0.40 (0.29-0.53)	-	1.70 (1.28-2.20)	-
f	HH	Groningen	1	1	0.18 (-)	-	0.63 (-)	-
f	MaH	Groningen	2	1	1.19 (1.18-1.20)	a	3.94 (2.57-5.31)	a
f	MaH	Noordoostpolder	5	3	0.73 (0.49-1.02)	b	2.79 (1.70-4.09)	a
f	MaH	NW Flanders	1	1	0.12 (-)	-	0.31 (-)	-
f	CB	Groningen	3	2	0.25 (0.09-0.35)	a	0.80 (0.68-0.90)	a
f	CB	Limburg	3	2	0.19 (0.14-0.25)	a	0.48 (0.45-0.52)	b
f	CB	NW Flanders	4	2	0.27 (0.21-0.32)	a	0.72 (0.58-0.85)	a
f	RK	Alsace	4	3	0.95 (0.62-1.27)	ab	2.18 (1.78-2.78)	a
f	RK	East NL	1	1	0.27 (-)	-	3.38 (-)	-
f	RK	Haute-Marne	2	2	1.43 (1.19-1.66)	a	5.07 (4.85-5.28)	b
f	RK	Limburg	1	1	0.76 (-)	-	3.19 (-)	-
f	RK	Luxembourg	20	8	0.76 (0.63-0.89)	b	2.49 (2.05-2.91)	a
f	STE	Provence	3	2	5.00 (2.15-6.74)	-	9.82 (7.56-11.04)	-
m	MoH	Aumelas	3	2	2.44 (1.64-3.05)	a	4.98 (3.64-5.70)	a
m	MoH	Champagne	7	5	2.40 (1.89-3.04)	a	5.53 (4.61-6.59)	a
m	MoH	Diepholz	1	1	2.77 (-)	-	7.21 (-)	-
m	MoH	Groningen	13	9	2.23 (1.84-2.72)	a	5.98 (4.85-7.11)	a
m	MoH	Hellwegbörde	3	3	1.61 (1.15-2.32)	a	4.39 (3.26-6.40)	a
m	MoH	Öland	1	1	2.24 (-)	-	4.95 (-)	-
m	MoH	SW Flanders	1	1	2.50 (-)	-	6.62 (-)	-
m	HH	Champagne	3	3	0.95 (0.40-1.41)	-	2.13 (1.24-3.25)	-
m	HH	Groningen	1	1	0.91 (-)	-	2.64 (-)	-
m	MaH	Groningen	5	2	0.84 (0.72-1.00)	a	2.50 (2.02-3.15)	a
m	MaH	Hellwegbörde	8	6	1.63 (1.09-2.29)	b	4.80 (3.27-6.33)	b
m	MaH	Noordoostpolder	1	1	0.59 (-)	-	1.48 (-)	-
m	MaH	NW Flanders	5	3	2.38 (1.39-2.99)	b	5.06 (4.72-5.39)	b
m	CB	Groningen	6	4	0.68 (0.42-0.98)	a	1.30 (0.93-1.80)	a
m	CB	Limburg	5	4	0.33 (0.26-0.39)	b	0.79 (0.53-1.12)	a
m	CB	NW Flanders	3	3	0.39 (0.24-0.69)	ab	0.72 (0.47-1.10)	a
m	RK	Alsace	8	5	2.26 (1.78-2.76)	a	4.03 (3.33-4.99)	a
m	RK	Haute-Marne	3	3	1.53 (1.24-1.97)	a	3.78 (2.86-4.46)	a
m	RK	Limburg	3	2	1.86 (0.94-2.35)	a	4.17 (2.15-5.31)	a
m	RK	Luxembourg	18	6	1.98 (1.74-2.22)	a	3.91 (3.49-4.31)	a

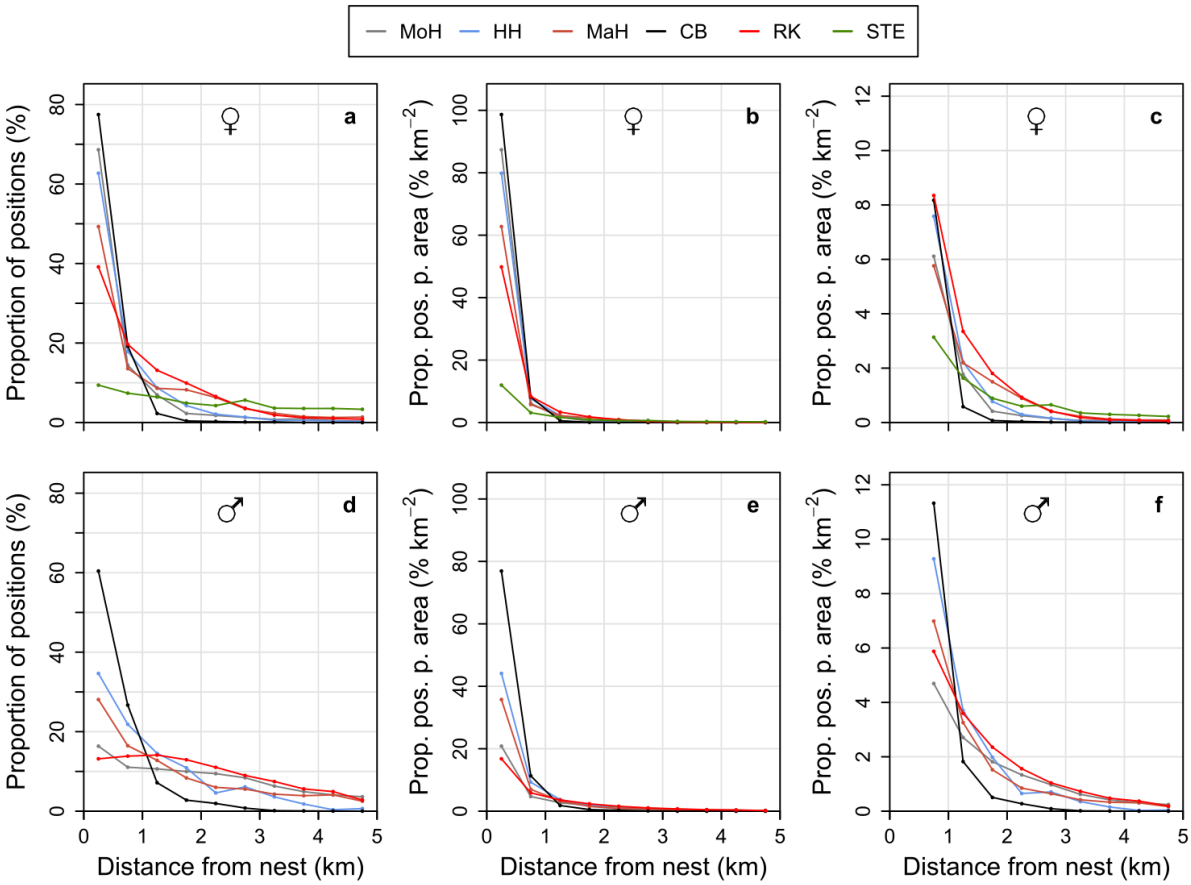

Figure A5.2.5: Proportion of GPS positions per class of distance from nest for complete successful breeding seasons (**a**, **d**) and proportion of positions per unit of area available per distance class (**b**, **c**, **e**, **f**; bins of 0.5 km; means across individual breeding seasons). Panels **c** and **f** are zoomed-in versions of **b** and **e** with shortened y-axis (distance bin 0.0-0.5 km excluded). See Figure A5.2.6-7 for individual variation. MoH = Montagu's Harrier, HH = Hen Harrier, MaH = Marsh Harrier, CB = Common Buzzard, RK = Red Kite, STE = Short-toed Eagle.

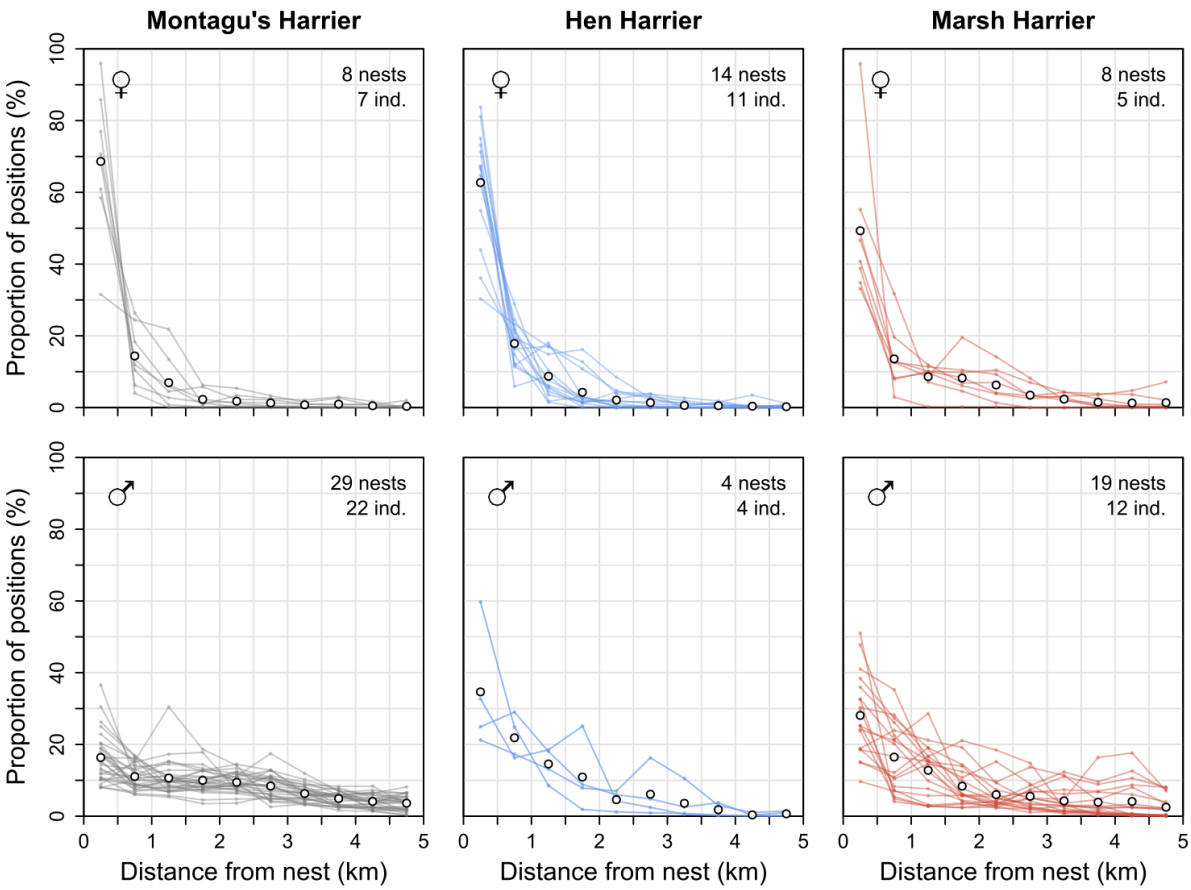

Figure A5.2.6: Proportion of GPS positions per class of distance from nest for complete successful breeding seasons of Montagu's Harriers, Hen Harriers and Marsh Harriers (bins of 0.5 km). Lines represent combinations of individual year and nest; overlaid white points indicate means per distance class. Ind. = individuals.

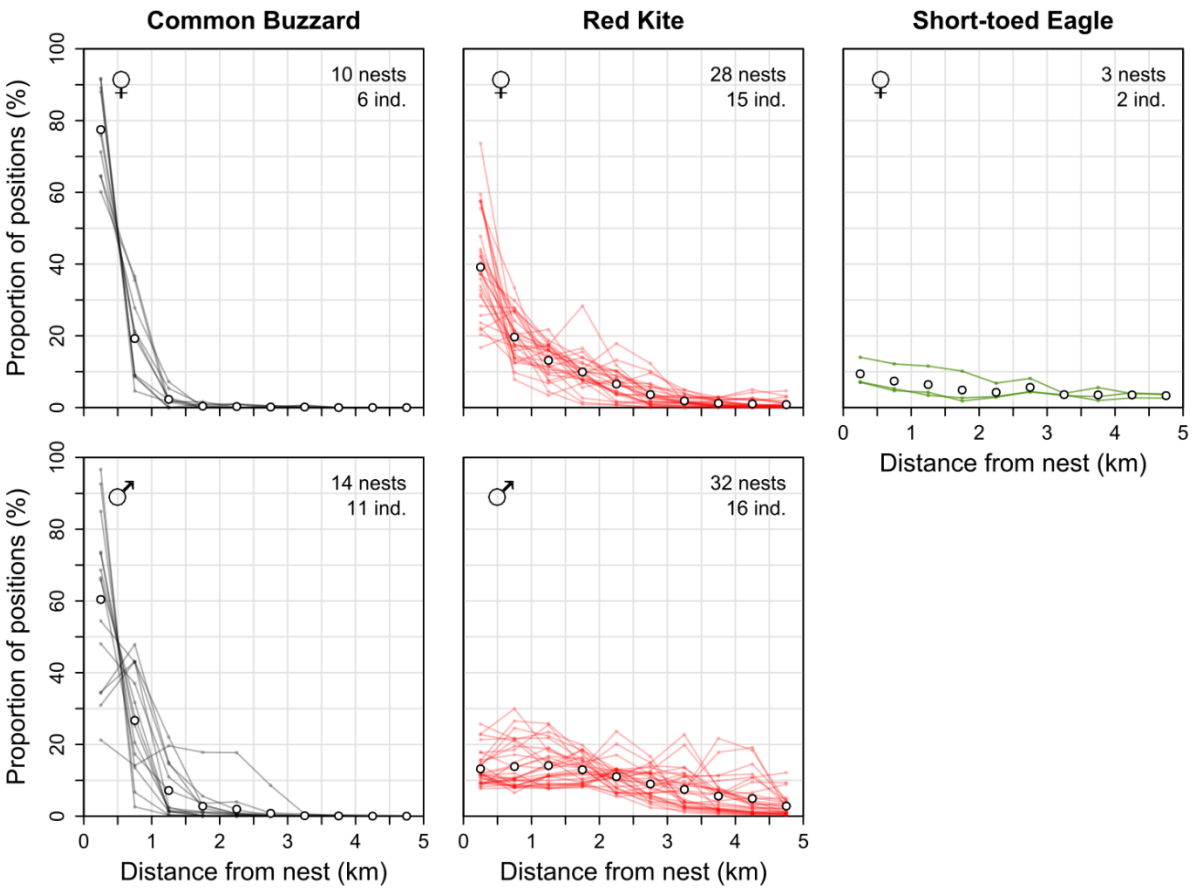

Figure A5.2.7: Proportion of GPS positions per class of distance from nest for complete successful breeding seasons of Common Buzzards, Red Kites and Short-toed Eagles (bins of 0.5 km). Lines represent combinations of individual year and nest; overlaid white points indicate means per distance class. Ind. = individuals.

Appendix 5.3: Information on local GPS-tracking projects (chapter 5)

Table A5.3.1: Information on local tracking projects. MoH = Montagu's Harrier, HH = Hen H., MaH = Marsh H., CB = Common Buzzard, RK = Red Kite.

Study area	Species	Involved persons (in addition to co-authors)	Funding	Permit
Alsace (FR)	RK	Jérôme Isambert, Sébastien Didier (LPO Alsace), Christelle Scheid (Ecofaune), Alexandre Gill (La Volerie des Aigles), Wouter Pieters and colleagues (Parc Animalier de Sainte-Croix), Alexandre Eich (Office National des Forêts)	ENGIE Green, CNR	PP 987 A. Mionnet (CRBPO)
Aumelas (FR)	MoH	Camille Montégu, Aurélie Béa (LPO Occitanie), Colin Moffa (Aix Marseille Univ), Carole Millon (GepB)	Aix Marseille Univ, Natural England	PP 633 T. Printemps (CRBPO)
Champagne (FR)	MoH, HH	José Dorey, Roland Faynot, Bernard Vacheret, Laurent Cocquyt, Gérard Crouzier, Claude Bouillon (GepB)	Aix Marseille Univ, Natural England	PP 633 T. Printemps (CRBPO)
Diepholz (DE)	MoH	Luise Boldt, Thorsten Obracay (BUND Diepholzer Moorniederung)		33.19-42502-04-18/2865 (LAVES Niedersachsen)
East NL & Limburg (NL)	RK	Arend van Dijk, Mark Zekhuis, René Janssen, Rick de Ruiter, Willem van Manen, Warner Jan de Wilde, Gijs Bouwmeester	Province of Limburg, Province of Drenthe, Werkgroep Roofvogels Nederland, Vogelbescherming Nederland, Netherlands (IJsvogelfonds), Bettie Wiegman Fonds, Vogelwerkgroep Noordwest-Achterhoek, Landschap Overijssel, Fonds 1999, Jeroen de Bruijn	IvD-light, 23 April 2009 (University of Groningen)
Groningen (NL/DE)	MoH, HH, MaH, CB	Almut Schlaich, Sylvia de Vries, Madeleine Postma, Jitty Hakkert, Toni Hoenders, Jan Ploeger, Danny Gerrets, Pien Tibbe (Dutch Montagu's Harrier Foundation); Ben Koks; René Janssen (Bionet Natuuronderzoek); Henk van der Noord and Marsh Harrier field team (Collectief Groningen West); Felix Jachmann, Marike Boekhoff	Province of Groningen, Dutch Ministry of Agriculture, Nature and Food Quality, Prins Bernhard Cultuurfonds, B.V. Oldambt, Dutch Montagu's Harrier Foundation. The UvA-BiTS infrastructure was facilitated by Infrastructures for EScience, developed with the support of the Netherlands eScience Centre (NLeSC) and LifeWatch, and conducted on the Dutch National E-Infrastructure with support from the SURF Foundation.	5869B, 6429B & 172544-01-001 (University of Groningen), 33.12-42502-04-14/1550 & 33.19-42502-04-16/2149 (LAVES Niedersachsen)

Table A5.3.1 (continued). MoH = Montagu's Harrier, MaH = Marsh H., CB = Common Buzzard, RK = Red Kite, STE = Short-toed Eagle.

Study area	Species	Involved persons (in addition to co-authors)	Funding	Permit
Haute-Marne (FR)	RK	Julien Rougé, Jérôme Chamoin, Patrick Demorgny (LPO Champagne-Ardenne), Lucas Graja (Fauconnerie 2000), Eric Graja (La Volerie des Templiers), Marine Felten (LOANA), Paul Supper, Benjamin Colonges	ENGIE Green, CNR, EDPR, Boralex	PP 987 A. Mionnet (CRBPO)
Hellwegbörde (DE)	MoH, MaH	Margret Bunzel-Drüke, Olaf Zimball, Patrick Hundorf (Arbeitsgemeinschaft Biologischer Umweltschutz), Thomas Laumeier (NABU-Station Münsterland)	Bezirksregierung Arnsberg	84-02.04.2017.A038 (Landesamt für Natur, Umwelt und Verbraucherschutz Nordrhein-Westfalen)
Limburg (NL)	CB		Gaiafund Zoo Kerkrade, Müskens Fauna	172544-01-001 (University of Groningen), 2017.D-0045.004 (Wageningen University & Research)
Luxembourg (LU)	RK	Katharina Klein (natur&ëmwelt a.s.b.l.), Simone Schneider (SICONA), Arnaud Beckers (CSD Ingénieurs)	Ministère de l'Environnement, du Climat et du Développement durable (MECDD): Fonds Environnement (SICONA-Project « Contribution du secteur communal à la mise en œuvre du 2ème Plan National concernant la Protection de la Nature dans le sud-ouest et le centre du Grand-Duché »); Soler	N/Réf 90832 CD/tw, N/Réf 93179 CD/gp, N/Réf 95445 CD/ne, N/Réf 102316 (Ministère de l'Environnement, du Climat et du Développement durable)
Noordoostpolder (NL)	MaH	Harold Boer, Jan Nagel, Jacques van der Ploeg and colleagues (Werkgroep Roofvogels Noordoostpolder), Nicolai Bolt (Province of Flevoland), Reinhard Vohwinkel	Province of Flevoland, Dutch Ministry of Agriculture, Nature and Food Quality in the context of WUR Knowledge Base Program KB36 Biodiversity in a Nature Inclusive Society	2017.D-0045.004 (Wageningen University & Research)
NW Flanders & SW Flanders (BE)	MaH, CB, MoH	Tanja Milotic, Peter Desmet (INBO); Natuurwerkgroep De Kerkuil	Flemish Agency for Nature and Forest, Research Foundation - Flanders (FWO) as part of the Belgian contribution to LifeWatch	INBO
Öland (SE)	MoH	Susanne Forslund, Helena Lager, Aron Edman (Kalmar County Administrative Board)	BirdLife Sweden, Kalmar County Administrative Board	01858-2020 (Linköpings djurförsöksetiska nämnd)
Provence (FR)	STE	Olivier Hameau, Alexandre Van der Yeught, Thomas Girard (LPO PACA), Alexandre Lautier (GS Sainte-Victoire), Elvin Miller	Aix Marseille Univ, LPO Provence-Alpes-Côte d'Azur	PP 1167 B. Van Hecke (CRBPO)

References

Acácio, M., Atkinson, P. W., Silva, J. P., & Franco, A. M. A. (2022). Performance of GPS/GPRS tracking devices improves with increased fix interval and is not affected by animal deployment. *PLoS ONE*, *17*(3). https://doi.org/10.1371/journal.pone.0265541

Adams, E. M., Gulka, J., & Williams, K. A. (2021). A review of the effectiveness of operational curtailment for reducing bat fatalities at terrestrial wind farms in North America. *PLoS ONE*, *16*(11), e0256382. https://doi.org/10.1371/journal.pone.0256382

Agisoft. (n.d.). *Global Geoid Models*. Retrieved March 2, 2023, from https://www.agisoft.com/downloads/geoids/

Albert, P., Bourrioux, J., Falkdalen, U., Lee, S., Millon, A., Persson, T., & Schaub, T. (2022). Breeding dispersal of an adult female Hen Harrier from France to Sweden. *Fåglar i Jämtland-Härjedalen*, *42*(2), 17–19. https://www.researchgate.net/publication/367168173_Faglar_i_Jamtland-Harjedalen_2022_-_Breeding_dispersal_of_an_adult_female_Hen_Harrier_from_France_to_Sweden

Ameijeiras-Alonso, J., Crujeiras, R. M., & Rodríguez-Casal, A. (2021). *multimode: An R Package for Mode Assessment*. *97*(9). https://doi.org/10.18637/jss.v097.i09

Anderson, D., Arkumarev, V., Bildstein, K., Botha, A., Bowden, C. G. R., Davies, M., Duriez, O., Forbes, N. A., Godino, A., Green, R. E., Krüger, S., Lambertucci, S. A., Orr-Ewing, D., Parish, C. N., Parry-Jones, J., & Weston, E. (2020). Practical Guide To Methods for Attaching Research Devices To Vultures and Condors. *Vulture News*, *78a*, 1–72. https://doi.org/http://dx.doi.org/10.4314/vulnew.v78ai1.1

Arnett, E. B., & May, R. (2016). Mitigating wind energy impacts on wildlife: Approaches for multiple taxa. *Human-Wildlife Interactions*, *10*(1), 28–41. https://doi.org/10.26077/1jeg-7r13

Arroyo, B., Mougeot, F., & Bretagnolle, V. (2013). Characteristics and sexual functions of sky-dancing displays in a semi-colonial raptor, the Montagu's Harrier (*Circus pygargus*). *Journal of Raptor Research*, *47*(2), 185–196. https://doi.org/10.3356/JRR-12-44.1

Aschwanden, J., Stark, H., Peter, D., Steuri, T., Schmid, B., & Liechti, F. (2018). Bird collisions at wind turbines in a mountainous area related to bird movement intensities measured by radar. *Biological Conservation*, *220*, 228–236. https://doi.org/10.1016/j.biocon.2018.01.005

Assandri, G., Bazzi, G., Bermejo-Bermejo, A., Bounas, A., Calvario, E., Catoni, C., Catry, I., Catry, T., Champagnon, J., De Pascalis, F., de la Puente, J., del Moral, J. C., Duriez, O., Evangelidis, A., Gameiro, J., García-Silveira, D., Garcés-Toledano, F., Jiguet, F., Kordopatis, P., … Cecere, J. G. (2024). Assessing exposure to wind turbines of a migratory raptor through its annual life cycle across continents. *Biological Conservation*, *293*. https://doi.org/10.1016/j.biocon.2024.110592

Avery, M. L., Humphrey, J. S., Daughtery, T. S., Fischer, J. W., Milleson, M. P., Tillman, E. A., Bruce, W. E., & Walter, W. D. (2011). Vulture flight behavior and implications for aircraft safety. *Journal of Wildlife Management*, *75*(7), 1581–1587. https://doi.org/10.1002/jwmg.205

Band, W. (2000). *Windfarms and birds: Calculating a theoretical collision risk assuming no avoiding action*. Scottish Natural Heritage. https://www.nature.scot/sites/default/files/2017-09/Guidance Note - Windfarms and birds - Calculating a theoretical collision risk assuming no avoiding action.pdf

Band, W. (2012). *Using a collision risk model to assess bird collision risks for offshore windfarms*. https://www.bto.org/sites/default/files/u28/downloads/Projects/Final_Report_SOSS02_Band1ModelGuidance.pdf

Band, W., Madders, M., & Whitfield, D. P. (2007). Developing field and analytical methods to assess avian collision risk at wind farms. In M. de Lucas, G. F. E. Janns, & M. Ferrer (Eds.), *Birds and wind farms. Risk assessment and mitigation* (pp. 259–275). Quercus.

Barclay, R. M. R., Baerwald, E. F., & Gruver, J. C. (2007). Variation in bat and bird fatalities at wind energy facilities: assessing the effects of rotor size and tower height. *Canadian Journal of Zoology*, *85*(3), 381–387. https://doi.org/10.1139/Z07-011

Barclay, R. M. R., Baerwald, E. F., & Rydell, J. (2017). Bats. In M. R. Perrow (Ed.), *Wildlife and Wind Farms, Conflicts and Solutions. Volume 1 Onshore: Potential Effects* (pp. 191–221). Pelagic Publishing.

Barrios, L., & Rodríguez, A. (2004). Behavioural and environmental correlates of soaring-bird mortality at on-shore wind turbines. *Journal of Applied Ecology*, *41*, 72–81. https://doi.org/10.1111/j.1365-2664.2004.00876.x

Bauer, H.-G., Bezzel, E., & Fiedler, W. (Eds.). (2005). *Das Kompendium der Vögel Mitteleuropas* (2nd ed.). Aula-Verlag.

Bell, W. J. (1990). Central place foraging. In W. J. Bell (Ed.), *Searching Behaviour: The behavioural ecology of finding resources* (pp. 171–187). Springer. https://doi.org/10.1007/978-94-011-3098-1_12

Bellebaum, J., Korner-Nievergelt, F., Dürr, T., & Mammen, U. (2013). Wind turbine fatalities approach a level of concern in a raptor population. *Journal for Nature Conservation*, *21*(6), 394–400. https://doi.org/10.1016/j.jnc.2013.06.001

Bennun, L., van Bochove, J., Ng, C., Fletcher, C., Wilson, D., Phair, N., & Carbone, G. (2021). *Mitigating biodiversity impacts associated with solar and wind energy development. Guidelines for project developers*. IUCN & The Biodiversity Consultancy. https://doi.org/10.2305/IUCN.CH.2021.04.en

Bilgili, M., & Alphan, H. (2022). Global growth in offshore wind turbine technology. *Clean Technologies and Environmental Policy*, *24*(7), 2215–2227. https://doi.org/10.1007/s10098-022-02314-0

Bivand, R., & Luque, S. (2023). *suntools: Calculate Sun Position, Sunrise, Sunset, Solar Noon and Twilight. R package version 1.0.0*.

Blary, C., Bonadonna, F., Dussauze, E., Potier, S., Besnard, A., & Duriez, O. (2023). Detection of wind turbines rotary motion by birds: A matter of speed and contrast. *Conservation Science and Practice*. https://doi.org/10.1111/csp2.13022

Bouten, W., Baaij, E. W., Shamoun-Baranes, J., & Camphuysen, C. J. (2013). A flexible GPS tracking system for studying bird behaviour at multiple scales. *Journal of Ornithology*, *154*(2), 571–580. https://doi.org/10.1007/s10336-012-0908-1

Bouzin, M. (2013). *Reproduction et mortalité du Busard cendré sur un parc éolien du sud de la France – Juillet 2013*. LPO Hérault.

Brenninkmeijer, A., & Klop, E. (2017). Bird Mortality in Two Dutch Wind Farms: Effects of Location, Spatial Design and Interactions with Powerlines. In J. Köppel (Ed.), *Wind Energy and Wildlife Interactions* (pp. 99–116). Springer. https://doi.org/10.1007/978-3-319-51272-3

Bright, J., & Muldoon, C. (2017). Spatial Planning. In M. R. Perrow (Ed.), *Wildlife and Wind Farms, Conflicts and Solutions. Volume 2 Onshore: Monitoring and Mitigation* (pp. 103–123). Pelagic Publishing.

Brook, B. W., Sodhi, N. S., & Bradshaw, C. J. A. (2008). Synergies among extinction drivers under global change. *Trends in Ecology and Evolution*, *23*(8), 453–460. https://doi.org/10.1016/j.tree.2008.03.011

Brownrigg, R., Becker, R. A., Wilks, A. R., Minka, T. P., & Deckmyn, A. (2018). *maps: Draw Geographical Maps. R package version 3.3.0.*

Bruderer, B., Peter, D., & Korner-Nievergelt, F. (2018). Vertical distribution of bird migration between the Baltic Sea and the Sahara. *Journal of Ornithology*, *159*(2), 315–336. https://doi.org/10.1007/s10336-017-1506-z

Buij, R., Moonen, S., Schaub, T., Janssen, K., Mañas, J., Müskens, G., Rijn, S. van, & Stralen, D. van. (2022). *Het risico op aanvaringen met windturbines van zeearend en bruine kiekendief in Flevoland*. Wageningen Environmental Research. https://research.wur.nl/en/publications/het-risico-op-aanvaringen-met-windturbines-van-zeearend-en-bruine [2023-07-06]

Caneco, B., Humphries, G., Cook, A., & Masden, E. (2022). *Estimating bird collisions at offshore windfarms with stochLAB. R package version 1.1.2*.

Carrete, M., Sánchez-Zapata, J. A., Benítez, J. R., Lobón, M., & Donázar, J. A. (2009). Large scale risk-assessment of wind-farms on population viability of a globally endangered long-lived raptor. *Biological Conservation*, *142*(12), 2954–2961. https://doi.org/10.1016/j.biocon.2009.07.027

Chamberlain, D. E., Rehfisch, M. R., Fox, A. D., Desholm, M., & Anthony, S. J. (2006). The effect of avoidance rates on bird mortality predictions made by wind turbine collision risk models. *Ibis*, *148*, 198–202. https://doi.org/10.1111/j.1474-919X.2006.00507.x

Christie, D., & Urquhart, B. (2015). A refinement of the Band spreadsheet for wind turbine collision risk allowing for oblique entry. *New Zealand Journal of Zoology*, *42*(4), 290–297. https://doi.org/10.1080/03014223.2015.1064456

Cleasby, I. R., Owen, E., Butler, A., Baer, J., Blackburn, J., Bogdanova, M. I., Coledale, T., Daunt, F., Dodd, S., Evans, J. C., Green, J. A., Guilford, T., Harris, M. P., Hughes, R., Newell, M. A., Newton, S. F., Robertson, G. S., Ruffino, L., Shoji, A., … Bolton, M. (2023). Assessing the importance of individual- and colony-level variation when using seabird foraging ranges as impact assessment and conservation tools. *Ibis*.

Cook, A. S. C. P., Humphreys, E. M., Masden, E. A., & Burton, N. H. K. (2014). The avoidance rates of collision between birds and offshore turbines. *Scottish Marine and Freshwater Science*, *5*(16). https://doi.org/10.7489/1616-1

Coppes, J., Braunisch, V., Bollmann, K., Storch, I., Mollet, P., Grünschachner-Berger, V., Taubmann, J., Suchant, R., & Nopp-Mayr, U. (2020). The impact of wind energy facilities on grouse: a systematic review. *Journal of Ornithology*, *161*(1), 1–15. https://doi.org/10.1007/s10336-019-01696-1

Corman, A.-M., & Garthe, S. (2014). What flight heights tell us about foraging and potential conflicts with wind farms: a case study in Lesser Black-backed Gulls (*Larus fuscus*). *Journal of Ornithology*, *155*, 1037–1043. https://doi.org/10.1007/s10336-014-1094-0

de Lucas, M., Ferrer, M., Bechard, M. J., & Muñoz, A. R. (2012). Griffon vulture mortality at wind farms in southern Spain: Distribution of fatalities and active mitigation measures. *Biological Conservation*, *147*, 184–189. https://doi.org/10.1016/j.biocon.2011.12.029

De Lucas, M., & Perrow, M. R. (2017). Birds: Collision. In M. R. Perrow (Ed.), *Wildlife and Wind Farms, Conflicts and Solutions. Volume 1 Onshore: Potential Effects* (pp. 155–190). Pelagic Publishing.

De Pascalis, F., Panuccio, M., Bacaro, G., & Monti, F. (2020). Shift in proximate causes of mortality for six large migratory raptors over a century. *Biological Conservation*, *251*(June), 108793. https://doi.org/10.1016/j.biocon.2020.108793

del Hoyo, J., Elliott, A., & Sargatal, J. (1994). *Handbook of the Birds of the World. Volume 2: New World Vultures to Guineafowl*. Lynx Edicions.

Desholm, M., & Kahlert, J. (2005). Avian collision risk at an offshore wind farm. *Biology Letters*, *1*, 296–298. https://doi.org/10.1098/rsbl.2005.0336

Dickinson, M. G., Orme, C. D. L., Suttle, K. B., & Mace, G. M. (2014). Separating sensitivity from exposure in assessing extinction risk from climate change. *Scientific Reports*, *4*, 1–6. https://doi.org/10.1038/srep06898

Diffendorfer, J. E., Stanton, J. C., Beston, J. A., Thogmartin, W. E., Loss, S. R., Katzner, T. E., Johnson, D. H., Erickson, R. A., Merrill, M. D., & Corum, M. D. (2021). Demographic and potential biological removal models identify raptor species sensitive to current and future wind energy. *Ecosphere*, *12*(6). https://doi.org/10.1002/ecs2.3531

Dodge, S., Bohrer, G., Weinzierl, R., Davidson, S., Kays, R., Douglas, D., Cruz, S., Han, J., Brandes, D., & Wikelski, M. (2013). The Environmental-Data Automated Track Annotation (Env-DATA) system: linking animal tracks with environmental data to facilitate research of external factors effects on movement. *Movement Ecology*, *1*, 1–14.

Duriez, O., Peron, G., Gremillet, D., Sforzi, A., & Monti, F. (2018). Migrating ospreys use thermal uplift over the open sea. *Biology Letters*, *14*(12). https://doi.org/10.1098/rsbl.2018.0687

Duriez, O., Pilard, P., Saulnier, N., Boudarel, P., & Besnard, A. (2022). Windfarm collisions in medium-sized raptors: even increasing populations can suffer demographic impacts. *Animal Conservation*, *26*(2), 264–275.

Dürr, T. (2011). Vogelunfälle an Windradmasten. *Der Falke*, *58*, 499–501.

Dürr, T. (2023). *Bird fatalities at wind turbines in Europe*. Staatliche Vogelschutzwarte im Landesamt für Umwelt Brandenburg. https://lfu.brandenburg.de/sixcms/media.php/9/Voegel-Uebersicht-Europa.xlsx

EEA. (2017). *European Digital Elevation Model (EU-DEM), version 1.1.* European Environment Agency. https://land.copernicus.eu/imagery-in-situ/eu-dem/eu-dem-v1.1

Efford, M. G., Dawson, D. K., Jhala, Y. V., & Qureshi, Q. (2016). Density-dependent home-range size revealed by spatially explicit capture–recapture. *Ecography*, *39*(7), 676–688. https://doi.org/10.1111/ecog.01511

Eichhorn, M., Johst, K., Seppelt, R., & Drechsler, M. (2012). Model-based estimation of collision risks of predatory birds with wind turbines. *Ecology and Society*, *17*(2), 1. https://doi.org/10.5751/ES-04594-170201

European Commission. (2022). *Commission staff working document. Implementing the REPower EU action plan: Investment needs, hydrogen accelerator and achieving the bio-methane targets*. European Commission.

European Commission. (2023). *COMMUNICATION FROM THE COMMISSION TO THE EUROPEAN PARLIAMENT, THE COUNCIL, THE EUROPEAN ECONOMIC AND SOCIAL COMMITTEE AND THE COMMITTEE OF THE REGIONS. European Wind Power Action Plan*. COM/2023/669 final. https://eur-lex.europa.eu/legal-content/EN/TXT/PDF/?uri=CELEX:52023DC0669

Everaert, J., & Stienen, E. W. M. (2007). Impact of wind turbines on birds in Zeebrugge (Belgium): Significant effect on breeding tern colony due to collisions. *Biodiversity and Conservation*, *16*(12), 3345–3359. https://doi.org/10.1007/s10531-006-9082-1

Fellows, I. (2016). OpenStreetMap*: Access to Open Street Map raster images*. *R* package version 0.3.3.

Ferguson-Lees, J., & Christie, D. A. (2001). *Raptors of the World*. Christopher Helm.

Fielding, A. H., Anderson, D., Benn, S., Dennis, R., Geary, M., Weston, E., & Whitfield, D. P. (2022). Responses of dispersing GPS-tagged Golden Eagles Aquila chrysaetos to multiple wind farms across. *Ibis*, *164*, 102–117.

Fijn, R. C., Krijgsveld, K. L., Poot, M. J. M., & Dirksen, S. (2015). Bird movements at rotor heights measured continuously with vertical radar at a Dutch offshore wind farm. *Ibis*, *157*(3), 558–566. https://doi.org/10.1111/ibi.12259

Gauld, J. G., Silva, J. P., Atkinson, P. W., Record, P., Acácio, M., Arkumarev, V., Blas, J., Bouten, W., Burton, N., Catry, I., Champagnon, J., Clewley, G. D., Dagys, M., Duriez, O., Exo, K. M., Fiedler, W., Flack, A., Friedemann, G., Fritz, J., … Franco, A. M. A. (2022). Hotspots in the grid: Avian sensitivity and vulnerability to collision risk from energy infrastructure interactions in Europe and North Africa. *Journal of Applied Ecology*, *59*(6), 1496–1512. https://doi.org/10.1111/1365-2664.14160

Gedeon, K., Grüneberg, C., Mitschke, A., Sudfeldt, C., Eikhorst, W., Fischer, S., Flade, M., Frick, S., Geiersberger, I., Koop, B., Kramer, M., Krüger, T., Roth, N., Ryslavy, T., Stübing, S., Sudmann, S. R., Steffens, R., Vökler, F., & Witt, K. (2014). *Atlas Deutscher Brutvogelarten*. Stiftung Vogelmonitoring Deutschland & Dachverband Deutscher Avifaunisten.

Grajetzky, B., & Nehls, G. (2017). Telemetric monitoring of Montagu's Harrier in Schleswig-Holstein. In H. Hötker, O. Krone, & G. Nehls (Eds.), *Birds of prey and wind farms. Analysis of problems and possible solutions* (pp. 97–148). Springer. https://doi.org/10.1007/978-3-319-53402-2

Grande, C. (2017). Unterscheidet sich das Kollisionsrisiko von Rohrweihen an Windenergieanlangen zwischen Männchen und Weibchen? In *Tagungsband 150. Jahresversammlung der Deutschen Ornithologen-Gesellschaft*. http://www.do-g.de/fileadmin/do-g_dokumente/DO-G_Tagungsband_Halle_2017_WEB.pdf

Grünkorn, T., & Welcker, J. (2019). *Erhebung von Grundlagendaten zur Abschätzung des Kollisionsrisikos von Uhus an Windenergieanlagen im im nördlichen Schleswig-Holstein*. BioConsult SH. https://bioconsult-sh.de/site/assets/files/1803/endbericht_uhutelemetrie_20191128.pdf

GWEC. (2023). *Global Wind Report 2023*. Global Wind Energy Council. https://gwec.net/wp-content/uploads/2023/04/GWEC-2023_interactive.pdf

Harel, R., Horvitz, N., & Nathan, R. (2016). Adult vultures outperform juveniles in challenging thermal soaring conditions. *Scientific Reports*, *6*. https://doi.org/10.1038/srep27865

Heinänen, S., Žydelis, R., Kleinschmidt, B., Dorsch, M., Burger, C., Morkūnas, J., Quillfeldt, P., & Nehls, G. (2020). Satellite telemetry and digital aerial surveys show strong displacement of red-throated divers (Gavia stellata) from offshore wind farms. *Marine Environmental Research*, *160*, 104989. https://doi.org/10.1016/j.marenvres.2020.104989

Hengl, T., Roudier, P., Beaudette, D., & Pebesma, E. (2015). plotKML: Scientific Visualization of Spatio-Temporal Data. *Journal Of Statistical Software*, *63*(5).

Herrera-Alsina, L., Villegas-Patraca, R., Eguiarte, L. E., & Arita, H. T. (2013). Bird communities and wind farms: A phylogenetic and morphological approach. *Biodiversity and Conservation*, *22*(12), 2821–2836. https://doi.org/10.1007/s10531-013-0557-6

Hersbach, H., Bell, B., Berrisford, P., Biavati, G., Horányi, A., Muñoz Sabater, J., Nicolas, J., Peubey, C., Radu, R., Rozum, I., Schepers, D., Simmons, A., Soci, C., Dee, D., & Thépaut, J.-N. (2018a). *ERA5 hourly data on pressure levels from 1959 to present*. Copernicus Climate Change Service (C3S) Climate Data Store (CDS). https://doi.org/10.24381/cds.bd0915c6

Hersbach, H., Bell, B., Berrisford, P., Biavati, G., Horányi, A., Muñoz Sabater, J., Nicolas, J., Peubey, C., Radu, R., Rozum, I., Schepers, D., Simmons, A., Soci, C., Dee, D., & Thépaut, J.-N. (2018b). *ERA5 hourly data on single levels from 1959 to present*. Copernicus Climate Change Service (C3S) Climate Data Store (CDS). https://doi.org/10.24381/cds.adbb2d47

Heuck, C., Herrmann, C., Levers, C., Leitão, P. J., Krone, O., Brandl, R., & Albrecht, J. (2019). Wind turbines in high quality habitat cause disproportionate increases in collision mortality of the white-tailed eagle. *Biological Conservation*, *236*(August 2018), 44–51. https://doi.org/10.1016/j.biocon.2019.05.018

Heuck, C., Sommerhage, M., Stelbrink, P., Höfs, C., Geisler, K., Gelpke, C., & Koschkar, S. (2019). *Untersuchung des Flugverhaltens von Rotmilanen in Abhängigkeit von Witterung und Landnutzung unter besonderer Berücksichtigung vorhandener Windenergieanlagen im Vogelschutzgebiet Vogelsberg - Abschlussbericht*. Im Auftrag des Hessischen Ministerium für Wirtschaft, Energie, Verkehr und Wohnen. https://landesplanung.hessen.de/sites/landesplanung.hessen.de/files/2022-11/flugverhaltenrotmilan_abschlussbericht_200206.pdf

Hijmans, R. J. (2015). *raster: Geographic Data Analysis and Modeling. R package version 2.5-2.*

Hijmans, R. J. (2022). *geosphere: Spherical Trigonometry. R package version 1.5-18*.

Hoover, S. L., & Morrison, M. L. (2005). Behavior of Red-Tailed Hawks in a Wind Turbine Development Author(s): *Journal of Wildlife Management*, *69*(1), 150–159.

Hötker, H. (2017). Birds: displacement. In M. R. Perrow (Ed.), *Wildlife and Wind Farms, Conflicts and Solutions. Volume 1 Onshore: Potential Effects* (pp. 119–154). Pelagic Publishing.

Hull, C. L., & Muir, S. C. (2013). Behavior and turbine avoidance rates of eagles at two wind farms in Tasmania, Australia. *Wildlife Society Bulletin*, *37*(1), 49–58. https://doi.org/10.1002/wsb.254

Huso, M., Dalthorp, D., & Korner-Nievergelt, F. (2017). Statistical principles of post-construction fatality monitoring. In M. R. Perrow (Ed.), *Wildlife and Wind Farms, Conflicts and Solutions. Volume 2 Onshore: Monitoring and Mitigation* (pp. 84–102). Pelagic Publishing.

IEA. (2021). *Net Zero by 2050: A Roadmap for the Global Energy Sector*. International Energy Agency. https://iea.blob.core.windows.net/assets/deebef5d-0c34-4539-9d0c-10b13d840027/NetZeroby2050-ARoadmapfortheGlobalEnergySector_CORR.pdf

IGN. (n.d.). *BD TOPO*®. Retrieved September 15, 2022, from https://geoservices.ign.fr/bdtopo

International Service for the Geoid. (n.d.). *Europe (EGG2008)*. Retrieved March 3, 2023, from https://www.isgeoid.polimi.it/Geoid/Europe/europe2008_g.html

ISO. (1975). *ISO 2533-1975. Standard Atmosphere*. International Organization for Standardization.

Janss, G. F. E. (2000). Avian mortality from power lines: A morphologic approach of a species-specific mortality. *Biological Conservation*, *95*(3), 353–359. https://doi.org/10.1016/S0006-3207(00)00021-5

Johnston, A., Cook, A. S. C. P., Wright, L. J., Humphreys, E. M., & Burton, N. H. K. (2014). Modelling flight heights of marine birds to more accurately assess collision risk with offshore wind turbines. *Journal of Applied Ecology*, *51*(1), 31–41. https://doi.org/10.1111/1365-2664.12191

Johnston, D. T., Thaxter, C. B., Boersch-Supan, P. H., Davies, J. G., Clewley, G. D., Green, R. M. W., Shamoun-Baranes, J., Cook, A. S. C. P., Burton, N. H. K., & Humphreys, E. M. (2023). Flight heights obtained from GPS versus altimeters influence estimates of collision risk with offshore wind turbines in Lesser Black-backed Gulls Larus fuscus. *Movement Ecology*, *11*(1), 1–15. https://doi.org/10.1186/s40462-023-00431-z

Johnston, D. T., Thaxter, C. B., Boersch-Supan, P. H., Humphreys, E. M., Bouten, W., Clewley, G. D., Scragg, E. S., Masden, E. A., Barber, L., Conway, G. J., Clark, N. A., Burton, N. H. K., & Cook, A. S. C. P. (2022). Investigating avoidance and attraction responses in lesser black-backed gulls Larus fuscus to offshore wind farms. *Marine Ecology Progress Series*, *686*, 187–200. https://doi.org/10.3354/meps13964

Kitzing, L., Jensen, M. K., Telsnig, T., & Lantz, E. (2020). Multifaceted drivers for onshore wind energy repowering and their implications for energy transition. *Nature Energy*, *5*(12), 1012–1021. https://doi.org/10.1038/s41560-020-00717-1

Klaassen, R. H. G., Hake, M., Strandberg, R., Koks, B. J., Trierweiler, C., Exo, K. M., Bairlein, F., & Alerstam, T. (2014). When and where does mortality occur in migratory birds? Direct evidence from long-term satellite tracking of raptors. *Journal of Animal Ecology*, *83*(1), 176–184. https://doi.org/10.1111/1365-2656.12135

Klaassen, R. H. G., Schlaich, A. E., Bouten, W., Both, C., & Koks, B. J. (2014). First results of year-round tracking of Hen Harriers *Circus cyaneus* breeding in the agricultural landscape of East-Groningen. *Limosa*, *87*, 135–148.

Kölzsch, A. (2022). *Extract Two Movement Speeds v1.1 (6).* MoveApps. https://github.com/movestore/Flight-Speed-Estimation.git

Krijgsveld, K. L., Akershoek, K., Schenk, F., Dijk, F., & Dirksen, S. (2009). Collision risk of birds with modern large wind turbines. *Ardea*, *97*(3), 357–366. https://doi.org/10.5253/078.097.0311

Krijgsveld, K. L., Kleyheeg-Hartman, J. C., Klop, E., & Brenninkmeijer, A. (2016). *Stilstandsvoorziening windturbines Eemshaven Mogelijkheden en consequenties*. Altenburg & Wymenga and Bureau Waardenburg. https://www.provinciegroningen.nl/fileadmin/user_upload/Documenten/Downloads/Downloads_2019/Stilstandsvoorziening_windturbines_Eemshaven.pdf

LAG VSW. (2014). Recommendations for distances of wind turbines to important areas for birds as well as breeding sites of selected bird species. *Berichte Zum Vogelschutz*, *51*, 15–42.

Lato, K. A., Stepanuk, J. E. F., Heywood, E. I., Conners, M. G., & Thorne, L. H. (2022). Assessing the accuracy of altitude estimates in avian biologging devices. *PLoS ONE*, *17*(10), 1–20. https://doi.org/10.1371/journal.pone.0276098

Lerner, H. R. L., & Mindell, D. P. (2005). Phylogeny of eagles, Old World vultures, and other Accipitridae based on nuclear and mitochondrial DNA. *Molecular Phylogenetics and Evolution*, *37*(2), 327–346. https://doi.org/10.1016/j.ympev.2005.04.010

Leroux, C., Le Viol, I., Valet, N., Kerbiriou, C., & Barré, K. (2023). Disentangling mechanisms responsible for wind energy effects on European bats. *Journal of Environmental Management*, *346*(July). https://doi.org/10.1016/j.jenvman.2023.118987

Liechti, F., Witvliet, W., Weber, R., & Bächler, E. (2013). First evidence of a 200-day non-stop flight in a bird. *Nature Communications*, *4*, 2554. https://doi.org/10.1038/ncomms3554

Lindström, Å., Alerstam, T., Andersson, A., Bäckman, J., Bahlenberg, P., Bom, R., Ekblom, R., Klaassen, R. H. G., Korniluk, M., Sjöberg, S., & Weber, J. K. M. (2021). Extreme altitude changes between night and day during marathon flights of great snipes. *Current Biology*, *31*(15), 3433-3439.e3. https://doi.org/10.1016/j.cub.2021.05.047

Longarini, A., Duriez, O., Shepard, E., Safi, K., Wikelski, M., & Scacco, M. (2023). Effect of harness design for tag attachment on the flight performance of five soaring species. *Movement Ecology*, *11*(1), 1–13. https://doi.org/10.1186/s40462-023-00408-y

Loss, S. R., Will, T., & Marra, P. P. (2015). Direct Mortality of Birds from Anthropogenic Causes. *Annual Review of Ecology, Evolution, and Systematics*, *46*, 99–120. https://doi.org/10.1146/annurev-ecolsys-112414-054133

Maderspacher, F. (2022). Flightless birds. *Current Biology*, *32*, R1042–R1172. https://doi.org/10.1016/j.cub.2022.09.039

Mammen, K., Mammen, U., & Resetaritz, A. (2017). Red Kite. In H. Hötker, O. Krone, & G. Nehls (Eds.), *Birds of prey and wind farms. Analysis of problems and possible solutions* (pp. 13–95). Springer.

Marques, A. T., Batalha, H., & Bernardino, J. (2021). Bird Displacement by Wind Turbines: Assessing Current Knowledge and Recommendations for Future Studies. *Birds*, *2*(4), 460–475. https://doi.org/10.3390/birds2040034

Marques, A. T., Batalha, H., Rodrigues, S., Costa, H., Pereira, M. J. R., Fonseca, C., Mascarenhas, M., & Bernardino, J. (2014). Understanding bird collisions at wind farms: An updated review on the causes and possible mitigation strategies. *Biological Conservation*, *179*, 40–52. https://doi.org/10.1016/j.biocon.2014.08.017

Martin, G. R. (2011). Understanding bird collisions with man-made objects: a sensory ecology approach. *Ibis*, *153*, 239–254. http://onlinelibrary.wiley.com/doi/10.1111/j.1474-919X.2011.01117.x/abstract

Masden, E. A., & Cook, A. S. C. P. (2016). Avian collision risk models for wind energy impact assessments. *Environmental Impact Assessment Review*, *56*, 43–49. https://doi.org/10.1016/j.eiar.2015.09.001

Masden, E. A., Cook, A. S. C. P., McCluskie, A., Bouten, W., Burton, N. H. K., & Thaxter, C. B. (2021). When speed matters: The importance of flight speed in an avian collision risk model. *Environmental Impact Assessment Review*, *90*, 106622. https://doi.org/10.1016/j.eiar.2021.106622

May, R. (2015). A unifying framework for the underlying mechanisms of avian avoidance of wind turbines. *Biological Conservation*, *190*, 179–187. https://doi.org/10.1016/j.biocon.2015.06.004

May, R. (2017). Mitigation for birds. In *Wildlife and Wind Farms, Conflicts and Solutions. Volume 2 Onshore: Monitoring and Mitigation* (pp. 124–144). Pelagic Publishing.

May, R. (2019). The Mitigation of Impact and the Impact of Mitigation: An Ethical Perspective. In *Wind Energy and Wildlife Impacts: Balancing Energy Sustainability with Wildlife Conservation* (pp. 93–113). https://doi.org/10.1007/978-3-030-05520-2_6

May, R., Masden, E. A., Bennet, F., & Perron, M. (2019). Considerations for upscaling individual effects of wind energy development towards population-level impacts on wildlife. *Journal of Environmental Management*, *230*(January 2018), 84–93. https://doi.org/10.1016/j.jenvman.2018.09.062

May, R., Nygård, T., Falkdalen, U., Åström, J., Hamre, Ø., & Stokke, B. G. (2020). Paint it black: Efficacy of increased wind turbine rotor blade visibility to reduce avian fatalities. *Ecology and Evolution*, *10*(16), 8927–8935. https://doi.org/10.1002/ece3.6592

May, R., Reitan, O., Bevanger, K., Lorentsen, S. H., & Nygård, T. (2015). Mitigating wind-turbine induced avian mortality: Sensory, aerodynamic and cognitive constraints and options. *Renewable and Sustainable Energy Reviews*, *42*, 170–181. https://doi.org/10.1016/j.rser.2014.10.002

McClure, C. J. W., Dunn, L., McCabe, J. D., Rolek, B. W., Botha, A., Virani, M. Z., Buij, R., & Katzner, T. E. (2021). Flight Altitudes of Raptors in Southern Africa Highlight Vulnerability of Threatened Species to Wind Turbines. *Frontiers in Ecology and Evolution*, *9*(October 2021), 1–7. https://doi.org/10.3389/fevo.2021.667384

McClure, C. J. W., Martinson, L., & Allison, T. D. (2018). Automated monitoring for birds in flight: Proof of concept with eagles at a wind power facility. *Biological Conservation*, *224*, 26–33. https://doi.org/10.1016/j.biocon.2018.04.041

McClure, C. J. W., Schulwitz, S. E., Anderson, D. L., Robinson, B. W., Mojica, E. K., Therrien, J. F., Oleyar, M. D., & Johnson, J. (2019). Commentary: Defining Raptors and Birds of Prey. *Journal of Raptor Research*, *53*(4), 419–430. https://doi.org/10.3356/0892-1016-53.4.419

McGregor, R. M., King, S., Donovan, C. R., Caneco, B., & Webb, A. (2018). *A Stochastic Collision Risk Model for Seabirds in Flight*. Marine Scotland Science. https://tethys.pnnl.gov/sites/default/files/publications/McGregor-2018-Stochastic.pdf

Mebs, T., & Schmidt, D. (2017). *Roofvogels van Europa* (4th ed.). Kosmos Uitgevers.

Mercker, M., Liedtke, J., Liesenjohann, T., & Blew, J. (2023). *Pilotstudie „Erprobung Probabilistik": Erprobung probabilistischer Methoden hinsichtlich ihrer fachlichen Voraussetzungen mit dem Ziel der Validierung der Methode zur Ermitt- lung des vorhabenbezogenen Tötungsrisikos von kollisionsgefährdeten Brutvogel- a*.

Ministère de la Transition Ecologique et Solidaire. (2020). Stratégie française pour l'énergie et le climat. Programmation pluriannuelle de l'énergie 2019-2023, 2024-2028. In *Programmation Pluriannuelle de l'Energie* (Vol. 1, Issue 1). https://www.ecologie.gouv.fr/sites/default/files/20200422 Programmation pluriannuelle de l%27énergie.pdf

NASA JPL. (2013). *NASA Shuttle Radar Topography Mission Global 1 arc second v003*. NASA EOSDIS Land Processes DAAC. https://doi.org/10.5067/MEaSUREs/SRTM/SRTMGL1.003

Nunez, S., Arets, E., Alkemade, R., Verwer, C., & Leemans, R. (2019). Assessing the impacts of climate change on biodiversity: is below 2 °C enough? *Climatic Change*, *154*(3–4), 351–365. https://doi.org/10.1007/s10584-019-02420-x

OIML. (2012). *International Vocabulary of Metrology – Basic and General Concepts and Associated Terms (VIM)* (3rd ed.). International Organization of Legal Metrology.

PDOK. (n.d.). *Dataset: Basisregistratie Topografie (BRT) TOPNL en TOPraster Historie*. Retrieved December 14, 2022, from https://www.pdok.nl/downloads/-/article/basisregistratie-topografie-brt-historie

Pearce-Higgins, J. W., Stephen, L., Langston, R. H. W., Bainbridge, I. P., & Bullman, R. (2009). The distribution of breeding birds around upland wind farms. *Journal of Animal Ecology*, *46*, 1323–1331. https://doi.org/10.1111/j.1365-2664.2009.01715.x

Pebesma, E. (2018). Simple features for R: Standardized support for spatial vector data. *R Journal*, *10*(1), 439–446. https://doi.org/10.32614/rj-2018-009

Pebesma, E. J., & Bivand, R. S. (2005). Classes and methods for spatial data in *R*. *R News*, *5*(2), 9–13.

Peery, M. Z. (2000). Factors Affecting Interspecies Variation in Home-Range Size of Raptors. *The Auk*, *117*(2), 511–517.

Perold, V., Ralston-Paton, S., & Ryan, P. (2020). On a collision course? The large diversity of birds killed by wind turbines in South Africa. *Ostrich*, 228–239. https://doi.org/10.2989/00306525.2020.1770889

Péron, G., Calabrese, J. M., Duriez, O., Fleming, C. H., García-Jiménez, R., Johnston, A., Lambertucci, S. A., Safi, K., & Shepard, E. L. C. (2020). The challenges of estimating the distribution of flight heights from telemetry or altimetry data. *Animal Biotelemetry*, *8*(5), 1–13. https://doi.org/10.1186/s40317-020-00194-z

Péron, G., Fleming, C. H., Duriez, O., Fluhr, J., Itty, C., Lambertucci, S., Safi, K., Shepard, E. L. C., & Calabrese, J. M. (2017). The energy landscape predicts flight height and wind turbine collision hazard in three species of large soaring raptor. *Journal of Applied Ecology*, *54*, 1895–1906. https://doi.org/10.1111/1365-2664.12909

Perrow, M. R. (Ed.). (2017). *Wildlife and Wind Farms, Conflicts and Solutions. Volume 1 Onshore: Potential Effects*. Pelagic Publishing.

Pfeiffer, T., & Meyburg, B. U. (2022). Flight altitudes and flight activities of adult Red Kites (*Milvus milvus*) in the breeding area as determined by GPS telemetry. *Journal of Ornithology*, *163*(4), 867–879. https://doi.org/10.1007/s10336-022-01994-1

Pörtner, H. O., Scholes, R. J., Agard, J., Archer, E., Arneth, A., Bai, X., Barnes, D., Burrows, M., Chan, L., Cheung, W. L., Diamond, S., Donatti, C., Duarte, C., Eisenhauer, N., Foden, W., Gasalla, M. A., Handa, C., Hickler, T., Hoegh-Guldberg, O., … Ngo, H. T. (2021). *Scientific outcome of the IPBES-IPCC co-sponsored workshop on biodiversity and climate change*. IPBES secretariat. https://doi.org/10.5281/zenodo.4659158.IPBES

Pretorius, M. D., Galloway-Griesel, T. L., Leeuwner, L., Michael, M. D., Durgapersad, K., & Chetty, K. (2023). Defining Collision Risk : Lesser Flamingo Phoeniconaias minor Power Line Collision Sensitivity and Exposure for Proactive Mitigation. *Birds*, *4*, 315–329.

R Core Team. (2020). *R: A Language and Environment for Statistical Computing. R version 4.0.3 (2020-10-10)*. R Foundation for Statistical Computing.

R Core Team. (2023). *R: A Language and Environment for Statistical Computing. Version 4.3.1 (2023-06-16)*. R Foundation for Statistical Computing.

Rasran, L., Grajetzky, B., & Mammen, U. (2017). Calculation of the Probability of a Collision of Territorial Birds of Prey with Wind Turbines. In H. Hötker, O. Krone, & G. Nehls (Eds.), *Birds of prey and wind farms. Analysis of problems and possible solutions* (pp. 297–307). Springer.

Reichenbach, M., Greule, S., Steinkamp, T., Reers, H., Akili, J., & Roselius, L. (2023). *Fachgutachten zur Ermittlung des Flugverhaltens des Rotmilans im Windparkbereich unter Einsatz von Detektionssystemen.pdf*. https://landesplanung.hessen.de/sites/landesplanung.hessen.de/files/2023-09/IDF Hessen Berichtsendfassung_11-09-2023.pdf

Ren, S., Lai, H., Tong, W., Aminzadeh, M., Hou, X., & Lai, S. (2010). Nonparametric bootstrapping for hierarchical data. *Journal of Applied Statistics*, *37*(9), 1487–1498. https://doi.org/10.1080/02664760903046102

Roeleke, M., Blohm, T., Kramer-Schadt, S., Yovel, Y., & Voigt, C. C. (2016). Habitat use of bats in relation to wind turbines revealed by GPS tracking. *Scientific Reports*, *6*, 28961. https://doi.org/10.1038/srep28961

Ross-Smith, V. H., Thaxter, C. B., Masden, E. A., Shamoun-Baranes, J., Burton, N. H. K., Wright, L. J., Rehfisch, M. M., Johnston, A., & Thompson, D. (2016). Modelling flight heights of lesser black-backed gulls and great skuas from GPS: a Bayesian approach. *Journal of Applied Ecology*, *53*(6), 1676–1685. https://doi.org/10.1111/1365-2664.12760

Šálek, M., Bažant, M., Klvaňa, P., Vermouzek, Z., & Václav, R. (2023). Historical changes in mortality patterns of diurnal and nocturnal raptors in the Czech Republic, Central Europe: 1913–2017. *Biological Conservation*, *282*(January). https://doi.org/10.1016/j.biocon.2023.110073

Sansom, A., Pearce-Higgins, J. W., & Douglas, D. J. T. (2016). Negative impact of wind energy development on a breeding shorebird assessed with a BACI study design. *Ibis*, *158*, 541–555. https://doi.org/10.1111/ibi.12364

Santos, C. D., Ferraz, R., Munõz, A. R., Onrubia, A., & Wikelski, M. (2021). Black kites of different age and sex show similar avoidance responses to wind turbines during migration. *Royal Society Open Science*, *8*, 201933. https://doi.org/10.1098/rsos.201933

Schaub, M. (2012). Spatial distribution of wind turbines is crucial for the survival of Red Kite populations. *Biological Conservation*, *155*, 111–118. https://doi.org/10.1016/j.biocon.2012.06.021

Schaub, T., Klaassen, R. H. G., Bouten, W., Schlaich, A. E., & Koks, B. J. (2020). Collision risk of Montagu's Harriers *Circus pygargus* with wind turbines derived from high-resolution GPS tracking. *Ibis*, *162*(2), 520–534. https://doi.org/10.1111/ibi.12788

Schaub, T., Millon, A., De Zutter, C., Buij, R., Chadœuf, J., Lee, S., Mionnet, A., & Klaassen, R. H. G. (2023). How to improve the accuracy of height data from bird tracking devices? An assessment of high-frequency GPS tracking and barometric altimetry in field conditions. *Animal Biotelemetry*, *11*(31), 1–16. https://doi.org/10.1186/s40317-023-00342-1

Schlaich, A. E., Bouten, W., Bretagnolle, V., Heldbjerg, H., Klaassen, R. H. G., Sørensen, I. H., Villers, A., & Both, C. (2017). A circannual perspective on daily and total flight distances in a long-distance migratory raptor, the Montagu's harrier, *Circus pygargus*. *Biology Letters*, *13*, 20170073. https://doi.org/10.1098/rsbl.2017.0073

Schlaich, A. E., Klaassen, R. H. G., Bouten, W., Both, C., & Koks, B. J. (2015). Testing a novel agri-environment scheme based on the ecology of the target species, Montagu's Harrier *Circus pygargus*. *Ibis*, *157*, 713–721. https://doi.org/10.1111/ibi.12299

Schuster, E., Bulling, L., & Köppel, J. (2015). Consolidating the state of knowledge: A synoptical review of wind energy's wildlife effects. *Environmental Management*, *56*, 300–331. https://doi.org/10.1007/s00267-015-0501-5

Sergio, F., Tavecchia, G., Tanferna, A., López Jiménez, L., Blas, J., De Stephanis, R., Marchant, T. A., Kumar, N., & Hiraldo, F. (2015). No effect of satellite tagging on survival, recruitment, longevity, productivity and social dominance of a raptor, and the provisioning and condition of its offspring. *Journal of Applied Ecology*, *52*(6), 1665–1675. https://doi.org/10.1111/1365-2664.12520

Serrano-González, J., & Lacal-Arántegui, R. (2016). Technological evolution of onshore wind turbines—a market-based analysis. *Wind Energy*, *19*(12), 2171–2187. https://doi.org/10.1002/we.1974

Shamoun-Baranes, J., van Loon, E., van Gasteren, H., van Belle, J., Bouten, W., & Buurma, L. (2006). A comparative analysis of the influence of weather on the flight altitudes of birds. *Bulletin of the American Meteorological Society*, *87*(1), 47–61. https://doi.org/10.1175/BAMS-87-1-47

Simpson, G. (2023). *gratia: Graceful ggplot-Based Graphics and Other Functions for GAMs Fitted using mgcv. R package version 0.8.1*.

Skov, H., Heinänen, S., Norman, T., Ward, R., Méndez-Roldán, S., & Ellis, I. (2018). *ORJIP Bird Collision Avoidance Study. Final report – April 2018*. The Carbon Trust. https://ctprodstorageaccountp.blob.core.windows.net/prod-drupal-files/documents/resource/public/orjip-bird-collision-avoidance-study_april-2018.pdf

Smales, I., Muir, S., Meredith, C., & Baird, R. (2013). A description of the biosis model to assess risk of bird collisions with wind turbines. *Wildlife Society Bulletin*, *37*(1), 59–65. https://doi.org/10.1002/wsb.257

Smallwood, K. S. (2013). Comparing bird and bat fatality-rate estimates among North American wind-energy projects. *Wildlife Society Bulletin*, *37*(1), 19–33. https://doi.org/10.1002/wsb.260

Smallwood, K. S., & Bell, D. A. (2020). Effects of Wind Turbine Curtailment on Bird and Bat Fatalities. *Journal of Wildlife Management*, *84*(4), 685–696. https://doi.org/10.1002/jwmg.21844

SNH. (2018). *Avoidance Rates for the onshore SNH Wind Farm Collision Risk Model*. https://www.nature.scot/sites/default/files/2018-09/Wind farm impacts on birds - Use of Avoidance Rates in the SNH Wind Farm Collision Risk Model.pdf

Spaar, R., & Bruderer, B. (1997). Migration by flapping or soaring: Flight strategies of Marsh, Montagu's and Pallid Harriers in southern Israel. *Condor*, *99*(2), 458–469. https://doi.org/10.2307/1369952

Stokke, B. G., Nygård, T., Falkdalen, U., Pedersen, H. C., & May, R. (2020). Effect of tower base painting on willow ptarmigan collision rates with wind turbines. *Ecology and Evolution*, *10*(12), 5670–5679. https://doi.org/10.1002/ece3.6307

Stumpf, J. P., Denis, N., Hamer, T. E., Johnson, G., & Verschuyl, J. (2011). Flight height distribution and collision risk of the Marbled Murrelet *Brachyramphus marmoratus*: Methodology and preliminary results. *Marine Ornithology*, *39*, 123–128.

Thaxter, C. B., Buchanan, G. M., Carr, J., Butchart, S. H. M., Newbold, T., Green, R. E., Tobias, J. A., Foden, W. B., O'Brien, S., & Pearce-Higgins, J. W. (2017). Bird and bat species' global vulnerability to collision mortality at wind farms revealed thr ough a trait-based assessment. *Proceedings of the Royal Society B: Biological Sciences*, *284*(1862). https://doi.org/10.1098/rspb.2017.0829

Thaxter, C. B., Ross-Smith, V. H., Bouten, W., Clark, N. A., Conway, G. J., Rehfisch, M. M., & Burton, N. H. K. (2015). Seabird-wind farm interactions during the breeding season vary within and between years: A case study of lesser black-backed gull *Larus fuscus* in the UK. *Biological Conservation*, *186*, 347–358. https://doi.org/10.1016/j.biocon.2015.03.027

Thaxter, C. B., Ross-Smith, V. H., Bouten, W., Masden, E. A., Clark, N. A., Conway, G. J., Barber, L., Clewley, G., & Burton, N. H. K. (2018). Dodging the blades: New insights into three-dimensional area use of offshore wind farms by Lesser Black-backed Gulls *Larus fuscus*. *Inter-Research Marine Ecology Progress Series*, *587*, 247–253. https://doi.org/10.3354/meps12415

The Wind Power. (2022). *Wind turbines database 22-05-2022*. The Wind Power.

The Wind Power. (2023). *Wind farms Europe database 07-06-2023*. The Wind Power.

Tikkanen, H., Balotari-Chiebao, F., Laaksonen, T., Pakanen, V. M., & Rytkönen, S. (2018). Habitat use of flying subadult white-tailed eagles (haliaeetus albicilla): Implications for land use and wind power plant planning. *Ornis Fennica*, *95*(4), 137–150.

Tikkanen, H., Rytkönen, S., Karlin, O. P., Ollila, T., Pakanen, V. M., Tuohimaa, H., & Orell, M. (2018). Modelling golden eagle habitat selection and flight activity in their home ranges for safer wind farm planning. *Environmental Impact Assessment Review*, *71*(April), 120–131. https://doi.org/10.1016/j.eiar.2018.04.006

Tomé, R., Canário, F., Leitão, A. H., Pires, N., & Repas, M. (2017). Wind Energy and Wildlife Interactions. In J. Köppel (Ed.), *Wind Energy and Wildlife Interactions* (pp. 119–133). Springer. https://doi.org/10.1007/978-3-319-51272-3

UN Global Compact, & IUCN. (2012). *A Framework for Corporate Action on Biodiversity and Ecosystem Services*. UN Global Compact and IUCN. https://doi.org/10.1016/b978-0-12-419964-4.00007-x

van Erp, J., Sage, E., Bouten, W., van Loon, E., Camphuysen, K., & Shamoun-Baranes, J. (2023). Thermal soaring over the North Sea and implications for wind farm interactions. *Marine Ecology Progress Series*. https://doi.org/10.3354/meps14315

van Rijn, S., & van Manen, W. (2019). Jonge Nederlandse Rode Wouwen Milvus milvus op de voet gevolgd met GPS-zenders. *De Takkeling*, *27*(3), 252–256.

Vansteelant, W. M. G., Klaassen, R., Strandberg, R., Janssens, K., T´Jollyn, F., Bouten, W., Koks, B. J., & Anselin, A. (2020). Western Marsh Harriers Circus aeruginosus from nearby breeding areas migrate along comparable loops, but on contrasting schedules in the West African–Eurasian flyway. *Journal of Ornithology*, *161*(4), 953–965. https://doi.org/10.1007/s10336-020-01785-6

Vasilakis, D. P., Whitfield, D. P., Schindler, S., Poirazidis, K. S., & Kati, V. (2016). Reconciling endangered species conservation with wind farm development: Cinereous Vultures (*Aegypius monachus*) in south-eastern Europe. *Biological Conservation*, *196*, 10–17. https://doi.org/10.1016/j.biocon.2016.01.014

Vignali, S., Lörcher, F., Hegglin, D., Arlettaz, R., & Braunisch, V. (2022). A predictive flight-altitude model for avoiding future conflicts between an emblematic raptor and wind energy development in the Swiss Alps. *Royal Society Open Science*, *9*, 211041. https://doi.org/10.1098/rsos.211041

Wickham, H., François, R., Henry, L., & Müller, K. (2022). *dplyr: A Grammar of Data Manipulation. R package version 1.0.8.*

Wilson, M., Fernández-Bellon, D., Irwin, S., & O'Halloran, J. (2015). *The interactions between Hen Harriers and wind turbines - WINDHARRIER* [Final project report. University College Cork]. https://www.ucc.ie/en/media/research/planforbio/forestecology/WINDHARRIERFinalProjectReport.pdf

WindEurope. (2023). *Wind energy in Europe. 2022 Statistics and the outlook for 2023-2027*. WindEurope.

Wood, S. (2017). *Generalized Additive Models: An Introduction with R* (2nd ed.). Chapman and Hall/CRC.

Zheng, Z., Rasouli, S., & Timmermans, H. (2014). Evaluating the Accuracy of GPS-based Taxi Trajectory Records. *Procedia Environmental Sciences*, *22*, 186–198. https://doi.org/10.1016/j.proenv.2014.11.019

Co-author affiliations

Albert, Pascal: Groupe d'Études et de Protection des Busards, Maison forestière de Blinfey, 10120 Beurville, France

Bedotti, Olivier: ENGIE Laborelec, Rodestraat 125, 1630 Linkebeek, Belgium

Bourrioux, Jean-Luc: Groupe d'Études et de Protection des Busards, Maison forestière de Blinfey, 10120 Beurville, France

Buij, Ralph: Wageningen Environmental Research, Droevendaalsesteeg 3A, 6708 PB Wageningen, The Netherlands

Chadœuf, Joël: Groupe d'Études et de Protection des Busards, Maison forestière de Blinfey, 10120 Beurville, France

De Zutter, Caroline: ENGIE Lab CRIGEN, 4 rue Joséphine Baker, 93240 Stains, France

Grande, Celia: Landscape Ecology Group, Carl von Ossietzky Universität Oldenburg, 26111 Oldenburg, Germany

Illner, Hubertus: Arbeitsgemeinschaft Biologischer Umweltschutz e.V., Biologische Station Soest, Teichstraße 19, 59505 Bad Sassendorf, Germany

Isambert, Jérôme: Ligue pour la Protection des Oiseaux Alsace, 1 rue du Wisch, 67560 Rosenwiller, France

Janssens, Kjell: Research Institute for Nature and Forest (INBO), VAC Herman Teirlinck, Havenlaan 88 bus 73, 1000 Brussel; Dutch Montagu's Harrier Foundation, Berkenweg 1, 9471 VA Zuidlaren, The Netherlands

Julius, Eike: TB Raab, Quadenstraße 13, 2232 Deutsch-Wagram, Austria

Keller, Arthur: Ligue pour la Protection des Oiseaux Alsace, 1 rue du Wisch, 67560 Rosenwiller, France

Klaassen, Raymond H. G.: Groningen Institute for Evolutionary Life Sciences (GELIFES), University of Groningen, PO Box 11103, 9700 CC Groningen, The Netherlands; Dutch Montagu's Harrier Foundation, Berkenweg 1, 9471 VA Zuidlaren, The Netherlands

Lee, Simon: Natural England, Sterling House, Dix's Field, Exeter, UK; Centre for Ecology and Conservation, University of Exeter, Penryn, UK

Millon, Alexandre: Aix Marseille Univ, Avignon Univ, CNRS, IRD, Institut Méditerranéen de Biodiversité et d'Ecologie, Technopôle Arbois-Méditerranée, BP 80, 13545 Aix-en-Provence, France; Groupe d'Études et de Protection des Busards, Maison forestière de Blinfey, 10120 Beurville, France

Mionnet, Aymeric: Ligue pour la Protection des Oiseaux Champagne-Ardenne, Der Nature, Ferme des Grands Parts, 51290 Outines, France

Müskens, Gerard: Müskens Fauna, van Nispenstraat 4, 6561 BG Groesbeek, The Netherlands

Raab, Rainer: TB Raab, Quadenstraße 13, 2232 Deutsch-Wagram, Austria

van Rijn, Stef: Deltamilieu Projecten, Edisonweg 53/D, 4382 NV Vlissingen, The Netherlands

Shamoun-Baranes, Judy: Institute for Biodiversity and Ecosystem Dynamics, University of Amsterdam, PO Box 94240, 1090 GE Amsterdam, The Netherlands

Spanoghe, Geert: Research Institute for Nature and Forest (INBO), VAC Herman Teirlinck, Havenlaan 88 bus 73, 1000 Brussel, Belgium

Van Hecke, Benoît: Groupe d'Études et de Protection des Busards, Maison forestière de Blinfey, 10120 Beurville, France

Waldenström, Jonas: Linnaeus University, Department of Ecology and Environmental Science, 39182 Kalmar, Sweden